System Design and Electrochemical Characterization of Lithium-Ion Active Material Suspensions

A Dissertation

Presented to

the faculty of the School of Engineering and Applied Science

University of Virginia

in partial fulfillment

of the requirements for the degree

Doctor of Philosophy

by

Zhaoxiang Qi

August

2017

APPROVAL SHEET

The dissertation

is submitted in partial fulfillment of the requirements

for the degree of

Doctor of Philosophy

Zhaoxiang Qi

AUTHOR

The dissertation has been read and approved by the examining committee:

Gary Koenig

Advisor

Geoffrey Geise

Robert Kelly

Joshua Choi

David Green

Accepted for the School of Engineering and Applied Science:

Craig H. Benson, Dean, School of Engineering and Applied Science

August

2017

Print Form

System Design and Electrochemical Characterization of Lithium-Ion Active Material Suspensions

A Dissertation

Presented to

The Faculty of the School of Engineering and Applied Science

University of Virginia

in partial fulfilment

of the requirements of the degree

Doctor of Philosophy in Chemical Engineering

by

Zhaoxiang Qi

August 2017

Executive Summary

To further reduce the usage of fossil fuels, large scale energy storage technologies are needed to store electrical energy and improve the energy quality from the renewable energies effectively at a low cost. Redox flow batteries are ideal for large scale energy storage because of the decoupling of the power and the energy in the system, which provides the flexibility to independently adjust and design the power and energy requirements for an application. The energy density in conventional flow batteries, however, is highly limited by the solubility of the active species. In this dissertation, a new type of flow battery with lithium-ion active materials is first demonstrated to address this limitation. The energy density is increased significantly comparing with conventional redox flow battery while maintaining the benefits of design flexibility.

This new type of flow battery incorporates solid electroactive materials dispersed in lithium-ion battery electrolyte as flowing suspensions. Such type of battery has never been investigated before. To fill this missing knowledge, challenges including active material selection, flow cell architecture design, rheological characterization, and electrochemical performance measurements were addressed in this dissertation. A half-cell design was demonstrated with $Li_4Ti_5O_{12}$ suspension, an anode active material. This was the first demonstration on this type of flow battery based on lithium-ion active materials in literature and discussed in Chapter II. Moving forward to the cathode material suspension demonstration, a sub-micrometer sized $LiCoO_2$ material was synthesized and characterized because of the need of a small sized cathode active material with high conductivity. This synthesis method was expected to be a scalable

synthesis approach and included in Chapter III. Based on this, another half-cell demonstration was further conducted with $LiCoO_2$ suspension as the first report on lithium-ion cathode material suspension as the energy storage media. Combining $Li_4Ti_5O_{12}$ suspension and $LiCoO_2$ suspension in the same system, a full cell demonstration was studied as well. Both pieces of work were discussed in Chapter IV.

In this route, the high resistance of the electrochemical reaction was found to be the key barrier limiting the cycling performance. Therefore, a technique to characterize the resistance and identify materials for best performance was developed and named "Dispersed Particle Resistance". Chapter V first introduced this concept with $Li_4Ti_5O_{12}$ anode material as the model material and characterized in organic lithium-ion electrolyte. This technique was also found to be effective to characterize the performance of active materials in conventional coin cells as the measured resistance parameter was inversely related with the rate capability of active materials in conventional cells. To further demonstrate the applicability of this technique, a new class of lithium-ion active materials – cathode materials was demonstrated using six $LiFePO_4$ cathode materials in aqueous electrolyte. This demonstration also introduced a new design using aqueous electrolyte suspensions for improved performance and was reported in Chapter VI. More detailed discussions are included in the following chapters of this dissertation.

Bibliography

The publications that resulted/will result from this dissertation are stated in each perspective chapter. A summary of all the publications is listed below:

Chapter I

Z. Qi, G.M. Koenig, Review Article: Flow battery systems with solid electroactive materials, *Journal of Vacuum Science & Technology B, Nanotechnology and Microelectronics: Materials, Processing, Measurement, and Phenomena*, 35 (2017) 040801.

Chapter II

Z. Qi, G.M. Koenig, A carbon-free lithium-ion solid dispersion redox couple with low viscosity for redox flow batteries, *Journal of Power Sources*, 323 (2016) 97-106.

Chapter III

Z. Qi, G.M. Koenig, High-Performance LiCoO2 Sub-Micrometer Materials from Scalable Microparticle Template Processing, *ChemistrySelect*, 1 (2016) 3992-3999.

Chapter IV

Z. Qi, A.L. Liu, G.M. Koenig, Carbon-free Solid Dispersion $LiCoO_2$ Redox Couple Characterization and Electrochemical Evaluation for All Solid Dispersion Redox Flow Batteries, *Electrochimica Acta*, 228 (2017) 91-99.

Chapter V

Z. Qi, G.M. Koenig, Electrochemical Evaluation of Suspensions of Lithium-Ion Battery Active Materials as an Indicator of Rate Capability, *Journal of The Electrochemical Society*, 164 (2017) A151-A155.

Chapter VI

Z. Qi, H. Dong, G.M. Koenig, Electrochemical Characterization of Lithium-Ion Battery Cathode Materials with Aqueous Flowing Dispersions, *in preparation*.

Table of Contents

Chapter I. Research Background: Flow Battery Systems with Solid Electroactive Materials

1.1. Overview

This chapter provides the background and scientific basis for the work in this dissertation. An outline of redox flow battery (RFB) technology and particularly RFB with solid active materials is reviewed. This is the first review on this emerging field of research on flow batteries with solid active material suspensions in the literature. Technical challenges for different types of RFB architecture designs, different materials, and operating methods are discussed in detail. The scope of the dissertation is then defined after reviewing the technical background. This chapter also provides the foundation for the arguments presented in subsequent chapters which provide more focused and detailed discussion on the research progress and achievements.

Elements of this chapter have been published in the following journal:
Z. Qi, G.M. Koenig, Review Article: Flow battery systems with solid electroactive materials, *Journal of Vacuum Science & Technology B, Nanotechnology and Microelectronics: Materials, Processing, Measurement, and Phenomena*, 35 (2017) 040801.

1.2. Introduction

Electrical energy storage devices have had dramatic increases in production due to the proliferation of personal digital devices, electric vehicles, and renewable energy technologies.[1-5] Dependent on the scale of the energy and power needs, the most common energy storage technologies include batteries, capacitors/supercapacitors, pumped hydropower, compressed air, and flywheels.[6-8] Among all of these energy storage technology options, batteries have attracted significant research attention recently in part because of the range of energy and power densities that can be achieved due to the variety of options with regards to battery chemistry and cell design.[8-11] Particular effort and success have been driven by high energy density rechargeable lithium-ion (Li-ion) batteries, which have seen their proliferation closely linked to the explosion in sales of the consumer devices where they dominate as the power source: smart phones, laptops, smart watches, fitness bands, and other portable electronics.[12] Li-ion batteries are also currently the dominant electric vehicle battery technology due to similar energy and power density advantages.[9, 13]

The battery technologies that are well-suited to portable electronics and transportation applications are not necessarily the best options for much larger scale stationary applications including emergency backup power and utility peak shaving or load levelling.[11, 14] Even when hydrocarbon fuel sources are at low price points, renewable energy generation is still important due to political and environmental concerns.[11, 15] Dealing with the intermittency of renewable sources such as solar and wind causes significant challenges for the electric grid due to the need for reliable power supply

regardless of time of day and weather, and often supplemental fossil fuel power plants are operated to compensate for the dramatic change in power supply of renewables.[11, 16] To operate renewable energies without non-renewable fossil fuels, large scale electrical energy storage devices are needed to store the energy at peak hours and release it at off-peak hours. The RFB is a promising technology for this particular application due to its decoupling of power output and energy storage capacity and has been demonstrated in numerous large scale energy storage projects.[11, 14, 17] RFBs date back to at least the 1940s,[18-21] and recently interest in RFBs has increased in part because of the drive to enable larger scale energy storage applications to which RFBs are well suited, but also due to recent advances that have shown the potential to dramatically increase the energy density of these types of energy storage devices.[14, 22-27] Transportation applications are also being explored for RFBs, and energy density advances would be particularly important in making RFBs more competitive for electric vehicles.[28]

1.2.1. Conventional Static Batteries

Batteries store electrical energy within chemical components of differing electrochemical potentials, the difference of which determines the battery voltage.[29] A wide variety of batteries have been developed and engineered depending on the application for different voltages, capacities, rate capabilities, geometries, energy densities, power densities, costs, etc.[12, 29-33] Rechargeable Li-ion batteries have found widespread use due to their high energy density and retention of capacity with extended cycling.[34, 35] One of the most well-known commercial Li-ion battery material pairings, a lithium cobalt oxide ($LiCoO_2$, or LCO) cathode and a graphite anode, is chosen to explain the working principles of a

rechargeable static battery. As shown in Figure 1a, a Li-ion battery consists of current collectors to transport electrons from the electrodes to the terminals of the battery, an anode (negative electrode), a cathode (positive electrode), a separator to prevent shorting of the electrodes, and electrolyte to provide ionic transport which is necessary to maintain charge neutrality during charge/discharge. LCO is an example of the material that would comprise the active material particles in the cathode and graphite would be the corresponding active material particles in the anode. Conductive carbon additives are mixed with the active materials to facilitate electron transfer within the composite electrode, which is held together by a polymeric binder that provides mechanical integrity, especially during cell manufacturing.[36-38] As indicated in Equation (1) and (2), Li ions are transferred from cathode to anode during the charging process and are transferred in the opposite direction during discharge. The total charge capacity is determined by the type and amount of active materials in the electrodes.

$$LiCoO_2 \underset{discharge}{\overset{charge}{\rightleftarrows}} Li_{1-x}CoO_2 + xLi^+ + xe^- \left(\text{Cathode}\right) \quad (1)$$

$$C_6 + xLi^+ + xe^- \underset{discharge}{\overset{charge}{\rightleftarrows}} Li_xC_6 \left(\text{Anode}\right) \quad (2)$$

Another type of electrical energy storage device, the supercapacitor, functions differently. Supercapacitors store electrical energy within the electrical double layer (EDL) near the surface of high surface area materials within an electrode, and redox reactions are not required.[29, 39] Cations and anions migrate to the electrode surfaces on the appropriate sides of the cell during charging of the supercapacitor (shown in Figure 1b). Opposing

surface charges on the electrodes balance the electric field created by the concentrated ions near the surface, generating a potential difference between the two electrodes. When the supercapacitor is discharged, the potential difference gradually diminishes while ions migrate away from the electrode surfaces and eventually the final result is a neutral electrolyte with minimal concentration gradient from anode to cathode.[29, 39] The total active surface area within the electrodes and the concentration of ions in the electrolyte are the key factors that determine the total charge capacity and energy density. There is also significant research interest in hybrid supercapacitors, where one electrode functions as a supercapacitor and the other undergoes battery redox reactions.[40-45] More detailed discussion of supercapacitors can be found in a number of recent reviews.[29, 40, 45-47]

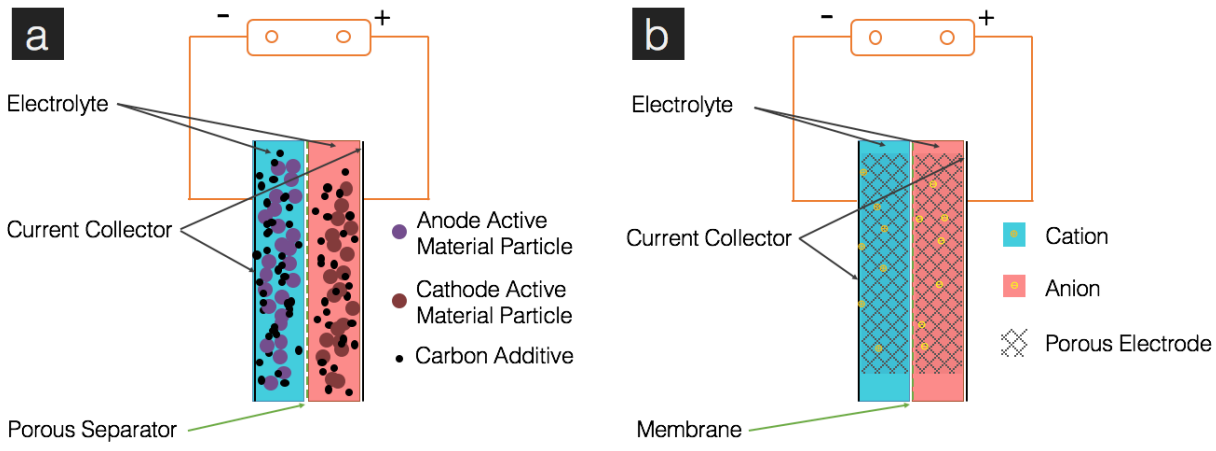

Figure 1. Schematic illustration of (a) a Li-ion battery and (b) a supercapacitor.

The electrical energy stored in batteries is primarily stored as chemical energy that is released by redox reactions, as opposed to within a surface double layer. Thus, a

straightforward approach to increase the cell capacity is to increase the amount of active material within the electrodes, either by increasing the relative fraction of active material within the electrodes or by increasing the electrode thickness. Unfortunately, this strategy only works within a limited range, because mass transfer resistance of the ions that must traverse through the electrodes will become limiting and the power output and current densities that the cell can operate at will become severely impaired.[48, 49] Some researchers have attempted to overcome the ion transport power limitations in the electrode by flowing the electrolyte through the electrode, which is different from a RFB since there is no active material being flowed through the system – only the electrolyte. One example was a convection battery proposed by Suppes *et al*., in which flowing electrolyte was used to facilitate ion transfer and reduce ionic resistance, resulting in a five-fold increase in achievable current densities; however, there were some performance limitations reported due to the separator and the operating efficiency after accounting for the pumping energy is unknown.[50-52]

One general challenge of using static batteries and static active material electrodes for stationary applications is that many smaller batteries must be connected in various combinations of parallel and series configurations to reach a final desired current and voltage output. The arrangement of many smaller batteries into a battery pack results in high costs due to the additional auxiliary parts, the need for a battery management system to safely and efficiently utilize all those cells, and typically the need for a heat removal system which also adds significant additional weight.[53-56] One promising approach to improve current density and also simplify battery system design and upgrades by

decoupling the power and energy units in the cell is a RFB, which will be discussed below.

1.2.2. Redox Flow Batteries

As shown in Figure 2, a typical RFB consists of the following main components: power output cells – electrochemical cells with porous electrodes separated by ion-selective ionically conducting membranes; energy storage tanks – these tanks contain electrolyte comprised of the desired amount of dissolved redox species as well as soluble ions that transport across the membrane; and a pumping system to connect the power output cells to the energy storage tanks.[57, 58] For the most common RFBs, the electroactive redox species are transition metal ions that have been dissolved in acidic aqueous electrolytes. During battery operation, the electrolytes are pumped through the electrochemical reaction cells to either oxidize or reduce the electroactive transition metal depending on which direction the current is flowing (charge or discharge) and which electrode the species is coming into contact with (anode or cathode). Note that in RFBs the electrolyte fed to the cathode is referred to as the catholyte, while the electrolyte fed to the anode is referred to as the anolyte. Reactions occur only on the surface of the porous electrodes in the reaction channel, which are typically comprised of porous carbon materials. The electrolytes are circled back to the original electrolyte energy storage tanks after exiting the electrochemical cell to mix with the remaining electrolyte solution while new electrolyte material is fed from the tank back to the electrochemical cell. In this system, total battery capacity is limited by the volume of electrolyte within the electrolyte energy storage tanks, which is dependent on the tank size and electroactive material

concentration. The power of the RFB, however, is limited by the performance and total number of electrochemical cells in the system.[57, 58] As an example, all-vanadium RFB, the most successful RFB for large scale applications, involves four different oxidation states of vanadium ions forming two redox couples dissolved in highly acidic electrolyte. VO_2^+ and VO^{2+} are dissolved in the catholyte and V^{3+} and V^{2+} in the anolyte.[14, 57-59] The active species are the same chemical element, vanadium, on both sides of the cell. Issues limiting all-vanadium RFB include corrosion in the cell and limiting operating conditions to suppress gas evolution which results in low material utilization.[59] The crossover of active materials through the membrane, which is a major issue for RFBs with two different active material elements, is less of a concern for all-vanadium RFB because the cell can be rebalanced by redistributing anolyte/catholyte as opposed to requiring complete electrolyte replacement and reprocessing. This advantage is also shared by all-iron RFBs in which Fe^{3+}/Fe^{2+} and Fe^{2+}/Fe serve as redox couples in catholyte and anolyte, respectively.[60]

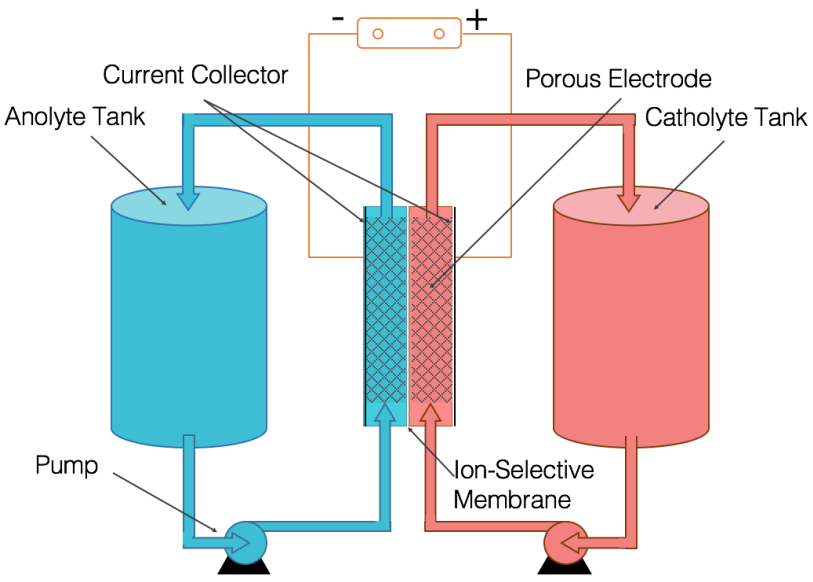

Figure 2. Schematic illustration of a redox flow battery.

The typical range of discharge current densities for RFBs based on dissolved transition metal species is between 20-80 mA cm^{-2}, though even higher current densities have been reported.[14, 58, 61, 62] RFB systems are highly modular, providing the flexibility to independently design the power output by changing the design and number of electrochemical reaction cells; and to modify the total battery energy by optimizing the size and/or number of the storage tanks. This decoupling of power and energy is particularly advantageous in large scale energy storage applications because of the flexibility and potentially low cost.[14] Many kW and MW scale RFB installations have been completed.[17] For example, two 500 kW/6-hour Zinc-Bromine RFBs were built in Massachusetts to lower peak energy demand and reduce the impact of power interruptions in 2016.[17, 63] One of these RFBs is accompanied by a 605 kW photovoltaic array and the other with a 600 kW wind turbine to demonstrate the concept of integrating an intermittent power source with a scalable and large scale electrochemical energy storage platform. As another example, a 5 MW Vanadium RFB was installed in China supporting 10% of a 50 MW wind farm.[17, 64] A few recent reviews provide good discussions on conventional RFBs.[14, 19, 22, 59, 65-67]

Efforts to improve the performance of RFBs for next generation concepts have largely been focused on improving RFB energy density. RFB energy density is determined by the energy density of the electrolytes, which is relatively low compared to other battery technologies.[59, 65, 68] Commercial systems such as vanadium RFBs have reported energy densities on the order of 25 Wh L^{-1},[59, 68] which is low in comparison to for example Li-ion technologies which range from 70 to 220 Wh kg^{-1} (100-450 Wh L^{-1}), or

even lead-acid (Pb-acid) batteries which have 25-50 Wh kg^{-1} (60-100 Wh L^{-1}).[65] The lower the energy density, the greater the size of the storage tank needed to meet a specific energy requirement. The tank footprint is not necessarily an issue in stationary energy storage, but it makes it challenging for RFBs to penetrate other applications such as transportation and even within stationary storage applications the footprint is particularly important where space involves a cost and access premium such as in urban environments. Equipment size also influences the overall shipping and installation cost of the system. Therefore, energy density is a key metric for RFBs that research groups have aimed to improve.

The root causes of the relatively low energy density for conventional RFBs are: 1) limited cell voltages due to the narrow electrolyte stability window and 2) low volumetric capacity due to solubility limits of the redox compounds.[57, 58] The electrolyte stability window is limited because the solvent for conventional RFBs is water, and the thermodynamic stability range for water is ~1.23 V (with the location of the upper and lower potentials highly dependent on the composition and concentration of the various solutes and additives).[69] To increase RFB operating voltages, much work has been and continues to be done to replace water with organic solvents with larger stability windows, and then to explore new redox compounds that are soluble and stable within organic electrolytes. Organic electrolytes provide a wider stability window to increase net cell voltage, and many new active materials and electrolytes have been reported.[67, 70-72] The cost and flammability of organic RFB systems are significant considerations; however, the possibility to increase the voltage and subsequently the performance of

these RFBs has driven significant interest. Most of the organic RFB reports have achieved at or above 2 V cells, though at this stage ionic conductivity limits the current densities to well below aqueous systems.[22, 73] The voltage has even been reported as high as ~3.5 V when paired with a Li metal anode.[65, 74] There have also been efforts to construct hybrid organic-aqueous RFBs to take advantage of the low potential achievable at the anode due to the organic electrolyte and suitable potential and high ionic conductivity offered by the aqueous electrolyte on the cathode side.[75] More comprehensive discussions on organic and/or Li-based RFBs can be found in these recent reviews.[19, 22, 65, 67, 76]

The second limitation, electroactive material solubility, is a challenge for both aqueous and organic RFBs. The higher the concentration of redox compounds in the electrolyte, the greater the number of electrons that can be exchanged for a given volume or mass of electrolyte and hence the higher the capacity and energy density of the RFB. Unfortunately, above the solubility limit for the electrolyte the redox compounds precipitate out as inactive solid particles, and thus the solubility limit provides one limitation on the cell energy density. Extensive research has been done to develop electrolytes with high solubility of active materials. For example, a number of reports demonstrated active material concentrations greater than 1 M for both aqueous and nonaqueous RFBs,[77-82] and even greater concentrations of over 5 M for the active material concentrations have been reported.[83-85] In addition, as the concentration of the redox compounds increases, and in particular if solid particles start to form, the viscosity of the electrolyte increases and the parasitic energy lost to pumping increases, in

some cases dramatically.[25, 86] Approaches have been developed for innovative solution preparations and solution chemistry, including the use of ionic liquids; however, significant increases in energy density and/or keeping viscosities reasonable is still a challenge.[22, 25, 87-89] One increasingly popular approach is to start with insoluble solid particles as the electroactive materials that participate in the redox reactions. By starting with electroactive solid particles solubility limitations are no longer a relevant barrier, though the trade-off between particle loading and electrolyte viscosity is still a consideration. This strategy of starting with solid electroactive particles in a RFB can be applied with both aqueous and organic electrolytes.

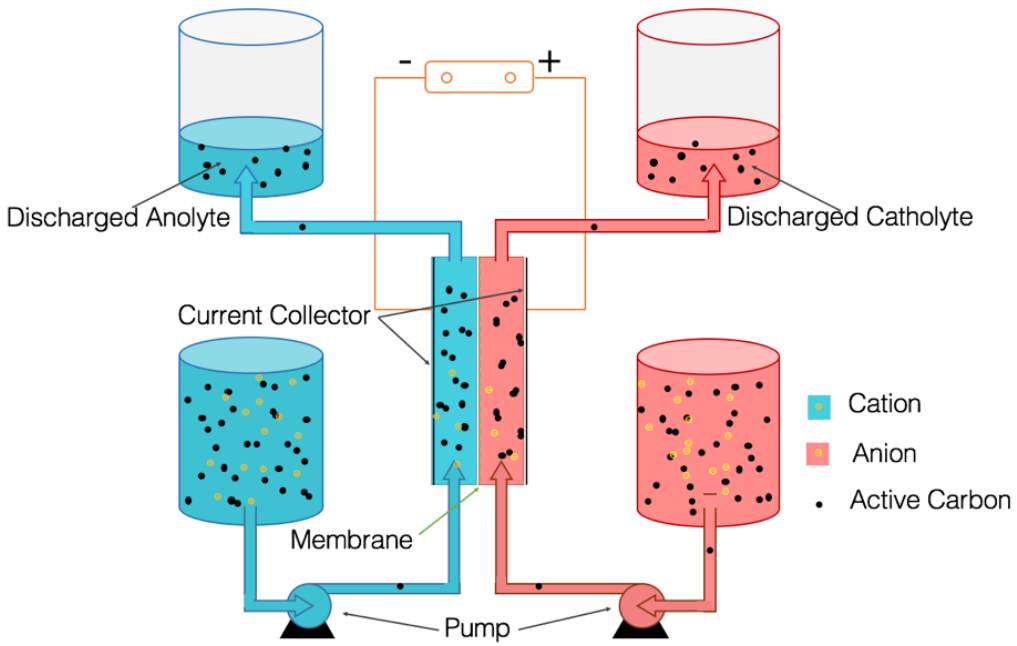

Figure 3. Schematic illustration of an electroactive flow capacitor undergoing cell discharge.

1.2.3. Solid Suspensions for Capacitive and Electrochemical Application

Solid suspensions are composed of nano- or micrometer sized solid particles dispersed within a continuous liquid phase. Solid suspensions have found a broad range of applications, and common design elements include the chemistry of the particles and/or liquid, solid particle size and morphology, particle surface chemistry, particle concentration and aggregate formation, and suspension rheological properties.[42, 90-97] For example, thermal conductivity can be dramatically modified with changes in particle concentration within a suspension, and thus solid dispersions have been popular for thermal storage and transfer applications.[93] Similarly, electrical conductivity of suspensions can also be manipulated by appropriate suspension design, which has particular relevance to electrochemical applications.[98]

One application of solid suspensions with active material dispersed within an electrolyte is flowing supercapacitors. As mentioned in Chapter 1.2.1, supercapacitors store electric charge in the form of electric double layers on the surfaces of electrodes. An electrochemical flow capacitor (EFC) combines aspects of both RFBs and supercapacitors (shown in Figure 3). Carbon suspensions, with the electrode surface being the surface area of the particulates within the suspension, are dispersed in storage tanks.[42, 90-92] Similar to conventional supercapacitors, cations and anions migrate to carbon surfaces at two opposite electrodes under applied potentials during the charging step. Instead of using static and limited carbon materials as in a conventional supercapacitor, in an EFC the charged carbon is pumped to storage tanks while fresh uncharged carbon materials are pumped to the electrochemical cell to accept more ions.

The discharge process is similar to the charge step with continuous carbon suspension supplied from storage tanks until the ions migrate to depletion from the carbon surfaces. The tank size is a parameter that can be changed to tune the total device capacity.[90] While EFCs in principle expand potential applications for supercapacitors, there are still challenges including low energy density and fast self-discharge. Research efforts have pursued new materials, flow cell designs, surface modification, and mathematical modelling.[42, 44, 92, 99-102] More detailed discussion on the current status and research perspectives for supercapacitors and EFCs can be found in these recent reviews.[29, 40, 45, 46, 103, 104]

Capacitive water deionization is another application where solid suspensions have been coupled into a system with electrodes and electrical potential driving forces.[104-107] In a conventional capacitive deionization system, a potential is applied between the two electrodes which forms electric double layers and drives ions toward the two electrode surfaces (shown in Figure 4a). Cations and anions are aggregated around the anode and cathode surfaces, respectively, which are both typically high surface area carbon materials.[108] As a result, relatively deionized water exits the cell. In a conventional capacitive water deionization system, the device needs to be periodically stopped and regenerated when it reaches its maximum capacitance. This intermittent operation limits the productivity and causes extra energy consumption during the regeneration procedure.[106] Solid carbon dispersions have also been applied to capacitive deionization applications (see Figure 4b). Once flowing carbon electrodes are integrated into the system, the device can run continuously with high capacity because the active

carbon can be regenerated without interfering with the deionization process by simply mixing the two carbon suspensions, filtering the carbon suspensions to separate the liquid with concentrated ions, and reinjecting the carbon into the fresh water flow.[106, 109, 110] The system can be adjusted to fit particular working loads by changing channel size and/or flow rate. More details and discussions on capacitive water deionization and electrochemical flow electrodes can be found in recent reviews.[104, 106, 108, 111-113]

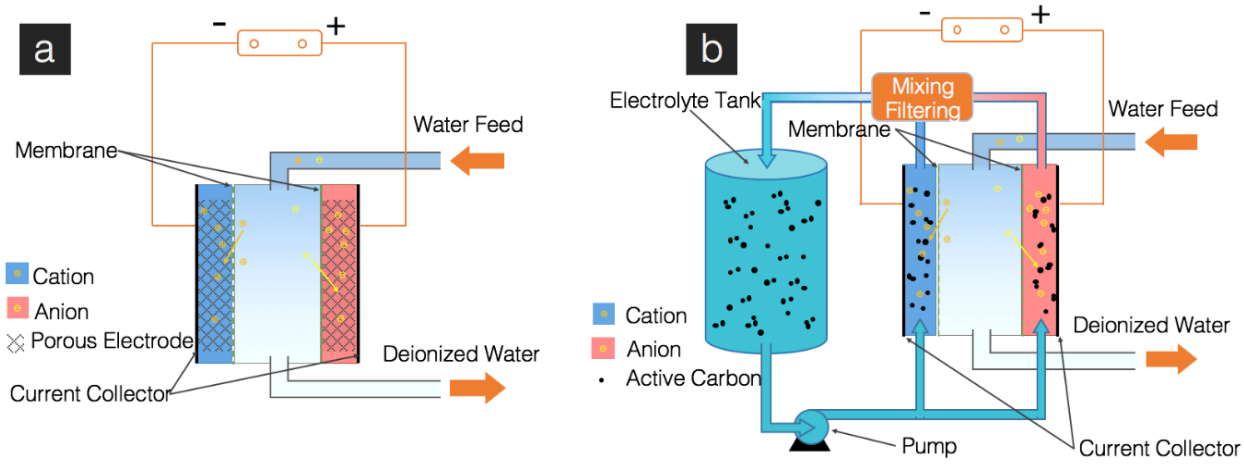

Figure 4. Schematic illustration of (a) a conventional capacitive water deionization device and (b) a flowing capacitive water deionization device.

Research on electrochemical flow capacitors and water capacitive deionization has demonstrated the applicability of solid suspensions for capacitive and electrochemical devices. Recently, progress has also been made in using solid suspensions in RFBs – where the move to solid particles provides a route to increase the battery energy density by overcoming the solubility limitation of active species. Many other considerations will be important for these new types of RFBs beyond electrolyte energy density, including

but not limited to operating efficiency, cost, safety, and reliability.[22, 114] The operating efficiency is hindered by the pressure drop of the flowing liquid. Depending on the cell design, the pressure drop could be due to pumping liquid through a porous and tortuous electrode and/or due to high viscosity of the carrier fluid. In either case significant energy is needed to keep the fluid moving and overcome the pressure drop. Efforts to address this challenge will be discussed in more detail in the following chapters. The cost of RFBs includes material cost, equipment cost, transport cost, maintenance cost, etc., and is an important factor to commercialization. A number of researchers are analyzing the cost metrics related to RFBs.[18, 26, 115-117] For example, ion-selective membranes are one of the primary contributors to material costs,[116] and hence research has been reported towards membrane-free RFBs.[118, 119] Addressing safety concerns is very important and necessary for wide scale adoption. Conventional RFBs use transition metals as active species, which in some cases can be expensive and/or have environmental concerns. Thus, research has pursued RFBs with abundant and non-toxic active materials.[18, 67, 77, 80, 120] For example, Lin *et al*. proposed an alkaline quinone RFB without transitional metals.[77] In addition, reliability and equipment life are also important for a long-term stationary battery application and have these topics have been addressed by many researchers as well.[18, 70, 121]

1.3. System Designs

Due to the complexity of dealing with the two-phase system of a suspension, RFBs with solid electroactive materials have had a number of different innovative engineering designs to enable their characterization and operation. These designs can be segmented into four main types dependent on the flowing conditions used and the role of carbon in the electrolyte. The mode of flowing the material through the system is a very important consideration for these systems, in particular because the viscosities in some cases become very high at increased particle loading. Carbon, with its relatively high electronic conductivity and low density, is a key component in many electrochemical devices and plays various roles in the RFBs described below.[91, 122-124] The designs for RFBs with solid electroactive dispersions are categorized as follows: Type I – flowing carbon as the electrochemical reaction electrodes, Type II – flowing solid active materials within a carbon conducting network, Type III – flowing active material particles colliding on current collectors without carbon, and Type IV – soluble redox mediators for power with solid active materials within tanks for energy. Each one of these systems is suited to different materials and has different advantages and disadvantages. The system designs will first be described in greater detail before more detailed discussion of the relevant chemistry.

1.3.1. Type I: Flowing Carbon as Electrochemical Reaction Electrodes

Carbon is a common electrode material in conventional RFBs, for example in the form of activated carbon foams, glassy carbon sheets, and carbon fiber cloth.[122] Porous carbon is preferred in order to increase the total surface area, which increases the net rate of

electrochemical reactions achievable per projected area of the electrochemical cell with the same cell volume. Thus, higher surface area porous electrodes result in higher area specific current density and increased total current and power from the RFB power module. Design of the porous electrodes must also take into consideration the pressure-drop of the electrolyte being forced through the electrode, which is relatively high and requires significant pumping power. For a solid electroactive material RFB Type I design, one way to conceptualize this type of device is that the porous carbon electrode of a conventional RFB has been broken apart into micro/nano-sized carbon particles flowing while dispersed in the energy-containing electrolyte. There would result in significantly less pressure-drop across the electrochemical reaction cells (the current collectors would be planar instead of porous carbon). As illustrated in Figure 5a, these flowing carbon particles form percolated aggregates and electrochemical reactions occur on the surface of carbon materials while in contact with the current collector – either directly or through particle-particle connections to the current collector surface. This type of design has been demonstrated for multiple battery systems including lithium-polysulfide (Li-PS),[125, 126] lithium-air (O_2), [127] and metal ions in aqueous solvents.[60, 68]

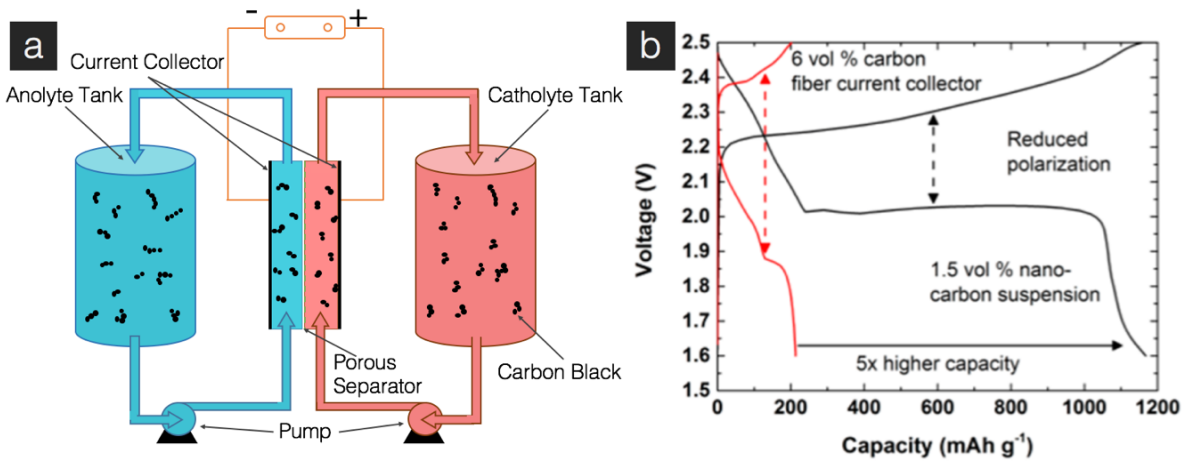

Figure 5. (a) Schematic illustration of a Type I design; (b) second galvanostatic charge/discharge cycle for 2.5 mol_{Sulfur} L^{-1} solutions with 6 vol% carbon fiber current collector (red) and 1.5 vol% nano-carbon suspension (black) at a current rate of C/4 [(b) reprinted with permission from F. Y. Fan, W. H. Woodford, Z. Li, N. Baram, K. C. Smith, A. Helal, G. H. McKinley, W. C. Carter, and Y. M. Chiang, Nano Lett, 14 (4), 2210-2218 (2014). Copyright 2014 American Chemical Society].

One example of a Type I design was a Li-PS half-cell system reported by Fan *et al.*, where nanocarbon material was dispersed within a Li-PS electrolyte before pumping through an electrochemical reaction cell.[125] The counter electrode was Li metal and a microporous separator film was adopted to separate the catholyte and the Li metal, with $LiNO_3$ added to the electrolyte to passivate the Li surface.[118, 119, 125, 128] In a conventional RFB design with Li-PS and a porous carbon electrode, the Li-PS electrochemical reaction window was limited to the range including only the soluble species between Li_2S_8 and Li_2S_4 and did not proceed to insoluble species such as elemental sulfur or Li_2S, restricting the total achievable capacity and energy in the

cell.[119, 128] However, with the flowing nanocarbon dispersed in the electrolyte, the electrochemical reaction window was expanded to include the solid species, which increased the energy density of the electrolyte significantly. The precipitation of the solid sulfur species onto the nanocarbon surfaces within the dispersion did not impact the flow of the catholyte and kept the solid species confined within the already solid and electronically conductive particles dispersed in the electrolyte. As shown in Figure 5b (adapted from Fan *et al*.[125]), four- to five-fold higher reversible capacity was achieved for the dispersed nanocarbon system over the conventional static porous carbon electrode.[125] In this design, the overpotential was also lower than conventional electrodes because the charge transfer resistance was lower even at a lower loading of carbon (1.5 vol% nanocarbon suspension over 6 vol% stationary carbon fiber within the electrochemical cell channel). This reduced resistance was attributed to the unique size and surface chemistry of the carbon nanoparticles compared to the micro-sized porous carbon fiber. The overall pumping cost was estimated to be lower for the dispersed nanocarbon relative to the conventional porous electrode because of the much lower pressure drop for the fluid flowing through the channel in the absence of the tortuous carbon fiber, though the viscosity of the catholyte with the carbon dispersion was higher than the carbon-free catholyte.

In this particular case, the addition of solid electrically conducting particles facilitated more complete oxidation and reduction using Li-PS chemistry due to the ability to go all the way to the solid products efficiently. This enabled higher total energy density in the electrolyte. For the Type I system, the added particles to the electrolyte are not

themselves the electroactive material undergoing redox chemistry, but rather facilitate and improve the rate or utilization of the redox chemistry that occurs within the electrolyte. The next type of RFB with particles dispersed in the electrolyte will involve the addition of electrochemically active particles that undergo redox reactions in the electrolyte.

1.3.2. Type II: Flowing Solid Active Materials with Flowing Carbon Conducting Network

In the Type I design, the carbon or other conductive additive needs to be small (nano-size) to provide a large surface area for electrochemical reactions with a relatively low loading of particles into the electrolyte. In contrast, the Type II design does not have electrochemical reactions occur on the carbon particles, and in this case the carbon functions as the conducting network for electrons between the electroactive solid particles and the current collector. In a Type II architecture shown in Figure 6a, both the active material particles and carbon additives are dispersed in the liquid electrolyte before flowing into the electrochemical reaction cells. This has previously been referred to as a semi-solid flow cell (SSFC), as proposed by Duduta *et al.*[27] This design has been exploited for Li-ion active materials as well as sodium-ion (Na-ion) materials in both organic and aqueous fluids,[76, 129-133] and some material choices will be discussed in more detail in later sections. The Type I design is suitable for soluble or liquid electrochemically active materials, including those that form solid deposits such as Li-PS, while the Type II design is desirable for systems where the electroactive material is always in the solid phase as particles dispersed in the electrolyte.

In Duduta *et al*.'s demonstration of the SSFC, half-cells were demonstrated with Li-ion active materials in the slurry dispersion vs. a Li metal anode, and also a full cell with both a slurry anode and a slurry cathode was reported.[27] The electrochemical charge and discharge was completed using both continuous and intermittent flow modes.[27] The cathode active material used was LCO which was dispersed into a suspension of 22.4 vol% LCO with 0.7 vol% Ketjen Black (KB) carbon conductive additive, with the balance of the dispersion being organic Li-ion electrolyte. During the continuous flow mode experiments the slurry had 127 mAh g^{-1}_{LCO} reversible capacity; however, there was significant energy lost to pumping under continuous flow mode due to the high viscosity of the dispersion. The pumping power dissipation was calculated to be 44.6% of the total discharge power at a flow rate of 15 mL min^{-1}. To optimize the operating efficiency, an intermittent flow mode was also demonstrated which reduced the reported average pumping requirements down to 0.6% of the discharge power. During intermittent flow mode, the process includes 1) pumping the suspension into the electrochemical cell, 2) fully charging and/or discharging the materials in the cell, and 3) pumping the suspensions out of the cell and replacing with fresh electrode materials for the next charge/discharge. The pumps only run intermittently to save pumping energy and hence increase the operating efficiency. As shown in Figure 6b (adapted from Duduta *et al*.[27]), a full cell under intermittent mode was demonstrated with 20 vol% LCO and 1.5 vol% KB suspension as the catholyte and 10 vol% $Li_4Ti_5O_{12}$ (LTO) with 2 vol% KB suspension as the anolyte, and both suspensions contained the same organic Li-ion electrolyte for the balance of the volume.[27] Although the coulombic efficiencies of the first two iterations for the intermittent flow (73% and 80%) were lower than the first two

charge/discharge cycles of static suspensions (98% and 88%), there are many possible optimization opportunities, for example, the channel geometry and flow rate. The company 24M was originally founded based on this technology, though the company subsequently pivoted towards using the slurries for static semi-solid batteries due to more favorable results from economic projections.[134]

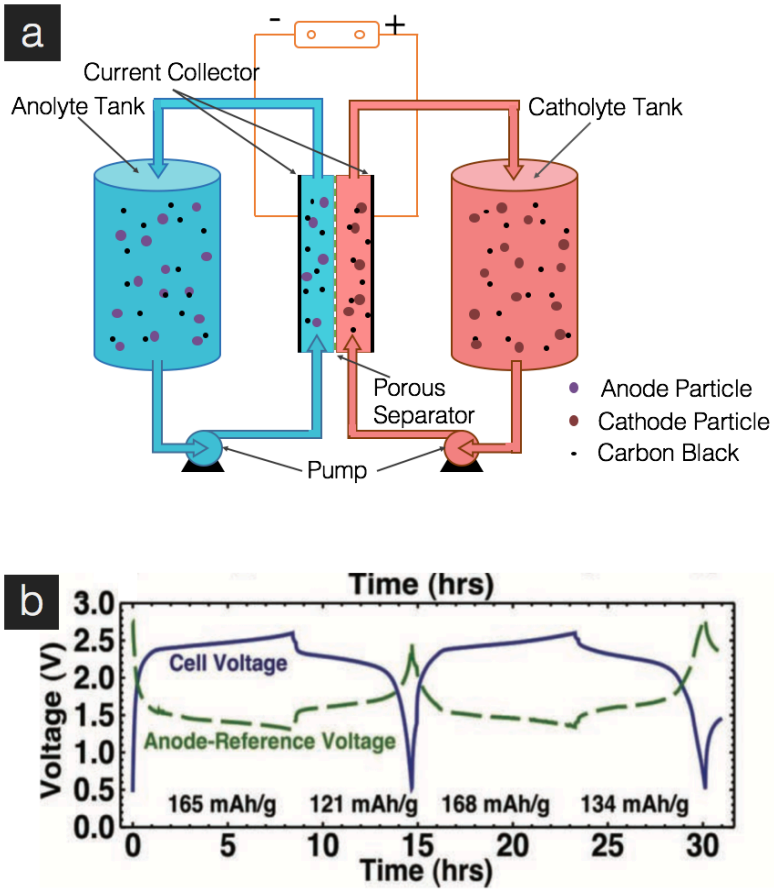

Figure 6. (a) Schematic illustration of a Type II design; (b) two iterations of injection and galvanostatic cycling for a cell of 20 vol% LCO and 1.5 vol% KB as the catholyte and 10 vol% LTO and 2 vol% KB as the anolyte using intermittent flow [(b) reprinted with permission from M. Duduta, B. Ho, V. C. Wood, P. Limthongkul, V. E. Brunini, W. C.

Carter, and Y. M. Chiang, Adv. Energy Mater., 1 (4), 511-516 (2011). Copyright 2011 John Wiley and Sons].

The main advantage of this Type II design is unlocking the opportunity to use solid active materials with high energy density in RFBs, in this case Li-ion battery active materials. Moving to solid active materials overcomes the solubility limitation on capacity per volume of conventional RFBs, and the use of Li-ion materials and organic electrolytes expands the possible voltage range to that of Li-ion batteries, which reaches >4 V for existing commercial systems and is even higher for next-generation materials.[135-137] For the system reported by Duduta et al., an optimized system with Li intercalation active materials is expected to achieve a theoretical energy density of 300-500 Wh L^{-1}, compared with a theoretical value of 40 Wh L^{-1} for a 2M aqueous vanadium RFB.[27] The Type II design can be further adapted to many other battery materials with high energy densities. Another attractive feature of this system is that the solid active materials and conductive carbon within the two slurries can be kept within separate channels by size exclusion. In principle this enables the use of porous separators, which are generally less expensive and when paired with liquid electrolytes have higher ionic conductivities than ion-conducting polymeric or solid-state membranes. There are also a few challenges for researchers with this system. The first major drawback is the pumping energy loss due to the high viscosity. For example, the viscosity reported for the slurries used by Duduta *et al*. were greater than 2 Pa·s at a shear rate of 10 s^{-1}. The viscosities need to be reduced to lower the pumping energy, which results in net improvements in the total energy efficiency. Pumping high viscosity slurries also requires larger duty and more complex or

expensive pumps. Using intermittent flow mode was one approach described above aimed at minimizing pumping losses, but there are challenges with this mode of operation, which will be discussed in more detail in following chapters. Another challenge is that not all of the active material particles are in sufficient contact with the conductive carbon network in this mechanically mixed suspension, and as a consequence there are losses in capacity utilization and coulombic efficiency.[126] Different carbon architectures have been reported to impact the electrochemical performance, thus carbon morphology and loading must be carefully controlled as well as the aggregation of the carbon particles.[125, 138, 139] Coatings on the carbon particles and suspension additives may provide opportunities to reduce suspension viscosity and/or reduce the total amount of carbon that must be dispersed in the slurry.[140-143] In addition, there is a tradeoff between the power density and the coulombic efficiency depending on the slurry conductivity. A high conductivity is needed to provide high power density with reasonable overpotential; however, shunt currents will be much more significant with a highly conductive carbon network, resulting a loss of coulombic efficiency for a system with cells in series.[121, 144-146] This conductivity tradeoff will be a more significant challenge for any flow battery with a conductive material network (e.g.; Types I and II). Exploration of flow profile control within the channel and the balance between active material and carbon material morphology and loading to improve the performance and efficiency of Type II systems could lead to major improvements for these relatively unusual battery cells.

1.3.3. Type III: Flowing Active Material Particles Colliding on Current Collectors without Carbon

The addition of carbon to the electrolyte results in a percolated network which has a significant impact on the suspension viscosity. For example, in the Type II SSFC system described earlier with 22.4 vol% LCO suspension, the addition of only 0.6 vol% carbon additive resulted in a >10-fold increase in the viscosity.[27] Therefore, eliminating carbon from the electrolyte in principle provides a route to significantly reduce pumping requirements while maintaining the high energy density that results from using high energy density materials and solid electroactive particles. The removal of carbon from the system results in the Type III system (schematic in Figure 7), which has two key features that differentiate it from the Type II system. First, due to the lack of carbon or other conductive additives, the Type III system has reduced viscosity while still relying on solid electroactive particles for redox reactions. The lack of carbon also reduces the mass and volume of components in the electrolyte that do not contribute to the cell energy density. Second, without the percolating network the electrochemical reaction no longer occurs throughout the cell channel facilitated by the electronic conductivity of the carbon, and thus only particles in contact with the current collector (directly or indirectly through other particles in for example a particle aggregate) participate in electrochemical reactions at any given time. In operation, Type III systems rely on the collisions of active material particles with the current collector and have very low electrochemical activity in the absence of flow.[147, 148] This Type III design is the focus of this thesis and will be discussed in further details in following chapters.

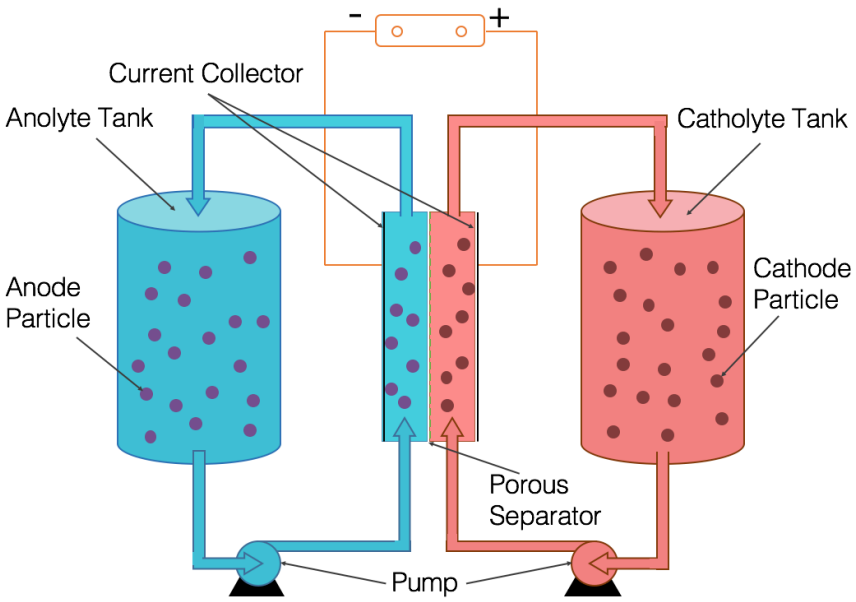

Figure 7. Schematic illustration of a Type III design.

In addition to research on battery geometry design and analysis, studies of battery material particles in isolation can also provide insights to understand and improve the performance of Type III batteries.[149, 150] Over the last two decades, a number of researchers have more generally explored particle collisions on electrode interfaces for a number of different systems and applications.[151] These studies can largely be divided into three groups of activities: 1) inert particles colliding with an electrode that block electrochemical reactions, 2) electrocatalytic particles that facilitate electrochemical reactions only during collisions with an electrode, and 3) direct oxidation/reduction of electrochemically active particles that only occurs upon collision with the electrode. In the first case, inert and electrically insulating particles partially block electrochemical reactions on the surface of the electrochemically active electrode upon collision, creating transient current changes by reducing the active area of the electrode (and in some cases

the adsorption was permanent).[152-154] In the second scenario, electrocatalytic particles are suspended in the electrolyte and only facilitate electrochemical reactions when a sufficient potential driving force is available, which is only provided when Brownian motion causes the particles to collide with the electrode surface resulting in a collision-dependent current response.[155, 156] For this electrocatalytic system, research has been performed to specifically understand the impact of surface chemistry,[157, 158] electrode size,[158] electrode material, and mass transfer effects.[159] One study of similar phenomena reported measurements of single particle collisions for a photovoltaic system that took advantage of semiconducting nanoparticle collisions to interpret spikes of photoelectrochemical current as individual particle events.[160] For the third case of direct oxidation/reduction of nanoparticles, the particles are electrochemically active for oxidation or reduction upon collision with the otherwise inert electrodes.[152] The measured current was quantitatively correlated to particle size, providing the capability to extract particle size information from electrochemical measurements.[161-164] More detailed discussions on the background and developments related to particle collisions on electrodes can be found in these recent reviews.[151, 161]

1.3.4. Type IV: Targeted Redox Mediators as the Power Carriers with Static Solid Active Materials Providing Energy Storage

RFBs are known for decoupling of the energy storage and power output components, providing the flexibility for customized designs for different applications.[57, 58] In a typical RFB design and all designs introduced above, the energy storage is provided by redox-active materials which are flowing through the electrochemical reaction cell for the

storage or delivery of power. The function of energy storage and power delivery is provided by the same materials, and thus even though the energy and power components are decoupled, the performance of the electrochemical cell is still coupled with the properties and state of the energy storage fluid. Early in 2006, Wang *et al*. proposed the concept of using targeted redox shuttles to improve the electrochemical performance of poorly conducting Li-ion battery materials to potentially eliminate the use of carbon additives.[165] Soluble redox mediators were introduced into the electrolyte within the cell that underwent electrochemical reactions and then the lithiation/delithiation of Li-ion active materials proceeded via chemical reduction/oxidation by the mediators.[165] Therefore, the energy storage and power output for the cell were provided by two different sets of materials; the energy storage was provided by the solid active material while the dissolved mediators actually underwent the electrochemical reactions during power delivery or charging. Integrating this concept with RFBs enabled further increases in capacity and flexibility. Wang's group proposed a design with flowing dissolved redox mediators to provide power output and static high energy density solid materials in separate tanks for energy storage.[24, 166-168] As shown in Figure 8a, solid active materials are stored in the energy tanks and only the dissolved mediators undergo electrochemical reactions in the flow channel. For example, after being discharged in the electrochemical reaction cell, the mediators get "recharged" through chemical redox reactions with the solid energy storage materials in the tanks until the solid materials have been fully chemically discharged. The charging process is then run in reverse. This design has been applied mainly to Li-ion active materials.[24, 165-167, 169, 170]

In Jia *et al.*'s report of a full cell demonstration, $LiFePO_4$ (LFP) and TiO_2 were used as the cathode and anode solid energy storage materials, respectively.[24, 166, 167] Two pairs of redox mediators were used, dibromoferrocene ($FcBr_2$) and ferrocene (Fc) for the catholyte, and cobaltocene [$Co(Cp)_2$] and bis(pentamethylcyclopentadienyl)cobalt [$Co(Cp^*)_2$] for the anolyte. A fully charged cathode includes static $FePO_4$ in the cathodic tank and dissolved $FcBr_2^+$ and Fc^+ flowing through the reaction channel and energy storage tank. As shown in Figure 8b (adapted from Jia *et al*.[24]), the $FcBr_2$ redox potential is above LFP and Fc is below LFP. When the cell is being discharged, $FcBr_2^+$ will be first reduced to $FcBr_2$. Then the only species participating electrochemically in the flowing liquid in the electrochemical reaction cell is Fc^+, which will be reduced to Fc thereafter. Fc will then be oxidized back to Fc^+ by $FePO_4$ through chemical oxidation when it comes into contact with the surface of the solid $FePO_4$ particles in the tank. This process continues until all $FePO_4$ is reduced to LFP. The residual Fc^+ continues to be reduced to Fc until depletion and the cell was then considered fully discharged. Corresponding reactions occur on the anode side and collectively the full cell is discharged in the order of Reaction (1) – (6) (reactions in Figure 8b). The charging process proceeds in the reverse sequence from reactions (6) to (1). Galvanostatic cycling at different current densities were demonstrated and are shown in Figure 8c (adapted from Jia *et al*.[24]). The discharge curves showed three plateau regions, with the highest potential plateau corresponding to reaction (1) and progressively the lowest attributed to reaction (5). This promising demonstration provides the opportunity to further increase the capacity and energy density by storing more static LFP/TiO_2 materials in the tanks. Increases in energy density by adding more solid particles to the tank does not change the

electrolyte viscosity as it would in Type II and III systems. Therefore, this design has a high theoretical energy density, ~500 Wh L^{-1} for TiO_2/LFP assuming 50% porosity is practically achievable.[24] The amount of redox shuttles in this system is in principle much less than that required for other system designs, and would result in significant volume reductions relative to an organic RFB that did not contain solid active material particles. This reduction in the amount of redox shuttles and electrolyte required provides a possibility for cost reductions. There are also safety advantages provided by the reduction in volume of flammable electrolyte required. In addition, the pumping energy loss is expected to be low because only low concentration mediator solutions with relatively low viscosities need to be circulated.

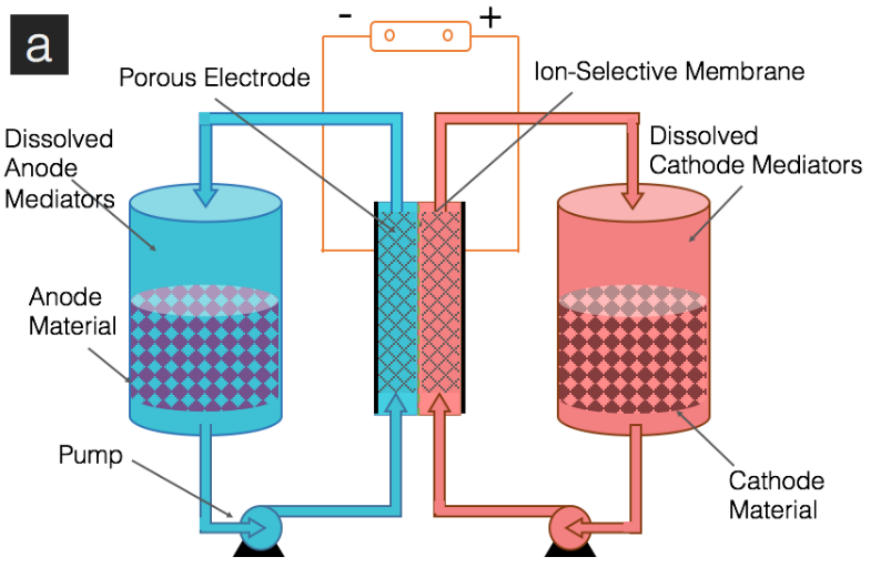

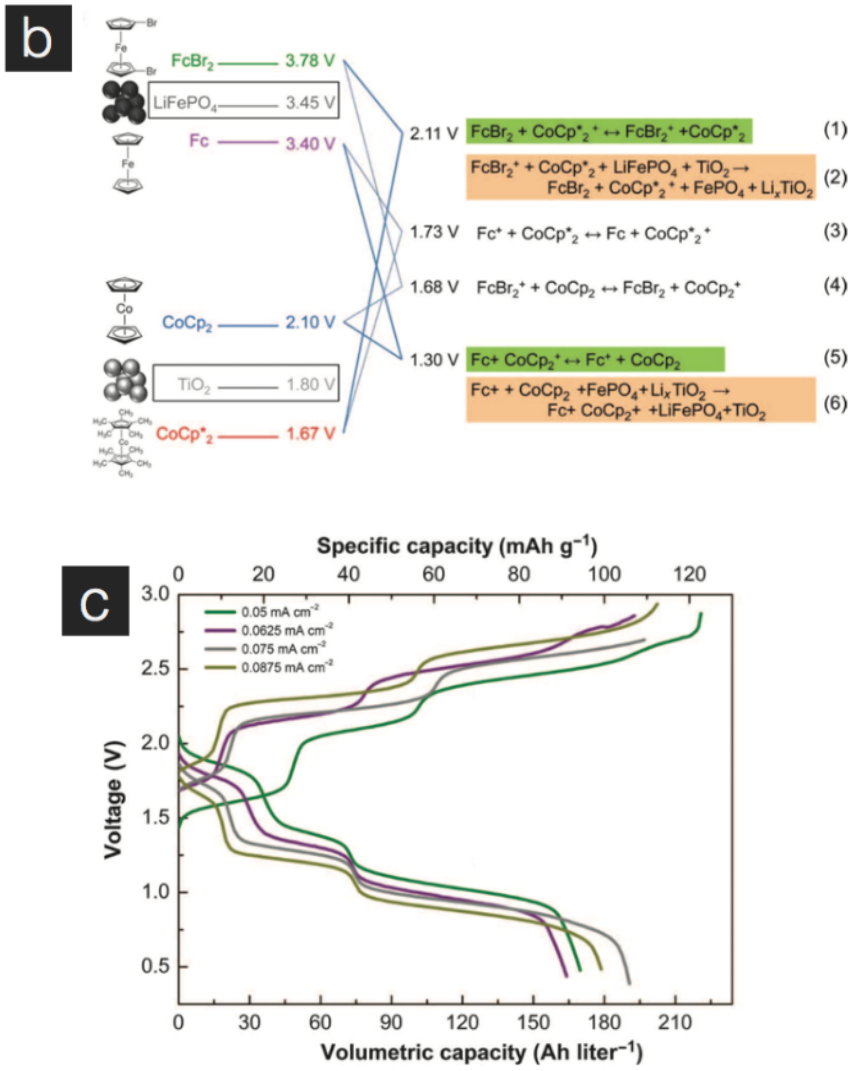

Figure 8. Schematic illustration of (a) a Type IV design. (b) The chemical and electrochemical reactions of the mediators and solid materials in the tank and (c) typical charge and discharge profiles of the cell at different current densities [(b) and (c) reprinted with permission from C. Jia, F. Pan, Y. G. Zhu, Q. Huang, and Q. Wang, Sci Adv, 1 (10), e1500886 (2015). Copyright 2015 American Association for the Advancement of Science].

However, the Type IV system still has some opportunities for innovation. At high loadings of solids in the energy storage tanks which are desired to increase system energy density, the pressure drop arising from the particle bed is likely to be high. The pressure drop associated with the active material packed in the tank may even exceed the pressure drop from passing through porous carbon in the flow channel, which is also present in this design incorporating mediator redox couples. To overcome this challenge, the particle bed would need to be designed to minimize the pressure drop, possibly at the expense of other metrics such as active material loading. A second challenge comes from the separator. The size-exclusion benefit of solid active materials in Types II and III is not applicable in this design because the redox active mediators are dissolved in the electrolyte and must be kept segregated via a more resistive membrane or thin film. Therefore, Li-ion conductive membranes compatible with organic solvents are needed. Although this is a greater issue relative to other RFBs with solid active materials that can rely on size exclusion at the separator, this challenge is shared by all other RFBs that rely on Li ions for ionic conductivity and have soluble redox shuttles. Jia *et al*. reported a custom Nafion/polyvinylidene difluoride (PVDF) composite membrane for this application after finding ceramic and commercial Nafion membranes to have performance limitations in their electrolyte.[24] Membrane cost will be a major factor to consider for Li-ion conductive membranes. A low-cost, stable, low resistance and low mediator crossover Li-ion conductive membrane will be needed to drive this design forward. The third challenge is the relatively low voltage efficiency due to the voltage difference needed between the mediators and the solid active materials to drive the additional chemical redox process. There was a 0.81 V difference between the expected

primary charge reaction (2.11 V, reaction 1 in Figure 8b) and discharge reaction (1.30 V, reaction 5 in Figure 8b). This significant voltage difference reduces the cycling energy efficiency. Future research will be needed to find more active material-mediator pairs that are effective with a lower potential difference, although voltaic efficiency loss due to the additional chemical oxidation/reduction processes between the redox shuttles and solid particles in this system is unique for RFBs and cannot be eliminated.

1.4. Active Materials

In batteries, the active materials store the chemical energy and participate in redox reactions. In RFBs, active materials are typically dissolved or dispersed in electrolytes, stored in energy storage tanks and pumped through electrochemical reaction cells during charge/discharge (illustrated in Figure 2). There have been many types of active materials developed since the RFB concept was introduced.[21, 22] The first group of active materials were dissolved single-elements in aqueous electrolytes, most commonly transition metal ions (e.g., Fe, V) and halogens (e.g. Br, Cl).[171] Some of the redox couple systems that have reached the greatest maturity are iron-chromium, soluble metal-bromine, iron-vanadium, and all-vanadium.[172] A more detailed discussion can be found in a recent review.[22] The second group of compounds are ligand-modified ions, which may be dissolved in aqueous or organic solvents.[22, 65, 171, 173-175] For example, additional capacity has been reported from the ligands of a vanadium complex.[173] More complex organic redox compounds can be modified by chemical functionalization to optimize both the redox potential and solubility.[19, 171] Beyond soluble compounds in RFBs, more recently research activity has increased toward solid active material tailored for RFBs.

1.4.1. Transition Metal Active Materials

Pb-acid batteries are one of the most widely known types of cells in part due to reliable performance and low cost.[176, 177] A conventional Pb-acid battery uses two electrochemical redox couples, Pb/Pb^{2+} as the anode and PbO_2/Pb^{2+} as the cathode. The electrochemical reactions are shown in Equation (3) and (4) (note: precipitation of Pb^{2+},

as is typical in Pb-acid cells, has been omitted). In the discharged state, both anode and cathode active materials have Pb in the Pb^{2+} state, typically as a $PbSO_4$ precipitate. However, if the Pb is under conditions where it remains as a soluble Pb^{2+} species, the possibility opens up of adopting Pb to a RFB system. For example, a RFB using Pb/Pb^{2+} as the anode and Fe^{2+}/Fe^{3+} cathode was reported.[178] More interestingly, Pletcher *et al*. reported a Pb-acid based RFB using a single flow channel without separators.[179] Electrolyte with dissolved Pb^{2+} is pumped through the flow channel and Pb and PbO_2 are electrochemically deposited on the anode and cathode, respectively, while being charged. Current densities in the range of 10-60 mA cm^{-2} were demonstrated and >85% coulombic efficiency and ~65% energy efficiency were reported.[179] The energy efficiency was improved to 79% with a cycle life of >2000 cycles after further optimization of the electrolyte, deposition conditions and current collectors.[180-183] However, there are a few challenges to apply this system widely. First, the energy density is highly limited by the solubility of Pb^{2+}, which may undergo precipitation at both the anode and cathode. Therefore, the operating efficiency is a challenge due to low energy density, low coulombic efficiency, low energy efficiency, and pumping energy dissipation. Second, the concentration overpotential is expected to be high due to a wide gap between the electrodes at low state of charge (SOC) after dissolution of solid material during discharge, although it is relatively low compared with conventional Pb-acid battery where often a thick layer of liquid sits in between two electrodes at all SOC. This challenge could potentially be overcome by promoting more compact surface deposition and/or engineering adjustable current collectors which minimize electrode separation during charge/discharge. Third, the benefit over conventional Pb-acid is not obvious because the

energy density of the chemistry has not changed but there is additional cost and complexity of RFB components including the pumps and tanks. The flexibility of decoupling power and energy is reduced due to high concentration overpotential at high overall capacity, in contrast to a conventional RFB where the electrodes have similar efficiency across a wide range of total capacity for the external tanks. In addition, the toxicity of Pb needs to be considered, particularly in the target large scale applications of RFBs. Dong *et al*. have noted, though, that recycled Pb could be used as the active materials for Pb-acid RFBs.[184]

$$Pb^{2+} + 2H_2O \underset{discharge}{\overset{charge}{\rightleftharpoons}} PbO_2 + 4H^+ + 2e^- \left(\text{Cathode, } E^0 = +1.685 V_{SHE}\right) \quad (3)$$

$$Pb^{2+} + 2e^- \underset{discharge}{\overset{charge}{\rightleftharpoons}} Pb\left(\text{Anode, } E^0 = -0.356 V_{SHE}\right) \quad (4)$$

A similar design to the Pb-acid RFB has been reported using Zn/Ni chemistry [redox reactions shown in Equation (5) and (6)], and for Zn/Ni the reported coulombic efficiency was 98% and energy efficiency was 88%, higher than those of Pb-acid.[185, 186] Optimization of electrolytes, Zn morphology, and current collectors were done to improve the overall performance.[186-189] Zn is also used as an electrode in other RFBs and has been paired with bromine,[190] polyhalides,[191] cerium,[192, 193] and polymer suspensions.[194] All-copper RFB based on reactions shown in Equation (7) and (8) was reported using aqueous solution of Cu^+.[195] The achieved energy density (20 Wh L^{-1}), cell voltage (0.6 V), and current density were low relative to other RFBs.[195, 196] Cu has also been paired with $PbO_2/PbSO_4$ electrodes, which increases the cell voltage to 1.29

V with an energy efficiency of 83%.[197] A similar design was applied to Cd/Cd^{2+} couple with a H_2SO_4-$(NH_4)_2SO_4$-$CdSO_4$ intermixture electrolyte as a RFB, achieving ~1.0 V discharge voltage and 82% energy efficiency.[198] MnO_2/Mn^{2+} is another commonly used solid cathode,[199] and has been paired with polymer suspension electrodes as well, to be discussed in more detail later.[200] MnO_2 has also been reported as a suspension electrode for flow capacitors in the form of percolating network, thus this material has shown the versatility to have been successfully demonstrated as a RFB active material in multiple different systems and cell designs.[42]

$$2Ni(OH)_2 + 2OH^- \underset{discharge}{\overset{charge}{\rightleftharpoons}} 2NiOOH + 2H_2O + 2e^- \left(\text{Cathode, } E^0 = +0.490\,V_{SHE}\right) \quad (5)$$

$$Zn(OH)_4^{2-} + 2e^- \underset{discharge}{\overset{charge}{\rightleftharpoons}} Zn + 4OH^- \left(\text{Anode, } E^0 = -1.215 V_{SHE}\right) \quad (6)$$

$$Cu^0 \underset{discharge}{\overset{charge}{\rightleftharpoons}} Cu^+ + e^- \left(\text{Cathode, } E^0 = +0.52 V_{SHE}\right) \quad (7)$$

$$Cu^{2+} + e^- \underset{discharge}{\overset{charge}{\rightleftharpoons}} Cu^+ \left(\text{Anode, } E^0 = -0.15 V_{SHE}\right) \quad (8)$$

All the materials just discussed share the same challenges as the Pb-acid RFB. One possible approach to improve performance is to apply Type I design. This design would be beneficial by keeping the separation between electrodes consistent during charge/discharge, which would reduce IR drop across the electrolyte. In Type I design, the solid material is deposited on or dissolved from the surface of the percolated conductive additive material and flows within the electrochemical reaction cell and the

storage tank, instead of building up as thick layers on the current collectors. Recently, Mubeen *et al*. demonstrated such a RFB.[68] For example, a Zn-Cu active solid suspension battery has the electrochemical redox reactions in Equation (9). In a fully charged state, Zn is deposited on carbon particle surfaces and Cu^{2+} is dissolved in the electrolyte, and both electrolytes contain flowing carbon suspensions. During discharge, Zn dissolves and Cu is electrochemically deposited onto the surface of carbon. The reaction is reversed during charging. A discharge voltage of 0.97 V was achieved with an overall energy efficiency of 70% at a constant current density of 5 mA cm^{-2}.[68]

$$Cu(solid) + Zn^{2+}(solution) \underset{discharge}{\overset{charge}{\rightleftarrows}} Cu^{2+}(solution) + Zn(solid) \qquad (9)$$

$$2Fe^{2+} \underset{discharge}{\overset{charge}{\rightleftarrows}} 2Fe^{3+} + 2e^{-} \left(\text{Cathode, } E^0 = +0.77 V_{SHE}\right) \qquad (10)$$

$$Fe^{2+} + 2e^{-} \underset{discharge}{\overset{charge}{\rightleftarrows}} Fe^0 \left(\text{Anode, } E^0 = -0.44 V_{SHE}\right) \qquad (11)$$

The all-iron RFB is another chemistry that relies on solid transition metal deposition. The redox reactions are shown in Equation (10) and (11). A conventional RFB with all-iron chemistry uses a Fe^{2+}/Fe^{3+} solution as the cathode flowing through a porous electrode and Fe/Fe^{2+} (Fe plating/stripping) as the anode.[201] Petek *et al*. demonstrated an all-iron RFB with Type I design and carbon particles added to the electrolytes.[60] Current density as high as 75 mA cm^{-2} was demonstrated, although the charge/discharge voltage efficiency was only just over 50%.[60] Applying Type I design to this transition metal chemistry provided the possibility to expand capacity significantly. All these cells share

the common challenges of conventional RFBs including relatively low voltage, energy density and round trip efficiency. On the other hand, many of these metal materials are relatively low cost due to their abundance.[60, 68] These technologies are also competitive in applications where space and footprint limitations are less of a concern.

1.4.2. Organic Active Materials, Including Polymers

Organic molecules have also been used as the active materials in both aqueous and organic RFBs. Some of these materials may offer cost and toxicity advantages over dissolved transition metals, and organic molecules provide a wide range of design flexibility and desirable attributes with regards to redox potentials and other physicochemical properties.[22, 65, 73, 79] For example, an acidic solution of 9,10-anthraquinone-2,7-disulphonic acid (AQDS) was used to undergo fast two-electron two proton reduction.[80] The quinone/hydroquinone couple was paired with a Br_2/Br^- redox couple yielding >99% capacity retention per cycle.[80] The quinone couple was demonstrated in alkaline solutions to improve safety and inhibit corrosion.[77] More detailed discussion on organic active materials and redox polymers can be found in recent reviews.[22, 65, 73, 202] One challenge facing dissolved organic molecules as active species is membrane crossover, which reduces cell capacity and operating lifetime. One option to mitigate this issue is to design new membrane materials; however, Montoto *et al*. proposed instead using redox active colloids (RAC) as the active materials to address this issue.[203] Solid cross-linked poly(vinylbenzyl chloride) (xPVBC) particles were synthesized through emulsion polymerization as backbones for redox couples, in this particular case ethyl viologen and (dimethylaminomethyl) ferrocene. The redox couples

were then grafted onto xPVBC through ion exchange by replacing –Cl on xPVBC with the functional redox species to form the final RAC particles. The functionalization efficiency was nearly 100%, indicating a high loading of redox species on the RAC polymer particles. These RACs had good size and shape stability during charge/discharge, chemical stability of the redox groups, and minimal membrane crossover,[203] A prototype RFB using low concentration RAC and a commercially available porous separator with a Type III flow cell design was demonstrated. The overall performance was comparable to typical RFBs based on dissolved organic active materials, showing a coulombic efficiency of ~94% at 43 $\mu A\ cm^{-2}$, and both energy and voltage efficiencies above 90%.[203]

Although RACs are a very promising technique, there are still a few challenges to be addressed. First, the capacity utilization was low in the initial demonstration, achieving 21% of the theoretical capacity. Notable causes including low loading and sedimentation at the counter electrode were mentioned by the authors. More research is needed to engineer the RAC design (e.g., particle size, morphology, flow pattern, and loading) and/or explore new backbone materials. Second, full charge/discharge cycling of a RAC fluid with high loading to increase energy and power density will be needed and parameters will need to be explored at the higher loadings including particle contact with the current collector, electrolyte tortuosity, and rheological properties. Successfully increasing the loading may also improve capacity utilization, as noted in the report.[203] A third challenge is the low energy density relative to conventional RFBs, which will likely be an issue even if higher particle loading in the electrolyte are achieved.

Assuming a high concentration of 40 wt% and an average discharge voltage of 0.85 V, the energy density would be approximately 12.5 Wh L^{-1}, which is significantly lower than a typical conventional all vanadium RFB (25 Wh L^{-1}).[19, 22] We note this energy density is limited not just by the mass loading, but also the cell voltage, which could potentially be improved by grafting other redox couples with different redox potentials. Increasing the cell voltage should be achievable because many organic redox couples are available and also because the system was designed for organic electrolytes which have stability windows exceeding 0.85 V. With regards to volumetric and gravimetric capacity limitations, future research could be directed towards other backbone materials with lower molecular weights and higher densities while maintaining or improving electrochemical properties. The key advantage of the RAC design is that it provided an opportunity to bypass the solubility limitation of the active species by grafting them onto backbone materials that were already solid particles. This feature is exciting because it opens a variety of materials that could potentially increase the energy density of RFBs with organic redox couples. The fourth challenge is the high viscosity at high RAC loadings. A 40 wt% RAC showed >10 Pa·s viscosity at 100 s^{-1} shear rate.[203] This is significantly higher than many other suspension-based systems.[27, 147, 148, 204] The high viscosity may result in low operating efficiencies. Further research efforts will likely explore lowering the viscosity by optimizing the RAC surface and electrolyte. Overall, the RAC system is promising due to the use of relatively low cost materials and their high initial capacity retention and lifetime estimates, though more research needs to address energy density, power density, and viscosity challenges.

Another polymer active material demonstrated in RFBs is polyaniline (PANI), where the redox couple involves Cl^- addition/subtraction with the PANI backbone [reactions in Equation (12)]. PANI has attracted attention for rechargeable batteries due to its high electronic conductivity, low cost, environmental stability, and good redox reversibility.[194, 205, 206] Zn–PANI batteries offer high capacity and discharge voltages close to 1.2 V [redox reactions in Equation (12) and (13)].[194, 205, 207, 208] Different methods have been reported to synthesize well controlled PANI films/particles.[206, 209, 210] Zhao *et al*. demonstrated a RFB based on PANI microparticle suspensions in aqueous electrolytes using a half-cell Type III design with a Zn counter electrode.[194] The results were promising, particularly relative to Zn-PANI thin film batteries, with a discharge capacity of 115.2 mAh g^{-1}_{PANI}, coulombic efficiency of 97% and minimal capacity decay at a current density of 20 mA cm^{-2}.[194] The high current density enables the possibilities of high power applications and fast cell charging, getting closer to the current densities achievable with RFBs based on dissolved transition metals.[194] In addition, the suspension viscosities were lower than Li-ion solid suspensions. This cell was further optimized by doping Ag on PANI particles, achieving high discharge capacity from oxidation of PANI particles.[207] PANI suspension redox has also been paired with PbO_2 electrodes, increasing the cell voltage.[211] Another micro-sized polymer particle suspension RFB cathode was reported by the same group.[200] This system included a polypyrrole (PPy) microparticle suspension paired with manganese dioxide for an average discharge voltage of ~0.95 V [anode redox reaction shown in Equation (14)).[200] This cell also showed a high capacity retention (97.2% after 90 cycles) and a stable coulombic efficiency of 92.1%.[200] These two

micro-polymer suspensions share similar promising advantages such as high capacity retentions and high current densities; however, they share similar challenges as well. First, these are aqueous systems and thus the cell voltage is low relative to organic electrolyte chemistry. Incorporating organic solvents may be possible, but particle stability and solubility in the organic electrolyte would need careful consideration. Second, the voltage efficiency is relatively low; researchers are currently addressing this challenge with new conducting polymers, modified polymer synthesis methods, and optimizing the supporting electrolyte.[205, 206, 210, 212, 213] Potential optimization on the counter electrode by adopting a Type I design may also be helpful to decrease the overpotential and to take advantage of the power-energy decoupling feature of RFBs. Oh *et al*. reported an all-organic RFB with polythiophene microparticle suspensions as both anode and cathode showing redox activities through two opposite electrochemical process, n-doping and p-doping.[214] Although a relatively high discharge voltage of ~2.4 V was achieved, the current density and efficiency were limited even with a high loading of KB to facilitate electron transfer.[214] Winsberg *et al*. demonstrated a RFB using 2,2,6,6-tetramethylpiperidinyl-N-oxyl (TEMPO) containing methacrylate/styrene block copolymers (PTMA-b-PS) micelles as cathode paired with Zn/Zn^{2+} anode achieving ~1.1 V discharge voltage with high coulombic efficiencies (99.8%) but low energy density (1.6 Wh L^{-1}) with limited current densities (fast capacity decline with increasing current densities with maximum at only 0.2 mA cm^{-2}).[215] Overall, these redox active polymer particles and grafted redox couples on inert backbone particles are promising approaches to overcome the solubility limitation of conventional RFBs, and

more innovations on material selection and engineering are expected to increase the performance significantly.

$$PANI + 2nCl \underset{discharge}{\overset{charge}{\rightleftharpoons}} PANI^{+}\left(Cl^{-}\right)_{2n} + ne^{-}\left(\text{Cathode}\right) \quad (12)$$

$$Zn^{2+} + 2ne^{-} \underset{discharge}{\overset{charge}{\rightleftharpoons}} nZn^{0}\left(\text{Anode, } \mathrm{E}^{0} = -0.762V_{SHE}\right) \quad (13)$$

$$2nPPy + nySO_4^{2-} \underset{discharge}{\overset{charge}{\rightleftharpoons}} \left[PPy_2^{y+}\left(SO_4^{2-}\right)_y \right]_n + 2nye^{-}\left(\text{Anode}\right) \quad (14)$$

1.4.3. Lithium-Ion and Sodium-Ion Active Materials

RFBs using Li metal or Li-ion battery redox chemistry stand out with regards to voltages and energy densities. One option is to use soluble cathode active redox couples dissolved in aqueous or organic solvents to form the flowing catholyte, and metallic Li or soluble anode active material as the anolyte separated by suitable ion conducting ceramics or polymers that serve the dual role of separator and electrolyte.[65] While Li metal anodes provide high cell voltages due to the anode potential, safety issues arise dependent on the ability of the electrolyte and separator to control the high reactivity of Li and the formation of Li dendrites that can cross to the cathode and short the cell.[61, 116, 216, 217] Another challenge of using soluble catholyte/anolyte species is that energy density is still limited by the solubility of the active species, just as is the case for conventional RFBs. More detailed discussion on this topic can be found in a recent review.[65] Given this limitation, it is not surprising that efforts have been made to incorporate solid Li-ion battery intercalation redox couples into RFBs in the past a few years. As static battery

cells, Li-ion batteries stand out among rechargeable battery materials with regards to energy density and cycling capacity retention.[34, 35] In this chapter, both cathode and anode solid active materials that have been adopted in RFBs will be discussed.

A. Lithium-Ion Cathode Materials

Li-PS is a low voltage but high capacity battery chemistry that typically uses sulfur as the cathode active material and Li as the anode. The overall cathode redox reaction, assuming complete conversion to Li_2S, is shown in Equation (15). The theoretical capacity of a Li-PS battery is 1672 mAh g^{-1}, significantly higher than transition metal–based commercial Li-ion cathode materials. However, this lithiation/delithiation is not a single step process; instead, Li_2S_x ($2 < x \leq 8$) forms throughout the process. While some of the product/intermediate species are insoluble in the electrolyte, the Li-PS Li_2S_x ($6 < x \leq 8$) are highly soluble. These dissolved PS have a shuttling effect, migrating to the counter electrode and reacting with Li resulting in capacity fade and low coulombic efficiency.[218] Numerous research efforts have attempted to address the issue of PS solubility in static battery configurations;[219-225] however, soluble PS can be conveniently incorporated into a RFB system. Li-PS RFBs have been reported where the operating voltage maintains the sulfur species always as the soluble Li_2S_8 and Li_2S_4 PS species.[119, 128, 226] Functioning like a conventional RFB, this Li-PS RFB only operates within the voltage window of the soluble PSs, and thus the theoretical capacity drops to 418 mAh g^{-1}. The experimentally achieved energy density was still high, at 108 Wh L^{-1}.[119] Conversion all the way to solid species is required to fully take advantage of the high capacity feature of sulfur. Therefore, a Type I RFB design using percolating

carbon network as flowing electrodes to provide both electron conduction and a surface for solid deposition was reported.[125] Four- to five-fold increase of capacity was achieved by expanding the redox window to the insoluble species.[125] Li-PS chemistry has attracted increased attention for RFBs in recent years, for example with new separator design,[227] applying Type IV mediator design,[170] and innovations on flow design.[228]

This promising chemistry, however, still faces a few technical challenges in RFBs. First, the PS shuttling effect remains a problem, causing self-discharge and capacity fade. The larger PSs migrate towards the anode, react with Li forming smaller PSs, and migrate back to the cathode to reform the larger PSs again.[225] This is a shared problem with conventional Li-PS batteries, and extensive research has been focused on this topic. There are currently three main reported approaches to reduce this effect. 1) Immobilizing sulfur in sulfur-porous carbon composites or other composite materials.[219-224] Sulfur immobilization strategies have already been applied to Li-PS RFBs.[125, 126] Although some Li-PS RFBs achieved very high capacity and good cycling performance, the S to C ratio in the cathode was very low, resulting in low energy density based on the total cathode mass or volume as pointed out by Zhang *et al.*[218, 229] 2) Nonporous ion-selective membranes are needed to provide a physical barrier for PS to cross between the cathode and anode in the electrochemical cell. Porous polypropylene separators, which are commonly used in static Li-PS batteries, have limited capability in blocking PS migration. There are a few reports demonstrating good blocking of PS by using selective ion-conducting membranes, for example lithiated Nafion membranes[230] and

perfluorinated polymer membranes with lithium sulfonyl dicyanomethide functional groups.[231] The membranes used in other Li RFBs are also good candidates for Li-PS RFBs, for example Nafion/PVDF membranes used in mediator RFBs by Jia *et al*.[24, 65] 3) Electrolytes have been designed to suppress PS dissolution, including the use of high Li salt concentration[232, 233] and ionic liquids,[234, 235] although these methods are expected to be less effective in RFB systems as these strategies significantly increase the viscosity. The second challenge for Li-PS RFB, for systems that choose Li metal anode, is the stability of Li metal. Metallic Li has been used as the anode in both conventional Li-PS batteries and RFBs to achieve high energy density. Li anodes are typically stabilized by a passive layer on the surface, however, the passive layer can be unstable and particularly in flowing systems the Li will be exposed to a relatively large amount of electrolyte and will face shear forces, which may impact the stability of the Li interface. Innovations on cell configuration and electrolyte design may help in this area.[236, 237] More detailed discussions on Li-S chemistry, especially for static Li-S cells, can be found in these recent reviews.[32, 65, 218, 238, 239]

$$Li_2S \underset{discharge}{\overset{charge}{\rightleftharpoons}} S + 2Li^+ + 2e^- \quad (15)$$

$$Li_xM_yO_z \underset{discharge}{\overset{charge}{\rightleftharpoons}} Li_{x-n}M_yO_z + nLi^+ + ne^- \quad (16)$$

The most well-known Li-ion battery active cathode materials are based on transition metal oxides with high redox potentials, from 3.0 to approaching 5.0 V vs. Li/Li^+.[240] In addition to the specific examples in Equation (1) and (2), a more general

redox reaction is shown in Equation (16), where M refers to one or multiple transition metals, and O refers to oxygen, though there are other anion species that have been reported such as phosphates.[240-243] During the discharge process, the metal oxides are lithiated by Li^+ insertion coupled with transition metal reduction by electrons originated from the anode. The charge process is the reaction reversed. The cycling profiles of a few representative cathode materials are shown in Figure 9 (adapted from Patoux *et al*.[244]). Some of these materials have already been demonstrated in RFBs and will be discussed first, followed by a discussion of other candidate materials.

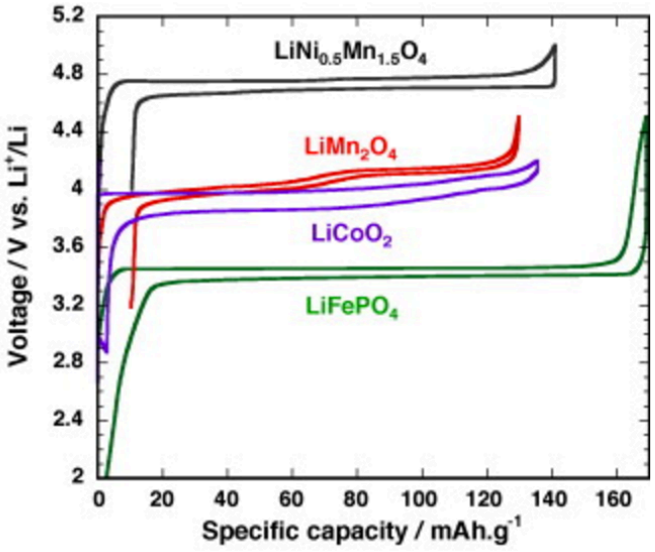

Figure 9. Representative cycling profiles of common Li-ion cathode materials paired with Li metal anodes (reprinted with permission from S. Patoux, L. Daniel, C. Bourbon, H. Lignier, C. Pagano, F. Le Cras, S. Jouanneau, and S. Martinet, J. Power Sources, 189 (1), 344-352 (2009). Copyright 2009 Elsevier).

LCO is one of the most widely used Li-ion cathode materials, especially in portable devices, and has a layered structure with its electrochemical properties widely reported.[12, 245-250] A suspension of 22.4 vol% LCO with 0.7 vol% KB showed a reversible capacity of 127 mAh g^{-1}_{LCO},[27] close to the capacity of 137 mAh g^{-1}_{LCO} corresponding to 50% delithiation/lithiation, a common approximation for the practical capacity of LCO materials. LCO has a discharge voltage of ~4.0 V vs. Li/Li^+ as shown in Figure 9 and higher energy density can be achieved if charged to higher potentials that further delithiate LCO, although charging to such potentials generally accelerates material degradation or failure.[251-254] Compared with other common Li-ion cathode materials, LCO has relatively high electronic and ionic conductivities (~10^{-4} S cm^{-1} electronic conductivity and 10^{-11}-10^{-7} cm^2 s^{-1} Li^+ diffusion coefficient reported),[255-257] both of which minimize the overpotential while operating in flow cell geometries.[148] There are a few additional considerations for the use of LCO in RFBs. First, the environmental impacts of Co needs to be addressed.[258] Although the recycling of Co from a flow cell system should be easier than static laminated Li-ion batteries, the toxicity of Co means that recovery and recycling is important. Second, the cost of Co is relatively high because of its relatively low earth abundance; and high energy inputs are needed during processing and manufacturing LCO, further demonstrating the need for implementation of effective material recycling.[259, 260] Third, the particle volume is expected to change by 2.32% during cycling.[261] The concern with volume change is that it may result in particle cracking, isolation of active materials, and hence capacity fade. However, particle fracture is less of an issue in a flow cell system because the particles are not statically connected in a solid composite and therefore there is no

isolation problem in the dynamic solid suspension.[148] The volume change in large scale RFB system may cause pressure fluctuations during cycling, which is a potential technical challenge. Additionally, particle fracture during cycling in a flow system would change the rheological properties of the electrolyte, which requires appropriate design to account for these changes in electrolyte properties.

$LiMn_{1.5}Ni_{0.5}O_4$ (LMNO) is a spinel-phase material with a high voltage of 4.7 V vs. Li/Li^+ (shown in Figure 9) and high theoretical capacity of 146 mAh g^{-1}, suggesting a theoretical energy density of 686 Wh kg^{-1}.[137] It also uses Ni and Mn, which are both less expensive than Co. These promising features have previously been noted, and LMNO has been demonstrated in a Type II design flow cell.[27] A suspension of 20 vol% LMNO and 2.5 vol% carbon was cycled as a half cell achieving close to theoretical voltage and high capacity.[27] Research effort has improved the electrochemical performance of LMNO in conventional Li-ion batteries using metrics such as rate capability, stability, and cycle life.[137, 262-266] Although the high energy density of LMNO is appealing, there are still challenges, in particular long-term cycle life due to the high potential of LMNO which is outside of the stability window of many Li-ion battery electrolytes.[137, 267] More detailed discussion about LMNO materials can be found in recent reviews.[137, 268]

Other transition metal oxide cathode materials may be potential candidates for RFBs. $LiMn_2O_4$ (LMO) has a spinel structure providing an average voltage of ~4.0 V vs. Li/Li^+ (shown in Figure 9) and a theoretical capacity of 148 mAh g^{-1}.[269-271] It has a lower

cost and is more environmental friendly than other transition metal oxides such as LCO or LMNO, but capacity loss is an issue due to manganese dissolution in the electrolyte and/or particle crystallinity change.[272, 273] The ionic and electronic conductivities are also relatively low (~10^{-6} S cm^{-1} electronic conductivity and 10^{-11}-10^{-9} cm^2 s^{-1} Li^+ diffusion coefficient reported),[148, 255, 274, 275] suggesting potential challenges of electrochemical performance in RFBs. Other materials like $Li(Ni_xMn_yCo_z)O_2$ (with varying compositions of x, y, and z) and vanadium oxides are also under active research.[276-279] To improve the performance of these cathode materials, doping with various metals has been explored. Dopants (e.g., aluminum, zinc, titanium, magnesium.) have been reported in specific material systems to increase crystal structure stability, battery capacity and capacity retention, material rate capability, and improve conductivity and dissolution rate.[260, 280] More detailed discussions on these materials are available in recent reviews.[135, 240, 260, 279, 281-283]

$LiFePO_4$ (LFP) is another appealing cathode material with a discharge voltage of ~3.5 V vs. Li/Li^+ (shown in Figure 9) and a theoretical capacity of 169 mAh g^{-1}.[284] LFP features cost, environmental, and safety advantages and has been adopted in electric vehicles and hybrid electric vehicle batteries.[285, 286] It also has a flat discharge voltage profile, which can be beneficial for Type III design based on stochastic particle collision because a stable voltage output is expected even for particles at different SOC.[147, 287] Extensive research has been done on synthesis methods, morphology control, dopants, and carbon coatings to improve the electrochemical performance of LFP.[285, 287-296] LFP was demonstrated as a cathode material for RFBs in both Type

II and Type IV.[24, 131, 132, 166] Other phosphates that have been researched in conventional Li-ion batteries can also potentially be adopted in RFBs such as $LiMnPO_4$,[297] $LiCoPO_4$,[242, 298, 299] $Li_3V_2(PO_4)_3$,[300] and mixed phosphates.[301] More discussions on this group of phosphate cathode materials, especially LFP, can be found in recent reviews.[142, 284, 302]

Li-ion solid active cathode materials generally have high voltage and capacity, providing the opportunity for RFBs with high energy densities. Development of these materials has been a very active field, but there are a few shared challenges and/or potential improvements to be addressed specifically for the application of RFBs. First, the suspension loaded with solid Li-ion battery particles generally results in high viscosity and causes operating complexity and cost to pump the high viscosity electrolyte. Second, the effects of particle size, morphology and microstructure are not well studied for RFBs, although there is a rich history with static Li-ion batteries to draw from. There are potential opportunities to improve the electrochemical performance of active material suspensions by designing the particle physical and electrochemical properties to be matched to a flowing suspension, rather than a static composite, system. In addition, surface modifications on active material particles could improve both the cycling performance and fluid properties.

B. Lithium-Ion Anode Materials

Besides metallic Li, which was discussed earlier with Li-PS chemistry, $Li_4Ti_5O_{12}$ (LTO) is a commonly used anode material in RFBs, and has been demonstrated in Type II and

Type III design geometries.[27, 131, 147, 148, 303, 304] LTO has material properties that make it desirable for RFB applications. It has reasonably high theoretical capacity of 175 mAh g^{-1}_{LTO} and a Li insertion/extraction voltage of ~1.55 V vs. Li/Li^+, which lies within the stability window of common organic electrolytes. The electrochemical potential being within the stability window of common Li-ion battery electrolytes mitigates solid electrolyte interphase (SEI) formation and electrolyte decomposition.[305] The discharge curve is very flat, providing a stable voltage output.[147] LTO is also reported as a zero-strain material, suggesting good particle morphology and crystal stabilities due to the lack of strain during Li insertion/extraction because there is no volume change during these processes.[306] In addition, LTO has excellent ionic and electronic conductivities (10^{-6}-10^{-8} cm^2 s^{-1} Li^+ diffusion coefficient and 10^{-6}-10^{-13} S cm^{-1} electronic conductivity), particularly after slight lithiation of the material which results in 10^0 S cm^{-1} electronic conductivity.[255, 307-310] As an example, a suspension of 25 vol% LTO and 0.8 vol% KB showed close to theoretical capacity with reasonably low overpotential at a rate of C/3 (the current that is able to theoretically charge or discharge the electrode in 3 hours).[27] LTO shares common challenges related to using solid dispersions in flowing electrolytes. A recent review provides a more detailed discussion on the materials development of LTO.[311]

Anatase TiO_2 is another titanium-based Li-ion anode material with an average potential of ~1.8 V vs. Li/Li^+ and a theoretical capacity of 330 mAh/g, and it has been reported in RFBs.[140, 167, 312, 313] A type IV cell configuration showed ~1.25 V vs. Li/Li^+ discharge voltage for $CoCp^*_2$ and $CoCp_2$ mediators and using TiO_2 particles as the

energy storage material that facilitated chemical redox with the mediators.[167] TiO_2 has cost, environmental, and safety advantages and a high ionic conductivity, but the electronic conductivity and rate capability are low relative to other anode materials.[313] More detailed discussions about the synthesis and development of TiO_2 as a Li-ion anode material can be found in these recent reviews.[313-315] Another titanium-based material that has been applied to RFBs is $LiTi_2(PO_4)_3$, which was paired with LFP and cycled in aqueous electrolyte, resulting in a ~0.9 V full cell.[132] The high redox potential (~1.8 V vs. Li/Li^+) is beneficial to minimize hydrogen evolution and enables using this material in an aqueous electrolyte; however, in an organic system the sacrifice in cell voltage would make this material unlikely to be chosen over other Ti-containing materials.[316]

Silicon is a Li-ion anode material under active research and development with a high theoretical capacity (3590 mAh g^{-1} by forming $Li_{15}Si_4$, ~10 times higher than graphite, the most commonly used anode material).[288, 317] A mixture of silicon and carbon in organic electrolyte was cycled showing a large capacity and low polarization.[130] However, silicon performance can suffer from large SEI formation which results in low coulombic and energy efficiency. The material also undergoes large volume change during cycling which can result in particle fracture during lithiation and delithiation cycles. More detailed discussions on silicon as Li-ion anode material can be found in these recent reviews.[318-322] There are many new anode materials besides graphite and those discussed above, and these reviews provide a good perspective on anode development of Li-ion batteries.[135, 315, 323-325] Anode materials require consideration of the tradeoff between energy and stability – lower potential materials are

desirable because they increase the net cell voltage, but below the stability window of the electrolyte there will be electrolyte decomposition and formation of an interfacial layer, the stability of which is critical to long-term charge/discharge cycling of the material.

C. Sodium-Ion Active Materials

Although the energy density, power density, and cycle life advantages of Li-ion battery chemistry has been established, Na-ion battery materials have attracted attention in part because Na is more earth abundant and thus cheaper than Li, and in some cases allows for alternative material choices in the battery cell (e.g.; Na does not alloy with aluminum, whereas Li does).[129, 326] Ventosa *et al*. reported a non-aqueous RFB using P2-type $Na_xNi_{0.22}Co_{0.11}Mn_{0.66}O_2$ (NaNCM) and $NaTi_2(PO_4)_3$ (NaTP) as the cathode and anode active materials, respectively.[129] NaTP operates at a flat potential of ~2.1 V vs. Na/Na^+, which is within the electrolyte stability window, and had a reported capacity of 125 mAh g^{-1}_{NaTP}.[129, 327] P2-type NaNCM was demonstrated to have a capacity of ~130 mAh g^{-1}_{NaNCM} with a range of potentials plateaus between 2.1-4.3 V vs. Na/Na^+.[129, 328] In their RFB system, a reversible 9 Wh L^{-1} energy density was demonstrated, although it was suggested 150 Wh L^{-1} would be achievable with a better selection of active materials and performance optimization.[129] The coulombic efficiencies were considerably low, 53% in the first cycle and ~88% in subsequent cycles. The main challenges in this system were 1) high overpotential, causing incomplete utilization of the active material capacities; 2) low gravimetric capacity relative to other demonstrated Li-ion materials, which is even further reduced when pumping power is included in the total power output for the viscous suspension. Na-ion

materials provide an alternate route to using solid intercalating particles in RFB systems. Recent reviews provide more detailed discussions on Na-ion battery materials.[326, 329-332]

1.5. Flow and Agitation Methods

Power needs to be applied in a RFB to drive the fluid for mass exchange between the electrochemical reaction cells and the energy storage tanks. In most scenarios, this energy is provided by pumps and the fluids run continuously as shown in Figure 2, 5a, 6a, 7, and 8a. There are other methods for providing this force to move the electrolyte fluid, as well as different operating modes, and both factors can have significant influence on the electrochemical performance of the cell. In this chapter, three operating modes will first be discussed and then two types of driving forces will be introduced that have previously been demonstrated for RFBs.

1.5.1. Continuous Pumping, Intermittent Pumping, and Batch Stirring

In a continuous pumping mode, both the catholyte and the anolyte are circulated between the reaction cells and the energy storage tanks continuously during charge/discharge. Such a mode is necessary for conventional soluble transition metal RFBs because 1) the energy densities of the fluids are limited and continuous refreshing of the active material solution is required to provide a stable power output; 2) the fluids that have been charged/discharged in the electrochemical reaction cells will be quickly mixed with the rest of the liquid in the energy tank, allowing a gradual change in electrolyte concentration of the oxidized/reduced electroactive species; 3) the fluid viscosities are typically low, making continuous pumping relatively easy to implement. This situation also applies to a Type IV RFB where dissolved mediators are pumped to circulate and the mediators have relatively low energy density. [24, 166, 167] Therefore, continuous pumping of electrolyte is also the best method for Type IV batteries. In a Type III design

where the reactions are based on collisions of active material particles on current collectors, suspension agitation is needed to charge/discharge the battery; therefore, a continuous pumping mode may be applicable provided the fluid is pumped with sufficient force to keep the particles well-dispersed.[147]

In other designs; however, the active materials have sufficient energy density to halt the flow before the active materials are fully discharged to save pumping energy. An intermittent flow mode, in which the active material suspensions are pumped to the electrochemical reaction cell in a batch manor and replaced after they are fully charged/discharged, was proposed and estimated to reduce the energy loss due to pumping. In a Type II system, the estimated loss of energy due to pumping dropped from 44.6% in the continuous mode to 0.6% when an intermittent pumping was implemented.[27] However, there are additional items to consider for this operation mode. First, it is important to note that the estimates from the report referenced were based on a flow rate assumption that did not account for the energy to initiate flow and the initial fluid viscosity. At very low shear rates the viscosity of the suspension is multiple orders of magnitude higher due to the shear thinning behavior of the solid suspensions.[27, 148, 204] Second, four suspension storage tanks are needed for intermittent flow operation because one tank is required for charged suspensions and one for discharged suspensions for each electrode.[104] Such a system must then account for the additional cost, space, and complexity requirements of 4 tanks as opposed to 2 per system. In addition, a stable method to switch active material batches is needed to avoid

power interruptions between batches of electrolyte suspension being pumped into the electrochemical reaction cell intermittently.[132]

Another design is to add electroactive suspensions in a custom electrochemical cell that uses stirring to agitate the suspension and create a simulated flow environment.[147, 148] This design is a modified version of the intermittent flow mode as fresh active material is pumped in after full charge/discharge. This method provides extra agitation via stirring while pumping is only needed during material exchanges. It is potentially useful in a Type III flow cell design since the reaction is based on collision between active materials and the current collectors and reliable agitation of the suspension is needed to run the cell. It also provides an approach to boost the power output in other designs because the quick mixing of active materials may facilitate ion diffusion and hence lower the cell overpotential. An extra energy input needed to drive the system agitation; therefore, the advantage of the additional agitation relative to its additional energy cost needs to be evaluated in detail for a system considering this design.

1.5.2. Other Driving Forces for Electrolyte Flow

Other innovative approaches in addition to pumping have been reported for flow cells. A gravity-induced flow cell design (GIFcell) was proposed by Chen *et al*.[228] As shown in Figure 10, the energy storage tanks and electrochemical reaction cells are directly connected and the mass transfer between these two units is induced by the force of gravity. The energy input to mechanically flip the cell is expected to be significantly smaller than pumping the viscous suspensions. One or more passes, or movements of the

suspension from one end of the cell to the other, may be required to fully charge/discharge the cell. The number of passes is dependent on the flow rate, which is further controlled by channel thickness and width, channel surface properties, tilt angle of the channels, and cycling rates.[228] In the first reported demonstration of this concept, a Li-PS chemistry was cycled within the potential window of Li_2S_8 and Li_2S_6 for the catholyte, and the counter electrode was Li metal. Chronoamperometry (CA) tests were conducted to charge the cell at 2.6 V and discharge at 2.05 V, with resulting current densities in the range of 0.5-1 mA cm^{-2}.[228] A complete charge/discharge required 25 passes (12.5 h in total) for a tilt angle optimized cell. The mechanical energy for flipping the cell 25 times was calculated to be only ~0.01% of the electrochemical energy stored in the cell.[228] Although the low energy input is appealing for a flow inducing method, there are a few challenges to be addressed in addition to the quick capacity fade, which may have been due to PS shuttling. First, optimizing channel design for various active material suspensions for system scale up will be challenging because the flow can have a viscous fingering effect which impacts the uniformity of the flow profile, though the authors note this can be mitigated by reducing the channel width to height ratio; and channel surface properties must be designed to form high wall slip interactions between the surface and the fluid to result in the desired unyielding plugs. Thus, channel surface modifications will be needed depending on the composition of the active material suspensions. Second, although the flow rate can be controlled by tilt angle, the range and control over flow rate is limited, and a large number of flips may still require high energy inputs. Third, other electrochemical characterization, including galvanostatic charge/discharge, need to be investigated for these systems. The drop in current density

during CA testing as the number of passes increases, including 54% during discharge, suggests high overpotential which needs to be addressed. The difficulties of controlling flow in tilted channels suggests adjusting elevation of only the energy storage tanks in a more conventional flow cell design may be worth exploring, and would simplify design by separating the energy storage and power components.

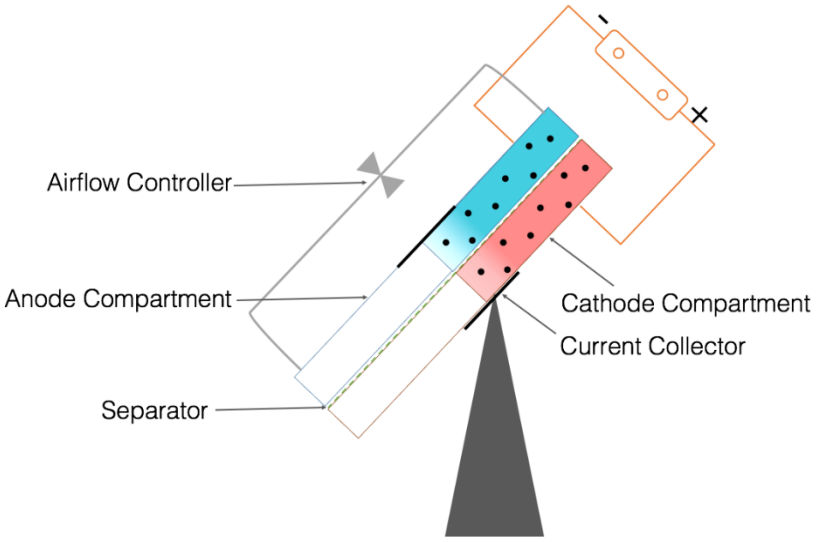

Figure 10. Illustration of gravity induced flow cell design.

Magnetic fields are another potential force to drive fluid movement in RFBs. γ-Fe_2O_3 nanoparticle suspensions are well-known as ferrofluids, and have also been reported as additives to energy storage fluids to promote using magnetic fields to provide transport advantages.[333] Li *et al*. reported a Li-PS battery with added γ-Fe_2O_3 particles in a conventional static cell geometry and used applied magnetic fields to improve electrochemical properties.[139] An optimized suspension of PS, γ-Fe_2O_3 particles and

carbon nanotubes achieved a high capacity of ~350 mAh g^{-1}_{sulfur} (corresponding to ~66 Wh L^{-1} of catholyte) while cycling between sulfur and Li_2S_4 under applied magnetic field, where the magnetic field improved cycling performance by concentrating the active material near the current collector.[139] In this suspension, γ-Fe_2O_3 nanoparticles absorbed PS on the surface and were concentrated near the current collector under an applied magnetic field, providing benefits with regards to mitigating PS shuttling and increasing the achievable discharge current densities. The magnetic particles also provide the possibility of driving the fluid with magnetic fields rather than pumps. The benefits of transporting the fluid with magnetic fields may include more precise control of the flow rate and direction, a simpler system, and possibly savings on pumping energy.[139] However, there a few challenges to implement these flow cell systems, especially at large scale. First, the composition of the electrolyte needs further research and optimization to be able to absorb PS and carry the flow with a minimum amount of γ-Fe_2O_3 loading to save both space and energy. Second, the electrochemical reaction cell has a relatively complex geometry, especially for large scale designs; therefore, the design of the magnetic field and the auxiliary components needed to generate the field and provide the flow pattern desired for numerous pipes and channels simultaneously will be needed. Third, while γ-Fe_2O_3 nanoparticles worked well with PS, it is not clear how general the use of this material will be, and surface modifications and/or alternative magnetic nanoparticles may need to be designed to match a given battery chemistry.

1.6. Characterization Methods

As discussed above, desirable properties such as high electrolyte energy density make RFBs with solid electroactive materials attractive battery systems to pursue. However, there are a number of challenges that span many of the cell designs that need to be addressed, and researchers have developed various methods to probe the fundamental properties of these systems or optimize the various battery components. Some of these advances are introduced below.

1.6.1. Suspension Viscosity

Viscosity of the electrolyte suspension has been noted as a key parameter of operating efficiency for RFBs and understanding the underlying causes of changes in viscosity and methods to decrease this parameter are important to improve the overall battery performance. Active material suspensions were found to be non-Newtonian fluids showing shear-thinning behavior.[27, 131, 138, 147, 148, 204] which is common for solid particle suspensions especially metal oxides.[94, 138, 334-336] Narayanan *et al*. reported a rheo-impedance study on KB suspensions and indicated that a high flow rate would minimize the electronic resistance for RFBs in continuous flow mode and that a high pre-shear through fast pumping or stirring would help minimize the electronic resistance and maximize the yield stress in intermittent flow mode.[337]

Carbon additives have significant impact on both the conductivities and viscosities of active material suspensions. Carbon material was added in Type I and Type II systems to

improve the electrochemical performance, and at the same time, the viscosities of the suspensions were also increased dramatically. For example, the addition of only 0.6 vol% carbon resulted a >10-fold increase in viscosity for a 22.4 vol% LCO suspension.[27] There is a tradeoff between conductivity and viscosity with varied carbon additive loading, with multiple groups previously reporting on this phenomena in the literature.[104, 337] Particle size, morphology, and salt concentration have previously been reported to have significant influence on the rheological properties of solid suspensions,[138, 204, 338-341] and hence provide potential directions to decrease the fluid viscosity. There are a few reports in the literature aimed at decreasing the fluid viscosities of battery material solid suspensions in particular. A nonionic dispersant, polyvinylpyrrolidone (PVP) was applied in LFP/KB suspensions to selectively stabilize only LFP particles, but not KB particles, resulting in a decrease in viscosity as well as an increase in the conductivity of the suspension, both of which resulted in improved electrochemical performance.[131] Similarly, the addition of non-ionic surfactant (isooctylphenylether of polyoxyethylene) to a LTO/KB suspension decreased the viscosity and improved the mixture homogeneity.[342] Surface modification of TiO_2 nanoparticles with a monolayer of propyl sulfonate groups was demonstrated to achieve high particle loading, low viscosity (below 10 cP with 50 wt% particle loading), and high colloidal stability while maintaining good electrochemical activity.[140] Surface grafting of small organic molecules onto γ-Fe_2O_3 was used to decrease suspension viscosity significantly, although the electrochemical activity was partially suppressed by the surface grafting.[333] Polyethyleneimine (PEI), a cationic surfactant, was found to effectively help disperse LFP and carbon suspensions and improve the homogeneity of

LFP-C slurry electrodes, hence improving the electrochemical performance via processing of the slurry electrodes for conventional Li-ion cells.[141] These results may be applicable to LFP/C suspensions for Type II semisolid designs for improving suspension homogeneity and hence preventing particle agglomeration and decreasing viscosities.[126, 141] While these examples are specific to battery particle suspensions, there have been many innovative methods reported to modify particle surfaces for improved rheological and/or electrochemical properties and are highlighted in recent related reviews.[343-345]

1.6.2. Mathematic Modeling and Other Studies for System Optimization

Mathematic modeling and simulations provide perspectives to understand the operating fundamentals and to optimize system performance. A 3D model of a RFB cell integrating ionic flux, electronic current, and hydrodynamic flow was developed to describe a Type II design flow cell.[346] Based on these calculations, active materials with flat charge/discharge potential profiles, i.e. electrochemical potential showing little variation with SOC such as LTO and LFP, are preferred to achieve more complete charge/discharge and higher energy efficiency than those materials with less flat potential profiles such as LCO.[346] Smith *et al*. simulated the energy loss mechanisms using LCO, LFP and the VO^{2+}/VO_2^+ couple, and provided four strategies to maximize the operating efficiency: 1) controlling the flow volume per pumping stroke; 2) promoting slip at interfaces; 3) reducing suspension rheology; and 4) selecting appropriate active material thermodynamics.[347] A simulation based on a LTO-carbon suspension in a battery stack model system was conducted and compared with experimental results,

indicating early-cycle coulombic inefficiencies and three recommendations were made to improve the energy inefficiency: 1) extend the length of the flow channel/current collector; 2) operate at high charge/discharge rates at the stack level; and 3) controlling the cutoff voltage window.[348] In addition, a half-cell model of a Type IV cell was reported to capture the distinct charge and discharge profiles, providing the possibility of accurate full cell simulations.[169]

Electronic and ionic limitations to electrochemical performance have been studied with LTO-carbon suspensions in static cells, noting the effects of the electrode thickness and LTO loading per area on charge/discharge profiles.[304] For example, anolytes with 15 and 20 wt% LTO accompanied by 3 wt% KB can form a perfect percolated network connecting all LTO particles with no isolated KB clusters; however, when the anolyte is loaded at 25 wt% LTO, the KB network (3 wt%) is fragmented with isolated KB clusters, and only a fraction of the LTO mass can contribute to the reversible cell capacity.[304] Different carbon black materials or carbon nanotubes also showed notable impacts on rheological and electrochemical properties.[60, 126, 138, 139, 349, 350] Ventosa *et al*. noted the importance of considering the SEI formation challenge with flowing electrodes since within flow systems the SEI formation occurs on the full surface of the current collector, as well as the anode particles.[351] As discussed earlier, SEI is a metastable layer typically formed on the surface of the low potential anode when the potential is below the stability window of the electrolyte. The SEI is critical to stabilizing the electrode in conventional Li-ion batteries. SEI production, however, also causes capacity loss and results in additional cell overpotential, hence lower energy efficiency. For an

electrode contacting a flowing electrolyte, new SEI can form continuously as new active material particles collide with the current collector, resulting in a much larger quantity of SEI formed and therefore lower energy efficiency. This effect was noted in a previous report as was the importance of selecting anode materials within the electrolyte stability window.[351] Petek *et al*. proposed the concept of an additional overpotential due to the distributed nature of the current between the electronic and ionic phases of the slurry to describe the high operating overpotential of suspension systems.[349] Electrochemical Impedance Spectroscopy (EIS) results showed an extra component in addition to traditional overpotential descriptions (Ohmic, activation and mass transfer overpotential), which is a function of slurry electrode charge transfer resistance and the ratio of the electronic and ionic phase conductivities.[349] Increasing the suspension electronic conductivity was found to be the key factor to decrease the overpotential and hence improve the electrochemical performance.[349] These results provided insights to improve RFB performance, and additional studies are needed to further understand the different types of solid active material RFBs and to further develop these technologies.

1.7. Summary and Perspectives

RFBs with solid electroactive materials have attracted increased attention, and recent research progress was discussed in this review. Much of the increased interest is driven by the energy density improvements that are possible for RFBs with solid active materials, as this route overcomes the intrinsic energy density thresholds set by solubility limitations of more established RFB systems that rely on soluble redox species. Significant achievements have been reported in research on flow cell design, material development, operating methods, and fundamental understanding. These projects all aim to provide the knowledge and tools necessary to enable large scale energy storage devices using these RFBs by improving energy density, energy efficiency and cost. The trend of using high energy density Li-ion solid active materials was noted, and this battery chemistry has been reported to provide high density energy storage in both conventional batteries and RFBs. In RFBs, the use of Li-ion battery materials was made possible due to the innovation of flow cell designs, introducing carbon percolating networks, taking advantage of the collision reactions, and mediating reactions with external chemical oxidants/reductants. Li-S chemistry in particular has attracted substantial attention due to its high capacity, earth abundancy, and flexibility to operate completely soluble in the electrolyte or only soluble during different stages of charge/discharge. The challenges and possible research directions for further development of RFBs with solid electroactive materials are briefly discussed below.

(1) Increasing energy density is desirable in every battery system. Using multiple electron redox couples in the suspension is an approach to further increase the energy density in

solid active material RFBs, and such materials have been reported for static battery cells.[352] Another option to increase energy density is to have multifunctional materials in the RFB. Chen *et al*. reported a catholyte containing solid sulfur/carbon composites and liquid lithium iodide (LiI) electrolyte, where the LiI serves as both a Li^+ conductor and energy storage active material.[353] This design achieved a high energy density (580 Wh L^{-1}) and columbic efficiency (>95%), providing the possibility to increase the energy density by storing energy in both the solid and liquid phases.[353] Further investigations applying similar designs with other materials, studying and optimizing the suspension viscosity, and finding more stable soluble species will improve the energy density and electrochemical performance. Electrolytes with high energy density, high ionic conductivity, and low viscosity are preferred.

(2) Another potential way to increase the energy density is to combine RFBs and EFCs, resulting in a high energy density and fast response energy storage system. Hybrid systems with one electrode providing high surface area for high capacitance and the other electrode with LTO for Li^+ intercalation have been reported.[41] Research on a hybrid system using nano-sized active material particles providing both electrochemical storage and capacitive energy storage could be possible and would help achieve relatively high energy and power densities.

(3) Increased operating efficiencies are needed. Operating improvements could be accomplished by reducing the fluid viscosity or investigating surface coatings on the tubing and channels to reduce flow resistance, especially for high loading systems where

the resistance due to the fluid being in contact with the tubing surface may be significant. Solid particle surface modifications were shown effective for reducing the fluid viscosity.[333] Research on lowering viscosity of Li-ion electrolytes explicitly for RFBs has not yet been pursued to the authors' knowledge.

(4) Increasing the electronic conductivity of solid electroactive particles is expected to improve the cell performance.[349] Methods to increase particle electronic conductivity includes changing to intrinsically higher conductivity materials and carbon coating particles,[142, 143, 287, 290] which has previously been demonstrated to improve electrochemical performance for active materials with low conductivities such as LFP and LMO.[255] Electronically conductive polymers may also be beneficial as particle surface coatings, particularly those providing high electronic conductivity as well as energy storage capability.[194, 200] These coatings might also reduce the fluid viscosity, given previous reports of such effects from experiments on the rheological properties of polymer-particle suspensions.[194, 211, 215] The polymer coatings will also need to be conductive to Li ions to be effective.

(5) Safety is always a concern for batteries, but is particularly important for large scale applications such as those suited to RFBs because at larger scales the failures could be catastrophic. A unique issue for RFBs relative to static cells are that clogging and unexpected pressure changes can be potential operating issues, which may cause unexpected failures. The safety concerns of fires and gas generation of Li-ion batteries are of course also relevant to the RFB systems with Li-ion materials and

electrolytes.[354] Future solid electroactive material RFB reports will likely present safety information on these systems, including abuse test and analysis.[355, 356] Fault detectors and/or mitigation strategies will be needed within the battery.[357]

(6) Although almost all RFBs are suited towards large scale applications, no large scale demonstrations have been done with solid electroactive material RFBs to date. Such demonstrations and experiments require significant capital investments; however, intermediate scale battery prototypes will need to be demonstrated in the near term to identify more realistic estimates of operating parameters.

(7) Aqueous – nonaqueous hybrid designs, which have an aqueous suspension as the catholyte and a nonaqueous suspension as the anolyte, are promising because they combine the aqueous suspension high ionic conductivity and low cost with the nonaqueous suspension low operating potential which enables high cell voltages.[74, 75, 358, 359] The key challenge in such a system is designing a membrane compatible with both electrolytes with long lifetime, reliable separation, high and selective ionic conductivity, and low cost.

(8) Battery temperature control is an important component of battery research, particularly for large scale applications to prevent potential safety hazards and ensure long battery lifetimes.[13, 55, 360-363] RFBs have temperature regulation advantages because heat exchangers may be constructed as an additional unit operation seamlessly

integrated with the flowing electrolyte through tubing, as opposed to complicated heat removal systems designed for static battery stacks. The efficiency of such a design for temperature regulation is expected to be tested in the future with flowing solid suspensions.

Overall, RFBs with solid electroactive material suspensions show promise to provide reliable energy storage with high capacity, efficiency, safety, and low cost. This thesis will focus on the demonstration of a Type II system with Li-ion active materials. Both electrochemical properties and rheological properties are characterized for carbon-free organic and aqueous Li-ion active material suspensions. The detailed research is presented in the following chapters.

1.8. Reference

1. *U.S. Battery Mfg. Industry*, in *2014 Industry & Market*. 2014, C. Barnes & Co.: USA.
2. Honda, W., et al., *Wearable, Human-Interactive, Health-Monitoring, Wireless Devices Fabricated by Macroscale Printing Techniques.* Advanced Functional Materials, 2014. **24**(22): p. 3299-3304.
3. *Hybrid and Electric Cars in the United States*, in *MarketLine Industry Profile*. 2015: London, United Kingdom.
4. Mullendore, S., *Energy Storage And Electricity Markets*, in *Resilient Power*. 2015, Clean Energy Group and Meridian Institute.
5. Yan, N.F., G.R. Li, and X.P. Gao, *Solar rechargeable redox flow battery based on Li2WO4/LiI couples in dual-phase electrolytes.* Journal of Materials Chemistry A, 2013. **1**(24): p. 7012-7015.
6. Yang, C.J. and R.B. Jackson, *Opportunities and barriers to pumped-hydro energy storage in the United States.* Renewable & Sustainable Energy Reviews, 2011. **15**(1): p. 839-844.
7. Dunn, B., H. Kamath, and J.M. Tarascon, *Electrical Energy Storage for the Grid: A Battery of Choices.* Science, 2011. **334**(6058): p. 928-935.
8. Dunn, B., H. Kamath, and J.M. Tarascon, *Electrical Energy Storage for the Grid: A Battery of Choices.* Science (Washington, DC, U. S.), 2011. **334**(6058): p. 928-935.
9. Wu, C., *Better batteries for electric vehicles.* Mrs Bulletin, 2010. **35**: p. 650-651.
10. Xu, C., et al., *Secondary batteries with multivalent ions for energy storage.* Sci Rep, 2015. **5**: p. 14120.
11. Yang, Z., et al., *Electrochemical energy storage for green grid.* Chem. Rev. (Washington, DC, U. S.), 2011. **111**(5): p. 3577-613.
12. Whittingham, M.S., *Lithium Batteries and Cathode Materials.* Chemical Reviews, 2004. **104**(10): p. 4271-4301.
13. Lu, L., et al., *A review on the key issues for lithium-ion battery management in electric vehicles.* Journal of Power Sources, 2013. **226**: p. 272-288.
14. Alotto, P., M. Guarnieri, and F. Moro, *Redox flow batteries for the storage of renewable energy: A review.* Renewable and Sustainable Energy Reviews, 2014. **29**: p. 325-335.
15. Yang, Z.G., et al., *Electrochemical Energy Storage for Green Grid.* Chemical Reviews, 2011. **111**(5): p. 3577-3613.
16. Future, C.o.A.s.E., et al., *America's Energy Future: Technology and Transformation: Summary Edition*. 2009, Washington, DC: The National Academies Press.
17. *DOE Global Energy Storage Database*. Available from: https://energy.gov/oe/office-electricity-delivery-and-energy-reliability.
18. Janoschka, T., et al., *An aqueous, polymer-based redox-flow battery using non-corrosive, safe, and low-cost materials.* Nature, 2015. **527**(7576): p. 78-81.
19. Winsberg, J., et al., *Redox-Flow Batteries: From Metals to Organic Redox-Active Materials.* Angew Chem Int Ed Engl, 2017. **56**(3): p. 686-711.

20. Kangro, W., *Verfahren zur Speicherung von elektrischer Energie*, G.p. DE, Editor. 1949: German.
21. Posner, A.M., *Redox fuel cell.* Fuel, 1955. **34**(3): p. 330-8.
22. Soloveichik, G.L., *Flow Batteries: Current Status and Trends.* Chemical Reviews, 2015. **115**(20): p. 11533-11558.
23. Skyllas-Kazacos, M., et al., *Progress in Flow Battery Research and Development.* Journal of the Electrochemical Society, 2011. **158**(8): p. R55-R79.
24. Jia, C., et al., *High-energy density nonaqueous all redox flow lithium battery enabled with a polymeric membrane.* Science Advances, 2015. **1**(10): p. e1500886.
25. Takechi, K., Y. Kato, and Y. Hase, *A highly concentrated catholyte based on a solvate ionic liquid for rechargeable flow batteries.* Adv Mater, 2015. **27**(15): p. 2501-6.
26. Li, Z., et al., *A high-energy and low-cost polysulfide/iodide redox flow battery.* Nano Energy, 2016. **30**: p. 283-292.
27. Duduta, M., et al., *Semi-Solid Lithium Rechargeable Flow Battery.* Adv. Energy Mater., 2011. **1**(4): p. 511-516.
28. *nanoFlowcell AG Achieves Breakthrough in Flow Cell Technology*. 2016, nanoFlowcell AG: Geneva.
29. Winter, M. and R.J. Brodd, *What Are Batteries, Fuel Cells, and Supercapacitors?* Chemical Reviews, 2004. **104**: p. 4245-4269.
30. Rahman, M.A., X. Wang, and C. Wen, *A review of high energy density lithium–air battery technology.* Journal of Applied Electrochemistry, 2013. **44**(1): p. 5-22.
31. Aurbach, D., et al., *Design of electrolyte solutions for Li and Li-ion batteries: a review.* Electrochimica Acta, 2004. **50**(2-3): p. 247-254.
32. Scheers, J., S. Fantini, and P. Johansson, *A review of electrolytes for lithium–sulphur batteries.* Journal of Power Sources, 2014. **255**: p. 204-218.
33. Chikkannanavar, S.B., D.M. Bernardi, and L. Liu, *A review of blended cathode materials for use in Li-ion batteries.* Journal of Power Sources, 2014. **248**: p. 91-100.
34. Manthiram, A., K. Chemelewski, and E.-S. Lee, *A perspective on the high-voltage LiMn1.5Ni0.5O4 spinel cathode for lithium-ion batteries.* Energy & Environmental Science, 2014. **7**(4): p. 1339.
35. Armand, M. and J.M. Tarascon, *Building better batteries.* Nature (London, U. K.), 2008. **451**(7179): p. 652-657.
36. Marks, T., et al., *A Guide to Li-Ion Coin-Cell Electrode Making for Academic Researchers.* Journal of the Electrochemical Society, 2011. **158**(1): p. A51-A57.
37. Daniel, C., *Lithium Ion Batteries and Their Manufacturing Challenges*, in *The Bridge*. 2015, National Academy of Sciences: Washington DC. p. 21-24.
38. Yoshio, M., R.J. Brodd, and A. Kozawa, *Lithium-ion Batteries: Science and Technologies*. 2009: Springer. 452.
39. Kotz, R. and M. Carlen, *Principles and applications of electrochemical capacitors.* Electrochimica Acta, 2000. **45**(15-16): p. 2483-2498.
40. Aravindan, V., et al., *Insertion-type electrodes for nonaqueous Li-ion capacitors.* Chem Rev, 2014. **114**(23): p. 11619-35.

41. Deng, S., et al., *Synthesis and electrochemical properties of Li4Ti5O12 spheres and its application for hybrid supercapacitors.* Electrochimica Acta, 2014. **146**: p. 37-43.
42. Hatzell, K.B., et al., *Composite manganese oxide percolating networks as a suspension electrode for an asymmetric flow capacitor.* ACS Appl Mater Interfaces, 2014. **6**(11): p. 8886-93.
43. Laldin, O., M. Moshirvaziri, and O. Trescases, *Predictive Algorithm for Optimizing Power Flow in Hybrid Ultracapacitor/Battery Storage Systems for Light Electric Vehicles.* Ieee Transactions on Power Electronics, 2013. **28**(8): p. 3882-3895.
44. Vonlanthen, D., et al., *A Stable Polyaniline-Benzoquinone-Hydroquinone Supercapacitor.* Adv Mater, 2014. **26**(30): p. 5095–5100.
45. Chotia, I. and S. Chowdhury, *Battery Storage and Hybrid Battery Supercapacitor Storage Systems: A Comparative Critical Review*, in *2015 Ieee Innovative Smart Grid Technologies - Asia (Isgt Asia)*. 2015, IEEE.
46. Fisher, R.A., M.R. Watt, and W.J. Ready, *Functionalized Carbon Nanotube Supercapacitor Electrodes: A Review on Pseudocapacitive Materials.* Ecs Journal of Solid State Science and Technology, 2013. **2**(10): p. M3170-M3177.
47. Aken, K.L.V. and Y. Gogotsi, *Recent Developments and Prospects of Nanostructured Supercapacitors*, in *Nanotechnology for Energy Sustainability*, B. Raj, M.V.d. Voorde, and Y. Mahajan, Editors. 2017, Wiley-VCH Verlag GmbH & Co. KGaA: Weinheim, Germany.
48. Dees, D., et al., *Electrochemical Modeling of Lithium-Ion Positive Electrodes during Hybrid Pulse Power Characterization Tests.* Journal of The Electrochemical Society, 2008. **155**(8): p. A603-A613.
49. Gallagher, K.G., P.A. Nelson, and D.W. Dees, *Simplified calculation of the area specific impedance for battery design.* Journal of Power Sources, 2011. **196**(4): p. 2289-2297.
50. Suppes, G.J., B.D. Sawyer, and M.J. Gordon, *High-Energy Density Flow Battery Validation.* Aiche Journal, 2011. **57**(7): p. 1961-1967.
51. Gordon, M. and G. Suppes, *Li-Ion Battery Performance in a Convection Cell Configuration.* Aiche Journal, 2013. **59**(5): p. 1774-1779.
52. Gordon, M. and G. Suppes, *Convection battery-modeling, insight, and review.* Aiche Journal, 2013. **59**(8): p. 2833-2842.
53. Schuster, S.F., et al., *Lithium-ion cell-to-cell variation during battery electric vehicle operation.* J. Power Sources, 2015. **297**: p. 242-251.
54. Mahamud, R. and C. Park, *Reciprocating air flow for Li-ion battery thermal management to improve temperature uniformity.* Journal of Power Sources, 2011. **196**(13): p. 5685-5696.
55. Rezvanizaniani, S.M., et al., *Review and recent advances in battery health monitoring and prognostics technologies for electric vehicle (EV) safety and mobility.* Journal of Power Sources, 2014. **256**: p. 110-124.
56. Waag, W., C. Fleischer, and D.U. Sauer, *Critical review of the methods for monitoring of lithium-ion batteries in electric and hybrid vehicles.* Journal of Power Sources, 2014. **258**: p. 321-339.

57. de Leon, C.P., et al., *Redox flow cells for energy conversion.* Journal of Power Sources, 2006. **160**(1): p. 716-732.
58. Weber, A.Z., et al., *Redox flow batteries: a review.* Journal of Applied Electrochemistry, 2011. **41**(10): p. 1137-1164.
59. Wang, W., et al., *Recent Progress in Redox Flow Battery Research and Development.* Advanced Functional Materials, 2013. **23**(8): p. 970-986.
60. Petek, T.J., et al., *Slurry electrodes for iron plating in an all-iron flow battery.* Journal of Power Sources, 2015. **294**: p. 620-626.
61. Kear, G., A.A. Shah, and F.C. Walsh, *Development of the all-vanadium redox flow battery for energy storage: a review of technological, financial and policy aspects.* International Journal of Energy Research, 2012. **36**(11): p. 1105-1120.
62. Janoschka, T., et al., *Aqueous Redox-Flow Battery with High Capacity and Power: The TEMPTMA/MV System.* Angew Chem Int Ed Engl, 2016. **55**: p. 1-5.
63. *VionX Energy Distributed Energy Storage System Project Description*. 2015; Available from: https://www.smartgrid.gov/document/premium_power_distributed_energy_storage_system.html.
64. *Rongke Power 5MW/10MWh VFB Energy Storage System successfully finish power transmission to Liaoning Power Grid*. Available from: http://www.rongkepower.com/index.php/article/show/id/140/language/en.
65. Zhao, Y., et al., *A chemistry and material perspective on lithium redox flow batteries towards high-density electrical energy storage.* Chemical Society Reviews, 2015. **44**(22): p. 7968-7996.
66. Huang, Q. and Q. Wang, *Next-Generation, High-Energy-Density Redox Flow Batteries.* ChemPlusChem, 2015. **80**(2): p. 312-322.
67. Gong, K., et al., *Nonaqueous redox-flow batteries: organic solvents, supporting electrolytes, and redox pairs.* Energy Environ. Sci., 2015. **8**(12): p. 3515-3530.
68. Mubeen, S., et al., *Solid Suspension Flow Batteries Using Earth Abundant Materials.* Acs Applied Materials & Interfaces, 2016. **8**(3): p. 1759-1765.
69. Li, X.M., et al., *Nanostructured catalysts for electrochemical water splitting: current state and prospects.* Journal of Materials Chemistry A, 2016. **4**(31): p. 11973-12000.
70. Shinkle, A.A., et al., *Degradation mechanisms in the non-aqueous vanadium acetylacetonate redox flow battery.* Journal of Power Sources, 2012. **206**: p. 490-496.
71. Brushett, F.R., J.T. Vaughey, and A.N. Jansen, *An All-Organic Non-aqueous Lithium-Ion Redox Flow Battery.* Advanced Energy Materials, 2012. **2**(11): p. 1390-1396.
72. Kaur, A.P., et al., *A Highly Soluble Organic Catholyte for Non-Aqueous Redox Flow Batteries.* Energy Technology, 2015. **3**(5): p. 476-480.
73. Darling, R.M., et al., *Pathways to low-cost electrochemical energy storage: a comparison of aqueous and nonaqueous flow batteries.* Energy & Environmental Science, 2014. **7**(11): p. 3459-3477.
74. Lu, Y.H. and J.B. Goodenough, *Rechargeable alkali-ion cathode-flow battery.* Journal of Materials Chemistry, 2011. **21**(27): p. 10113-10117.

75. Wang, Y., P. He, and H. Zhou, *Li-Redox Flow Batteries Based on Hybrid Electrolytes: At the Cross Road between Li-ion and Redox Flow Batteries.* Advanced Energy Materials, 2012. **2**(7): p. 770-779.
76. Hamelet, S., et al., *Non-Aqueous Li-Based Redox Flow Batteries.* Journal of the Electrochemical Society, 2012. **159**(8): p. A1360-A1367.
77. Lin, K., et al., *Alkaline quinone flow battery.* Science, 2015. **349**(6255): p. 1529-32.
78. Winsberg, J., et al., *Aqueous 2,2,6,6-Tetramethylpiperidine-N-oxyl Catholytes for a High-Capacity and High Current Density Oxygen-Insensitive Hybrid-Flow Battery.* Acs Energy Letters, 2017. **2**(2): p. 411-416.
79. Hu, B., et al., *Long-Cycling Aqueous Organic Redox Flow Battery (AORFB) toward Sustainable and Safe Energy Storage.* J Am Chem Soc, 2017. **139**: p. 1207-1204.
80. Huskinson, B., et al., *A metal-free organic-inorganic aqueous flow battery.* Nature, 2014. **505**(7482): p. 195-8.
81. Beh, E.S., et al., *A Neutral pH Aqueous Organic-Organometallic Redox Flow Battery with Extremely High Capacity Retention.* Acs Energy Letters, 2017. **2**(3): p. 639-644.
82. Lin, K.X., et al., *A redox-flow battery with an alloxazine-based organic electrolyte.* Nature Energy, 2016. **1**.
83. Li, B., et al., *Ambipolar zinc-polyiodide electrolyte for a high-energy density aqueous redox flow battery.* Nature Communications, 2015. **6**.
84. Wei, X.L., et al., *TEMPO-Based Catholyte for High-Energy Density Nonaqueous Redox Flow Batteries.* Advanced Materials, 2014. **26**(45): p. 7649-7653.
85. Weng, G.M., et al., *Unlocking the capacity of iodide for high-energy-density zinc/polyiodide and lithium/polyiodide redox flow batteries.* Energy & Environmental Science, 2017. **10**(3): p. 735-741.
86. Rahman, F. and M. Skyllas-Kazacos, *Vanadium redox battery: Positive half-cell electrolyte studies.* Journal of Power Sources, 2009. **189**(2): p. 1212-1219.
87. Pratt, H.D., et al., *Synthesis and characterization of ionic liquids containing copper, manganese, or zinc coordination cations.* Dalton Transactions, 2011. **40**(43): p. 11396-11401.
88. Cong, G., et al., *A Highly Concentrated Catholyte Enabled by a Low-Melting-Point Ferrocene Derivative.* ACS Energy Letters, 2017. **2**(4): p. 869-875.
89. Bai, P. and M.Z. Bazant, *Performance and Degradation of A Lithium-Bromine Rechargeable Fuel Cell Using Highly Concentrated Catholytes.* Electrochimica Acta, 2016. **202**: p. 216-223.
90. Presser, V., et al., *The Electrochemical Flow Capacitor: A New Concept for Rapid Energy Storage and Recovery.* Advanced Energy Materials, 2012. **2**(7): p. 895-902.
91. Campos, J.W., et al., *Investigation of carbon materials for use as a flowable electrode in electrochemical flow capacitors.* Electrochimica Acta, 2013. **98**: p. 123-130.
92. Porada, S., et al., *Continuous operation of an electrochemical flow capacitor.* Electrochemistry Communications, 2014. **48**: p. 178-181.

93. Keblinski, P., J.A. Eastman, and D.G. Cahill, *Nanofluids for thermal transport.* Materials Today, 2005. **8**(6): p. 36-44.
94. Mueller, S., E.W. Llewellin, and H.M. Mader, *The rheology of suspensions of solid particles.* Proceedings of the Royal Society A: Mathematical, Physical and Engineering Sciences, 2009. **466**(2116): p. 1201-1228.
95. Besra, L. and M. Liu, *A review on fundamentals and applications of electrophoretic deposition (EPD).* Progress in Materials Science, 2007. **52**(1): p. 1-61.
96. van Dinther, A.M.C., et al., *Suspension flow in microfluidic devices - A review of experimental techniques focussing on concentration and velocity gradients.* Advances in Colloid and Interface Science, 2012. **173**: p. 23-34.
97. Fabian, D.M., et al., *Particle suspension reactors and materials for solar-driven water splitting.* Energy & Environmental Science, 2015. **8**(10): p. 2825-2850.
98. Ohshima, H., *Electrical conductivity of a concentrated suspension of spherical colloidal particles.* Journal of Colloid and Interface Science, 1999. **212**(2): p. 443-448.
99. Dennison, C.R., et al., *Effects of flow cell design on charge percolation and storage in the carbon slurry electrodes of electrochemical flow capacitors.* Journal of Power Sources, 2014. **247**: p. 489-496.
100. Lee, J.H., et al., *Use of Surfactants for Continuous Operation of Aqueous Electrochemical Flow Capacitors.* Energy Technology, 2016. **4**(1): p. 75-84.
101. Hoyt, N.C., J.S. Wainright, and R.F. Savinell, *Current Density Scaling in Electrochemical Flow Capacitors.* Journal of the Electrochemical Society, 2015. **162**(6): p. A1102-A1110.
102. Hoyt, N.C., J.S. Wainright, and R.F. Savinell, *Mathematical Modeling of Electrochemical Flow Capacitors.* Journal of the Electrochemical Society, 2015. **162**(4): p. A652-A657.
103. Boota, M., et al., *Activated Carbon Spheres as a Flowable Electrode in Electrochemical Flow Capacitors.* Journal of the Electrochemical Society, 2014. **161**(6): p. A1078-A1083.
104. Hatzell, K.B., M. Boota, and Y. Gogotsi, *Materials for suspension (semi-solid) electrodes for energy and water technologies.* Chemical Society Reviews, 2015. **44**(23): p. 8664-8687.
105. Jeon, S.-i., et al., *Desalination via a new membrane capacitive deionization process utilizing flow-electrodes.* Energy & Environmental Science, 2013. **6**(5): p. 1471.
106. Porada, S., et al., *Carbon flow electrodes for continuous operation of capacitive deionization and capacitive mixing energy generation.* Journal of Materials Chemistry A, 2014. **2**(24): p. 9313-9321.
107. Hatzell, K.B. and Y. Gogotsi, *Suspension Electrodes for Flow-Assisted Electrochemical Systems*, in *Nanomaterials in Advanced Batteries and Supercapacitors*, K.I. Ozoemena and S. Chen, Editors. 2016, Springer International Publishing: Cham. p. 377-416.
108. Thamilselvan, A., A.S. Nesaraj, and M. Noel, *Review on carbon-based electrode materials for application in capacitive deionization process.* International Journal of Environmental Science and Technology, 2016. **13**(12): p. 2961-2976.

109. Jeon, S.I., et al., *Desalination via a new membrane capacitive deionization process utilizing flow-electrodes.* Energy & Environmental Science, 2013. **6**(5): p. 1471-1475.
110. Yang, S., et al., *Flow-Electrode Capacitive Deionization Using an Aqueous Electrolyte with a High Salt Concentration.* Environmental Science & Technology, 2016. **50**(11): p. 5892-5899.
111. Oren, Y., *Capacitive delonization (CDI) for desalination and water treatment - past, present and future (a review).* Desalination, 2008. **228**(1-3): p. 10-29.
112. Porada, S., et al., *Review on the science and technology of water desalination by capacitive deionization.* Progress in Materials Science, 2013. **58**(8): p. 1388-1442.
113. AlMarzooqi, F.A., et al., *Application of Capacitive Deionisation in water desalination: A review.* Desalination, 2014. **342**: p. 3-15.
114. Gyuk, I., et al., *Grid Energy Storage*. 2013, U.S. Department of Energy, Office of Electricity Delivery & Energy Reliability: Washington, DC.
115. Darling, R.M., et al., *Pathways to low-cost electrochemical energy storage: a comparison of aqueous and nonaqueous flow batteries.* Energy Environ. Sci., 2014. **7**(11): p. 3459-3477.
116. Viswanathan, V., et al., *Cost and performance model for redox flow batteries.* Journal of Power Sources, 2014. **247**: p. 1040-1051.
117. Zhang, H.P., et al., *A hybrid redox flow battery with high energy efficiency using a low cost sandwiched membrane as a separator and LiMn2O4 as a cathode.* Journal of Materials Chemistry A, 2013. **1**(46): p. 14476-14479.
118. Ding, Y., Y. Zhao, and G. Yu, *A Membrane-Free Ferrocene-Based High-Rate Semiliquid Battery.* Nano Lett, 2015. **15**(6): p. 4108-4113.
119. Yang, Y., G.Y. Zheng, and Y. Cui, *A membrane-free lithium/polysulfide semi-liquid battery for large-scale energy storage.* Energy & Environmental Science, 2013. **6**(5): p. 1552-1558.
120. Iordache, A., et al., *Monothioanthraquinone as an organic active material for greener lithium batteries.* Journal of Power Sources, 2014. **267**: p. 553-559.
121. Xing, F., H. Zhang, and X. Ma, *Shunt current loss of the vanadium redox flow battery.* Journal of Power Sources, 2011. **196**(24): p. 10753-10757.
122. Chakrabarti, M.H., et al., *Application of carbon materials in redox flow batteries.* Journal of Power Sources, 2014. **253**: p. 150-166.
123. Hatzell, K.B., et al., *Effect of oxidation of carbon material on suspension electrodes for flow electrode capacitive deionization.* Environ Sci Technol, 2015. **49**(5): p. 3040-7.
124. D.D.L.CHUNG, *Electrical applications of carbon materials.* Journal of Materials Science, 2004. **39**: p. 2645-2661.
125. Fan, F.Y., et al., *Polysulfide flow batteries enabled by percolating nanoscale conductor networks.* Nano Lett, 2014. **14**(4): p. 2210-8.
126. Chen, H.N., et al., *Sulphur-impregnated flow cathode to enable high-energy-density lithium flow batteries.* Nature Communications, 2015. **6**: p. 5877.
127. Ruggeri, I., C. Arbizzani, and F. Soavi, *A novel concept of Semi-solid, Li Redox Flow Air (O2) Battery: a breakthrough towards high energy and power batteries.* Electrochimica Acta, 2016. **206**: p. 291-300.

128. Dong, K., S.P. Wang, and J.X. Yu, *A lithium/polysulfide semi-solid rechargeable flow battery with high output performance.* Rsc Advances, 2014. **4**(88): p. 47517-47520.
129. Ventosa, E., et al., *Non-aqueous semi-solid flow battery based on Na-ion chemistry. P2-type NaxNi0.22Co0.11Mn0.66O2-NaTi2(PO4)(3).* Chemical Communications, 2015. **51**(34): p. 7298-7301.
130. Hamelet, S., et al., *Silicon-Based Non Aqueous Anolyte for Li Redox-Flow Batteries.* Journal of the Electrochemical Society, 2013. **160**(3): p. A516-A520.
131. Wei, T.S., et al., *Biphasic Electrode Suspensions for Li-Ion Semi-solid Flow Cells with High Energy Density, Fast Charge Transport, and Low-Dissipation Flow.* Advanced Energy Materials, 2015. **5**(15): p. 1500535.
132. Li, Z., et al., *Aqueous semi-solid flow cell: demonstration and analysis.* Physical Chemistry Chemical Physics, 2013. **15**(38): p. 15833-15839.
133. Biendicho, J.J., et al., *Static and Dynamic Studies on LiNi1/3Co1/3Mn1/3O2-Based Suspensions for Semi-Solid Flow Batteries.* Chemsuschem, 2016. **9**(15): p. 1938-1944.
134. LeVine, S., *The story of the invention that could revolutionize batteries—and maybe American manufacturing as well*, in *Quartz*. 2015, Quartz Media LLC.
135. Mekonnen, Y., A. Sundararajan, and A.I. Sarwat, *A Review of Cathode and Anode Materials for Lithium-Ion Batteries*, in *Southeastcon 2016*. 2016, IEEE.
136. Hong, S.-K., et al., *Structural and electrochemical characteristics of morphology-controlled Li[Ni0.5Mn1.5]O4 cathodes.* Electrochim. Acta, 2015. **156**: p. 29-37.
137. Liu, G.Q., L. Wen, and Y.M. Liu, *Spinel LiNi0.5Mn1.5O4 and its derivatives as cathodes for high-voltage Li-ion batteries.* Journal of Solid State Electrochemistry, 2010. **14**(12): p. 2191-2202.
138. Youssry, M., et al., *Non-aqueous carbon black suspensions for lithium-based redox flow batteries: rheology and simultaneous rheo-electrical behavior.* Phys Chem Chem Phys, 2013. **15**(34): p. 14476-86.
139. Li, W.Y., et al., *Magnetic Field-Controlled Lithium Polysulfide Semiliquid Battery with Ferrofluidic Properties.* Nano Letters, 2015. **15**(11): p. 7394-7399.
140. Sen, S., et al., *Surface Modification Approach to TiO2 Nanofluids with High Particle Concentration, Low Viscosity, and Electrochemical Activity.* ACS Appl Mater Interfaces, 2015. **7**(37): p. 20538-47.
141. Li, J.L., et al., *Optimization of LiFePO4 Nanoparticle Suspensions with Polyethyleneimine for Aqueous Processing.* Langmuir, 2012. **28**(8): p. 3783-3790.
142. Wang, J. and X. Sun, *Understanding and recent development of carbon coating on LiFePO4 cathode materials for lithium-ion batteries.* Energy & Environmental Science, 2012. **5**(1): p. 5163.
143. Kim, J.-K., et al., *Effect of carbon coating methods on structural characteristics and electrochemical properties of carbon-coated lithiumiron phosphate.* Solid State Ionics, 2014. **262**: p. 25-29.
144. Smith, K.C., et al., *Electroactive-Zone Extension in Flow-Battery Stacks.* Electrochimica Acta, 2014. **147**: p. 460-469.
145. Tang, A., et al., *Investigation of the effect of shunt current on battery efficiency and stack temperature in vanadium redox flow battery.* Journal of Power Sources, 2013. **242**: p. 349-356.

146. Butler, P.C., et al., *ZINC/BROMINE BATTERIES*, in *Handbook of Batteries*, D. Linden and T.B. Reddy, Editors. 2002, The McGraw-Hill Companies, Inc.
147. Qi, Z. and G.M. Koenig, *A carbon-free lithium-ion solid dispersion redox couple with low viscosity for redox flow batteries.* J. Power Sources, 2016. **323**: p. 97-106.
148. Qi, Z., A.L. Liu, and G.M.K. Jr., *Carbon-free Solid Dispersion LiCoO2 Redox Couple Characterization and Electrochemical Evaluation for All Solid Dispersion Redox Flow Batteries.* Electrochimica Acta, 2017. **228**: p. 91-99.
149. Dokko, K., et al., *In situ Raman spectroscopy of single microparticle Li+-intercalation electrodes.* Journal of Physical Chemistry B, 2003. **107**(46): p. 12549-12554.
150. Palencsar, A. and D.A. Scherson, *Electrochemical and in situ optical characterization of single micrometer-size particles of spherical nickel oxide in alkaline aqueous electrolytes.* Electrochemical and Solid State Letters, 2003. **6**(4): p. E1-E4.
151. Rees, N.V., *Electrochemical insight from nanoparticle collisions with electrodes: A mini-review.* Electrochemistry Communications, 2014. **43**: p. 83-86.
152. Ko, J.K., et al., *Transport, phase reactions, and hysteresis of iron fluoride and oxyfluoride conversion electrode materials for lithium batteries.* ACS Appl Mater Interfaces, 2014. **6**(14): p. 10858-69.
153. Suraniti, E., et al., *Electrochemical detection of single microbeads manipulated by optical tweezers in the vicinity of ultramicroelectrodes.* Anal Chem, 2013. **85**(19): p. 8902-9.
154. Fosdick, S.E., et al., *Correlated electrochemical and optical tracking of discrete collision events.* J Am Chem Soc, 2013. **135**(16): p. 5994-7.
155. Guo, Z., S.J. Percival, and B. Zhang, *Chemically resolved transient collision events of single electrocatalytic nanoparticles.* J Am Chem Soc, 2014. **136**(25): p. 8879-82.
156. Dasari, R., et al., *Influence of the redox indicator reaction on single-nanoparticle collisions at mercury- and bismuth-modified Pt ultramicroelectrodes.* Langmuir, 2013. **29**(48): p. 15100-6.
157. Chen, C.H., et al., *Impact of Surface Chemistry on Nanoparticle-Electrode Interactions in the Electrochemical Detection of Nanoparticle Collisions.* Langmuir, 2015. **31**: p. 11932-11942.
158. Kim, J., et al., *Tunneling ultramicroelectrode: nanoelectrodes and nanoparticle collisions.* J Am Chem Soc, 2014. **136**(23): p. 8173-6.
159. Alligrant, T.M., et al., *Single nanoparticle collisions at microfluidic microband electrodes: the effect of electrode material and mass transfer.* Langmuir, 2014. **30**(44): p. 13462-9.
160. Fernando, A., S. Parajuli, and M.A. Alpuche-Aviles, *Observation of individual semiconducting nanoparticle collisions by stochastic photoelectrochemical currents.* J Am Chem Soc, 2013. **135**(30): p. 10894-7.
161. Rees, N.V., Y.G. Zhou, and R.G. Compton, *Making contact: charge transfer during particle-electrode collisions.* Rsc Advances, 2012. **2**(2): p. 379-384.

162. Qiu, D., et al., *One at a time: counting single-nanoparticle/electrode collisions for accurate particle sizing by overcoming the instability of gold nanoparticles under electrolytic conditions.* Nanotechnology, 2013. **24**(50): p. 505707.
163. Cheng, W., X.F. Zhou, and R.G. Compton, *Electrochemical Sizing of Organic Nanoparticles.* Angewandte Chemie-International Edition, 2013. **52**(49): p. 12980-12982.
164. Stuart, E.J.E., et al., *Electrochemical Observation of Single Collision Events: Fullerene Nanoparticles.* ACS Nano, 2014. **8**(8): p. 7648–7654.
165. Wang, Q., et al., *Redox targeting of insulating electrode materials: A new approach to high-energy-density batteries.* Angewandte Chemie-International Edition, 2006. **45**(48): p. 8197-8200.
166. Huang, Q.Z., et al., *Reversible chemical delithiation/lithiation of LiFePO4: towards a redox flow lithium-ion battery.* Physical Chemistry Chemical Physics, 2013. **15**(6): p. 1793-1797.
167. Pan, F., et al., *Redox Targeting of Anatase TiO2for Redox Flow Lithium-Ion Batteries.* Advanced Energy Materials, 2014. **4**(15): p. 1400567.
168. Huang, Q.Z., et al., *A redox flow lithium battery based on the redox targeting reactions between LiFePO4 and iodide.* Energy & Environmental Science, 2016. **9**(3): p. 917-921.
169. Sharma, A.K., et al., *Mathematical modeling and experiments of a half-cell redox flow lithium ion battery system.* Electrochimica Acta, 2016. **204**: p. 1-8.
170. Li, J., et al., *The Application of Redox Targeting Principles to the Design of Rechargeable Li-S Flow Batteries.* Advanced Energy Materials, 2015. **5**(24): p. 1501808.
171. Perry, M.L. and A.Z. Weber, *Advanced Redox-Flow Batteries: A Perspective.* Journal of the Electrochemical Society, 2016. **163**(1): p. A5064-A5067.
172. Rychcik, M. and M. Skyllas-Kazacos, *Characteristics of a New All-Vanadium Redox Flow Battery.* Journal of Power Sources, 1988. **22**(1): p. 59-67.
173. Cappillino, P.J., et al., *Application of Redox Non-Innocent Ligands to Non-Aqueous Flow Battery Electrolytes.* Advanced Energy Materials, 2014. **4**(1): p. 1300566.
174. Yamamura, T., et al., *Characterization of tetraketone ligands for active materials of all-uranium redox flow battery.* Journal of Alloys and Compounds, 2004. **374**(1-2): p. 349-353.
175. Park, J.W., et al., *Nonaqueous redox flow battery employing redox couples with aromatic ligands.* Abstracts of Papers of the American Chemical Society, 2011. **242**.
176. Frost, P.C., *Developments in lead-acid batteries: a lead producer's perspective.* Journal of Power Sources, 1999. **78**(1-2): p. 256-266.
177. Jung, J., *Lead-Acid Battery*, in *Electrochemical Technologies for Energy Storage and Conversion*, R.-S. Liu, et al., Editors. 2012, Wiley-VCH Verlag GmbH & Co.KGaA: Weinheim, Germany.
178. Zeng, Y.K., et al., *A novel iron-lead redox flow battery for large-scale energy storage.* Journal of Power Sources, 2017. **346**: p. 97-102.

179. Pletcher, D. and R. Wills, *A novel flow battery: A lead acid battery based on an electrolyte with soluble lead(II) - Part II. Flow cell studies.* Physical Chemistry Chemical Physics, 2004. **6**(8): p. 1779-1785.
180. Verde, M.G., et al., *Achieving high efficiency and cyclability in inexpensive soluble lead flow batteries.* Energy & Environmental Science, 2013. **6**(5): p. 1573-1581.
181. Pletcher, D. and R. Wills, *A novel flow battery - A lead acid battery based on an electrolyte with soluble lead(II) - III. The influence of conditions on battery performance.* Journal of Power Sources, 2005. **149**: p. 96-102.
182. Collins, J., et al., *A novel flow battery: A lead acid battery based on an electrolyte with soluble lead(II). Part IX: Electrode and electrolyte conditioning with hydrogen peroxide.* Journal of Power Sources, 2010. **195**(9): p. 2975-2978.
183. Collins, J., et al., *A novel flow battery: A lead acid battery based on an electrolyte with soluble lead(II) Part VIII. The cycling of a 10 cm x 10 cm flow cell.* Journal of Power Sources, 2010. **195**(6): p. 1731-1738.
184. Dong, J.X., et al., *A study on Pb2+/Pb electrodes for soluble lead redox flow cells prepared with methanesulfonic acid and recycled lead.* Journal of Applied Electrochemistry, 2016. **46**(8): p. 861-868.
185. Cheng, J., et al., *Preliminary study of single flow zinc-nickel battery.* Electrochemistry Communications, 2007. **9**(11): p. 2639-2642.
186. Zhang, L., et al., *Study of zinc electrodes for single flow zinc/nickel battery application.* Journal of Power Sources, 2008. **179**(1): p. 381-387.
187. Ito, Y., et al., *Zinc morphology in zinc-nickel flow assisted batteries and impact on performance.* Journal of Power Sources, 2011. **196**(4): p. 2340-2345.
188. Cheng, Y.H., et al., *A high power density single flow zinc-nickel battery with three-dimensional porous negative electrode.* Journal of Power Sources, 2013. **241**: p. 196-202.
189. Ito, Y., et al., *Gas evolution in a flow-assisted zinc-nickel oxide battery.* Journal of Power Sources, 2011. **196**(15): p. 6583-6587.
190. Lai, Q.Z., et al., *A novel single flow zinc-bromine battery with improved energy density.* Journal of Power Sources, 2013. **235**: p. 1-4.
191. Zhang, L.Q., et al., *A High-Energy-Density Redox Flow Battery based on Zinc/Polyhalide Chemistry.* Chemsuschem, 2012. **5**(5): p. 867-869.
192. Leung, P.K., et al., *Characterization of a zinc-cerium flow battery.* Journal of Power Sources, 2011. **196**(11): p. 5174-5185.
193. Xie, Z.P., et al., *The developments and challenges of cerium half-cell in zinc-cerium redox flow battery for energy storage.* Electrochimica Acta, 2013. **90**: p. 695-704.
194. Zhao, Y.F., S.H. Si, and C. Liao, *A single flow zinc//polyaniline suspension rechargeable battery.* Journal of Power Sources, 2013. **241**: p. 449-453.
195. Sanz, L., et al., *Description and performance of a novel aqueous all-copper redox flow battery.* Journal of Power Sources, 2014. **268**: p. 121-128.
196. Lloyd, D., T. Vainikka, and K. Kontturi, *The development of an all copper hybrid redox flow battery using deep eutectic solvents.* Electrochimica Acta, 2013. **100**: p. 18-23.

197. Pan, J.Q., et al., *Study on a new single flow acid Cu-PbO2 battery.* Electrochemistry Communications, 2008. **10**(9): p. 1226-1229.
198. Xu, Y., et al., *Study on a single flow acid Cd-chloranil battery.* Electrochemistry Communications, 2009. **11**(7): p. 1422-1424.
199. Cheng, F.Y., et al., *High-power alkaline Zn-MnO(2) batteries using gamma-MnO2 nanowires/nanotubes and electrolytic zinc powder.* Advanced Materials, 2005. **17**(22): p. 2753–2756.
200. Zhao, Y.F., et al., *Electrochemical study on polypyrrole microparticle suspension as flowing anode for manganese dioxide rechargeable flow battery.* Journal of Power Sources, 2014. **248**: p. 962-968.
201. Hruska, L.W. and R.F. Savinell, *Investigation of Factors Affecting Performance of the Iron-Redox Battery.* Journal of the Electrochemical Society, 1981. **128**(1): p. 18-25.
202. Burgess, M., J.S. Moore, and J. Rodriguez-Lopez, *Redox Active Polymers as Soluble Nanomaterials for Energy Storage.* Accounts of Chemical Research, 2016. **49**(11): p. 2649-2657.
203. Montoto, E.C., et al., *Redox Active Colloids as Discrete Energy Storage Carriers.* J Am Chem Soc, 2016. **138**: p. 13230-13237.
204. Youssry, M., et al., *Formulation of flowable anolyte for redox flow batteries: Rheo-electrical study.* Journal of Power Sources, 2015. **274**: p. 424-431.
205. Jugovic, B.Z., et al., *Novel electrolyte for zinc-polyaniline batteries.* Journal of Power Sources, 2006. **160**(2): p. 1447-1450.
206. Dearmitt, C. and S.P. Armes, *Synthesis of Novel Polyaniline Colloids Using Chemically Grafted Poly(N-Vinylpyrrolidone)-Based Stabilizers.* Journal of Colloid and Interface Science, 1992. **150**(1): p. 134-142.
207. Wu, S., et al., *An asymmetric Zni//Ag doped polyaniline microparticle suspension flow battery with high discharge capacity.* Journal of Power Sources, 2015. **275**: p. 305-311.
208. Karami, H., M.F. Mousavi, and M. Shamsipur, *A new design for dry polyaniline rechargeable batteries.* Journal of Power Sources, 2003. **117**(1-2): p. 255-259.
209. Armes, S.P., et al., *Aqueous Colloidal Dispersions of Polyaniline Formed by Using Poly(Vinylpyridine)-Based Steric Stabilizers.* Langmuir, 1990. **6**(12): p. 1745-1749.
210. Armes, S.P., J.F. Miller, and B. Vincent, *Aqueous Dispersions of Electrically Conducting Monodisperse Polypyrrole Particles.* Journal of Colloid and Interface Science, 1987. **118**(2): p. 410-416.
211. Zhao, Y.F., et al., *Electrochemical Behavior of Polyaniline Microparticle Suspension as Flowing Anode for Rechargeable Lead Dioxide Flow Battery.* Journal of the Electrochemical Society, 2014. **161**(3): p. A330-A335.
212. Armes, S.P. and B. Vincent, *Dispersions of Electrically Conducting Polypyrrole Particles in Aqueous-Media.* Journal of the Chemical Society-Chemical Communications, 1987(4): p. 288-290.
213. Bjorklund, R.B. and B. Liedberg, *Electrically Conducting Composites of Colloidal Polypyrrole and Methylcellulose.* Journal of the Chemical Society-Chemical Communications, 1986(16): p. 1293-1295.

214. Oh, S.H., et al., *A metal-free and all-organic redox flow battery with polythiophene as the electroactive species.* Journal of Materials Chemistry A, 2014. **2**(47): p. 19994-19998.
215. Winsberg, J., et al., *Polymer/zinc hybrid-flow battery using block copolymer micelles featuring a TEMPO corona as catholyte.* Polymer Chemistry, 2016. **7**(9): p. 1711-1718.
216. Crowther, O. and A.C. West, *Effect of electrolyte composition on lithium dendrite growth.* Journal of the Electrochemical Society, 2008. **155**(11): p. A806-A811.
217. Na, W., et al., *Lithium Dendrite Suppression with UV-Curable Polysilsesquioxane Separator Binders.* Acs Applied Materials & Interfaces, 2016. **8**(20): p. 12852-12858.
218. Manthiram, A., et al., *Rechargeable Lithium-Sulfur Batteries.* Chemical Reviews, 2014. **114**(23): p. 11751-11787.
219. Zhang, B., et al., *Enhancement of long stability of sulfur cathode by encapsulating sulfur into micropores of carbon spheres.* Energy & Environmental Science, 2010. **3**(10): p. 1531-1537.
220. Li, X.L., et al., *Optimization of mesoporous carbon structures for lithium-sulfur battery applications.* Journal of Materials Chemistry, 2011. **21**(41): p. 16603-16610.
221. Su, Y.S., Y.Z. Fu, and A. Manthiram, *Self-weaving sulfur-carbon composite cathodes for high rate lithium-sulfur batteries.* Physical Chemistry Chemical Physics, 2012. **14**(42): p. 14495-14499.
222. Zheng, W., et al., *Novel nanosized adsorbing sulfur composite cathode materials for the advanced secondary lithium batteries.* Electrochimica Acta, 2006. **51**(7): p. 1330-1335.
223. Liang, C.D., N.J. Dudney, and J.Y. Howe, *Hierarchically Structured Sulfur/Carbon Nanocomposite Material for High-Energy Lithium Battery.* Chemistry of Materials, 2009. **21**(19): p. 4724-4730.
224. Brun, N., et al., *Hydrothermal carbon-based nanostructured hollow spheres as electrode materials for high-power lithium-sulfur batteries.* Physical Chemistry Chemical Physics, 2013. **15**(16): p. 6080-6087.
225. Cheon, S.E., et al., *Rechargeable lithium sulfur battery - I. Structural change of sulfur cathode during discharge and charge.* Journal of the Electrochemical Society, 2003. **150**(6): p. A796-A799.
226. Pan, H.L., et al., *On the Way Toward Understanding Solution Chemistry of Lithium Polysulfides for High Energy Li-S Redox Flow Batteries.* Advanced Energy Materials, 2015. **5**(16): p. 1500113.
227. Li, C.Y., et al., *Polysulfide-Blocking Microporous Polymer Membrane Tailored for Hybrid Li-Sulfur Flow Batteries.* Nano Letters, 2015. **15**(9): p. 5724-5729.
228. Chen, X.W., et al., *A low-dissipation, pumpless, gravity-induced flow battery.* Energy & Environmental Science, 2016. **9**(5): p. 1760-1770.
229. Zhang, S.S., *Liquid electrolyte lithium/sulfur battery: Fundamental chemistry, problems, and solutions.* Journal of Power Sources, 2013. **231**: p. 153-162.
230. Jin, Z.Q., et al., *Application of lithiated Nafion ionomer film as functional separator for lithium sulfur cells.* Journal of Power Sources, 2012. **218**: p. 163-167.

231. Jin, Z.Q., K. Xie, and X.B. Hong, *Electrochemical performance of lithium/sulfur batteries using perfluorinated ionomer electrolyte with lithium sulfonyl dicyanomethide functional groups as functional separator.* Rsc Advances, 2013. **3**(23): p. 8889-8898.
232. Shin, E.S., et al., *Polysulfide dissolution control: the common ion effect.* Chemical Communications, 2013. **49**(20): p. 2004-2006.
233. Suo, L.M., et al., *A new class of Solvent-in-Salt electrolyte for high-energy rechargeable metallic lithium batteries.* Nature Communications, 2013. **4**: p. 1481.
234. Park, J.W., et al., *Ionic Liquid Electrolytes for Lithium-Sulfur Batteries.* Journal of Physical Chemistry C, 2013. **117**(40): p. 20531-20541.
235. Wu, F., et al., *Ionic liquid-based electrolyte with binary lithium salts for high performance lithium-sulfur batteries.* Journal of Power Sources, 2015. **296**: p. 10-17.
236. Ji, X.L., et al., *Spatially heterogeneous carbon-fiber papers as surface dendrite-free current collectors for lithium deposition.* Nano Today, 2012. **7**(1): p. 10-20.
237. Zhamu, A., et al., *Reviving rechargeable lithium metal batteries: enabling next-generation high-energy and high-power cells.* Energy & Environmental Science, 2012. **5**(2): p. 5701-5707.
238. Manthiram, A., Y.Z. Fu, and Y.S. Su, *Challenges and Prospects of Lithium-Sulfur Batteries.* Accounts of Chemical Research, 2013. **46**(5): p. 1125-1134.
239. Fedorkova, A., et al., *New Composite Cathode Materials for Li/S Batteries: A Review.* International Journal of Electrochemical Science, 2013. **8**(8): p. 10308-10319.
240. Zhang, Y.D., et al., *High-energy cathode materials for Li-ion batteries: A review of recent developments.* Science China-Technological Sciences, 2015. **58**(11): p. 1809-1828.
241. Wu, H.X., Q.J. Liu, and S.W. Guo, *Composites of Graphene and LiFePO4 as Cathode Materials for Lithium-Ion Battery: A Mini-review.* Nano-Micro Letters, 2014. **6**(4): p. 316-326.
242. Ouml;rnek, A., M. Can, and A. Yesildag, *Improving the cycle stability of LiCoPO4 nanocomposites as 4.8 V cathode: Stepwise or synchronous surface coating and Mn substitution.* Materials Characterization, 2016. **116**: p. 76-83.
243. Rui, X.H., et al., *Li3V2(PO4)(3) cathode materials for lithium-ion batteries: A review.* Journal of Power Sources, 2014. **258**: p. 19-38.
244. Patoux, S., et al., *High voltage spinel oxides for Li-ion batteries: From the material research to the application.* Journal of Power Sources, 2009. **189**(1): p. 344-352.
245. Kim, J., et al., *Electrochemical Properties of Li1+xCoO2 Synthesized for All-Solid-State Lithium Ion Batteries with Li2S-P2S5 Glass-Ceramics Electrolyte.* J. Electrochem. Soc., 2015. **162**(6): p. A1041-A1045.
246. Otoyama, M., et al., *Raman imaging for LiCoO2 composite positive electrodes in all-solid-state lithium batteries using Li2S–P2S5 solid electrolytes.* Journal of Power Sources, 2016. **302**: p. 419-425.

247. Ensling, D., et al., *Nonrigid Band Behavior of the Electronic Structure of LiCoO2Thin Film during Electrochemical Li Deintercalation.* Chemistry of Materials, 2014. **26**(13): p. 3948-3956.
248. Ruffo, R., et al., *Electrochemical characterization of LiCoO2 as rechargeable electrode in aqueous LiNO3 electrolyte.* Solid State Ionics, 2011. **192**(1): p. 289-292.
249. Gummow, R.J. and M.M. Thackeray, *Structure and electrochemistry of lithium cobalt oxide synthesised at 400℃.* Material Research Bulletin, 1992. **27**: p. 327-337.
250. Antolini, E., *LiCoO2: formation, structure, lithium and oxygen nonstoichiometry, electrochemical behaviour and transport properties.* Solid State Ionics, 2004. **170**(3-4): p. 159-171.
251. Belov, D. and M.H. Yang, *Investigation of the kinetic mechanism in overcharge process for Li-ion battery.* Solid State Ionics, 2008. **179**(27-32): p. 1816-1821.
252. Doh, C.H., et al., *Thermal and electrochemical behaviour of C/LixCoO2 cell during safety test.* Journal of Power Sources, 2008. **175**(2): p. 881-885.
253. Tang, W., et al., *Nano-LiCoO2 as cathode material of large capacity and high rate capability for aqueous rechargeable lithium batteries.* Electrochem. Commun., 2010. **12**(11): p. 1524-1526.
254. Tan, K.S., et al., *High-performance LiCoO2 by molten salt (LiNO3 : LiCl) synthesis for Li-ion batteries.* J. Power Sources, 2005. **147**(1-2): p. 241-248.
255. Park, M., et al., *A review of conduction phenomena in Li-ion batteries.* J. Power Sources, 2010. **195**(24): p. 7904-7929.
256. Dokko, K., et al., *Kinetic characterization of single particles of LiCoO2 by AC impedance and potential step methods.* Journal of the Electrochemical Society, 2001. **148**(5): p. A422-A426.
257. Barker, J., et al., *An electrochemical investigation into the lithium insertion properties of LixCoO2.* Electrochimica Acta, 1996. **41**(15): p. 2481-2488.
258. Paustenbach, D.J., et al., *A review of the health hazards posed by cobalt.* Critical Reviews in Toxicology, 2013. **43**(4): p. 316-362.
259. Qi, Z. and G.M.K. Jr., *High-Performance LiCoO2 Sub-Micrometer Materials from Scalable Microparticle Template Processing.* ChemistrySelect, 2016. **1**(13): p. 3992-3999.
260. Fergus, J.W., *Recent developments in cathode materials for lithium ion batteries.* J. Power Sources, 2010. **195**(4): p. 939-954.
261. Rieger, B., et al., *A New Method to Model the Thickness Change of a Commercial Pouch Cell during Discharge.* Journal of The Electrochemical Society, 2016. **163**(8): p. A1566-A1575.
262. Zhou, L., D.Y. Zhao, and X.W. Lou, *LiNi0.5Mn1.5O4 Hollow Structures as High-Performance Cathodes for Lithium-Ion Batteries.* Angewandte Chemie-International Edition, 2012. **51**(1): p. 239-241.
263. Deng, Y.-F., et al., *Impact of P-Doped in Spinel LiNi0.5Mn1.5O4on Degree of Disorder, Grain Morphology, and Electrochemical Performance.* Chemistry of Materials, 2015. **27**(22): p. 7734-7742.

264. Zhu, Z., et al., *Preparation of spherical hierarchical LiNi0.5Mn1.5O4 with high electrochemical performances by a novel composite co-precipitation method for 5V lithium ion secondary batteries.* Electrochimica Acta, 2014. **115**: p. 290-296.
265. Lee, E.-S., et al., *Influence of Cation Ordering and Lattice Distortion on the Charge–Discharge Behavior of LiMn1.5Ni0.5O4Spinel between 5.0 and 2.0 V.* Chem. Mater., 2012. **24**(18): p. 3610-3620.
266. Liu, J., et al., *Nanoscale Ni/Mn Ordering in the High Voltage Spinel Cathode LiNi0.5Mn1.5O4.* Chemistry of Materials, 2016. **28**(19): p. 6817-6821.
267. Yang, L., B. Ravdel, and B.L. Lucht, *Electrolyte Reactions with the Surface of High Voltage LiNi0.5Mn1.5O4 Cathodes for Lithium-Ion Batteries.* Electrochemical and Solid State Letters, 2010. **13**(8): p. A95-A97.
268. Dou, S.M., *Review and prospect of layered lithium nickel manganese oxide as cathode materials for Li-ion batteries.* Journal of Solid State Electrochemistry, 2013. **17**(4): p. 911-926.
269. Robinson, J.P. and G.M. Koenig, *Tuning solution chemistry for morphology control of lithium-ion battery precursor particles.* Powder Technol., 2015. **284**: p. 225-230.
270. Dou, S.M., *Review and prospects of Mn-based spinel compounds as cathode materials for lithium-ion batteries.* Ionics, 2015. **21**(11): p. 3001-3030.
271. Yi, T.F., et al., *A review of recent developments in the surface modification of LiMn2O4 as cathode material of power lithium-ion battery.* Ionics, 2009. **15**(6): p. 779-784.
272. Liu, Y.J., et al., *Electrochemical performance and capacity fading reason of LiMn2O4/graphite batteries stored at room temperature.* Journal of Power Sources, 2009. **189**(1): p. 721-725.
273. Doi, T., et al., *Electrochemical AFM study of LiMn2O4 thin film electrodes exposed to elevated temperatures.* Journal of Power Sources, 2008. **180**(1): p. 539-545.
274. Molenda, J. and W. Kucza, *Transport properties of LiMn2O4.* Solid State Ionics, 1999. **117**(1-2): p. 41-46.
275. Guan, J. and M.L. Liu, *Transport properties of LiMn2O4 electrode materials for lithium-ion batteries.* Solid State Ionics, 1998. **110**(1-2): p. 21-28.
276. Xu, J., et al., *Elucidation of the surface characteristics and electrochemistry of high-performance LiNiO2.* Chemical Communications, 2016. **52**(22): p. 4239-4242.
277. Zhao, H.Y., et al., *A simple and facile one-step strategy to synthesize orthorhombic LiMnO2 nano-particles with excellent electrochemical performance.* Ceramics International, 2015. **41**(10): p. 15266-15271.
278. Fei, H.L., W.J. Feng, and Y.S. Lin, *Facile synthesis of vanadium oxide microspheres for lithium-ion battery cathodes.* Solid State Sciences, 2016. **55**: p. 36-41.
279. Zhao, X.R., et al., *Structure Design and Performance of LiNixCoyMn1-x-yO2 Cathode Materials for Lithium-ion Batteries: A Review.* Journal of the Chinese Chemical Society, 2014. **61**(10): p. 1071-1083.

280. Li, Y., et al., *A New Way for Preparation and Characterization of Cr-Doped LiMnO2 Cathode Materials for Lithium Ion Batteries.* Synthesis and Reactivity in Inorganic Metal-Organic and Nano-Metal Chemistry, 2016. **46**(6): p. 892-895.
281. Tan, T.Q., et al., *A Brief Review of Layered Rock Salt Cathode Materials for Lithium Ion Batteries.* 2nd International Conference on Sustainable Materials (Icosm 2013), 2013. **795**: p. 245-250.
282. Nichelson, A., et al., *A Brief Review on Integrated (Layered and Spinel) and Olivine Nanostructured Cathode Materials for Lithium Ion Battery Applications.* Materials Focus, 2016. **5**(4): p. 324-334.
283. Daniel, C., et al., *Cathode Materials Review.* Review on Electrochemical Storage Materials and Technology, 2014. **1597**: p. 26-43.
284. Zhang, W.J., *Structure and performance of LiFePO4 cathode materials: A review.* Journal of Power Sources, 2011. **196**(6): p. 2962-2970.
285. Vu, A. and A. Stein, *Lithium iron phosphate spheres as cathode materials for high power lithium ion batteries.* J. Power Sources, 2014. **245**: p. 48-58.
286. Axsen, J., K.S. Kurani, and A. Burke, *Are batteries ready for plug-in hybrid buyers?* Transport Policy, 2010. **17**(3): p. 173-182.
287. Chen, Z., et al., *Polyacene coated carbon/LiFePO4 cathode for Li ion batteries: Understanding the stabilized double coating structure and enhanced lithium ion diffusion kinetics.* Electrochimica Acta, 2013. **109**: p. 262-268.
288. Liang, B., Y. Liu, and Y. Xu, *Silicon-based materials as high capacity anodes for next generation lithium ion batteries.* J. Power Sources, 2014. **267**: p. 469-490.
289. Li, Y., et al., *Effects of Particle Size, Electronic Connectivity, and Incoherent Nanoscale Domains on the Sequence of Lithiation in LiFePO4 Porous Electrodes.* Adv. Mater. (Weinheim, Ger.), 2015. **27**(42): p. 6591-7.
290. Gaberscek, M., R. Dominko, and J. Jamnik, *Is small particle size more important than carbon coating? An example study on LiFePO4 cathodes.* Electrochem. Commun., 2007. **9**(12): p. 2778-2783.
291. Miao, C., et al., *A novel synthesis and characterization of LiFePO4 and LiFePO4/C as a cathode material for lithium-ion battery.* J. Power Sources, 2014. **246**: p. 232-238.
292. Yu, F., et al., *Optimized electrochemical performance of three-dimensional porous LiFePO4/C microspheres via microwave irradiation assisted synthesis.* Journal of Power Sources, 2014. **271**: p. 223-230.
293. Wang, S., et al., *A simple and inexpensive synthesis route for LiFePO4/C nanoparticles by co-precipitation.* J. Power Sources, 2013. **233**: p. 43-46.
294. Wang, J., et al., *Size-dependent surface phase change of lithium iron phosphate during carbon coating.* Nat Commun, 2014. **5**: p. 3415.
295. Zhong, K., et al., *Study on the stability of the LiFePO4 Li-ion battery via an electrochemical method.* Journal of Power Sources, 2014. **250**: p. 296-305.
296. Lva, Y.-J., et al., *Synthesis of bowl-like mesoporous LiFePO4/C composites as cathode materials for lithium ion batteries.* Electrochim. Acta, 2014. **119**: p. 155-163.
297. Kim, S.W., et al., *Phase Stability Study of Li1-xMnPO4 (0 <= x <= 1) Cathode for Li Rechargeable Battery.* Journal of the Electrochemical Society, 2009. **156**(8): p. A635-A638.

298. Kosova, N.V., et al., *Approaching better cycleability of LiCoPO4 by vanadium modification.* Materials Science and Engineering B-Advanced Functional Solid-State Materials, 2016. **213**: p. 105-113.
299. Maeyoshi, Y., et al., *Effect of organic additives on characteristics of carbon-coated LiCoPO4 synthesized by hydrothermal method.* Journal of Power Sources, 2017. **337**: p. 92-99.
300. He, W., et al., *Li3V2(PO4)(3)/LiFePO4 composite hollow microspheres for wide voltage lithium ion batteries.* Electrochimica Acta, 2016. **219**: p. 682-692.
301. Wang, X.J., et al., *Li-storage in LiFe1/4Mn1/4Co1/4Ni1/4PO4 solid solution.* Electrochemistry Communications, 2008. **10**(9): p. 1347-1350.
302. Xu, Z.R., et al., *Review-Recent Developments in the Doped LiFePO4 Cathode Materials for Power Lithium Ion Batteries.* Journal of the Electrochemical Society, 2016. **163**(13): p. A2600-A2610.
303. Qi, Z. and G.M.K. Jr., *Electrochemical Evaluation of Suspensions of Lithium-Ion Battery Active Materials as an Indicator of Rate Capability.* Journal of The Electrochemical Society, 2017. **164**(2): p. A151-A155.
304. Madec, L., et al., *Electronic vs Ionic Limitations to Electrochemical Performance in Li4Ti5O12-Based Organic Suspensions for Lithium-Redox Flow Batteries.* Journal of the Electrochemical Society, 2014. **161**(5): p. A693-A699.
305. Belharouak, I., G.M. Koenig, and K. Amine, *Electrochemistry and safety of Li4Ti5O12 and graphite anodes paired with LiMn2O4 for hybrid electric vehicle Li-ion battery applications.* J. Power Sources, 2011. **196**(23): p. 10344-10350.
306. Ohzuku, T., A. Ueda, and N. Yamamoto, *Zero-Strain Insertion Material of Li[Li1/3Ti5/3]O4 for Rechargeable Lithium Cells.* J. Electrochem. Soc, 1995. **142**(5): p. 1431-1435.
307. Young, D., et al., *Electronic Conductivity in the Li4/3Ti5/3O4-Li7/3Ti5/3O4 System and Variation with State-of-Charge as a Li Battery Anode.* Advanced Energy Materials, 2013. **3**(9): p. 1125-1129.
308. Yang, Z., et al., *Nanostructures and lithium electrochemical reactivity of lithium titanites and titanium oxides: A review.* J. Power Sources, 2009. **192**(2): p. 588-598.
309. Takai, S., et al., *Diffusion coefficient measurement of lithium ion in sintered Li1.33Ti1.67O4 by means of neutron radiography.* Solid State Ionics, 1999. **123**(1-4): p. 165-172.
310. Zaghib, K., et al., *Electrochemical study of Li4Ti5O12 as negative electrode for Li-ion polymer rechargeable batteries.* Journal of Power Sources, 1999. **81**: p. 300-305.
311. Zhao, B., et al., *A comprehensive review of Li4Ti5O12-based electrodes for lithium-ion batteries: The latest advancements and future perspectives.* Materials Science & Engineering R-Reports, 2015. **98**: p. 1-71.
312. Bresser, D., et al., *Percolating networks of TiO2 nanorods and carbon for high power lithium insertion electrodes.* Journal of Power Sources, 2012. **206**: p. 301-309.
313. Liu, Y. and Y.F. Yang, *Recent Progress of TiO2-Based Anodes for Li Ion Batteries.* Journal of Nanomaterials, 2016. **2016**: p. 8123652.

314. Wei, J., et al., *A review of Nanostructured TiO2 Application in Li-Ion Batteries.* Advanced Engineering Materials Iii, Pts 1-3, 2013. **750-752**: p. 301-306.
315. Goriparti, S., et al., *Review on recent progress of nanostructured anode materials for Li-ion batteries.* Journal of Power Sources, 2014. **257**: p. 421-443.
316. Shivashankaraiah, R.B., et al., *Electrochemical Characterization of LiTi2(PO4)(3) as Anode Material for Aqueous Rechargeable Lithium Batteries.* Journal of the Electrochemical Society, 2012. **159**(7): p. A1074-A1082.
317. Szczech, J.R. and S. Jin, *Nanostructured silicon for high capacity lithium battery anodes.* Energy & Environmental Science, 2011. **4**(1): p. 56-72.
318. Ma, D.L., Z.Y. Cao, and A.M. Hu, *Si-Based Anode Materials for Li-Ion Batteries: A Mini Review.* Nano-Micro Letters, 2014. **6**(4): p. 347-358.
319. Ge, M., et al., *Review of porous silicon preparation and its application for lithium-ion battery anodes.* Nanotechnology, 2013. **24**(42): p. 422001.
320. Kamali, A.R. and D.J. Fray, *Review on Carbon and Silicon Based Materials as Anode Materials for Lithium Ion Batteries.* Journal of New Materials for Electrochemical Systems, 2010. **13**(2): p. 147-160.
321. Luo, F., et al., *Review-Nano-Silicon/Carbon Composite Anode Materials Towards Practical Application for Next Generation Li-Ion Batteries.* Journal of the Electrochemical Society, 2015. **162**(14): p. A2509-A2528.
322. Zamfir, M.R., et al., *Silicon nanowires for Li-based battery anodes: a review.* Journal of Materials Chemistry A, 2013. **1**(34): p. 9566-9586.
323. Cheng, X.B., et al., *A Review of Solid Electrolyte Interphases on Lithium Metal Anode.* Advanced Science, 2016. **3**(3): p. 1500213.
324. Balogun, M.S., et al., *A review of the development of full cell lithium-ion batteries: The impact of nanostructured anode materials.* Nano Research, 2016. **9**(10): p. 2823-2851.
325. Sri Devi Kumari, T., T. Prem Kumar, and A.K. Shukla, *Nanostructured Materials for Next-Generation Lithium-Ion Batteries*, in *Nanotechnology for Energy Sustainability*, B. Raj, M.V.d. Voorde, and Y. Mahajan, Editors. 2017, Wiley-VCH Verlag GmbH & Co. KGaA: Weinheim, Germany.
326. Kim, S.W., et al., *Electrode Materials for Rechargeable Sodium-Ion Batteries: Potential Alternatives to Current Lithium-Ion Batteries.* Advanced Energy Materials, 2012. **2**(7): p. 710-721.
327. Bhide, A., et al., *Electrochemical stability of non-aqueous electrolytes for sodium-ion batteries and their compatibility with Na0.7CoO2.* Physical Chemistry Chemical Physics, 2014. **16**(5): p. 1987-1998.
328. Buchholz, D., et al., *Toward Na-ion Batteries-Synthesis and Characterization of a Novel High Capacity Na Ion Intercalation Material.* Chemistry of Materials, 2013. **25**(2): p. 142-148.
329. Huang, L., et al., *Electrode Nanomaterials for Room Temperature Sodium-Ion Batteries: A Review.* Journal of Nanoscience and Nanotechnology, 2015. **15**(9): p. 6295-6307.
330. Zhu, Z.Q. and J. Chen, *Review-Advanced Carbon-Supported Organic Electrode Materials for Lithium (Sodium)-Ion Batteries.* Journal of the Electrochemical Society, 2015. **162**(14): p. A2393-A2405.

331. Pan, H.L., Y.S. Hu, and L.Q. Chen, *Room-temperature stationary sodium-ion batteries for large-scale electric energy storage.* Energy & Environmental Science, 2013. **6**(8): p. 2338-2360.
332. Slater, M.D., et al., *Sodium-Ion Batteries.* Advanced Functional Materials, 2013. **23**(8): p. 947-958.
333. Sen, S., et al., *Engineering nanofluid electrodes: controlling rheology and electrochemical activity of gamma-Fe2O3 nanoparticles.* Journal of Nanoparticle Research, 2015. **17**(11): p. 437.
334. Smith, T.L. and C.A. Bruce, *Intrinsic Viscosities and Other Rheological Properties of Flocculated Suspensions of Nonmagnetic and Magnetic Ferric Oxides.* Journal of Colloid and Interface Science, 1979. **72**(1): p. 13-26.
335. Zhou, Z., P.J. Scales, and D.V. Boger, *Chemical and physical control of the rheology of concentrated metal oxide suspensions.* Chemical Engineering Science, 2001. **56**: p. 2901-2920.
336. Tseng, W.J. and K.-C. Lin, *Rheology and colloidal structure of aqueous TiO2 nanoparticle suspensions.* Materials Science and Engineering: A, 2003. **355**(1-2): p. 186-192.
337. Narayanan, A., F. Mugele, and M.H. Duits, *Mechanical History Dependence in Carbon Black Suspensions for Flow Batteries: A Rheo-Impedance Study.* Langmuir, 2017. **33**: p. 1629-1638.
338. Mewis, J. and N.J. Wagner, *Colloidal suspension rheology*. Cambridge series in chemical engineering. 2012, Cambridge, UK New York: Cambridge University Press.
339. Nguyen, C.T., et al., *Temperature and particle-size dependent viscosity data for water-based nanofluids-Hysteresis phenomenon.* International Journal of Heat and Fluid Flow, 2007. **28**(6): p. 1492-1506.
340. Timofeeva, E.V., et al., *Particle size and interfacial effects on thermo-physical and heat transfer characteristics of water-based alpha-SiC nanofluids.* Nanotechnology, 2010. **21**(21): p. 215703.
341. Timofeeva, E.V., et al., *Base fluid and temperature effects on the heat transfer characteristics of SiC in ethylene glycol/H2O and H2O nanofluids.* Journal of Applied Physics, 2011. **109**(1): p. 014914.
342. Madec, L., et al., *Surfactant for Enhanced Rheological, Electrical, and Electrochemical Performance of Suspensions for Semisolid Redox Flow Batteries and Supercapacitors.* ChemPlusChem, 2015. **80**(2): p. 396-401.
343. Ata, M.S., Y. Liu, and I. Zhitomirsky, *A review of new methods of surface chemical modification, dispersion and electrophoretic deposition of metal oxide particles.* Rsc Advances, 2014. **4**(43): p. 22716-22732.
344. Caruso, F., *Nanoengineering of particle surfaces.* Advanced Materials, 2001. **13**(1): p. 11-22.
345. Kango, S., et al., *Surface modification of inorganic nanoparticles for development of organic-inorganic nanocomposites-A review.* Progress in Polymer Science, 2013. **38**(8): p. 1232-1261.
346. Brunini, V.E., Y.-M. Chiang, and W.C. Carter, *Modeling the hydrodynamic and electrochemical efficiency of semi-solid flow batteries.* Electrochimica Acta, 2012. **69**: p. 301-307.

347. Smith, K.C., Y.M. Chiang, and W.C. Carter, *Maximizing Energetic Efficiency in Flow Batteries Utilizing Non-Newtonian Fluids.* Journal of the Electrochemical Society, 2014. **161**(4): p. A486-A496.
348. Smith, K.C., et al., *Electroactive-Zone Extension in Flow-Battery Stacks.* Electrochimica Acta, 2014. **147**: p. 460-469.
349. Petek, T.J., et al., *Characterizing Slurry Electrodes Using Electrochemical Impedance Spectroscopy.* Journal of the Electrochemical Society, 2016. **163**(1): p. A5001-A5009.
350. Cerbelaud, M., et al., *Numerical and Experimental Study of Suspensions Containing Carbon Blacks Used as Conductive Additives in Composite Electrodes for Lithium Batteries.* Langmuir, 2014. **30**(10): p. 2660-2669.
351. Ventosa, E., et al., *Solid electrolyte interphase in semi-solid flow batteries: a wolf in sheep's clothing.* Chemical Communications, 2015. **51**(81): p. 14973-14976.
352. Lin, M.C., et al., *An ultrafast rechargeable aluminium-ion battery.* Nature, 2015. **520**(7547): p. 325-8.
353. Chen, H.N. and Y.C. Lu, *A High-Energy-Density Multiple Redox Semi-Solid-Liquid Flow Battery.* Advanced Energy Materials, 2016. **6**(8): p. 1502183.
354. Doughty, D. and E.P. Roth, *A General Discussion of Li Ion Battery Safety.* The Electrochemical Society Interface, 2012. **21**(2): p. 37-44.
355. Singh, J. and D. Tee, *Contributions to Electric Vehicle Power Safety through Battery Testing Calorimetry (Btc).* Hazards Xxii: Process Safety and Environmental Protection, 2011(156): p. 625-633.
356. Ichimura, M., *The safety characteristics of lithium-ion batteries for mobile phones and the nail penetration test.* Intelec 07 - 29th International Telecommunications Energy Conference, Vols 1 and 2, 2007: p. 687-692.
357. Wu, H., et al., *Improving battery safety by early detection of internal shorting with a bifunctional separator.* Nature Communications, 2014. **5**: p. 5193.
358. Lu, Y.H., J.B. Goodenough, and Y. Kim, *Aqueous Cathode for Next-Generation Alkali-Ion Batteries.* Journal of the American Chemical Society, 2011. **133**(15): p. 5756-5759.
359. Wang, Y.R., Y.G. Wang, and H.S. Zhou, *A Li-Liquid Cathode Battery Based on a Hybrid Electrolyte.* Chemsuschem, 2011. **4**(8): p. 1087-1090.
360. Park, H., *A design of air flow configuration for cooling lithium ion battery in hybrid electric vehicles.* Journal of Power Sources, 2013. **239**: p. 30-36.
361. Jarrett, A. and I.Y. Kim, *Design optimization of electric vehicle battery cooling plates for thermal performance.* Journal of Power Sources, 2011. **196**(23): p. 10359-10368.
362. Duan, X. and G.F. Naterer, *Heat transfer in phase change materials for thermal management of electric vehicle battery modules.* International Journal of Heat and Mass Transfer, 2010. **53**(23-24): p. 5176-5182.
363. Rao, Z.H. and S.F. Wang, *A review of power battery thermal energy management.* Renewable & Sustainable Energy Reviews, 2011. **15**(9): p. 4554-4571.

Chapter II. A Carbon-Free Lithium-Ion Solid Dispersion Redox Couple with Low Viscosity for Redox Flow Batteries

2.1. Overview

This chapter describes the initial demonstration of a carbon-free RFB with solid lithium-ion active materials (Type III design described in Chapter I). This is the first report of RFB based on lithium-ion active material suspensions in the literature. $Li_4Ti_5O_{12}$ (LTO) in non-aqueous electrolyte with different loadings has been characterized in two specially designed lithium half-cell configurations. This chapter describes the electrochemical performance of the LTO suspensions after characterizing LTO in conventional coin cells and carbon-free coin cells. LTO suspensions were electrochemically active and could be reversibly cycled. The electrochemical reaction was based on LTO particle collisions on the current collector and was active under agitation. Power density was limited by the high resistance of the electrochemical reaction. This chapter also provides the initial system designs for following chapters.

Elements of this chapter have been published in Journal of Power Sources:

Z. Qi, G.M. Koenig, A carbon-free lithium-ion solid dispersion redox couple with low viscosity for redox flow batteries, *Journal of Power Sources*, 323 (2016) 97-106.

2.2. Abstract

A new type of non-aqueous redox couple without carbon additives for flow batteries is proposed and the target anolyte chemistry is demonstrated. The so-called “Solid Dispersion Redox Couple” incorporates solid electroactive materials dispersed in organic lithium-ion battery electrolyte as its flowing suspension. In this piece of work, a unique and systematic characterization approach has been used to study the flow battery redox couple in half cell demonstrations relative to a lithium electrode. An electrolyte laden with LTO has been characterized in multiple specially designed lithium half-cell configurations. The flow battery redox couple described in this report has relatively low viscosity, especially in comparison to other flow batteries with solid active materials. The lack of carbon additive allows characterization of the electrochemical properties of the electroactive material in flow without the complication of conductive additives and unambiguous observation of the electrorheological coupling in these dispersed particle systems.

2.3. Introduction

Redox flow batteries are ideal for large scale energy storage because of the decoupling of the power and the energy in the system, which provides the flexibility to independently adjust and design the power and energy requirements for an application.[1] The electrochemical energy is stored in electrolyte tanks, which in principle results in total energy only being limited by tank size. Conventional flow batteries are typically comprised of transition metal redox couples dissolved in highly acidic aqueous electrolytes.[2, 3] Different approaches have been pursued in the literature to improve flow battery performance, including investigating new redox couples, [4] designing more efficient current collectors, [1, 5-7] incorporating electrolyte additives,[8] and modifying the ion-transferring membrane.[9] The energy density in conventional flow batteries is highly limited by the solubility of the active species, because beyond the solubility limit inactive precipitates form in the electrolyte.[2, 3] The long-term performance or cycle life of these systems is also limited by the significant loss of stored energy (i.e., capacity loss) in the electrolytes over time due to transport of the active species across the separator.[9]

Alternative flow battery systems beyond the conventional dissolved transition metal electrolytes have also been reported in the literature, including lead-based flow batteries with soluble lead [10] and polymer suspensions.[11] Another modified flow battery that has been developed is a convection battery with the electroactive materials fixed and electrolyte flowing to improve the mass transport of ionic species in the electrolyte.[12, 13] These reported systems, however, have performance limitations due to maximum practical electrode thicknesses or the inefficient pumping due to high pressure drop. More

recently, the possibility of combining lithium-ion battery chemistries with flow batteries has been proposed due to the high energy density and high operating voltages of lithium-ion battery active electrode materials.[14] While energy density is not necessarily a major concern for some stationary applications, higher energy density flow battery chemistries will be needed for flow batteries to be implemented in electric vehicles or stationary applications in urban areas where space is limited and energy demand is high. In some cases the active electrolyte materials are still soluble compounds, for example in the report of a membrane-free semiliquid flow battery composed of a ferrocene-based catholyte and a passivated metallic Li anode.[15] Other groups have moved to solid electroactive material flow battery designs, and recently the concept of semi-solid flow cells (SSFC) was demonstrated by Chiang's group for both organic and inorganic systems.[16, 17] In these reports, electrochemically active particles were suspended in the electrolytes together with conductive carbon, forming an interconnected network structure with relatively high conductivity. Other research groups have expanded on this concept and incorporated different chemistries into SSFC-type systems, including $LiFePO_4$.[18] These SSFC-type systems have also explored improvements by incorporation of surfactants within the electrolyte and by developing electrochemical models.[19, 20] A high energy storage density (>130 Wh kg^{-1}) compared to conventional flow batteries was achieved in these SSFC-type systems as a result of the high energy density solid electroactive materials.[16] However, the operating cost of SSFC-type systems will likely be extremely high due to high viscosities (>1 Pa·s at the shear rate of 35 s^{-1}) of the viscous electrolyte suspensions.[16, 21] Inactive carbon conductive additives in these systems also reduce the total electrolyte energy density.

Herein, we first demonstrate a redox couple for a new type of flow battery without carbon additives and hence with a relatively low viscosity. The functional design of the system is similar to a SSFC, but the flowing suspension is comprised of only electroactive material particles dispersed in an organic lithium-ion battery electrolyte. In contrast to previous SSFC reports, electrochemical charge/discharge of our redox couple does not rely on an interconnected particle network throughout the electrolyte, but instead relies on the collisions of particles directly with the current collector (or through interparticle contacts to the current collector). For this initial experimental work, we took advantage of a lithium half cell configuration to characterize an electrolyte laden with $Li_4Ti_5O_{12}$ (LTO). LTO was chosen because of its high capacity and good electrochemical performance at a variety of charge/discharge rates.[22-24] The details of LTO's material properties and electrochemical mechanisms have also been well described in the literature.[25-28] The flat charge/discharge profile for LTO should be advantageous at providing a consistent voltage during charge/discharge, regardless of the state of lithiation of the active material in contact with the current collector at any given time. LTO is also a zero-strain lithium insertion material,[25, 29] which prevents fractures of the particles during electrochemical cycling. In addition, the charge/discharge potential of LTO (~1.55 V vs. Li/Li^+) is within the stability window of the electrolyte, which removes the complication of significant electrolyte decomposition and solid-electrolyte interphase formation.[30] We note that at this voltage the long term goal is to use LTO as an anolyte paired with a catholyte that contains a lithium-ion battery solid cathode active material. Thus, although

for initial half cell characterization studies reported here relative to lithium metal LTO is a cathode, the eventual goal is to use the LTO as an anolyte in a full cell flow battery.

Since this system was derived from conventional lithium-ion battery electrode materials, we adopted a distinct approach to demonstrate the as-proposed flow battery redox couple step-by-step. A conventional lithium-ion battery coin cell with LTO was prepared as a benchmark, and then a particle coin cell was constructed free of binders and conductive additives to show that the LTO active material could be successfully charged and discharged through direct contact with the current collector. After that, a vial cell was prepared to electrochemically characterize the LTO suspension during electrochemical cycling in a turbid flowing environment, and finally a flow cell was assembled to demonstrate the as-proposed flow battery redox couple. Rheological tests were conducted to demonstrate the viscosity of our particle-laden electrolyte as a function of particle loading and relative to other flow battery systems.

2.4. Experimental

2.4.1. Preparation and Characterization of Materials

LTO (NEI Corporation) powders were obtained from the U.S. Department of Energy's (DOE) CAMP (Cell Analysis, Modeling, and Prototyping) Facility, Argonne National Laboratory. Detailed materials characterization of LTO powder from NEI can be found in other reports in the literature.[31, 32] The electrolyte (BASF Corporation) was 1.2 M lithium hexafluorophosphate ($LiPF_6$) in ethylene carbonate (EC) and ethyl methyl carbonate (EMC) with EC/EMC = 3:7 by volume ratio. The LTO suspensions of different loadings (5 vol%, 10 vol%, 20 vol%) were prepared by mixing the LTO powders with electrolyte under stirring overnight within an argon-filled glove box (with concentrations of O_2 < 1 ppm and H_2O < 1 ppm) at room temperature.

To characterize the LTO powder morphologies, scanning electron microscope (SEM) images were taken with a Quanta 650 SEM. X-ray diffraction (XRD) patterns were obtained with a Panalytical X'pert diffractometer using Cu Kα radiation. Rheology testing of the LTO suspensions was performed with an Anton Paar rheometer (Physica MCR 301, with a 5 cm plate-plate geometry).

2.4.2. Electrochemical Characterization

A conventional LTO electrode was fabricated from a slurry comprised of 80 wt % LTO powder, 10 wt % carbon black as conductive additive, and 10 wt % polyvinylidene fluoride binder (PVDF) dissolved in N-methylpyrrolidone (NMP, Sigma-Aldrich®). The slurry was agitated in a slurry mixer for 5 minutes and pasted (with a doctor blade with a

gap height of 200 μm) onto aluminum foil. The pasted slurry was dried in an oven at 70 °C overnight and further dried in a vacuum oven at 70 °C for 3 hrs. Electrodes composed of only LTO particles as the electrode material without binders or conductive additives on the aluminum foil were also prepared. LTO particles were suspended in acetone (Fisher Scientific) with a concentration of ~50 mg mL^{-1}, dropped on pre-punched aluminum foil discs (1.6 cm^2), and dried in a vacuum oven at 70 °C for 2 hrs. A coin cell using the as-prepared electrode was referred to as a "particle coin cell".

All coin cells were assembled in the glove box. LTO half cells were assembled with the LTO electrode as the cathode and lithium foil as the anode. The electrodes were separated by a polypropylene/polyethylene/polypropylene trilayer membrane. The galvanostatic charge-discharge cycling of coin cells was performed on a Maccor battery cycler. For all cycling tests where C rates are given, 1C was assumed to be 174.55 mA g^{-1} (the theoretical capacity of LTO) and the current adjusted by the amount of LTO active material.

2.4.3. Vial Cell and Flow Cell Testing

A customized cell was set up in the glove box as illustrated in Figure 1a, which we refer to as a "vial cell". An aluminum wire (99.999%, Alfa Aesar) of 1.5 mm in diameter and 20 cm in length was immersed in an LTO suspension of desired particle loading. Lithium foil, which was attached to a copper foil extended to the external circuit, was immersed into the electrolyte within a glass tube and separated from the LTO suspension by a trilayer membrane separator. Typically, particles would remain dispersed in the

suspension for ~30 minutes if agitation was stopped, however, particles were kept suspended via agitation continuously during all electrochemical experiments. Addition of surfactant would have been one approach to further stabilize the suspension,[33-35] however, the surfactant components would have introduced additional complications and sources for electrochemical currents within our system, and for this initial demonstration we focus on the electrochemical activity of just the active LTO particles free of conductive or stabilizing additives.[33, 36]

A customized flow cell was set up as illustrated in Figure 1b. The flow channels were formed by cutting compact stacks of laboratory films (Parafilm®) to provide the desired spacing and trilayer membrane separators were used. Aluminum wire was used as the cathode current collector. A piece of lithium foil was attached on a stainless steel foil (McMaster-Carr) as the anode and connected to a potentiostat (Bio-Logic, SP-150) to perform electrochemical tests. The whole cell was sealed with two polypropylene plates (McMaster-Carr). Electrochemical tests for both the vial cell and flow cell were performed within the glove box.

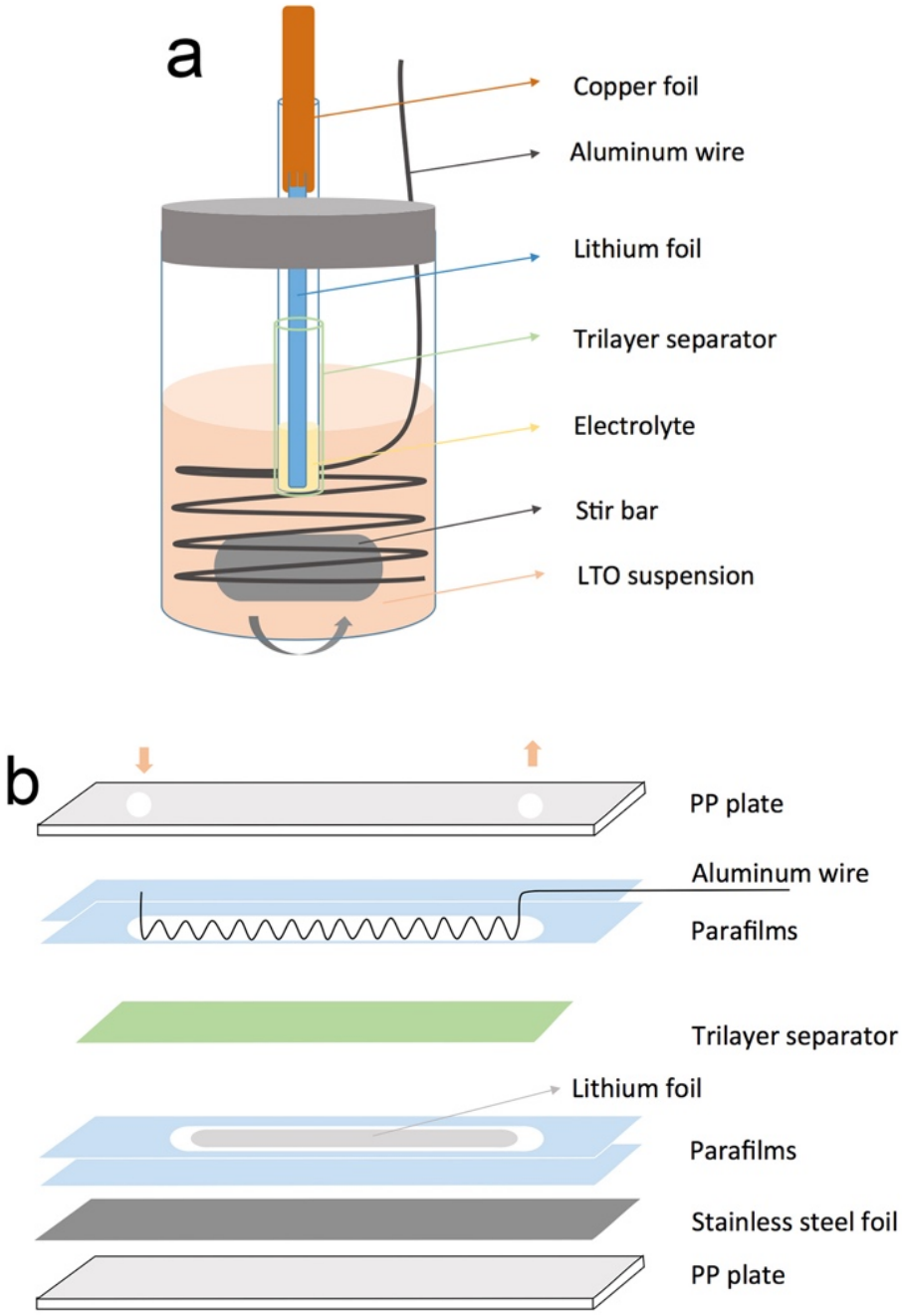

Figure 1. Cartoon schematic of cell configurations: (a) a vial cell with the aluminum wire in the LTO suspension as the cathode current collector and the lithium foil in the glass tube as the anode; (b) a flow cell with an aluminum wire current collector in the channel containing the LTO suspension and lithium foil attached on the stainless steel foil as the anode.

2.5. Results and Discussions

2.5.1. Materials Characterization

Figure 2 shows XRD patterns for the LTO powder (Figure 2a), as well as reference patterns for spinel phase LTO material (Figure 2b, obtained from PDF 00-049-0207 [37]) and rutile TiO_2 (Figure 2c, obtained from PDF 00-001-1292 [38]). The peaks for the LTO powder are consistent with the majority of the powder being spinel phase LTO. There are two small but distinguishable peaks in the XRD pattern at 27.49° and 54.36°, which are consistent with an impurity rutile TiO_2 phase also being present in the LTO powder. Rutile TiO_2 impurity is a common impurity observed for LTO materials, and has been reported as an intermediate compound during solid-state synthesis of LTO using anatase TiO_2 and Li_2CO_3.[26, 39] The morphology of the LTO powder is shown in the SEM image in Figure 3. The LTO powder consisted of irregularly shaped particulates with average particle lengths of 340 ± 200 nm (based on the measured lengths of 35 particles). The XRD and SEM results for this NEI LTO material was consistent with previous reports on LTO materials from NEI.[31]

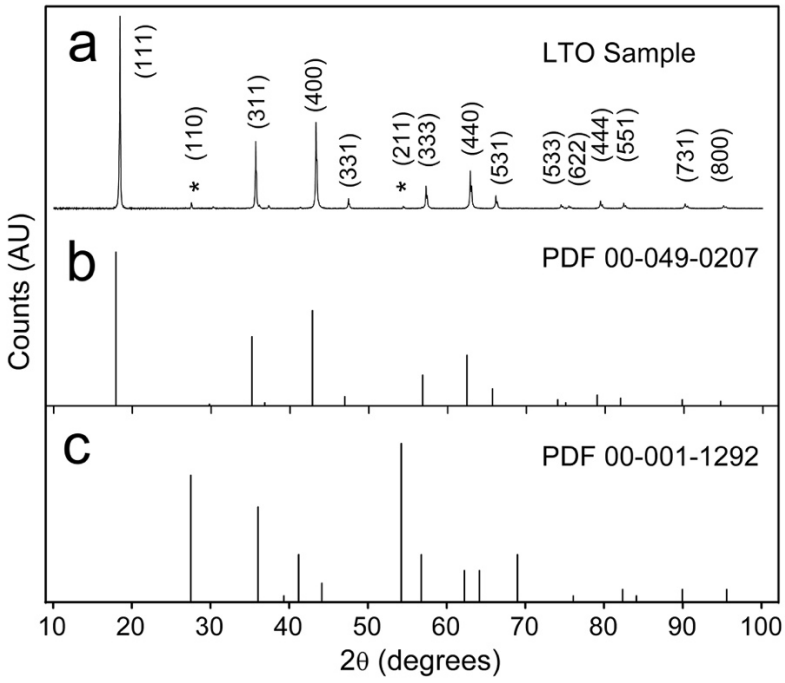

Figure 2. XRD patterns for (a) the LTO powder, as well as reference patterns for (b) spinel-phase LTO material (obtained from PDF 00-049-0207) and (c) rutile TiO_2 (obtained from PDF 00-001-1292).

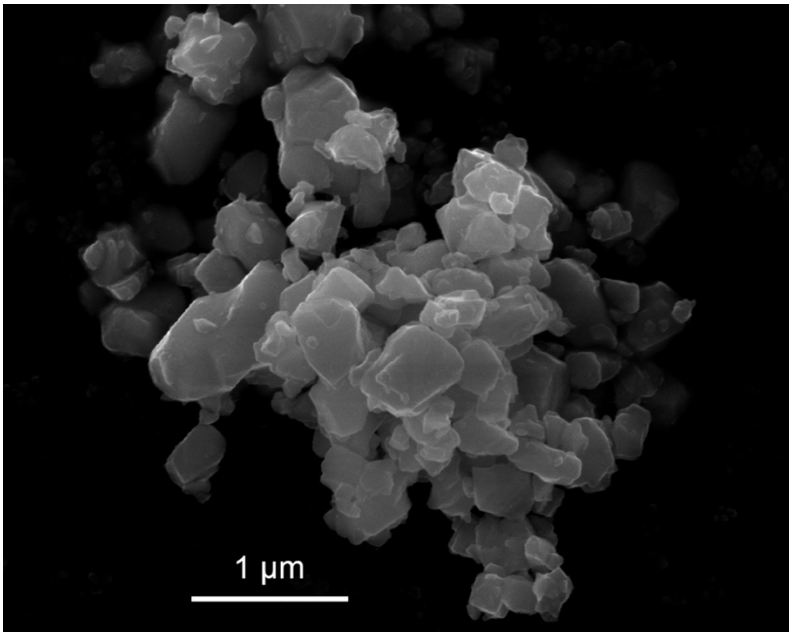

Figure 3. Scanning electron microscope (SEM) image of the LTO particles.

2.5.2. Conventional Coin Cell Electrochemical Characterization

Before using the LTO powder in our custom electrochemical cell geometries, we evaluated its electrochemical performance in conventional composite electrode architectures within coin cells. The first discharge and charge cycle of a conventional Li/LTO half cell is shown in Figure 4a. This cell was cycled at a rate of 0.1C and had a first cycle discharge capacity of 131 mAh g^{-1} and charge capacity of 132 mAh g^{-1}. While the first cycle had ~1% irreversible capacity loss, the columbic efficiency of subsequent cycles at 0.1C was ~100%. The LTO electrode had a flat charge/discharge plateau at approximately 1.55 V (vs. Li), consistent with literature reports.[22, 23, 40-42] Interestingly, even though the XRD patterns provided evidence of rutile TiO_2 (Figure 2), we did not observe associated discharge plateaus at 1.4 and 1.1 V.[43] The lack of capacity in these voltage regions was attributed to the small amount of the rutile TiO_2 impurities and the location of rutile TiO_2 phase possibly being segregated within the particle cores, making the rutile phase more difficult for lithium ions to access.[26, 44]

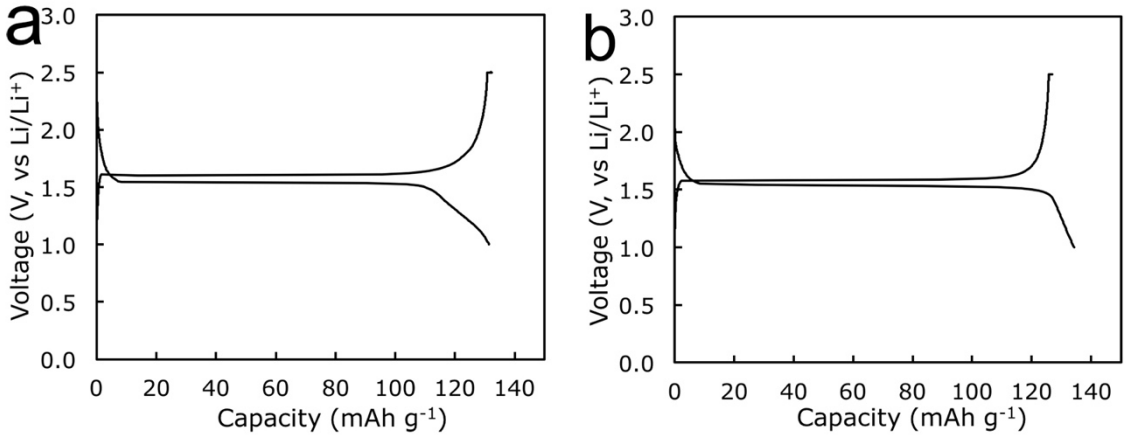

Figure 4. First discharge and charge cycle of (a) a conventional Li/LTO half cell and (b) a Li/LTO particle coin cell, both charged/discharged at a rate of ~ 0.1C.

2.5.3. Particle Coin Cell Electrochemical Characterization

To confirm that our LTO active material could maintain electrochemical activity in the absence of binders and conductive additives, a static particle coin cell battery was assembled where the electrode was comprised of only the LTO powder. The first charge/discharge cycle at a constant rate of 0.1C is shown in Figure 4b. This was the same rate (adjusted for active LTO mass) used for the conventional coin cells. The initial discharge capacity was 134 mAh g^{-1}, while the charge capacity was 127 mAh g^{-1}. Although the first cycle had 5.50% irreversible capacity loss, the columbic efficiency of subsequent cycles at 0.1C was ~99%. The particle coin cell had approximately equivalent gravimetric capacity within the same potential regions as the conventional coin cell, suggesting that electrochemical capacity was delivered from the entire thickness of the LTO electrode layer. The particle coin cell electrodes prepared for the tests had a thickness of greater than 70 μm, which was far greater than the length scale of the particles (340 ± 200 nm). These results indicate LTO particles separated from the current collector by multiple layers of other LTO particles were participating in electrochemical lithiation/delithiation reactions. Thus, LTO-to-LTO particle contacts provided sufficient electronic conductivity for particles far from the current collector to contribute electrochemical capacity. Electrodes of different LTO loadings (and hence different thicknesses) were also prepared and tested (see Appendix A, Figure A1). The total capacity of the particle coin cells with increased LTO loading increased almost proportionally to the total LTO loading, further confirming that electrochemical capacity was contributed by LTO particles far from the current collector. An inverse relationship was observed between particle loading and rate capability of the particle coin cells. Thus,

there are limits to the electrochemical capacity that can be extracted from particles far from the current collector, particularly at higher rates of charge/discharge. This was likely due to the increased resistance experienced by the electrons that had to traverse the extra distance via particle-to-particle LTO contact, as well as the lower lithium-ion accessibility to LTO close to the current collector for the thicker films. These results above, when combined, indicate that the LTO particles should be able to cycle when in contact with the current collector in the flow cell, and that capacity can also be contributed by particles far from the current collector if particle loadings are high enough to allow interconnected aggregated particle flocculation.

The charge/discharge voltages for the particle coin cells were very flat with plateaus near 1.55 V, indicating minimal electrode polarization. This low polarization confirmed LTO as a good candidate active material for the flow cell. While the flow cell will have polarization due to other factors, including the low contact and loose packing of the suspended particles and larger electrolyte distance, the low polarization in the particle coin cell demonstrated the intrinsic capabilities of the LTO for the electrochemical flow cell. Interestingly, the particle coin cell had an even lower difference between the average charge and discharge potentials, even though the particle cell does not contain conductive additives or binders. We attribute this observation to the excellent electronic and ionic conductivity of LTO material.[45] Although the initial electrical conductivity of LTO has been reported to be $10^{-6} \sim 10^{-13}$ S cm^{-1},[46] the conductivity has been demonstrated to rise sharply to 10^{0} S cm^{-1} after very low levels of lithiation.[45] The electrochemical performance of the particle coin cells demonstrated that conductive additives were not

necessary to effectively charge and discharge the LTO material when in contact with the current collector. These results provided additional motivation that a flow battery redox couple with LTO dispersed in electrolyte could be effectively charged and discharged through the contact of LTO particles with the current collector.

2.5.4. Rheological Characterization

Before evaluating the LTO material in custom flow geometries, we determined the rheological properties of LTO powder dispersed into the electrolyte. The rheological properties of a dispersed flow battery system are important both from an energy efficiency perspective and from a performance perspective. With regards to energy efficiency, the higher the viscosity of the particle-laden suspensions, the greater the energy demands of the pumps to move the particle dispersion through the flow battery system. Assuming the energy to drive the pumps is also provided by the flow battery, this parasitic energy loss will need to be considered in optimization of the overall energy efficiency of the battery.[21] Some SSFC-type batteries have extremely high viscosities, for example a recently reported value of more than 2 Pa·s for the mixture of LCO and carbon additive, and thus high pumping energy demands are necessary to flow such a slurry.[16] The rheological properties of the suspension will impact the distribution of particles in the suspension, the access of material to the current collector, and the collision frequency and residence time for the particles in contact with the current collector. Various factors contribute to the rheological behavior, such as particle size and morphology, salt concentration, temperature and pressure, and particle loading.[47, 48] Considering the critical influence of particle loading on both rheological properties and

energy density, we measured the viscosity of our LTO particle suspensions as a function of applied shear at a variety of particle loadings.

Figure 5 displays the viscosity as a function of shear rate for the particle-free electrolyte (1.2 M $LiPF_6$ in EC/EMC = 3:7) and the electrolyte laden with 5, 10, and 20 vol% LTO. The viscosity for all samples changed multiple orders of magnitude over the shear range investigated. The electrolyte both with and without particles displayed shear-thinning behavior, with the viscosity decreasing with increasing shear rate.[47] The particle-free electrolyte had Newtonian behavior with a flat plateau at shear rates higher than 10 s^{-1}.[47] The viscosity increased with a higher LTO loading. For the lowest particle concentration of 5 vol%, the measured viscosity was close to that of the particle-free electrolyte at low shear rates. The drag force provided by the LTO particles in the electrolyte became more pronounced at higher shear rates. This behavior indicates that at the lowest concentration (5 vol%), the LTO particles had a minor influence on the viscosity of the fluid dispersion. However, at 10 and 20 vol% LTO concentration, the viscosities were significantly higher than particle-free electrolyte and 5 vol% LTO within the full range of applied shear. Also, the Newtonian plateau at higher shear rate disappeared, and instead an extended shear-thinning behavior was observed. This behavior is consistent with the extreme shear-thinning behavior of flocculated metal oxide suspensions [49, 50] and previous research on LTO suspensions, which have reported that the flocculated network breaks up into smaller flocculates after sufficient shear, resulting in the steep decrease in viscosity.[48]

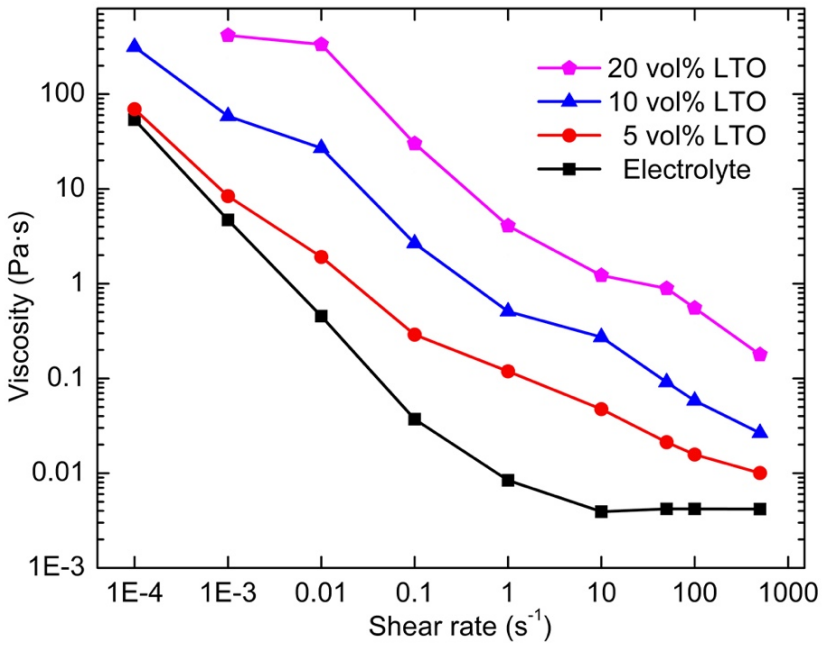

Figure 5. The viscosity as a function of shear rate for the particle-free electrolyte (1.2 M $LiPF_6$ in EC/EMC = 3:7 solvents, black squares) and the electrolyte laden with 5 (red circles), 10 (blue triangles), and 20 (purple pentagons) vol% LTO.

The relation between the viscosity and shear rate in the shear thinning region can be described by a power law or Ostwald–de Waele relationship,[51] taking the form of Equation 1, where η is the viscosity, γ is the shear rate, and K and n are fitting parameters. K is known as the flow consistency index, giving the viscosity at a shear rate of 1 s^{-1}. The dimensionless power law index describes the fluid behavior compared with a Newtonian fluid. For a Newtonian fluid, n = 1; for a shear-thinning fluid, n < 1 and for a shear-thickening fluid n is greater than 1.

$$\eta = K\gamma^{n-1} \qquad (1)$$

Experimental data from the LTO suspensions in Figure 5 were used to obtain the fitting parameters K and n. The fits of the 5 vol% LTO suspension was K = 0.18 and n = 0.44 (R^2 = 0.98); the 10 vol% LTO suspension was K = 0.96 and n = 0.39 (R^2 = 0.99); and the 20 vol% LTO suspension was K = 7.80 and n = 0.38 (R^2 = 0.97). These results and the quality of the fitting parameters further confirmed the shear-thinning behavior of the LTO suspensions.[47] The increasing K values with increased particle loadings indicated that suspensions with higher loadings generally have greater viscosities as would be expected; however, the decreasing n values with increased particle loading indicated that suspensions with higher loadings have more extensive shear-thinning behavior. The increased shear thinning with increasing particle loading is consistent with the higher loading suspensions being more flocculated, and with the flocculates becoming less stable and breaking up with sufficient applied shear. We also note that the n values are very close for 10 vol% and 20 vol% LTO, indicating that the transition to a more flocculated suspension occurs between 5 vol% and 10 vol% LTO. The observed shear-thinning is important to the operation of a carbon-free solid dispersion flow battery, because the rheological data indicate that there will be advantages from the perspective of reducing the suspension viscosity to operating at higher shear rates. A higher shear rate of the suspension means a higher flow rate in the tubing and the electrochemical channels of the flow cell. While the flow battery cannot be operated at an arbitrarily high flow rate, operation beyond the limit where flocculates break up would be desirable from the standpoint of reducing suspension viscosity. Also, the increases in viscosity for higher LTO concentration means that there is a trade off in the flow cell between energy density

and energy efficiency. Future studies will be conducted to understand the structure of the particle aggregates and the conditions that control the onset of the flocculation.

2.5.5. Vial Cell Electrochemical Characterization

In advance of constructing a full flow cell to characterize the dispersed particle electrolyte suspensions, the vial cell was used to characterize our particle suspensions electrochemically. For vial cell Chronoamperometry (CA) experiments, a fixed discharge potential of 1.2 V was used and the current was measured for 120 seconds. This voltage was chosen because it was below the 1.55 V discharge plateau of LTO, but above the potential where electrolyte decomposition and lithium aluminum alloy formation would be expected to compete with lithium intercalation for the currents measured.[52-54] The short measuring time of 120 s was chosen because it was enough to observe a stable current output and time-efficient to perform the tests. The results of CA using the vial cell for increasing particle loadings in the electrolyte dispersions can be found in Figure 6a. The electrolyte without particles dispersed was used as a control, and as expected the measured current was very low, with the steady-state value approaching 0 mA. Compared with the electrolyte baseline, all the other samples achieved a measureable current output (the currents were negative because the cell was discharging). Therefore, the LTO particles in the suspension were the source of the observed electrochemical activity. To further understand if the reactions were caused by lithium insertion into the LTO particles, cyclic voltammetry (CV) testing was performed for these suspensions in the vial cell at 5 mV s^{-1} and the results are shown in Figure 6b. The reduction and oxidation peaks were around 1.55 V. No other peaks were observed, indicating no other major

redox reactions were occurring in the vial cell system except for the desired oxidation/reduction of LTO. The electrochemical responses that were observed could have been caused either by LTO particles attached on the aluminum wire or by the particles in the suspension colliding with the aluminum wire. To provide insights into whether electrochemical activity originated from attached or colliding LTO particles, a CA test was performed in the vial cell where the suspension stirring was halted during the test. If the electrochemical activity was from adsorbed particles, the current signal would be expected to remain approximately constant, while if the current was due to colliding particles we expected the measured current to drop to approximately zero due to the absence of stirring initiating particle collisions with the current collector. This CA experiment was conducted at 1.2 V with the 10 vol% LTO suspension. As shown in Figure 7a, when the stirring was stopped at ~160 s, the current response quickly dropped to the background level. The measured current increased back to ~0.2 mA (0.02 mA cm^{-2}) as the stirring was resumed at ~360 s. The results in Figure 7a demonstrate that the discharge current from the LTO suspension is dependent on the agitation of the solution provided by stirring. The results above lead us to conclude that the electrochemical reactions observed were due to lithium insertion and extraction into/out of LTO particles as they collided with the aluminum wire current collector.

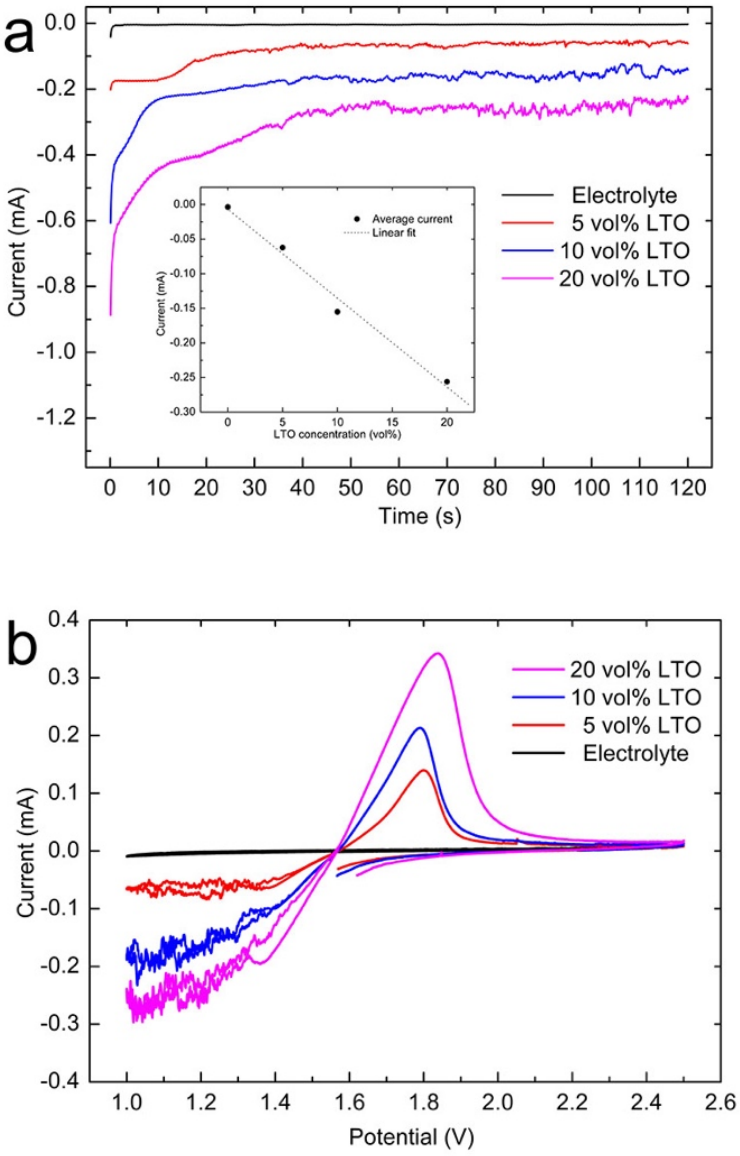

Figure 6. (a) Chronoamperometry (CA) profiles at 1.2 V and (b) cyclic voltammetry (CV) scans at the rate of 5 mV s^{-1} for the particle-free electrolyte and the electrolyte laden with 5 (red), 10 (blue), and 20 (purple) vol% LTO as measured in the vial cell. Inset in (a) is the steady state current as a function of the LTO concentration in the suspension.

As shown in the insert of Figure 6a, the discharge current linearly increased with the LTO concentration. This dependence of the measured CA current on LTO loading could be caused by the change in the collision frequencies of LTO particles on the aluminum wire. In the simplest case where the LTO particles were discrete units, a higher LTO concentration would provide more LTO particles within the range of the electron transfer distance from the aluminum wire, and hence more LTO particles would be able to collide on the aluminum wire and subsequently were discharged, resulting in the increased observed output currents. In addition, as discussed previously, rheological data suggested a more flocculated particle structure formed as the suspended particle concentration was increased. The flocculated aggregates would promote inter-particle charge transfer, further increasing the discharge current. The electrochemical plateaus had surprisingly little noise in the measured current for the first ~20 s of each CA curve, especially when compared to the steady-state current. This behavior was attributed to the electrochemical activity of a small amount of LTO powder attached on the aluminum wire. These attached particles were discharged as soon as the test started and were fully discharged quickly due to their small total capacity in the system. The steady-state current plateau; however, was attributed to the electrochemical discharge of LTO particles from the suspension colliding with the aluminum surface. We note that the CA curves were not flat but had fluctuations in the measured current. We attribute the fluctuations of the CA curves to the LTO particles not being perfectly homogeneously dispersed within the electrolyte. Thus, the concentration of LTO particles near the current collector, as well as number of particles/aggregates in direct contact, varies at any given instant. This local inhomogeneity in the dispersion results in the fluctuation in the observed current because

when more total particles/aggregates were in contact with the current collector, greater electrochemical current was produced.

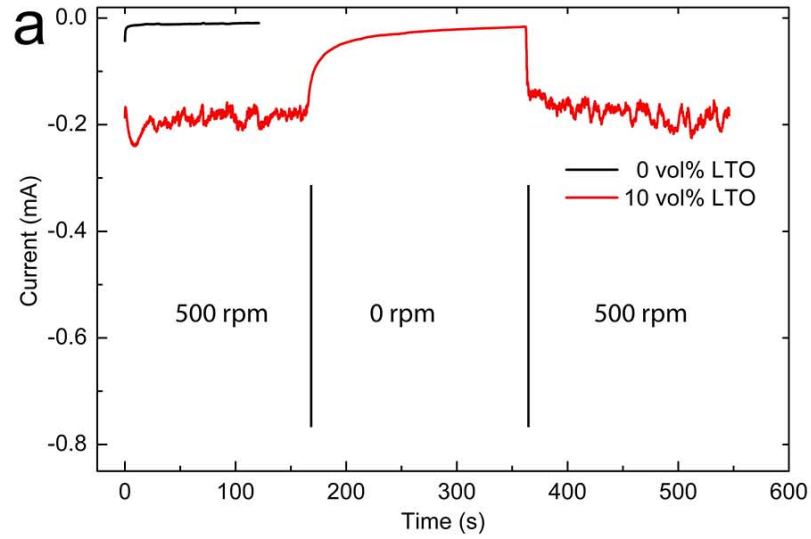

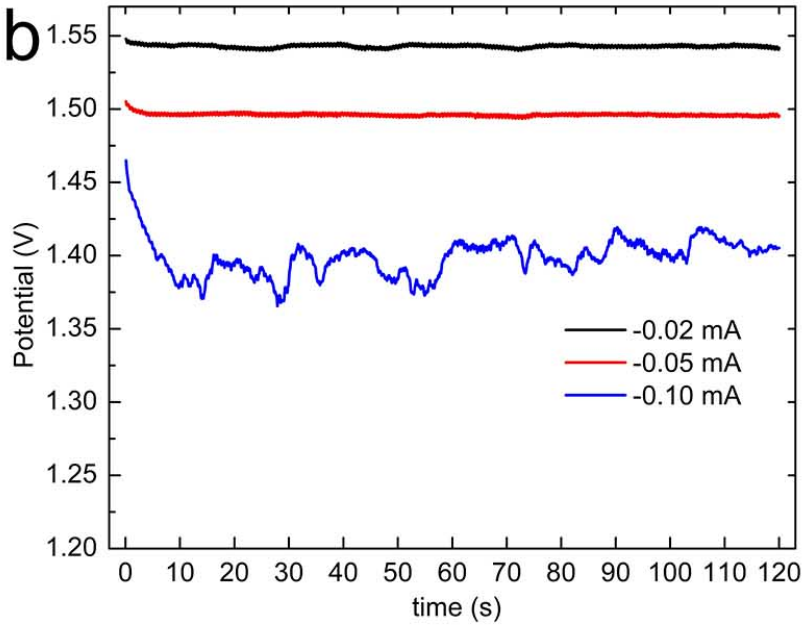

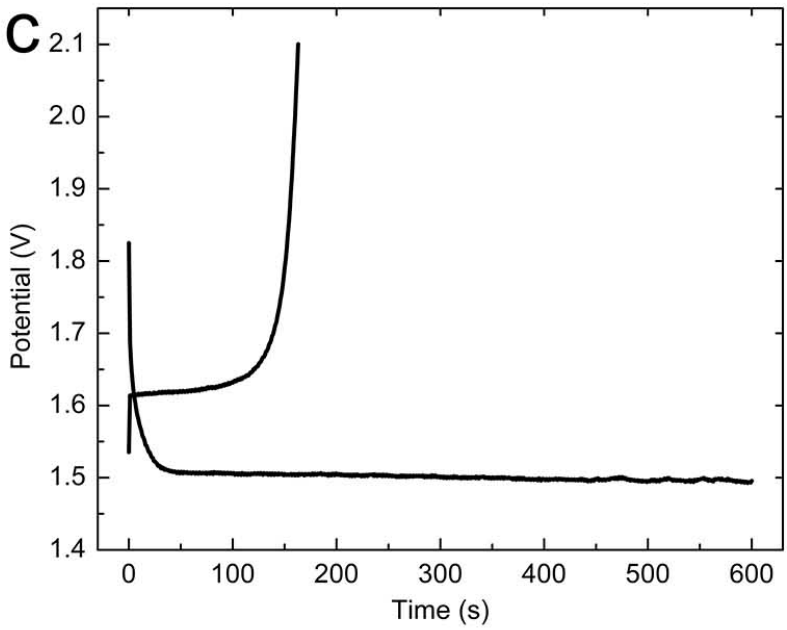

Figure 7. (a) Chronoamperometry (CA) profiles at 1.2 V with the stirring halted during the test, (b) Chronopotentiometry (CP) profiles with applied discharge currents 0.02, 0.05, 0.10 mA (0.002, 0.005, and 0.010 mA cm^{-2}, respectively), and (c) discharge and charge curves for the vial cell with an LTO concentration of 10 vol%.

The CV curves in Figure 6b were also influenced by the LTO concentration in the suspension. The CV results were consistent with the CA measurements from the perspective that there was an increase in the measured current as the LTO loading was increased. During electrochemical reduction of the LTO in the CV scan, a typical CV peak is not observed. These CV scans were not taken in quiescent solution, but instead were in a highly turbid constantly stirred suspension. We attribute the lack of a reduction peak and the increased noise in the measured current at lower voltages on reduction to the electrochemical reactions in this regime being limited by the collision rate of particles in the suspension with the current collector wire. An interesting phenomenon observed in

the CV curves was that there were significant oxidation peaks, even though only a very small fraction of the LTO particles (which initially should all be in the oxidized state) have been reduced. We estimate the fraction of the LTO material in the suspension that has been reduced before the oxidation half cycle to be only < 0.01% of the total electrochemical capacity within the dispersion. Thus, the significant LTO oxidation peaks in the CV scans indicate that the same LTO particles that participated in electrochemical reduction were still available to participate in electrochemical oxidation reactions on the aluminum wire current collector. The polarization of the CV curves was observed to be independent of loading of LTO particles. Great care was taken to use the same aluminum wire, lithium foil, and the wire-foil separation for all measurements at the different loadings and hence the IR drop associated with these components would be expected to be equivalent for all the measurements.[55]

To further characterize the discharging behavior of the vial cell system, chronopotentiometry (CP) testing was performed for the 10 vol% sample. For currents of -0.02, -0.05, and -0.10 mA (-0.002, -0.005, and -0.010 mA cm^{-2}, respectively), the potentials measured for the vial cell are shown in Figure 7b. Decreasing steady-state potentials were observed as the current was increased, consistent with previous reports.[23, 42, 56-58] The observed behavior was attributed to the increased IR drop in the vial cell with increasing current. The open cell voltage (OCV) was measured to be 1.57 V, and the steady-state potentials for 0.02, 0.05 and 0.10 mA discharge currents were 1.54, 1.49 and 1.40 V, respectively. These results were consistent with an almost linear relationship of the IR drop with increasing current. We note that the CP curve for

the 0.10 mA test was relatively unstable compared to the 0.02 mA and 0.05 mA currents. We speculate that at 0.10 mA we are starting to reach the limits of the stable current that we can draw for the stochastic particle collision process, at least for the level of agitation and amount of exposed surface area on the current collector in the vial cell.

Constant current discharging and charging was performed with the vial cell to demonstrate the viability of charging and discharging the vial cell as a battery. The constant current charge/discharge tests were performed using the 10 vol% dispersion. As shown in Figure 7c, the cell was first discharged at 0.05 mA (0.005 mA cm^{-2}) for 10 minutes and was then switched over to charge at the same current, with the cell being successfully charged for ~3 minutes before hitting the upper voltage cut-off of 2.1 V, resulting a coulombic efficiency of 38%. The charge and discharge plateaus were both at ~1.55 V, consistent with lithium insertion and extraction into/out of LTO particles with low polarization.[22, 23, 40-42] While the total capacities charged/discharged were relatively low (the total discharge capacity was 8.33×10^{-3} mAh and the total charge capacity was 3.18×10^{-3} mAh, corresponding to < 0.01% of the capacity of the LTO particles in the suspension), full discharge and charge of the cell would have been impractical because of the relatively low current densities and large amount of LTO active particles in the vial cell. The columbic efficiency also appears artificially low because most of the discharged material was exchanged into the solution laden with LTO particles in the oxidized state, limiting the total capacity available. The primary purpose of the test was to demonstrate 1) that the vial cell was capable of charge and discharge with colliding LTO particles, and 2) that the polarization during charge and discharge

was low. Both of these principles were demonstrated in the vial cell, and thus we moved to finally demonstrating electrochemical capacity of the LTO suspension within a custom flow cell geometry.

2.5.6. Flow Cell Electrochemical Characterization

We assembled a custom flow cell (Figure 1b) using the 10 vol% LTO suspension. The flow rate used for the LTO suspension through the flow channel and tubing was 120 mL min^{-1}. A CA test was performed for the flow cell at a fixed potential of 1.2 V and the results are shown in Figure 8a. The CA curve displayed similar behavior to that observed for the vial cell. The significant current measured in excess of the baseline confirmed that the LTO particles were discharged in the flow cell. CV was used to further confirm that there was electrochemical capacity from the LTO within the flow cell (Figure 8b). The redox peaks at ~1.55 V were consistent with the lithiation and delithiation of LTO particles.[22, 23, 40-42] Similar to the vial cell, the current output fluctuated due to the local inhomogeneity of the LTO suspension. The CV profile in the flow cell was similar to the vial cell, although the oxidation peak was much smaller. This was because the amount of LTO material in the flow cell experiment was larger than the amount used in the vial cell, while the surface area available from the current collector was less, resulting in a decrease in the relative amount of LTO particles discharged. In the flow cell, the oxidation current was smaller relative to the vial cell because a much smaller portion of LTO particles were discharged; and the "peak" was broadened because the residence time was short and the reaction was not limited by lithium-ion diffusion but rather by the available discharged LTO particle concentration.

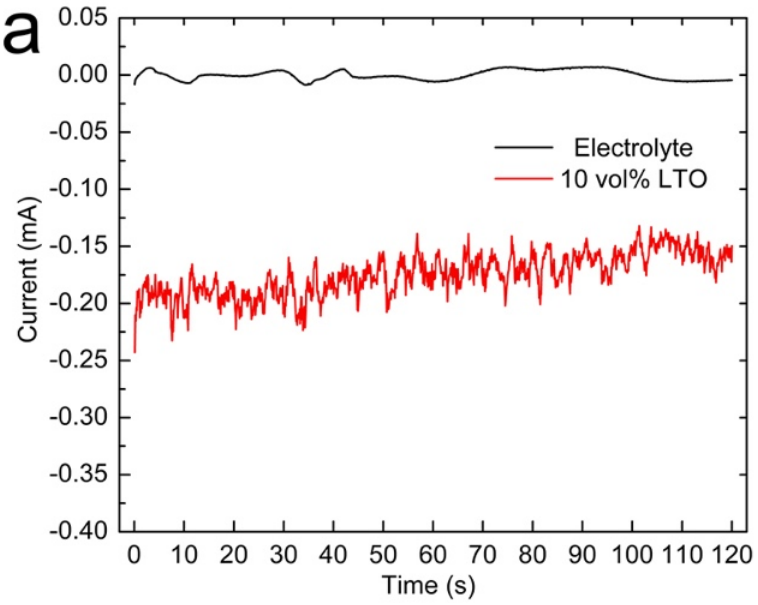
a
0.05
0.00
-0.05
-0.10
-0.15
-0.20
-0.25
-0.30
-0.35
-0.40
Current (mA)
0 10 20 30 40 50 60 70 80 90 100 110 120
Time (s)
Electrolyte
10 vol% LTO

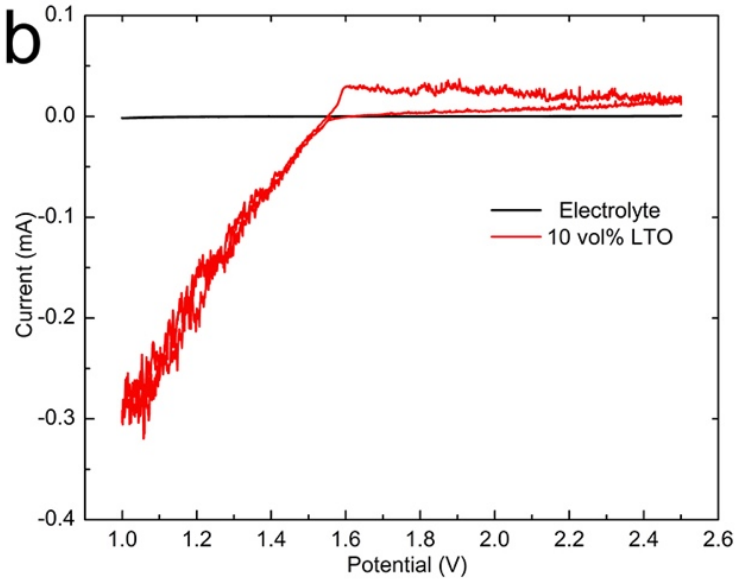
b
0.1
0.0
-0.1
-0.2
-0.3
-0.4
Current (mA)
1.0 1.2 1.4 1.6 1.8 2.0 2.2 2.4 2.6
Potential (V)
Electrolyte
10 vol% LTO

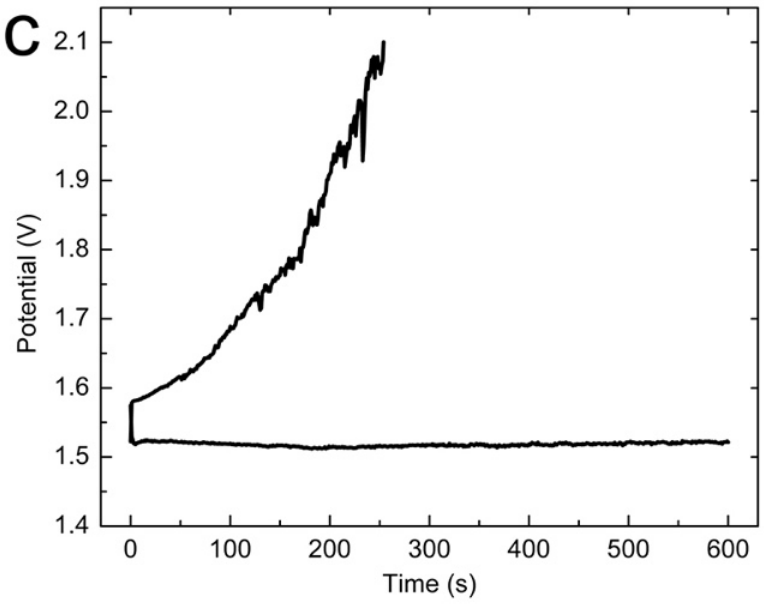

Figure 8. (a) Chronoamperometry (CA) profile at 1.2 V, (b) cyclic voltammetry (CV) scan at the rate of 5 mV s^{-1}, and (c) discharge and charge curve for the flow cell with an LTO concentration in the electrolyte of 10 vol%.

A constant current discharge and charge was also performed for the same 10 vol% sample (Figure 8c). The profile used was similar to the vial cell described previously. A constant current discharge was performed at 0.02 mA (0.0064 mA cm^{-2}) for 10 minutes, followed by a constant current charge at the same current that reached the upper voltage cut-off after ~4 minutes. The discharge plateau was at ~1.55 V, and the charge cycle starts at a plateau at ~1.55 V before quickly increasing in potential. The capacities were of 3.33×10^{-3} mAh for discharge and 1.49×10^{-3} mAh on charge, resulting a coulombic efficiency of 45%. It is not surprising that only a fraction of the discharge capacity is recovered on charge, as a very small portion of LTO particles were discharged. We note

that the charging curve has more noticeable fluctuations and a greater polarization relative to the vial cell. This is because the vial cell had constant access to the discharged particles during testing while the flow cell was only able to charge the small portion of the discharged particles that was in the flow chamber at any given time. While the capacities obtained in this cell are relatively modest, they successfully demonstrate the galvanic cycling of a solid dispersion LTO flow battery redox couple that relies on collision of LTO particles with the current collector to store and deliver electrochemical energy. Future efforts will be taken to increase the power of the cell to achieve full discharge and charge cycles within practical time limits.

We will note here that both the vial cell and flow cell experiments were limited in their discharge and charge times due to practical constraints of our system and its low current and power densities in this initial demonstration, and this limitation was not due to limited capacity of the LTO in the suspension. The mass of LTO in the vial cell with a 10 vol% suspension was 2.98 g. Based on the total cycling current in the cell of 0.02 mA, the time to fully discharge the cell would be ~348 days (2.98 g LTO at ~140 mAh g^{-1} is ~417 mAh). The ~12 months to discharge our vial cell made complete cycles impractical. These factors highlight the need for current collector designs to increase the current density in our system. We also note our Li/LTO flow cell has a power density of ~0.01 mW cm^{-2}, in this initial half cell demonstration flow system. The particle size of the LTO particles is also expected to have a major impact on the power density measured in the flow and vial cells. The resistance from the LTO particles will be dependent on the ionic and electronic conductivity of the particles and their diameters.[59, 60] Minimizing

active material particle sizes has been a typical approach to enhance conventional battery performance by increasing active surface areas, decreasing lithium ion diffusion distance and compensating the electronic conductivity.[24, 59, 61-65] Previous reports have established that the electrode resistance per unit mass of active material follows a general power law relationship with the particle diameter.[59] In the case of our uncoated LTO particles with no carbon in the slurry, we expect the particle collisions result in active particles with effectively a point-contacted conductor. Considering the relatively low ionic conductivity of LTO particles compared to their electronic conductivity (in particular after partial lithiation), we expect the resistance per unit mass of particles undergoing electrochemical reactions in our system to scale with the square of the particle diameters.[59] A smaller particle size is also generally preferable in the solid dispersion redox couple because with smaller particles lithium ions need a shorter diffusion distance from the surface to the center of the particles to fully discharge/charge the particle, and there is a finite residence time during collision with the current collector. Future experiments will be conducted to understand the detailed impacts of particle size and polydispersity on the power density in our dispersed particle electrochemical system.

It is instructive to discuss the carbon-free solid dispersion flow system relative to existing flow battery systems. Assuming that we can achieve capacities for the LTO in our LTO dispersions comparable what was reversibly measured for our LTO particle coin cells, the anolyte within our flow cell setup would be able to achieve a capacity of 55.6 mAh g^{-1} (total anolyte mass basis) with a viscosity of ~0.17 Pa·s at 20 vol% LTO loading. Some of the highest reported vanadium anolyte concentrations for vanadium redox flow

batteries have theoretical capacities and viscosities within a similar range,[66] however, the dispersion flow battery has the advantages of the ability to pair our anolyte with higher voltage lithium-ion catholyte materials and we are exploring the possibility of increasing LTO particle loading which would result in an even higher capacity dispersion. Also, relative to the semi-solid flow battery systems reported in the literature,[16] for similar particle volume loadings of particles the solid dispersion flow battery redox couple reported here operates without carbon additives and has a lower viscosity. The maximum packing volume fraction is the upper limit for the active material loading. Depending on the particle size and morphology, this limit will range from 52.4 vol% [67] to 71 vol% [47, 68]. The energy density for the carbon-free solid dispersion redox flow battery system is only dependent on the energy density of the solid active material itself and the volume fraction of the active material that can be stably dispersed and efficiently pumped.

2.6. Conclusions

A carbon-free solid dispersion redox flow couple consisting of an organic lithium-ion electrolyte laden with LTO was demonstrated and characterized electrochemically with a unique and systematic approach. It was found that LTO-to-LTO particle contacts provide sufficient electronic conductivity to allow particles multiple LTO particle distances from the current collector to contribute to battery capacity. The LTO suspension has a shear-thinning behavior and the current output of the LTO suspensions was linearly dependent on the LTO concentration. Electrochemical characterization of LTO dispersions in custom flow geometries indicates electrochemical capacity is provided by collision of LTO particles with the current collector, and that design of a flow cell relying on collision from a particle dispersion can be successfully reversibly electrochemically oxidized and reduced.

A carbon-free solid dispersion flow battery system inherits the advantages of conventional redox flow batteries to decouple the power and the energy in the system, providing the flexibility to independently adjust and design the power and energy requirements for an application. This system also has the potential to provide a much higher energy density with a lower viscosity compared with vanadium flow battery and semi-solid flow battery, provided the anolyte described in this study can be paired with a suitable catholyte and sufficient capacity utilization of active materials can be achieved. The characterization methods described in this paper provide a systematic step-by-step method to study dispersed solid flow batteries.

2.7. References

1. Chakrabarti, M.H., et al., *Application of carbon materials in redox flow batteries.* Journal of Power Sources, 2014. **253**: p. 150-166.
2. de Leon, C.P., et al., *Redox flow cells for energy conversion.* Journal of Power Sources, 2006. **160**(1): p. 716-732.
3. Weber, A.Z., et al., *Redox flow batteries: a review.* Journal of Applied Electrochemistry, 2011. **41**(10): p. 1137-1164.
4. Parasuraman, A., et al., *Review of material research and development for vanadium redox flow battery applications.* Electrochimica Acta, 2013. **101**: p. 27-40.
5. Ke, X., et al., *Flow distribution and maximum current density studies in redox flow batteries with a single passage of the serpentine flow channel.* Journal of Power Sources, 2014. **270**: p. 646-657.
6. Yue, L., et al., *Highly hydroxylated carbon fibres as electrode materials of all-vanadium redox flow battery.* Carbon, 2010. **48**(11): p. 3079-3090.
7. Park, M.S., et al., *High-energy redox-flow batteries with hybrid metal foam electrodes.* ACS Appl Mater Interfaces, 2014. **6**(13): p. 10729-35.
8. Wu, X.J., et al., *Influence of organic additives on electrochemical properties of the positive electrolyte for all-vanadium redox flow battery.* Electrochimica Acta, 2012. **78**: p. 475-482.
9. Sun, C.X., et al., *Investigations on transfer of water and vanadium ions across Nafion membrane in an operating vanadium redox flow battery.* Journal of Power Sources, 2010. **195**(3): p. 890-897.
10. Pletcher, D. and R. Wills, *A novel flow battery: A lead acid battery based on an electrolyte with soluble lead(II) - Part II. Flow cell studies.* Physical Chemistry Chemical Physics, 2004. **6**(8): p. 1779-1785.
11. Zhao, Y.F., et al., *Electrochemical Behavior of Polyaniline Microparticle Suspension as Flowing Anode for Rechargeable Lead Dioxide Flow Battery.* Journal of the Electrochemical Society, 2014. **161**(3): p. A330-A335.
12. Gordon, M. and G. Suppes, *Convection battery-modeling, insight, and review.* Aiche Journal, 2013. **59**(8): p. 2833-2842.
13. Gordon, M. and G. Suppes, *Li-Ion Battery Performance in a Convection Cell Configuration.* Aiche Journal, 2013. **59**(5): p. 1774-1779.
14. Dunn, B., H. Kamath, and J.M. Tarascon, *Electrical Energy Storage for the Grid: A Battery of Choices.* Science (Washington, DC, U. S.), 2011. **334**(6058): p. 928-935.
15. Ding, Y., Y. Zhao, and G. Yu, *A Membrane-Free Ferrocene-Based High-Rate Semiliquid Battery.* Nano Lett, 2015. **15**(6): p. 4108-4113.
16. Duduta, M., et al., *Semi-Solid Lithium Rechargeable Flow Battery.* Adv. Energy Mater., 2011. **1**(4): p. 511-516.
17. Li, Z., et al., *Aqueous semi-solid flow cell: demonstration and analysis.* Physical Chemistry Chemical Physics, 2013. **15**(38): p. 15833-15839.
18. Hamelet, S., et al., *Non-Aqueous Li-Based Redox Flow Batteries.* Journal of the Electrochemical Society, 2012. **159**(8): p. A1360-A1367.

19. Madec, L., et al., *Surfactant for Enhanced Rheological, Electrical, and Electrochemical Performance of Suspensions for Semisolid Redox Flow Batteries and Supercapacitors.* Chempluschem, 2015. **80**(2): p. 396-401.
20. Brunini, V.E., Y.-M. Chiang, and W.C. Carter, *Modeling the hydrodynamic and electrochemical efficiency of semi-solid flow batteries.* Electrochimica Acta, 2012. **69**: p. 301-307.
21. Viswanathan, V., et al., *Cost and performance model for redox flow batteries.* Journal of Power Sources, 2014. **247**: p. 1040-1051.
22. Deng, S., et al., *Synthesis and electrochemical properties of Li4Ti5O12 spheres and its application for hybrid supercapacitors.* Electrochimica Acta, 2014. **146**: p. 37-43.
23. He, N.D., B.S. Wang, and J.J. Huang, *Preparation and electrochemical performance of monodisperse Li4Ti5O12 hollow spheres.* Journal of Solid State Electrochemistry, 2010. **14**(7): p. 1241-1246.
24. Yang, Z., et al., *Nanostructures and lithium electrochemical reactivity of lithium titanites and titanium oxides: A review.* J. Power Sources, 2009. **192**(2): p. 588-598.
25. Ohzuku, T., A. Ueda, and N. Yamamoto, *Zero-Strain Insertion Material of Li[Li1/3Ti5/3]O4 for Rechargeable Lithium Cells.* J. Electrochem. Soc, 1995. **142**(5): p. 1431-1435.
26. Shen, Y., et al., *Solid State Formation Mechanism of Li4Ti5O12from an Anatase TiO2Source.* Chem. Mater., 2014. **26**(12): p. 3679-3686.
27. Ziebarth, B., et al., *Lithium diffusion in the spinel phase of lithium titanate from first principles.* Physical Review B, 2014. **89**(17).
28. Kim, C., et al., *Mechanism of Phase Propagation During Lithiation in Carbon-Free Li4Ti5O12 Battery Electrodes.* Advanced Functional Materials, 2013. **23**(9): p. 1214-1222.
29. Ohzuku, T. and A. Ueda, *Why transition metal (di)oxides are the most attractive materials for batteries.* Solid State Ionics, 1994. **69**(3-4): p. 201-211.
30. Belharouak, I., G.M. Koenig, and K. Amine, *Electrochemistry and safety of Li4Ti5O12 and graphite anodes paired with LiMn2O4 for hybrid electric vehicle Li-ion battery applications.* J. Power Sources, 2011. **196**(23): p. 10344-10350.
31. Martha, S.K., et al., *Li4Ti5O12/LiMnPO4 Lithium-Ion Battery Systems for Load Leveling Application.* Journal of the Electrochemical Society, 2011. **158**(7): p. A790-A797.
32. Viswanathan, V.V., et al., *Effect of entropy change of lithium intercalation in cathodes and anodes on Li-ion battery thermal management.* Journal of Power Sources, 2010. **195**(11): p. 3720-3729.
33. Patey, T.J., et al., *Electrode engineering of nanoparticles for lithium-ion batteries-Role of dispersion technique.* Journal of Power Sources, 2009. **189**(1): p. 590-593.
34. Sun, Z., et al., *Quantitative evaluation of surfactant-stabilized single-walled carbon nanotubes: Dispersion quality and its correlation with zeta potential.* Journal of Physical Chemistry C, 2008. **112**(29): p. 10692-10699.
35. Lotya, M., et al., *High-Concentration, Surfactant-Stabilized Graphene Dispersions.* Acs Nano, 2010. **4**(6): p. 3155-3162.

36. Wachtler, M., J.O. Besenhard, and M. Winter, *Tin and tin-based intermetallics as new anode materials for lithium-ion cells.* Journal of Power Sources, 2001. **94**(2): p. 189-193.
37. Tsubone, D., et al., J. Ceram. Soc. Jpn. Inter. Ed., 1994. **102**(179).
38. Hanawalt, J., et al., Anal. Chem., 1938. **10**(475).
39. Yuan, T., et al., *A mechanism study of synthesis of Li4Ti5O12 from TiO2 anatase.* Journal of Alloys and Compounds, 2010. **505**(1): p. 367-373.
40. He, Z., et al., *Spherical Li4Ti5O12 synthesized by spray drying from a different kind of solution.* Journal of Alloys and Compounds, 2012. **540**: p. 39-45.
41. Yi, T.-F., et al., *Synthesis and application of a novel Li4Ti5O12 composite as anode material with enhanced fast charge-discharge performance for lithium-ion battery.* Electrochimica Acta, 2014. **134**: p. 377-383.
42. Lin, C.F., et al., *Monodispersed mesoporous Li4Ti5O12 submicrospheres as anode materials for lithium-ion batteries: morphology and electrochemical performances.* Nanoscale, 2014. **6**(12): p. 6651-6660.
43. Kubiak, P., et al., *Electrochemical evaluation of rutile TiO2 nanoparticles as negative electrode for Li-ion batteries.* Journal of Power Sources, 2009. **194**(2): p. 1099-1104.
44. Shin, J.-W., et al., *Effects of TiO2 Starting Materials on the Solid-State Formation of Li4Ti5O12.* Journal of the American Ceramic Society, 2012. **95**(6): p. 1894-1900.
45. Young, D., et al., *Electronic Conductivity in the Li4/3Ti5/3O4-Li7/3Ti5/3O4 System and Variation with State-of-Charge as a Li Battery Anode.* Advanced Energy Materials, 2013. **3**(9): p. 1125-1129.
46. Park, M., et al., *A review of conduction phenomena in Li-ion batteries.* J. Power Sources, 2010. **195**(24): p. 7904-7929.
47. Mewis, J. and N.J. Wagner, *Colloidal suspension rheology*. Cambridge series in chemical engineering. 2012, Cambridge, UK New York: Cambridge University Press.
48. Youssry, M., et al., *Formulation of flowable anolyte for redox flow batteries: Rheo-electrical study.* Journal of Power Sources, 2015. **274**: p. 424-431.
49. Smith, T.L. and C.A. Bruce, *Intrinsic Viscosities and Other Rheological Properties of Flocculated Suspensions of Nonmagnetic and Magnetic Ferric Oxides.* Journal of Colloid and Interface Science, 1979. **72**(1): p. 13-26.
50. Zhou, Z., P.J. Scales, and D.V. Boger, *Chemical and physical control of the rheology of concentrated metal oxide suspensions.* Chemical Engineering Science, 2001. **56**: p. 2901-2920.
51. Ostwald, W., *Ueber die rechnerische Darstellung des Strukturgebietes der Viskosität.* Kolloid-Zeitschrift, 1929. **47**(2): p. 176 - 187.
52. Zhang, X. and T.M. Devine, *Identity of Passive Film Formed on Aluminum in Li-Ion Battery Electrolytes with LiPF[sub 6].* Journal of The Electrochemical Society, 2006. **153**(9): p. B344-B351.
53. Myung, S.-T. and H. Yashiro, *Electrochemical stability of aluminum current collector in alkyl carbonate electrolytes containing lithium bis(pentafluoroethylsulfonyl)imide for lithium-ion batteries.* Journal of Power Sources, 2014. **271**: p. 167-173.

54. Morita, M., et al., *Anodic behavior of aluminum in organic solutions with different electrolytic salts for lithium ion batteries.* Electrochemica Acta, 2002. **47**(17): p. 2787-2793.
55. Hamann, C.H., A. Hamnett, and W. Vielstich, *Electrochemistry*. 2 ed. 2007: Wiley-VCH.
56. Madec, L., et al., *Electronic vs Ionic Limitations to Electrochemical Performance in Li4Ti5O12-Based Organic Suspensions for Lithium-Redox Flow Batteries.* Journal of the Electrochemical Society, 2014. **161**(5): p. A693-A699.
57. Bai, X., et al., *Enhancing the Long-Term Cyclability and Rate Capability of Li4Ti5O12 by Simple Copper-Modification.* Electrochimica Acta, 2015. **155**: p. 132-139.
58. Liu, J., et al., *Self-supported Li4Ti5O12-C nanotube arrays as high-rate and long-life anode materials for flexible Li-ion batteries.* Nano Lett, 2014. **14**(5): p. 2597-603.
59. Gaberscek, M., R. Dominko, and J. Jamnik, *Is small particle size more important than carbon coating? An example study on LiFePO4 cathodes.* Electrochem. Commun., 2007. **9**(12): p. 2778-2783.
60. Li, H. and H. Zhou, *Enhancing the performances of Li-ion batteries by carbon-coating: present and future.* Chem. Commun. (Cambridge, U. K.), 2012. **48**(9): p. 1201-17.
61. Kim, K.H. and K.B. Kim, *Ultrasound assisted synthesis of nano-sized lithium cobalt oxide.* Ultrason. Sonochem., 2008. **15**(6): p. 1019-1025.
62. Tang, W., et al., *Nano-LiCoO2 as cathode material of large capacity and high rate capability for aqueous rechargeable lithium batteries.* Electrochem. Commun., 2010. **12**(11): p. 1524-1526.
63. Zhao, X., et al., *Nano LiMn2O4 with spherical morphology synthesized by a molten salt method as cathodes for lithium ion batteries.* RSC Adv., 2012. **2**(19): p. 7462-7469.
64. Arico, A.S., et al., *Nanostructured materials for advanced energy conversion and storage devices.* Nat. Mater., 2005. **4**(5): p. 366-377.
65. Lazarraga, M.G., et al., *Nanosize LiNiyMn2-yO(4) (0, y <= 0.5) spinels synthesized by a sucrose-aided combustion method. Characterization and electrochemical performance.* J. Mater. Chem., 2004. **14**(10): p. 1640-1647.
66. Rahman, F. and M. Skyllas-Kazacos, *Vanadium redox battery: Positive half-cell electrolyte studies.* Journal of Power Sources, 2009. **189**(2): p. 1212-1219.
67. Shapiro, A.P. and R.F. Probstein, *Random Packings of Spheres and Fluidity Limits of Monodisperse and Bidisperse Suspensions.* Physical Review Letters, 1992. **68**(9): p. 1422-1425.
68. Dekruif, C.G., et al., *Hard-Sphere Colloidal Dispersions - Viscosity as a Function of Shear Rate and Volume Fraction.* Journal of Chemical Physics, 1985. **83**(9): p. 4717-4725.

Chapter III. High-Performance $LiCoO_2$ Sub-Micrometer Materials from Scalable Microparticle Template Processing

3.1 Overview

This chapter describes a synthesis method to produce high-performance sub-micrometer $LiCoO_2$ material in a scalable way. Moving towards a full cell design of carbon-free RFB with lithium-ion active materials, a suitable cathode material is needed. $LiCoO_2$ is chosen because it is a commonly used lithium-ion cathode material with relatively high electronic and ionic conductivity. This chapter describes the template-based synthesis method in detail and discusses the electrochemical performance. $LiCoO_2$ synthesized with this method has high rate capabilities and is also used as the cathode active material in the next chapter to demonstrate a carbon-free lithium-ion RFB in which both electrodes are lithium-ion active material suspensions.

Elements of this chapter have been published in ChemistrySelect:

Z. Qi, G.M. Koenig, High-Performance $LiCoO_2$ Sub-Micrometer Materials from Scalable Microparticle Template Processing, *ChemistrySelect*, 1 (2016) 3992-3999.

3.2. Abstract

One attribute that has limited performance for some lithium-ion battery active material systems is large particle size. While many methods have been reported in the literature for producing high-performance sub-micrometer sized battery particles, often these procedures are difficult to adapt to large battery electrode powder production and/or the processing is relatively expensive compared to traditional methods. We report a highly scalable process to produce high performance sub-micrometer battery active material using an initial demonstration cathode chemistry, $LiCoO_2$ (LCO). We adopted a template-based process which took advantage of a cobalt oxalate precursor material with a rod morphology. Lithiation of the precursor via calcination produced loosely connected sub-micrometer sized LCO particles which were easily dispersed into individual particles through a low energy mechanical method. The sub-micrometer sized LCO particulates exhibited excellent electrochemical performance as lithium-ion battery cathode active materials, including high discharge capacity, rate capability, and coulombic efficiency.

3.3. Introduction

Batteries are currently used for many different scales of applications, from personal watches to large backup battery banks.[1] Lithium-ion chemistries are among the most popular for batteries being used and developed due to their high energy density on both a mass and volume basis.[2] While lithium-ion batteries have historically been very popular for consumer electronic applications, their high energy density has also resulted in the adoption of these chemistries in electric vehicle applications.[3, 4] Larger-scale stationary energy storage projects have also demonstrated the use of lithium-ion batteries, and as these batteries are applied to larger and larger scales the cost of the materials that comprise the cells needs to be continuously reduced to make advanced batteries cost-competitive.[5-8] Scalable processes must be developed for high performance battery materials, including sub-micrometer and nano-sized materials, which can have very complex architectures and/or processing.[9, 10]

One challenge that has previously been encountered for some lithium-ion battery active material systems is large particle size.[11] For materials where the ionic and/or electronic conductivity within the active material are relatively low, large particles result in unacceptably high mass transport and/or electronic resistance due to the dependence of the resistance on particle size.[12-18] Not only do these resistances result in lower energy efficiency for the cell, the wasted energy results in increased heat generation within the battery, and increased cell temperatures are detrimental to both battery cycling performance and safety.[19, 20] With sub-micrometer sized active material particles, the individual per particle resistance can be substantially reduced, providing a higher rate

capability and round trip energy efficiency.[12-18, 21-24] Smaller active material particles have also been demonstrated to mitigate mechanical stress in the active material during cycling which reduces particle cracking, often a major factor in battery capacity fading with cycling.[21, 25] We note that drawbacks to using active material sub-micrometer particles can include relatively low tap density and higher relative surface area that can participate in deleterious side reactions, however, these materials are finding increasing importance in new less conventional battery systems, such as printed electrodes and semi-solid type flow batteries.[26, 27] One major challenge shared by many sub-micrometer and nano-sized battery materials is relatively complex or expensive material handling and processing.[9, 10]

There are a variety of approaches reported in literature to synthesize sub-micrometer sized lithium-ion battery active materials. High-energy planetary ball milling is one of the most popular approaches adopted in research labs to produce sub-micrometer and nano-sized particles from a synthesized final material with an initially larger particle size.[24, 28] This process is done using individual batch methods and involves an inert grinding media breaking up the active material particles under high accelerating speeds (in some cases >1000 rpm).[24] These processes are challenging to scale because of their energy intensity and relatively low throughput. Hydrothermal processes are another popular approach to synthesize sub-micrometer and nano-sized active materials, however, reproducibility is typically low because of the high sensitivity of hydrothermal reactions to multiple process conditions.[29-32] Ultrasonic assisted hydrothermal synthesis.[33] sol-gel approaches,[34] molten salt synthesis,[35-38] and electrodeposition techniques

[39] have also been used to produce sub-micrometer materials, but the scalability and cost of these methods are challenging to move to high volume processing. While many methods have been reported for producing high-performance sub-micrometer and nano-sized battery particles, often these techniques are very difficult to scale up to the quantities needed for battery electrode powder synthesis and/or the processing is relatively expensive compared to traditional existing processes.

Template-based synthesis approaches starting from precipitate precursors have been reported by multiple research groups as an attractive method to produce lithium-ion battery active materials.[40-46] A precursor template is first synthesized/purchased and then subsequently lithiated with lithium salt to produce the final active material. The morphology of the precursor is controllable and will typically be maintained during the high temperature lithiation process.[40, 42] This method provides the opportunity to produce scalable materials of controllable morphologies that are adaptable to existing high volume calcination processes currently used in battery material manufacturing.[47] An important distinction of these previous research efforts with template materials is that the templates are typically micrometer-sized particles, and a major goal was to produce active materials with high tap densities to improve active material loading within the battery electrodes.[40, 46, 48] Our strategy for lithium-ion battery material templates is to synthesize a precursor that decomposes to give low tap density because it forms loosely agglomerated primary sub-micrometer particles in a secondary particle with large voids. Herein, we report this highly scalable and low energy process to produce high

performance battery sub-micrometer active material particles using an initial demonstration cathode chemistry, $LiCoO_2$ (LCO).

3.4. Experimental

3.4.1. Preparation of Precursor and LCO Materials

$CoC_2O_4 \cdot 2H_2O$ precursor was synthesized via a co-precipitation method, similar to other battery precursor co-precipitation reports in the literature.[49-52] While a batch process was used in these experiments, multiple groups have extended similar methods to continuous co-precipitation processes.[53-59] Equal volume of 0.1 M $(NH_4)_2C_2O_4$ (Fisher Scientific) and 0.1 M $Co(NO_3)_2$ (Fisher Scientific) solutions were preheated to 50 °C prior to mixing and the temperature was maintained between 50°C and 60 °C during the synthesis. The mixture was stirred intensely for 30 minutes before vacuum filtration to collect the solid particles. The solid particles were dried at 80 °C overnight and then dried in a vacuum oven at 80°C for 2 hours. The $CoC_2O_4 \cdot 2H_2O$ precursor was mixed with LiOH (Fisher Scientific, with Li : Co stoichiometric of 1.05 : 1) and calcined in a Carbolite CWF 1300 box furnace in an air atmosphere. The mixture was held at 200 °C for 2 hours to degas before increasing to the final calcination temperature (750 °C, 800 °C, 850 °C, and 900 °C were used in this study) at a rate of 1 °C/min. The furnace was immediately turned off upon reaching the target calcination temperature and allowed to cool to ambient temperature. The LCO product was milled to smaller particles through a wet soft milling procedure involving mixing the powder with 1-butanol and 12 mm zirconia beads and then soft milling on a roller (US Stoneware).

3.4.2. Characterization of Precursor and LCO Materials

To characterize the morphologies of the precursor, unmilled and milled LCO powder, scanning electron microscope (SEM) images were taken with a Quanta 650 SEM. X-ray diffraction (XRD) patterns were obtained with a Panalytical X'pert diffractometer using Cu Kα radiation. Thermogravimetric analysis (TGA) of the $CoC_2O_4 \cdot 2H_2O$ precursor in air was conducted with a TA Instruments Q50. Surface area of the milled LCO powder was determined with a surface area and pore size analyzer (NOVA 2200e). Tap density was measured using a tap density analyzer (Quantachrome Instruments).

3.4.3. Electrochemical Characterizations

Electrochemical characterization was done by using CR2032-type coin cells with an LCO electrode as the cathode paired with either lithium foil or graphite as the anode active material. The electrodes were separated by a polypropylene / polyethylene / polypropylene trilayer membrane. The LCO electrodes were fabricated from slurries comprised of 80 wt % LCO powder, 10 wt % carbon black as conductive additive, and 10 wt % polyvinylidene difluoride binder (PVDF) dissolved in *N*-methylpyrrolidone (NMP, Sigma-Aldrich®). Graphite electrodes were fabricated from a slurry comprised of 92 wt % graphite and 8 wt % PVDF dissolved in NMP. The slurries were prepared by agitation in a slurry mixer for 5 minutes, followed by pasting onto metal foil using a doctor blade (aluminum foil was used for the LCO electrodes and copper foil for the graphite electrodes). The pasted slurries were dried in an oven at 70 °C overnight and further dried in a vacuum oven at 70 °C for 3 hrs. The electrolyte (BASF Corporation) used was 1.2 M lithium hexafluorophosphate ($LiPF_6$) in ethylene carbonate (EC) and ethyl methyl

carbonate (EMC) with EC/EMC = 3:7 by volume ratio. All cells were assembled within an argon-filled glove box (with concentrations of O_2 < 1 ppm and H_2O < 1 ppm) at room temperature. The galvanostatic charge-discharge cycling of coin cells was performed on a Maccor battery cycler. For all cycling tests where C rates are given, 1C was assumed to be 180 mA g^{-1} (empirical value based on preliminary tests) of LCO active material in the electrode. For graphite half cell testing (Figure B7), 1C was assumed to be 372 mA g^{-1} of graphite in the graphite electrode.

3.4.4. Williamson−Hall Analysis

To determine if the milling process resulted in changes in microstrain within the LCO, the Williamson−Hall method was applied to the XRD patterns of the unmilled and milled materials. This method is based on a combination of Scherrer's equation and Bragg's law into Equation 1:

$$B \cos \theta = K(\lambda/t) + k\varepsilon \sin\theta \qquad (1)$$

where B is the line broadening at half the maximum peak intensity, θ is the angle of diffraction, K and k are constants, λ is the x-ray wavelength, t is the crystallite size, and ε is the microstrain. Microstrain is thus proportional to the slope of a plot of B cos θ - sinθ, which is shown in Figure B4. Both plots are flat and show undetectable change of B cos θ over sinθ, indicating that both materials have a good crystallinity without notable microstrain, and importantly the microstrain does not appreciably change with milling.

This method is not appropriate to measure the grain size because it lies out of the applicable range for particle size.

3.5. Results and Discussions

3.5.1. $CoC_2O_4 \cdot 2H_2O$ Precursor Characterization

As discussed in the Experimental Section, $CoC_2O_4 \cdot 2H_2O$ was first synthesized as the precursor to be used for calcination to LCO powder. Oxalate precursor precipitate chemistry was chosen because it has previously been demonstrated to be highly reproducible with regards to stoichiometry, crystal structure, and morphology for cations of interest to battery materials.[49, 51, 60] In addition, oxalate loses a substantial fraction of its mass during calcination to evolved CO_2 and H_2O. This mass loss results in void spaces that are typically undesirable for battery electrode materials due to reduction in tap density. In this study, however, large voids were desirable to keep the resulting primary LCO particles loosely connected and processible to sub-micrometer and nano-sized particles without high-energy techniques such as planetary ball milling. The x-ray diffraction (XRD) pattern for the $CoC_2O_4 \cdot 2H_2O$ precursor is shown in Figure 1a. The peaks observed in the $CoC_2O_4 \cdot 2H_2O$ precursor match with other reports in literature of orthorhombic β-$CoC_2O_4 \cdot 2H_2O$ material, confirming the desired oxalate phase was synthesized.[60-64] Energy dispersive x-ray spectroscopy (EDS) was also conducted on the precursor sample and confirmed the presence of Co, C, and O in the particles, with no impurities detected (Figure B1a in Appendix B).

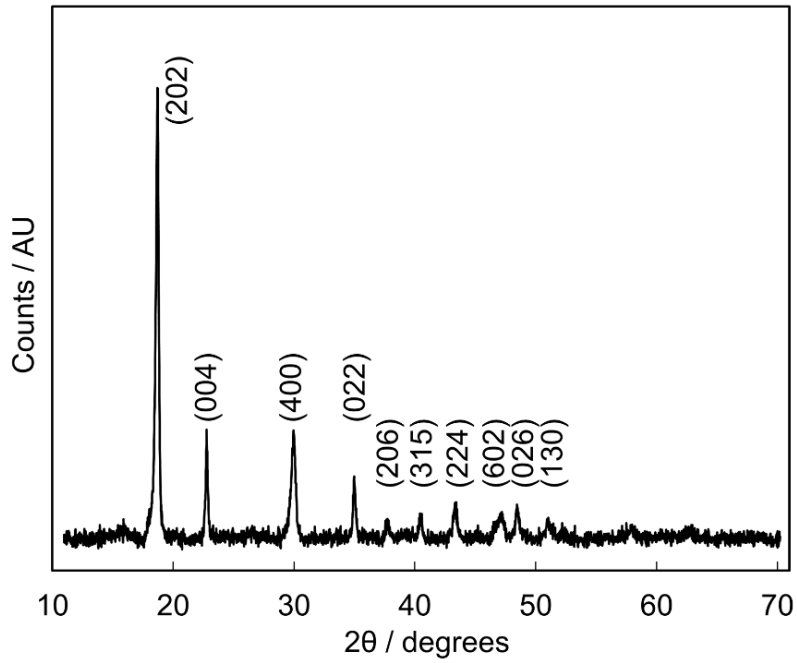

Figure 1. X-ray diffraction (XRD) patterns for $CoC_2O_4 \cdot 2H_2O$ sample

The morphology of the $CoC_2O_4 \cdot 2H_2O$ material can be seen in the scanning electron micrograph (SEM) image shown in Figure 2a (more images are available at Figure B2a and B2b in Appendix B). The rod-shaped $CoC_2O_4 \cdot 2H_2O$ materials have an average length of 7.88 ± 2.12 μm and width of 0.37 ± 0.10 μm (standard deviations based on the measurement of 100 rods in SEM images). The XRD and SEM results are consistent with previous reports in the literature for cobalt oxalate co-precipitated particles.[60-63, 65-67] Thermogravimetric analysis (TGA) was conducted to confirm the structural water content and decomposition temperatures of the precursor. As shown in Figure 2b, there was a mass loss of 18.45% at ~160 °C. This weight loss was attributed to the removal of structural water and was consistent with a stoichiometry of two structural water units per CoC_2O_4 in the material.[60, 61, 63, 65] The second mass loss was 37.37% at ~275 °C, which corresponds to the decomposition of CoC_2O_4 to Co_3O_4.[61] These observed

decomposition temperatures were consistent with previous reports of cobalt oxalate synthesized in an aqueous environment.[61] The TGA analysis also provided the necessary extent of hydration required to accurately account for the amount of lithium salt needed to provide the appropriate lithium stoichiometry in the final LCO powder. Based on the TGA results, a hold temperature of 200 °C was used during lithiation of the precursor with LiOH before ramping up to the final calcination temperature to allow for the removal of the structural water from the precursor.

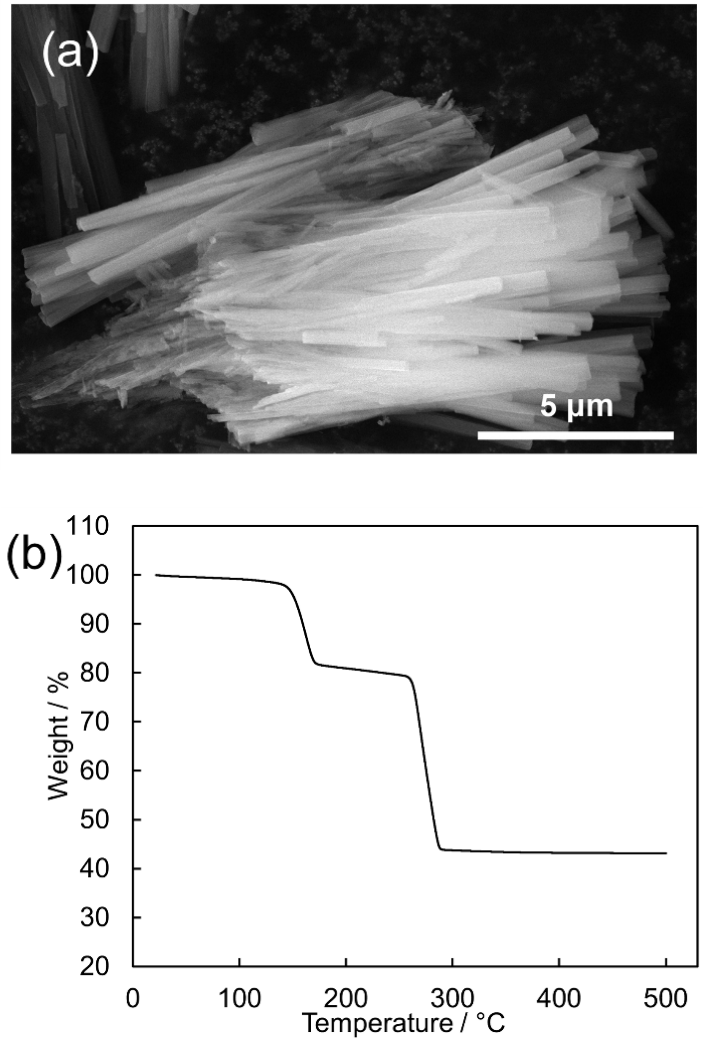

Figure 2. (a) Scanning electron micrograph (SEM) image of the $CoC_2O_4 \cdot 2H_2O$ rods; (b) $CoC_2O_4 \cdot 2H_2O$ thermogravimetric analysis (TGA) profile in an air atmosphere with 5 °C min^{-1} temperature ramp rate.

3.5.2. LCO Material Characterization

LCO material was obtained by calcining $CoC_2O_4 \cdot 2H_2O$ with LiOH at different final set temperatures. Temperatures were adjusted to control the primary particle size, as the LCO primary particles were expected to sinter into larger particles as a function of increasing temperature. SEM images were taken for the samples after calcination at

750 °C (Figure 3a), 800 °C (Figure 3b and Figure B2c, B2d in Appendix B), 850 °C (Figure 3c), and 900 °C (Figure 3d). The LCO calcined at 750 °C and 800 °C had similar morphologies of rod-shaped secondary particulates that retained the overall morphology of the original $CoC_2O_4 \cdot 2H_2O$ precursor and much smaller primary particulates that were loosely agglomerated to form the resulting secondary morphology. The volume of the secondary rod morphology in the LCO was slightly smaller than the volume of the precursor rods, likely due to some amount of sintering at the elevated temperature. The shape and size of the primary particulates varies, and the length of the particle in different dimensions was measured using the SEM images and the average and standard deviation of this length was determined (based on 100 measurements, this method was used for all LCO materials shown in Figure 3). For the material calcined at 750°C the primary particle size was 400 ± 170 nm, and for the material calcined at 800°C the size was 410 ± 230 nm. The sub-micrometer sized primary particle aggregates have been seen in other transition metal oxides synthesized from calcined oxalates and the fine primary particle structure is in part enabled by the large voids created during the loss of CO_2 and H_2O from the particles.[49] The majority of the primary particulates were still loosely interconnected to form the secondary rod morphology. These loosely interconnected agglomerates were easily broken into individual sub-micrometer sized particulates (discussed below). Interestingly, the primary particle size after calcination at 750°C and 800°C (400 and 410 nm, respectively) is very close to the width of the $CoC_2O_4 \cdot 2H_2O$ precursor material (370 nm). The primary particle formation is very complex and involves precursor decomposition, LCO formation, and LCO sintering, however, the role of precursor dimensions on templating primary particle size will be an area of future

research. At higher final furnace temperatures, such as 850 °C and 900 °C, the secondary rod shape was no longer apparent and larger primary particles were formed. The primary particles were 1.54 ± 0.73 μm and 2.44 ± 1.46 μm for the materials calcined at 850°C and 900 °C, respectively. The primary particle size increased by a factor of ~7 when the calcination temperature was increased from 800°C to 900°C. The primary particles also had a greater extent of agglomeration with greater degrees of contact between the primary particulates and no obvious secondary rod morphology. Due to the goal of easily dispersible, sub-micrometer sized active material particles only the material calcined at 750 °C and 800°C was chosen for further material characterization and electrochemical analysis.

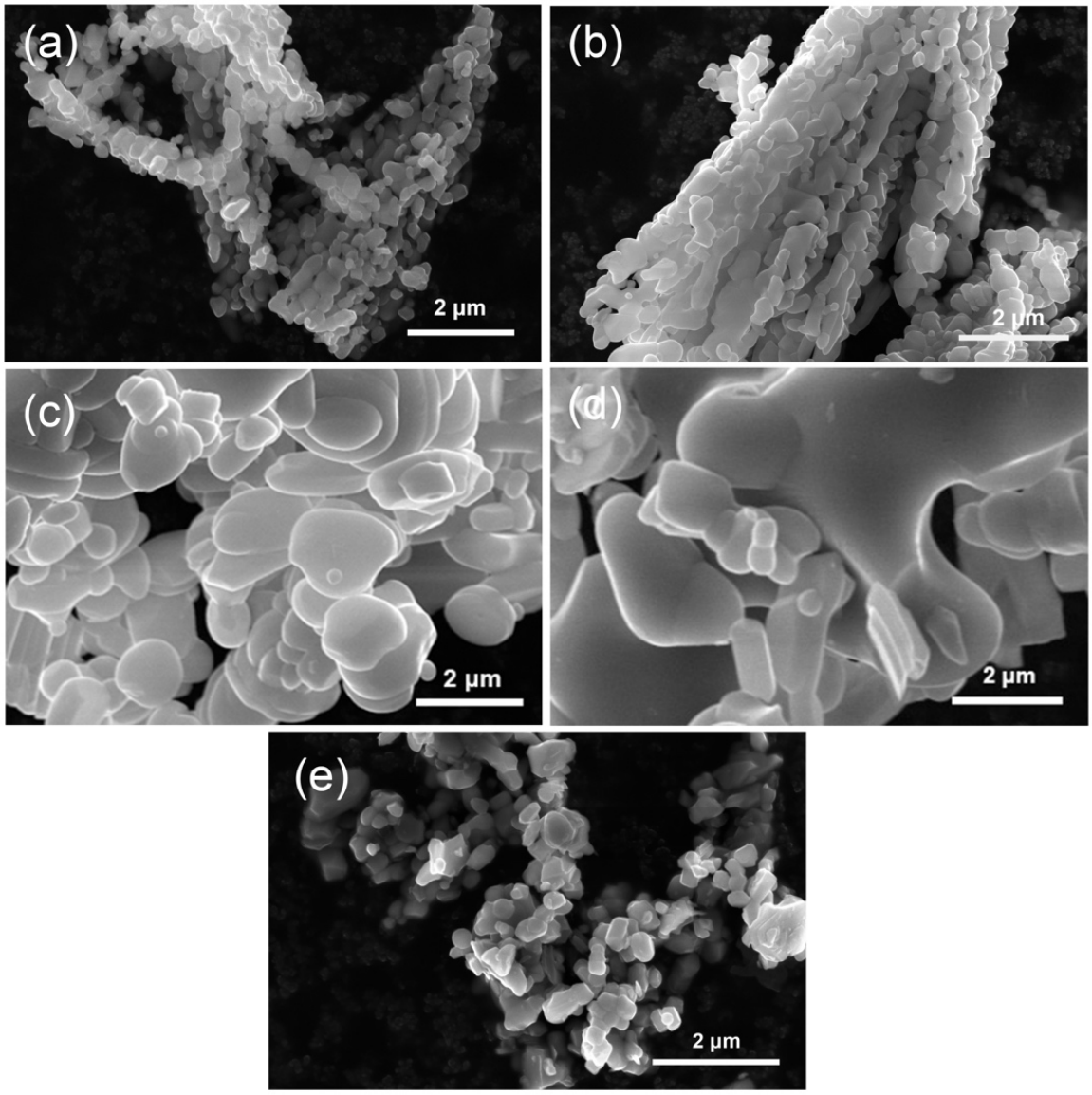

Figure 3. Scanning electron micrograph (SEM) images of calcined $LiCoO_2$ (LCO) materials fired at (a) 750 °C, (b) 800 °C, and (c) 850 °C, and (d) 900 °C; (e) LCO morphology after soft milling the material fired to 800 °C (material shown in (b)).

XRD was used to characterize the LCO prepared at 750 °C and at 800 °C to determine the crystal structure of the material. Both LCO materials (see Figure B3 for the 750 °C sample and Figure 4a for the 800°C sample) closely matched the reference pattern, which

has R$\bar{3}$m symmetry (from PDF 00-016-0427, Figure 4c).[68] The LCO material calcined at 750 °C had significant impurity peaks at both ~31.2 and ~36.8 degrees (Figure B2). We attribute these peaks to the (222) and (311) reflection for Co_3O_4, a common impurity phase from LCO synthesis.[69] This Co_3O_4 phase likely resulted from the incomplete lithiation of the LCO material.[60] The LCO material calcined at 800 °C only had a minor impurity peak at ~36.8 degrees (indicated with stars in Figure 4). Due to the impurities in the LCO fired to 750 °C and the very similar primary particle size for the two materials, we focused on the LCO fired to 800 °C for the rest of our analysis. LCO fired at 800 °C was soft milled on a roller mill with 12 mm zirconia beads to attempt to disperse the individual primary particles. XRD was also conducted for the LCO after milling to determine any changes that may have occurred to the crystal structure of the material. As can be seen in Figure 4, the XRD patterns of LCO after milling (Figure 4b) matched well with the pattern collected before milling (Figure 4a). No notable structural changes were observed to be caused by the soft milling procedure. The *a* and *c* lattice parameters for a hexagonal (R$\bar{3}$m) unit cell for LCO were determined both before and after milling. Before milling, the lattice parameters were a = 2.816 Å and c = 14.074 Å and after milling the lattice parameters were a = 2.815 Å and c = 14.033 Å. The lattice parameters were all consistent with other reports of LCO materials in the literature [29, 35, 37, 68, 70, 71]. Our LCO particles both before and after milling are likely too large to observe significant crystallite size effects on the lattice parameters as reported by others in the literature for nanocrystalline LCO.[72] EDS analysis confirmed Co was the only transition metal detectable within the material (Figure B1b in Appendix B). The results above, when combined, were consistent with the conversion of the oxalate precursor to

LCO cathode material. The milling procedure resulted in LCO sub-micrometer sized dispersed particulates with no detectable change in the crystal structure of the material using powder XRD. We note that based on the Williamson−Hall method (see Figure B4 IN Appendix B),[73, 74] There was no detectable change in the microstrain between the material before and after milling.

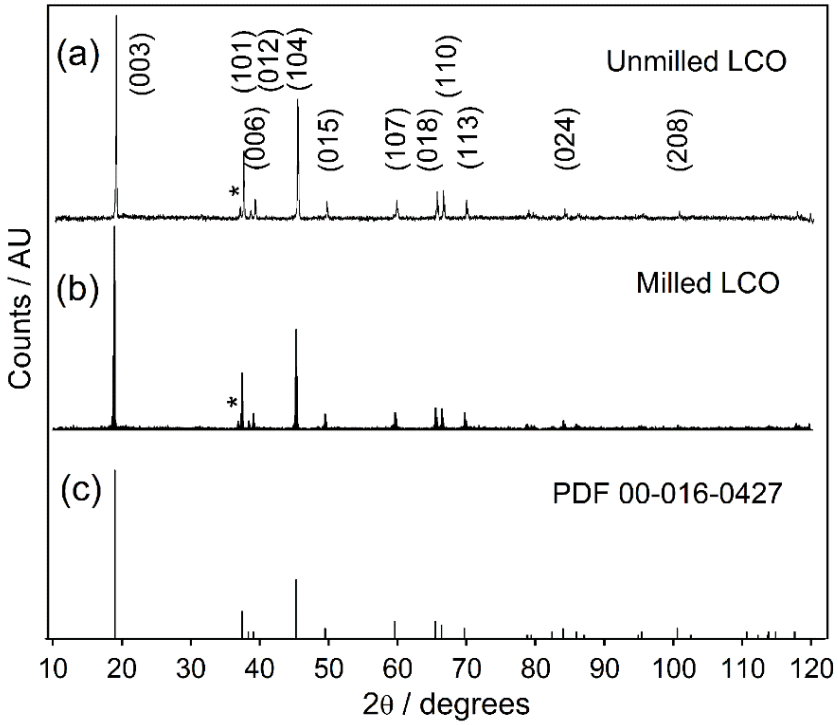

Figure 4. X-ray diffraction (XRD) patterns for $LiCoO_2$ (LCO) fired at 800 °C (a) before and (b) after soft milling the powder. (c) Reference pattern for LCO material (obtained from PDF 00-016-0427).

The morphology of the material after soft milling on a roller can be found in the SEM image in Figure 3e (and Figure B2e and B2f in Appendix B). After milling, the LCO particles were isolated to sub-micrometer sized particulates with an average length of 370 ± 150 nm (standard deviation based on the 100 measurements from SEM images; image

in Figure 3e is representative of other sample regions). This size was very similar to (e.g., within the standard deviation) but slightly smaller than the average size of the primary particles in the LCO material before milling (410 ± 230 nm). The similarity between the primary particle size for the premilled LCO and particle sizes for the postmilled LCO suggests that the simple soft milling procedure provides sufficient mechanical agitation to break the primary particles into individual dispersible particulates that approximately retain the size of the primary particles from the initial template material. The slightly reduced average particle size for the postmilled material may be due to breaking apart of some inter-connected primary particles that were counted as single particles during analysis of SEM images of the material (Figure 3b). The results above demonstrate the successful production of a sub-micrometer sized LCO powder via breaking apart the weakly connected LCO primary particulates form the LCO parent template material, as well approximately retaining the particle size of the primary particles from the LCO template.

Tap density was also measured for the powder comprised of the sub-micrometer sized particles (Figure 3e). The tap density of the milled LCO powder was measured to be 1.56 g mL^{-1}. This tap density was relatively low for a lithium-ion battery cathode material but was consistent with previous reports for sub-micrometer and nano-sized transition metal oxide cathode particulates.[75] Adsorption isotherm measurements were conducted to evaluate the surface area and porosity of the sub-micrometer sized particulate product. The nitrogen adsorption and desorption curves of milled LCO are shown in Figure 5. The adsorption isotherm appears to be a Type II curve, indicating a lack of micropores or

mesopores.[76, 77] The BET surface area is 3.58 $m^2 g^{-1}$ and the BJH pore volume was determined to be 9.84×10^{-3} $cm^3 g^{-1}$. The relatively low surface area and pore volume for the LCO powder indicated the absence of significant porosity within the LCO particulate interiors. The nitrogen adsorption isotherms and tap density measurements were consistent with dense, sub-micrometer sized LCO particles after the soft milling procedure.

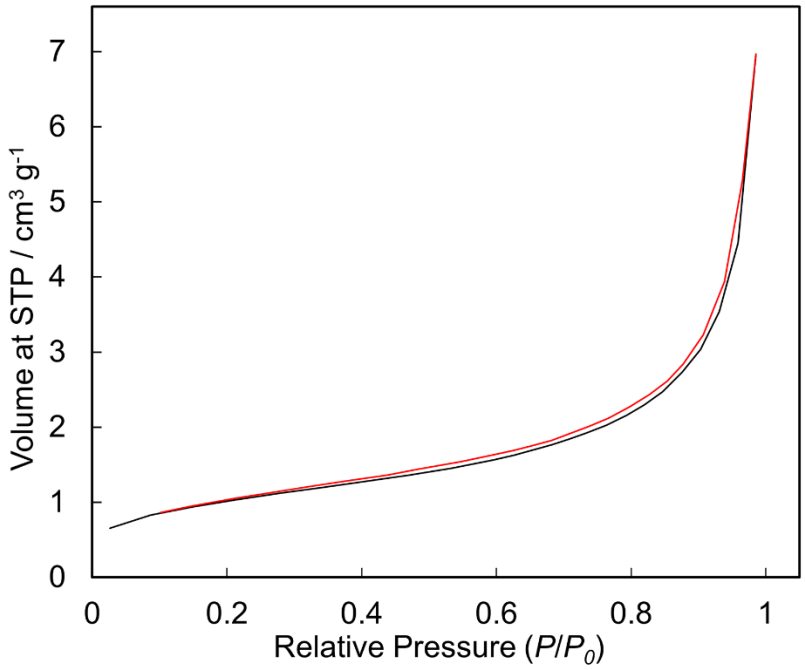

Figure 5. Adsorption (black) and desorption (red) isotherms for nitrogen at -195.8 °C on the soft milled $LiCoO_2$ (LCO) powder.

3.5.3. Electrochemical Characterization

The electrochemical performance of the milled, sub-micrometer sized LCO was first characterized with conventional composite electrode architectures within coin cells paired with a lithium metal anode. The composite LCO electrodes used in these coin cells were comprised of the LCO powder, conductive carbon additive, and binder as described

in the Experimental section. The first charge and discharge cycle of the milled LCO at 0.1C is shown in Figure 6. The charge and discharge voltage profile was consistent with other reports in the literature for LCO materials.[34, 35, 37, 78-80] The dQ/dV relationship also confirmed electrochemical capacity in voltage regions typical for LCO materials (Figure B5 in Appendix B). The first charge capacity was 197 mAh g^{-1} and the discharge capacity was 172 mAh g^{-1}. The discharge capacity was high relative to other reports in literature, though we will note that our cycling window was 2.5 to 4.5 V, which is relatively large.[29, 34-37, 78-80] While the first cycle had 12.52% irreversible capacity loss, the coulombic efficiency of subsequent cycles at 0.1C was > 95%. We attributed the relatively high irreversible capacity loss in the first cycle to the high surface area of the LCO powder, as well as the high charge cutoff voltage, which resulted in electrolyte decomposition at the LCO interface.[21, 80-82]

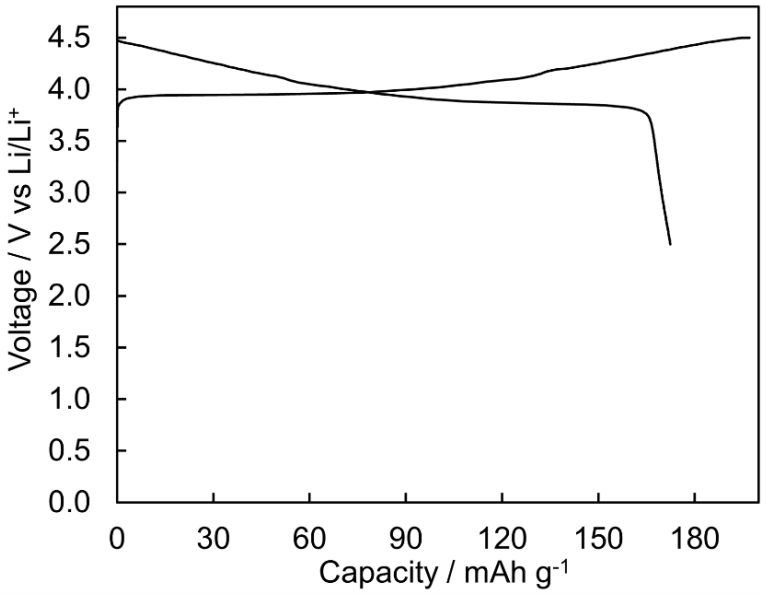

Figure 6. First charge and discharge cycle of a Li/ $LiCoO_2$ half-cell at a rate of 0.1C.

To understand the rate capability of the LCO material, the LCO electrode was paired with graphite anodes to perform cycling tests at increasing charge/discharge rates. As shown in Figure 7a, the cell retained high discharge capacity even at very high cycling rates. The average discharge capacity at 0.2C was 120 mAh g^{-1}, while at 2C the capacity decreased by 10.3% to 108 mAh g^{-1} and at 5C the capacity decreased by 21.9% (relative to 0.2C) to 94 mAh g^{-1} (gravimetric capacities are on a LCO active material mass basis). The rate capability of the LCO material was excellent, as the 21.9% reduction from 0.2C to 5C was much better than many LCO materials reported in the literature.[22, 78, 80] The rate capability of the sub-micrometer particles significantly outperformed the bulk LCO material with particles many micrometers in size as indicated in Figure B6 in Appendix B. We attribute this promising rate capability to the sub-micrometer scale particle size, which provides more surface area and shorter lithium diffusion pathways, resulting a lower cycling resistance.[21-24] We note that the coulombic efficiency of the first cycle for the graphite/LCO cell was low (~67%). This was primarily due to the irreversible first cycle capacity loss of our graphite anode material (Figure B7 in the Appendix B), and was not a reflection of our LCO material irreversible capacity loss (~12%, as mentioned above).

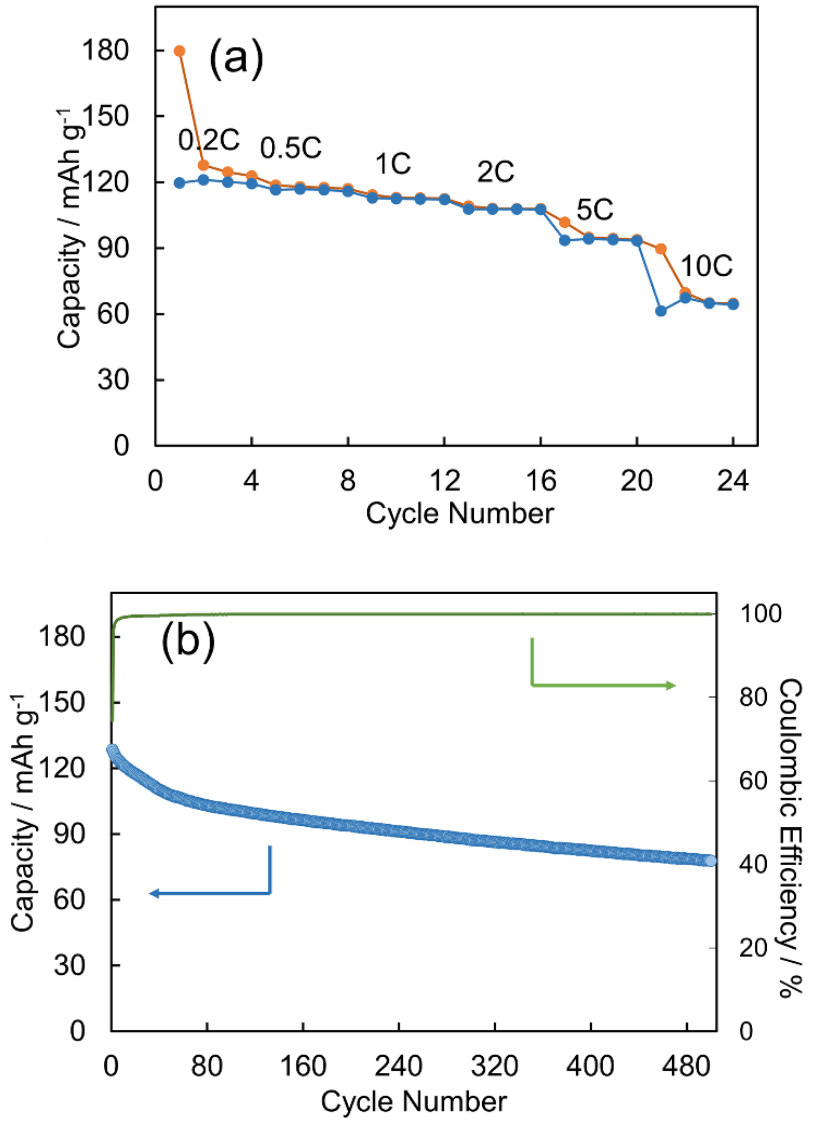

Figure 7. (a) Charge (orange) and discharge (blue) capacity of a graphite/ $LiCoO_2$ cell at increasing charge/discharge rates of 0.2C, 0.5C, 1C, 2C, 5C, and 10C. Four charge/discharge cycles were conducted at each rate; (b) discharge capacity (blue) and coulombic efficiency (green) of a graphite/LCO cell during a cycle life test of 500 charge/discharge cycles at a charge/discharge rate of 1C (1C based on LCO mass loading).

Cycle life testing was conducted with the graphite/LCO cells as well. A graphite/LCO cell was cycled at 1C charge and discharge rates for a total of 500 cycles (Figure 7b). The cell maintained a discharge capacity of ~100 mAh g^{-1} (cathode mass basis) even after 100 cycles. The cycling coulombic efficiency was ~97% after the first cycle, when the efficiency was relatively low due to SEI layer formation.[83] The coulombic efficiency further increased to >99% after 8 cycles. The capacity retention of the LCO material was very promising even when in comparison to other reports on LCO from the literature.[29, 80, 84] These results are very preliminary, however, previous literature reports have attributed cycling stability for sub-micrometer or nano-sized particles to the ability to withstand cracking during the mechanical stress of cycling and mitigate particle fracture and isolation from the electrode.[21, 36]

The process reported herein to synthesize sub-micrometer sized LCO particles is highly scalable because it is adaptable to continuous processing and requires low energy processing to break up the primary particulates. The co-precipitation process in aqueous solutions to produce the precursor template has the benefits of low cost, continuous production, and relatively simple operation.[10, 49, 54] In addition to using cheap and environmentally-friendly water as the precipitation solvent, the starting raw materials are simple salts with low cost and a high solubility in the solvent.[49] Previous reports have demonstrated that a continuous stirred tank reactor (CSTR) can be adopted for continuous production of precipitate battery precursors, providing a route to high volume production.[53-59] The calcination procedure to produce LCO agglomerates is very similar to current methods used in battery powder manufacturing.[47] The soft milling

step reported above requires much less energy compared to high-energy planetary milling.[24, 28] In fact, the mechanical intensity is very similar to the current technology used for grinding in large-scale high throughput LCO production.[47] Thus, the processing route used to produce sub-micrometer sized LCO described in this report is adaptable to current industrial methods for high throughput manufacturing of battery electrode active material particles.

The strategy described in this report is to use precursor templates explicitly designed to decompose to result in *low* tap density loosely agglomerated active material sub-micrometer particles within secondary particle structures with large voids. These voids were necessary to generate sub-micrometer scale discrete LCO particles that were loosely agglomerated such that low energy methods could be employed to break the primary particulates apart. These submicrometer particulate LCO materials have length scales that reduce the resistance experienced by individual particles to ionic/electronic transport that limits the rate capability of many battery electrode materials.[17, 18] Interestingly, the length scale of our particles is approximately the critical LCO particle size of 420 nm that was previously reported in a model as the size necessary to avoid grain boundary microfracture during electrochemical cycling which suggests mechanical advantages at and below the size range of the LCO particles reported in our study.[85] The results reported above also lead us to speculate that the initial diameters of the precursor oxalate rods serve to template the size of the final sub-micrometer LCO material after the milling procedure, suggesting synthesis strategies to control precursor morphology may yield direct routes to templating final material particle size. Future research efforts to template

the precursor material morphologies to tune the resulting size range of the final transition metal oxide sub-micrometer or nano-sized materials may lead to a general route to control the particle size of a variety of lithium-ion battery transition metal oxide materials via the simple and scalable method reported in this paper.

3.6. Conclusion

In this report, we demonstrate a scalable method to combine co-precipitation of battery precursor particles and a low energy soft milling method to synthesize sub-micrometer sized LCO lithium-ion battery active material particles. A rod-shaped cobalt oxalate precursor provided a convenient and desirable template structure for the formation of loosely connected sub-micrometer sized LCO primary particle aggregates. The weakly connected primary particle aggregates could be broken into individual particles through a low energy mechanical method, and the size of the particles was tunable with the calcination temperature. Batteries fabricated using electrodes comprised of the LCO sub-micrometer sized particulates as the active material showed excellent electrochemical performance, including high discharge capacity, rate capability, and coulombic efficiency. This simple scalable method for producing sub-micrometer sized active material battery electrode particles should be adaptable to a variety of lithium-ion cathode materials; especially those involving transition metal oxides where the transition metal also forms a stable oxalate precipitate.

3.7. References

1. Armand, M. and J.M. Tarascon, *Building better batteries.* Nature (London, U. K.), 2008. **451**(7179): p. 652-657.
2. Fergus, J.W., *Recent developments in cathode materials for lithium ion batteries.* J. Power Sources, 2010. **195**(4): p. 939-954.
3. Schuster, S.F., et al., *Lithium-ion cell-to-cell variation during battery electric vehicle operation.* J. Power Sources, 2015. **297**: p. 242-251.
4. Belharouak, I., G.M. Koenig, and K. Amine, *Electrochemistry and safety of Li4Ti5O12 and graphite anodes paired with LiMn2O4 for hybrid electric vehicle Li-ion battery applications.* J. Power Sources, 2011. **196**(23): p. 10344-10350.
5. Dunn, B., H. Kamath, and J.M. Tarascon, *Electrical Energy Storage for the Grid: A Battery of Choices.* Science (Washington, DC, U. S.), 2011. **334**(6058): p. 928-935.
6. Yang, Z., et al., *Electrochemical energy storage for green grid.* Chem. Rev. (Washington, DC, U. S.), 2011. **111**(5): p. 3577-613.
7. Mullendore, S., *Energy Storage And Electricity Markets*, in *Resilient Power*. 2015, Clean Energy Group and Meridian Institute.
8. Seitz, R., et al., *Nanotechnology in the sectors of solar energy and energy storage*. 2013, Fraunhofer Institute for Systems and Innovation Research ISI: Germany.
9. Daniel, C., *Lithium Ion Batteries and Their Manufacturing Challenges*, in *The Bridge*. 2015, National Academy of Sciences: Washington DC. p. 21-24.
10. Wood, D.L., J. Li, and C. Daniel, *Prospects for reducing the processing cost of lithium ion batteries.* J. Power Sources, 2015. **275**: p. 234-242.
11. Park, M., et al., *A review of conduction phenomena in Li-ion batteries.* J. Power Sources, 2010. **195**(24): p. 7904-7929.
12. Yu, Y.S., et al., *Dependence on Crystal Size of the Nanoscale Chemical Phase Distribution and Fracture in LiFePO.* Nano Lett., 2015. **15**(7): p. 4282-4288.
13. Qi, Z. and G.M. Koenig, *A carbon-free lithium-ion solid dispersion redox couple with low viscosity for redox flow batteries.* J. Power Sources, 2016. **323**: p. 97-106.
14. Yang, Z., et al., *Nanostructures and lithium electrochemical reactivity of lithium titanites and titanium oxides: A review.* J. Power Sources, 2009. **192**(2): p. 588-598.
15. Li, Y., et al., *Effects of Particle Size, Electronic Connectivity, and Incoherent Nanoscale Domains on the Sequence of Lithiation in LiFePO4 Porous Electrodes.* Adv. Mater. (Weinheim, Ger.), 2015. **27**(42): p. 6591-7.
16. Wang, S., et al., *A simple and inexpensive synthesis route for LiFePO4/C nanoparticles by co-precipitation.* J. Power Sources, 2013. **233**: p. 43-46.
17. Li, H. and H. Zhou, *Enhancing the performances of Li-ion batteries by carbon-coating: present and future.* Chem. Commun. (Cambridge, U. K.), 2012. **48**(9): p. 1201-17.
18. Gaberscek, M., R. Dominko, and J. Jamnik, *Is small particle size more important than carbon coating? An example study on LiFePO4 cathodes.* Electrochem. Commun., 2007. **9**(12): p. 2778-2783.

19. Al Hallaj, S., et al., *Thermal modeling and design considerations of lithium-ion batteries.* J. Power Sources, 1999. **83**(1-2): p. 1-8.
20. Saw, L.H., Y.H. Ye, and A.A.O. Tay, *Electrochemical-thermal analysis of 18650 Lithium Iron Phosphate cell.* Energy Convers. Manage., 2013. **75**: p. 162-174.
21. Arico, A.S., et al., *Nanostructured materials for advanced energy conversion and storage devices.* Nat. Mater., 2005. **4**(5): p. 366-377.
22. Scott, I.D., et al., *Ultrathin Coatings on Nano-LiCoO2 for Li-Ion Vehicular Applications.* Nano Lett., 2011. **11**(2): p. 414-418.
23. Goodenough, J.B. and Y. Kim, *Challenges for Rechargeable Li Batteries.* Chem. Mater., 2010. **22**(3): p. 587-603.
24. Liang, B., Y. Liu, and Y. Xu, *Silicon-based materials as high capacity anodes for next generation lithium ion batteries.* J. Power Sources, 2014. **267**: p. 469-490.
25. Li, J., et al., *Studies on the cycle life of commercial lithium ion batteries during rapid charge-discharge cycling.* J. Power Sources, 2001. **102**: p. 8.
26. Hu, L., et al., *Thin, Flexible Secondary Li-Ion Paper Batteries.* ACS Nano, 2010. **4**(10): p. 5843-5848.
27. Duduta, M., et al., *Semi-Solid Lithium Rechargeable Flow Battery.* Adv. Energy Mater., 2011. **1**(4): p. 511-516.
28. Crain, D., et al., *Electrochemical features of ball-milled lithium manganate spinel for rapid-charge cathodes of lithium ion batteries.* J. Solid State Electrochem., 2012. **16**(8): p. 2605-2615.
29. Burukhin, A., et al., *Hydrothermal synthesis of LiCoO2 for lithium rechargeable batteries.* Solid State Ionics, 2002. **151**(1-4): p. 259-263.
30. Tabuchi, M., et al., *Preparation of LiCoO2 and LiCo1-xFexO2 using hydrothermal reactions.* J. Mater. Chem., 1999. **9**(1): p. 199-204.
31. Miao, C., et al., *A novel synthesis and characterization of LiFePO4 and LiFePO4/C as a cathode material for lithium-ion battery.* J. Power Sources, 2014. **246**: p. 7.
32. Yamada, A., S.C. Chung, and K. Hinokuma, *Optimized LiFePO4 for lithium battery cathodes.* J. Electrochem. Soc., 2001. **148**(3): p. A224-A229.
33. Kim, K.H. and K.B. Kim, *Ultrasound assisted synthesis of nano-sized lithium cobalt oxide.* Ultrason. Sonochem., 2008. **15**(6): p. 1019-1025.
34. Tang, W., et al., *Nano-LiCoO2 as cathode material of large capacity and high rate capability for aqueous rechargeable lithium batteries.* Electrochem. Commun., 2010. **12**(11): p. 1524-1526.
35. Tan, K.S., et al., *High-performance LiCoO2 by molten salt (LiNO3 : LiCl) synthesis for Li-ion batteries.* J. Power Sources, 2005. **147**(1-2): p. 241-248.
36. Liang, H., et al., *High performance lithium cobalt oxides prepared in molten KCl for rechargeable lithium-ion batteries.* Electrochem. Commun., 2004. **6**(5): p. 505-509.
37. Liang, H.Y., et al., *Analysis of high rate performance of nanoparticled lithium cobalt oxides prepared in molten KNO3 for rechargeable lithium-ion batteries.* Electrochem. Commun., 2004. **6**(8): p. 789-794.
38. Zhao, X., et al., *Nano LiMn2O4 with spherical morphology synthesized by a molten salt method as cathodes for lithium ion batteries.* RSC Adv., 2012. **2**(19): p. 7462-7469.

39. Xiao, A., et al., *Electrodeposited porous metal oxide films with interconnected nanoparticles applied as anode of lithium ion battery.* Mater. Res. Bull., 2014. **60**: p. 864-867.
40. Robinson, J.P. and G.M. Koenig, *Tuning solution chemistry for morphology control of lithium-ion battery precursor particles.* Powder Technol., 2015. **284**: p. 225-230.
41. Vu, A. and A. Stein, *Lithium iron phosphate spheres as cathode materials for high power lithium ion batteries.* J. Power Sources, 2014. **245**: p. 48-58.
42. Gu, Y.-J., Z. Guo, and H.-Q. Liu, *Structure and electrochemical properties of Li4Ti5O12 with Li excess as an anode electrode material for Li-ion batteries.* Electrochim. Acta, 2014. **123**: p. 576-581.
43. Shen, Y., et al., *Solid State Formation Mechanism of Li4Ti5O12from an Anatase TiO2Source.* Chem. Mater., 2014. **26**(12): p. 3679-3686.
44. Kim, D.K., et al., *Spinel LiMn2O4 Nanorods as Lithium Ion Battery Cathodes.* Nano Lett., 2008. **8**(11): p. 3948-3952.
45. Hong, S.-K., et al., *Structural and electrochemical characteristics of morphology-controlled Li[Ni0.5Mn1.5]O4 cathodes.* Electrochim. Acta, 2015. **156**: p. 29-37.
46. Gao, J., et al., *Strategy for synthesizing spherical LiNi0.5Mn1.5O4 cathode material for lithium ion batteries.* Mater. Chem. Phys., 2015. **152**: p. 177-182.
47. Yoshio, M., R.J. Brodd, and A. Kozawa, *Lithium-ion Batteries: Science and Technologies*. 2009: Springer. 452.
48. Bommel, A.v. and J.R. Dahn, *Analysis of the Growth Mechanism of Coprecipitated Spherical and Dense Nickel, Manganese, and Cobalt-Containing Hydroxides in the Presence of Aqueous Ammonia.* Chem. Mater., 2009(21): p. 1500-1503.
49. Wang, D., et al., *Synthesis of Lithium and Manganese-Rich Cathode Materials via an Oxalate Co-Precipitation Method.* J. Electrochem. Soc., 2013. **160**(5): p. A3108-A3112.
50. Wang, D., et al., *Synthesis of high capacity cathodes for lithium-ion batteries by morphology-tailored hydroxide co-precipitation.* Journal of Power Sources, 2015. **274**: p. 451-457.
51. Cho, T.-H., Y. Shiosaki, and H. Noguchi, *Preparation and characterization of layered LiMn1/3Ni1/3Co1/3O2 as a cathode material by an oxalate co-precipitation method.* J. Power Sources, 2006. **159**(2): p. 1322-1327.
52. Zhu, Z., et al., *Preparation of spherical hierarchical LiNi0.5Mn1.5O4 with high electrochemical performances by a novel composite co-precipitation method for 5V lithium ion secondary batteries.* Electrochimica Acta, 2014. **115**: p. 290-296.
53. Wang, D., et al., *Growth mechanism of Ni0.3Mn0.7CO3 precursor for high capacity Li-ion battery cathodes.* J. Mater. Chem., 2011. **21**(25): p. 9290.
54. Wang, D., et al., *Chemistry and electrochemistry of concentric ring cathode Li1.42Ni0.25Mn0.75O2+γ for lithium batteries.* J. Mater. Chem., 2012. **22**(24): p. 12039.
55. Lim, J.-H., et al., *Electrochemical characterization of Li2MnO3–Li[Ni1/3Co1/3Mn1/3]O2–LiNiO2 cathode synthesized via co-precipitation for lithium secondary batteries.* J. Power Sources, 2009. **189**(1): p. 571-575.

56. Lee, M.H., et al., *Synthetic optimization of Li[Ni1/3Co1/3Mn1/3]O2 via co-precipitation.* Electrochim. Acta, 2004. **50**(4): p. 939-948.
57. Lee, D.K., et al., *High capacity Li[Li0.2Ni0.2Mn0.6]O2 cathode materials via a carbonate co-precipitation method.* J. Power Sources, 2006. **162**(2): p. 1346-1350.
58. Camardese, J., et al., *Synthesis of Spherical Core-Shell Ni(OH)2-Ni1/2Mn1/2(OH)2 Particles via a Continuously Stirred Tank Reactor.* J. Electrochem. Soc., 2014. **161**(6): p. A890-A895.
59. Park, S.H., et al., *Physical and electrochemical properties of spherical Li1+x(Ni1/3Co1/3Mn1/3)1−xO2 cathode materials.* J. Power Sources, 2008. **177**(1): p. 177-183.
60. Wang, D., Q. Wang, and T. Wang, *Morphology-controllable synthesis of cobalt oxalates and their conversion to mesoporous Co3O4 nanostructures for application in supercapacitors.* Inorg. Chem., 2011. **50**(14): p. 6482-92.
61. Wang, W.-W. and Y.-J. Zhu, *Microwave-assisted synthesis of cobalt oxalate nanorods and their thermal conversion to Co3O4 rods.* Mater. Res. Bull., 2005. **40**(11): p. 1929-1935.
62. Ren, L., et al., *Synthesis of CoC2O4 center dot 2H(2)O nanorods and their thermal decomposition to Co3O4 nanoparticles.* Chem. Phys. Lett., 2009. **476**(1-3): p. 78-83.
63. Ahmed, J., et al., *Development of a microemulsion-based process for synthesis of cobalt (Co) and cobalt oxide (Co3O4) nanoparticles from submicrometer rods of cobalt oxalate.* J. Colloid Interface Sci., 2008. **321**(2): p. 434-41.
64. Park, Y.-U., et al., *Synthesis of Multicomponent Olivine by a Novel Mixed Transition Metal Oxalate Coprecipitation Method and Electrochemical Characterization.* Chem. Mater., 2010. **22**(8): p. 2573-2581.
65. Majumdar, S., et al., *A study on isothermal kinetics of thermal decomposition of cobalt oxalate to cobalt.* Thermochim. Acta, 2008. **473**(1-2): p. 45-49.
66. Salavati-Niasari, M., N. Mir, and F. Davar, *Synthesis and characterization of Co3O4 nanorods by thermal decomposition of cobalt oxalate.* J. Phys. Chem. Solids, 2009. **70**(5): p. 847-852.
67. Baco-Carles, V., et al., *Correlation between the morphology of cobalt oxalate precursors and the microstructure of metal cobalt powders and compacts.* Powder Technol., 2008. **185**(3): p. 231-238.
68. Johnston, W.D., R.R. Heikes, and D. Sestrich, *The preparation, crystallography, and magnetic properties of the LixCo(1-x)O system.* J. Phys. Chem. Solids, 1958. **7**: p. 1-13.
69. Natl. Bur. Stand. Circ. (U. S.), 1960. **539**(9): p. 29.
70. Ohzuku, T. and A. Ueda, *Solid-State Redox Reactions of LiCoO (R3m) for 4 Volt Secondary Lithium Cells.* J. Electrochem. Soc, 1994. **141**(11): p. 2972-2977.
71. Cho, J., Y.J. Kim, and B. Park, *Novel LiCoO2 Cathode Material with Al2O3 Coating for a Li Ion Cell.* Chem. Mater., 2000. **12**: p. 3788-3791.
72. Okubo, M., et al., *Nanosize Effect on High-Rate Li-Ion Intercalation in LiCoO2 Electrode.* J. Am. Chem. Soc., 2007. **129**: p. 7444-7452.

73. Lee, E.-S., et al., *Influence of Cation Ordering and Lattice Distortion on the Charge–Discharge Behavior of LiMn1.5Ni0.5O4Spinel between 5.0 and 2.0 V.* Chem. Mater., 2012. **24**(18): p. 3610-3620.
74. Williamson, G.K. and W.H. Hall, *X-ray line broadening from filed aluminium and wolfram.* Acta Metall., 1953. **1**(1): p. 22-31.
75. Guo, D., et al., *Electrochemical performance of solid sphere spinel LiMn2O4 with high tap density synthesized by porous spherical Mn3O4.* Electrochim. Acta, 2014. **123**: p. 254-259.
76. Rouquerol, F., J. Rouquerol, and K. Sing, *Adsorption by powders and porous solids- principles, methodology and applications*. 1999, London: Academic Press.
77. Lazarraga, M.G., et al., *Nanosize LiNiyMn2-yO(4) (0, y <= 0.5) spinels synthesized by a sucrose-aided combustion method. Characterization and electrochemical performance.* J. Mater. Chem., 2004. **14**(10): p. 1640-1647.
78. Huang, B., et al., *Electrochemical evaluation of LiCoO2 synthesized by decomposition and intercalation of hydroxides for lithium-ion battery applications.* J. Appl. Electrochem., 1998. **28**(12): p. 1365-1369.
79. Kim, J., et al., *Electrochemical Properties of Li1+xCoO2 Synthesized for All-Solid-State Lithium Ion Batteries with Li2S-P2S5 Glass-Ceramics Electrolyte.* J. Electrochem. Soc., 2015. **162**(6): p. A1041-A1045.
80. Reddy, M.J.K., S.H. Ryu, and A.M. Shanmugharaj, *Synthesis of nanostructured lithium cobalt oxide using cherry blossom leaf templates and its electrochemical performances.* Electrochim. Acta, 2016. **189**: p. 237-244.
81. Xu, K., *Electrolytes and Interphases in Li-Ion Batteries and Beyond.* Chem. Rev. (Washington, DC, U. S.), 2014(114): p. 11503-11618.
82. Handel, P., et al., *Thermal aging of electrolytes used in lithium-ion batteries – An investigation of the impact of protic impurities and different housing materials.* J. Power Sources, 2014. **267**: p. 255-259.
83. Buqa, H., et al., *SEI film formation on highly crystalline graphitic materials in lithium-ion batteries.* J. Power Sources, 2006. **153**(2): p. 385-390.
84. Zhao, H., et al., *Improvement of electrochemical stability of LiCoO2 cathode by a nano-crystalline coating.* J. Power Sources, 2004. **132**(1-2): p. 195-200.
85. Woodford, W.H., W.C. Carter, and Y.-M. Chiang, *Design criteria for electrochemical shock resistant battery electrodes.* Energy Environ. Sci., 2012. **5**(7): p. 8014.

Chapter IV. Electrochemical Evaluation of $LiCoO_2$ Redox Couple Dispersion and All Solid Dispersion Redox Flow Batteries

4.1 Overview

This chapter first discusses the demonstration of $LiCoO_2$ suspension in organic lithium-ion electrolyte as the cathode for solid dispersion flow battery. This is the first demonstration of lithium-ion cathode material in the solid suspension based flow battery in the literature. A full cell with $Li_4Ti_5O_{12}$ suspension as the anode and $LiCoO_2$ suspension as the cathode is also demonstrated in a custom cell. This first report on all solid dispersion redox flow battery provides the electrochemical performance of the full cell as well as the rheological properties of anode and cathode suspensions.

Elements of this chapter have been published in Electrochimica Acta:

Z. Qi, A.L. Liu, G.M. Koenig, Carbon-free Solid Dispersion $LiCoO_2$ Redox Couple Characterization and Electrochemical Evaluation for All Solid Dispersion Redox Flow Batteries, *Electrochimica Acta*, 228 (2017) 91-99.

Respective author contribution:

Aaron Liu: $LiCoO_2$ material synthesis.

4.2. Abstract

Semi-solid flow batteries have been reported to have among the highest energy densities for redox flow batteries, however, they rely on percolated carbon networks which increase the electrolyte viscosity significantly. We report the first demonstration of carbon-free redox flow couples comprised of dispersed lithium-ion battery active material suspensions, with sub-micrometer $LiCoO_2$ (LCO) particles at the cathode and $Li_4Ti_5O_{12}$ (LTO) particles at the anode. Both electrochemical and rheological properties of the LCO suspensions are reported and compared to previous reports for LTO dispersed electrochemical redox couples. A LTO anode and LCO cathode full cell was constructed and reversible electrochemical redox reaction of the dispersed particles was successfully demonstrated. This carbon-free dispersed lithium-ion active material full cell provides a proof-of-concept for a system that lies between the relatively high viscosity semi-solid flow cells with percolated carbon networks and the relatively low energy density conventional flow cells comprised of dissolved transition metals, providing a system for future study of the trade-off between energy density and viscosity for electrochemical flow cells that rely on solid active materials.

4.3. Introduction

Redox flow batteries provide the flexibility to independently design the power and energy for applications by separating energy storage via electrolyte storage tanks and the power output in the electrochemical reaction cells.[1, 2] This is important for large-scale applications, and stationary flow battery technology has been commercially demonstrated in kW and even MW scales in recent years.[3, 4] One challenge for many flow batteries is that the solubility of the active species in the electrolyte is limiting the energy density due to formation of inactive precipitates at high concentrations.[3, 5, 6] Various efforts have been explored to increase the energy density, for example, polymer based flow batteries,[7-10] new active materials,[11, 12] ionic liquids,[13] and hybrid flow batteries with multiple redox couples.[14] Another recently explored redox flow battery, so-called semi-solid flow battery, bypasses the limitation of active material solubility on energy density by starting with solid active material particles in the electrolyte. This technology is promising because it provides significant improvements in energy density and also uses lithium-ion active materials, which results in a high operating voltage.[15, 16] However, the high viscosity of the carbon-percolated electrolyte in these systems is a challenge due to the relatively high parasitic energy required to pump the semi-solid electrolyte.[16, 17] Recently, our group reported initial results for a system that lies between conventional flow batteries (relatively low viscosity and energy density) and semi-solid flow batteries (relatively high viscosity and energy density) by dispersing a lithium-ion battery active material within an electrolyte and reversibly electrochemically oxidizing and reducing the active material particles during collisions with a current collector in the suspension.[18] Relatively low viscosities are achieved by not adding carbon to form a percolated

network in the system while theoretically high energy density is maintained by starting with solid electroactive materials. This previous initial report of what was termed a "dispersion flow battery" redox couple was a half-cell demonstration that paired a lithium metal anode with a target anolyte material dispersion containing $Li_4Ti_5O_{12}$ (LTO) active material. However, a target catholyte material for a carbon-free solid dispersion flow battery has previously not been reported, nor has a reversible full cell comprised of only dispersed lithium-ion active material particles for both the anode and cathode reactions.

Herein, we detail the first report of a carbon-free solid dispersion flow battery target catholyte material by using $LiCoO_2$ (LCO) as a redox couple. LCO was chosen as the target cathode material for a solid dispersion flow redox couple because of its relatively high electronic and ionic conductivities relative to other common lithium-ion cathode materials.[19] High ionic and electronic conductivity are necessary such that ambipolar diffusion is sufficient to not result in a prohibitive resistance in the collision electrochemical environment without carbon additives in a supporting electrode.[18, 20] LCO's conductivity has previously been reported to be sufficient to provide full charge/discharge cycles of thick carbon-free pellet electrodes, suggesting charge and discharge of LCO particles in contact with a current collector while dispersed into an electrolyte should be possible.[21] LCO is also one of the most widely used cathode materials and both structural and electrochemical properties have been widely reported in the literature.[22-27] LCO has a discharge voltage of ~4.0 V vs. Li/Li^+ and a high energy density.[28, 29]

We also report the first demonstration of an electrochemical dispersion cell comprised exclusively of solid dispersions of electroactive lithium-ion battery particles by pairing carbon-free solid dispersions of a catholyte containing LCO and an anolyte containing LTO. A full cell with LCO as the cathode and LTO as the anode in a conventional static lithium-ion battery cell has previously been reported to have a stable ~2.5 V cell voltage,[30] which would be significantly greater than the average discharge voltage of common conventional flow batteries such as vanadium-containing systems.[31] While the power density of the initial electrochemical cell in this report is very low, the theoretical capacity and cell voltage of a solid dispersion electrochemical cell with LTO and LCO shows promise in flow-based electrochemical energy storage applications.

4.4. Experimental

4.4.1. Preparation and Characterization of LCO and LTO Materials

The synthesis of LCO was described in detail in a previous report.[32] In brief, $CoC_2O_4 \cdot 2H_2O$ precursor was synthesized via a co-precipitation method. Equal volume of 0.1 M $(NH_4)_2C_2O_4$ and 0.1 M $Co(NO_3)_2$ solutions were mixed at 60 °C to form $CoC_2O_4 \cdot 2H_2O$. The solid particle precipitates were dried at 80 °C before being mixed with LiOH and calcined in a Carbolite CWF 1300 box furnace in an air atmosphere. The mixture was fired to 800 °C at a rate of 1 °C/min before turning off the furnace and allowing cooling to ambient temperature. The LCO product was milled to smaller particles through a wet soft milling procedure on a roller (US Stoneware) with zirconia beads.

LTO (NEI Corporation) powders were used as delivered. The characterization of the LTO material from NEI has been reported previously by our group and others.[18, 33, 34] The electrolyte (BASF Corporation) in the LCO suspensions and all electrochemical tests was 1.2 M lithium hexafluorophosphate ($LiPF_6$) in ethylene carbonate (EC) and ethyl methyl carbonate (EMC) with EC/EMC = 3:7 by volume ratio. The LCO suspensions of different loadings (0.5 vol%, 5 vol%, 10 vol%, 20 vol%) were prepared by mixing LCO powders with electrolyte under stirring overnight within an argon-filled glove box (with concentrations of O_2 < 1 ppm and H_2O < 1 ppm) at room temperature. The LTO suspension was prepared in the same way. Rheology characterization of the LCO suspensions was performed with an Anton Paar rheometer (Physica MCR 301, with

a 5 cm plate-plate geometry). Scanning electron micrograph (SEM) images were taken for both LCO and LTO with a Quanta 650 SEM.

4.4.2. Electrochemical Testing

A. Conventional Coin Cell Fabrication

Electrochemical characterization was done by using CR2032 type coin cells with the LCO electrode as the cathode and lithium foil as the anode for half-cell tests and an LTO electrode as the anode for full cell tests. The electrodes were separated by a polypropylene / polyethylene / polypropylene trilayer membrane. LCO or LTO electrodes used in coin cells were fabricated from slurries comprised of 80 wt % LCO or LTO powder, 10 wt % carbon black as conductive additive, and 10 wt % polyvinylidene fluoride binder (PVDF) dissolved in N-methylpyrrolidone (NMP, Sigma-Aldrich®). The slurry was agitated in a slurry mixer for 5 minutes and pasted (with a doctor blade) onto aluminum foil. The pasted slurry was dried in an oven at 70 °C overnight and further dried in a vacuum oven at 70 °C for 3 h.

B. Particle Coin Cell Fabrication

Electrodes composed of only LCO particles as the electrode material without binders or conductive additives on the aluminum foil were prepared. LCO particles were suspended in acetone (Fisher Scientific), dropped on pre-punched aluminum foil discs (1.6 cm^2), and then dried in a vacuum oven at 70 °C for 2 h. A coin cell using the as-prepared electrode was referred to as a "particle coin cell".

C. Conventional and Particle Coin Cell Electrochemical Characterization

All coin cells were assembled in the glove box. The galvanostatic charge-discharge cycling of coin cells was performed on a Maccor battery cycler. For all cycling tests where C rates are given, 1C was assumed to be 180 mA g^{-1} with the mass being the mass of LCO and the current was adjusted by the amount of LCO active material in the electrode.

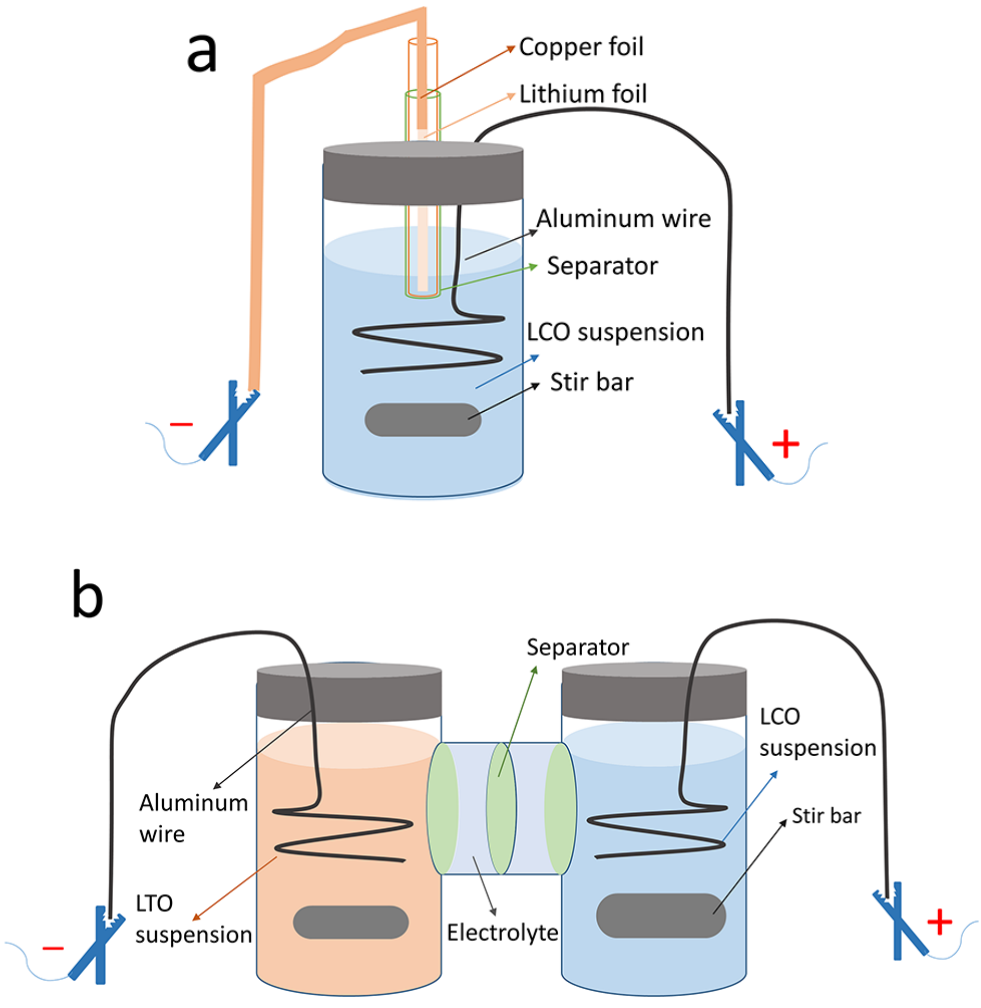

Figure 1. Schematic of cell configurations: (a) a vial cell with the aluminum wire in the LCO suspension as the cathode current collector and lithium foil in a glass tube as the

anode; (b) a full cell with aluminum wires in the LCO suspension as the cathode current collector and in the LTO suspension as the anode current collector.

D. Active Material Suspension Characterization in Customized Cells

A customized cell (referred to as a "vial cell") as illustrated in Figure 1a was set up in the glove box to perform half-cell tests. An aluminum wire (9.4 cm^2, Alfa Aesar) was immersed in an LCO suspension of a desired particle loading. Lithium foil, which was attached to a copper foil extended to the external circuit, was immersed into the electrolyte within a glass tube and separated from the LCO suspension by a trilayer membrane separator. A potentiostat (Bio-Logic, SP-150) was used to perform electrochemical tests while the suspension was agitated by stirring.

Another customized cell was set up in the glove box to perform full cell tests as illustrated in Figure 1b. An aluminum wire (14.1 cm^2, Alfa Aesar) was immersed in a 0.5 vol% LCO suspension and another one in a 1 vol% LTO suspension. The two electrodes were separated by three polypropylene / polyethylene / polypropylene trilayer membranes to prevent active material crossover. The potentiostat was used to perform electrochemical tests while both suspensions were agitated by stirring.

4.5. Results and Discussion

4.5.1. Electrochemical Characterization of the LCO Coin Cells

We adopted a synthesis method to produce sub-micrometer sized LCO material that had been previously reported,[32] because sub-micrometer sized or nano-sized particles are

needed to form stable suspensions in the electrolyte and we were not able to obtain suitable sized commercial LCO materials. Figure 2a displays typical charge/discharge profiles for the first 4 cycles of a Li/LCO cell with the LCO distributed within a conventional composite electrode. The voltage window for the cell was 2.5 - 4.5 V and the charge/discharge rate was 0.1 C. The voltage profile was consistent with previous reports on LCO materials.[22, 28, 29, 35-39] The first charge capacity reached 196 mAh g^{-1} with a discharge capacity of 171 mAh g^{-1}. We attribute the loss of capacity during the first cycle to both SEI formation and electrolyte decomposition at the relatively high cutoff voltage.[40-42] Subsequent cycles after the first charge/discharge had coulombic efficiency of >95%.

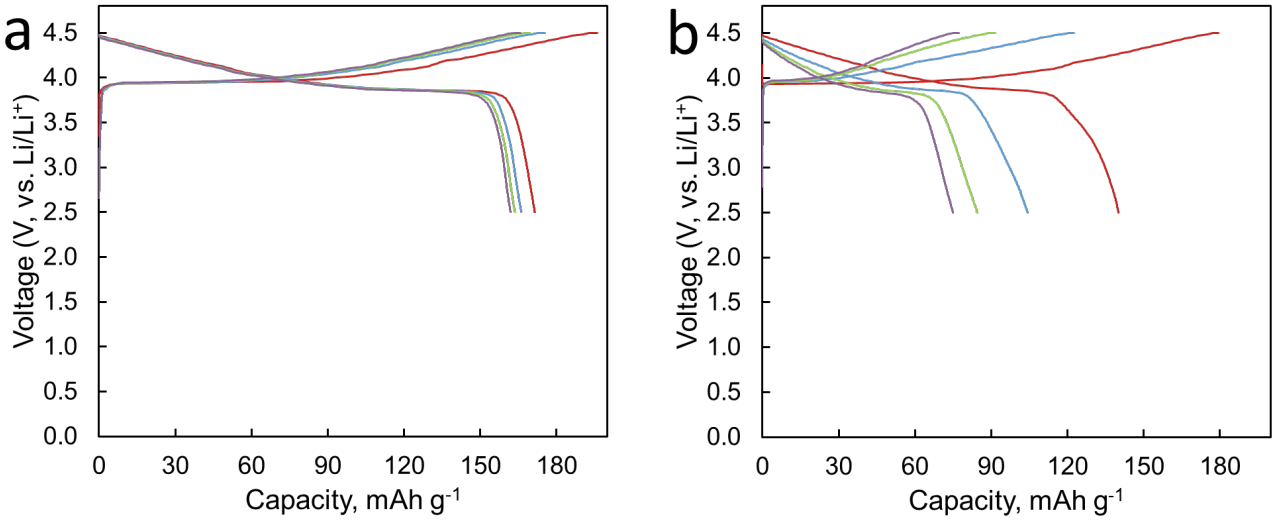

Figure 2. Charge/discharge profiles for cycles 1 (red), 2 (blue), 3 (green), and 4 (purple) for (a) a LCO conventional coin cell and (b) a LCO particle coin cell, both charged/discharged at a rate of 0.1 C between a voltage window of 2.5 to 4.5 V.

Two key differences between electrochemical oxidation/reduction of LCO particles in a conventional lithium-ion battery composite electrode compared to dispersion of the active material particles in a flowing electrolyte are that 1) the dispersion system does not contain conductive carbon additives and binder materials and 2) due to the active material being dispersed in the electrolyte only the LCO material in contact with the current collector at any given time participates in the electrochemical reaction. Therefore, we fabricated particle coin cells described in the Experimental section to confirm the electrochemical activity of the LCO material directly deposited on the current collector and in the absence of binders and conductive additives, which is more similar to the environment the LCO material will experience in the custom flow cells. The first 4 charge/discharge profiles for a Li/LCO particle coin cell using the same C rate and voltage window as the conventional LCO electrode coin cell are shown in Figure 2b. The initial charge capacity was 179 mAh/g, while the discharge capacity was 140 mAh/g. The overall capacity was lower than the conventional coin cell and only 78% capacity was retained for discharge in the first cycle. The capacity on following cycles dropped significantly and only 42% of the discharge capacity was retained after only four cycles at 0.1C. We attribute the loss in discharge capacity to the volume change of LCO particles during cycling, which caused disconnection of loosely packed LCO particles from the current collector, resulting in a loss of capacity.[43] Particle coin cells containing LTO retain a much greater fraction of initial discharge capacity with cycling at low rates of charge/discharge (see [18] and Figure C1 in Appendix C) compared to the LCO material. LTO has been reported to be a zero-strain material that does not undergo volume change during cycling, while LCO has been reported to have volume changes of

~2.3% during charge/discharge.[44-46] We thus suspect the strain from the volume change of the LCO material accelerates the disconnection of material from the current collector due to mechanical forces accompanying the particle strain and accelerates the fade in the discharge capacity for LCO particle coin cells relative to LTO. However, the initial charge capacity for the LCO particle coin cell was close to that observed for the conventional LCO coin cell and the potential for lithium extraction and insertion was not significantly impacted, suggesting that the LCO particles can be successfully charged and discharged without conductive carbon additives or binders. Thus, these results provided motivation and support that a dispersion of LCO particles could be effectively charged and discharged through direct contact of LCO particles with the current collector during collisions within a flowing suspension.

4.5.2. Rheological Characterization

Before studying the electrochemical properties of the LCO suspensions, the rheological properties of the LCO particles dispersed in the electrolyte were investigated, and also were compared to the rheological data reported for similar suspensions containing LTO particles.[18] The viscosities as a function of shear rate for LCO can be found in Figure C2 in Appendix C. Both the particle-free and particle-laden electrolytes show shear-thinning behavior, with the viscosity increasing as the particle volume fraction is increased across all measured shear rates. From these data for LCO suspensions and previous data for LTO suspensions,[18] we have extracted the viscosity and relative viscosity (the suspension viscosity divided by the carrier electrolyte viscosity) as a function of particle volume fraction at a shear rate of 100 s^{-1} (Figure 3). For equivalent

volume fractions, the viscosities of both the LCO and LTO suspensions are very similar. This is consistent with the similar approximate sizes and morphologies for both of the suspensions (360 ± 140 nm for LCO and 340 ± 200 nm for LTO, representative SEM images can be found in Figure C3 in Appendix C) [18, 32]. Particle size has previously been reported to have significant influence on rheological properties of solid suspensions,[47, 48] where suspensions with smaller solid particles generally have measured higher viscosities.[48, 49] The viscosity of metal oxide suspensions are also dependent on the volume fraction of solid particles loaded in the dispersion and can be modeled by the relationship in Equation 1.[50, 51]

$$\eta = ae^{b\phi} \quad (1)$$

where η is the viscosity of the suspension, ϕ is the volumetric solid particle loading, and *a* and *b* are fitting parameters. The parameter *b* indicates the viscosity's exponential dependence on volumetric loading. A higher *b* means a stronger exponential relationship with ϕ. With the extracted viscosity data for LCO and LTO at different particle loadings, we can fit the data in Figure 3 to this power law relationship to extract the *a* and *b* parameters (the fit curves are shown in Figure C4 in Appendix C). For LTO, a_{LTO} = 0.0043 Pa·s and b_{LTO} = 24.66 (R^2 = 0.997); and for LCO, a_{LCO} = 0.0041 Pa·s and b_{LCO} = 24.97 (R^2 = 0.998). The high R^2 correlation coefficients and *a* parameters being close to the viscosity of the electrolyte (0.0039 Pa·s) indicate this is a good model for LTO and LCO suspensions. The similar values for both *a* and *b* in the fits for the measured viscosities of LTO and LCO suspension indicate similar dependence of the viscosity on

particle loading and similar interparticle interactions in the suspensions. Both suspensions have high values of parameter b, indicating that the viscosities of both suspensions have strong dependence of particle loading. The parameter b_{LCO} is slightly greater than a_{LTO}; therefore, the viscosities of LCO suspensions are expected to increase at a slightly faster rate than LTO suspensions. Nevertheless, the two suspensions showed very similar exponential increase of viscosities over particle volumetric loading. While higher particle loadings increase the energy density of the electrolytes, the viscosity increases rapidly with the increased loading. This trend opens a new challenging task for increasing the energy density by increasing the loading. Surfactants have previously been reported to help stabilize particulate suspensions and decrease the viscosity,[52, 53] and future research efforts will be needed on incorporating surfactants and determining the detailed tradeoffs between loading and pumping requirements for various electrochemical cell configurations.

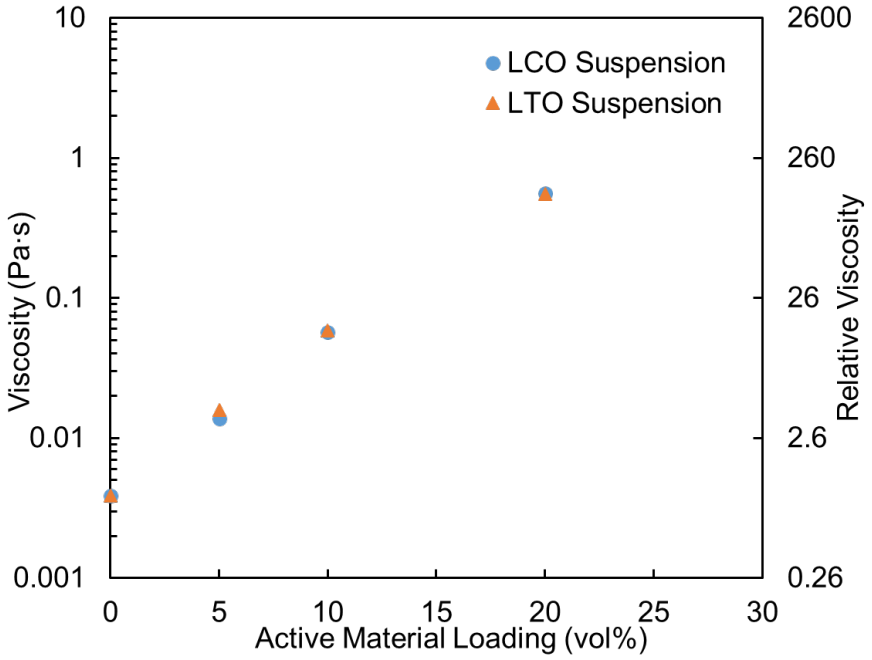

Figure 3. The viscosities and relative viscosities for the particle-free electrolyte (1.2 M $LiPF_6$ in EC/EMC = 3:7 solvents) and the electrolyte laden with 5, 10, and 20 vol% LCO (blue circle) and LTO (orange triangle) measured at 100 s^{-1}.

4.5.3. LCO Dispersions Half Cell Electrochemical Characterization

Vial cells were used for electrochemical characterization of the LCO dispersed in the electrolyte. As depicted in Figure 1a, the cathode is the LCO suspension with aluminum wire as the current collector, while a single lithium foil is adopted as the anode and reference electrode. This customized geometry was selected for three reasons. First, the suspension can be easily and continuously agitated to keep the LCO particles in suspension by rotation of the magnetic stirring bar. Second, the distance between the cathode and anode is controllable, reproducible, and kept small to minimize the IR drop. Third, the cell is relatively easy to assemble and disassemble for changing out different

dispersion solutions for analysis. Cyclic voltammetry (CV) was first adopted to confirm the potentials of the redox reactions in the LCO dispersion electrolyte. A typical CV scan at 5 mV/s for a 10 vol% LCO suspension is shown in Figure 4a. The oxidation reaction started at ~3.9 V and the current continued to increase, whereas the reduction curve showed a peak at ~3.8 V. The location of the onset potential for oxidation and peak potential for reduction were consistent with the electrochemical redox potentials for the LCO material in the suspension and indicated that the LCO particles were electrochemically active for lithium extraction/insertion and corresponding cobalt oxidation/reduction in the flowing dispersion.[32, 38, 54] Note that the cathodic current kept increasing without an obvious peak during the scan. This was because the LCO suspension was being agitated throughout the test and the current response was low, showing no diffusion limitation for the continuous exchange of fresh electroactive LCO particles in the flowing environment. However, an anodic peak was clearly observed, which we attribute to be a consequence of the small amount of LCO material that was oxidized during the cathodic scan. Thus, the reduction current was quickly limited by the low concentration of the oxidized LCO and the current decreased quickly as the anodic scan continued down to 3.0 V because very little “charged” LCO was available in the suspension. The CV scan suggests that the electrochemical oxidation of LCO in the suspension was reversible. Also, we note that the oxidation curve was fluctuating at high potentials >~4.3 V. We attribute this phenomenon to three factors: first, the inhomogeneity of collision frequencies of LCO particles on the current collector caused current fluctuations throughout the experiments; second, this fluctuation was greater when a higher voltage was applied because of the greater total currents in response to the

greater applied potential; third, the electrolyte decomposition and aluminum corrosion also became significant and contributed to the observed current at these high potentials.[55-58]

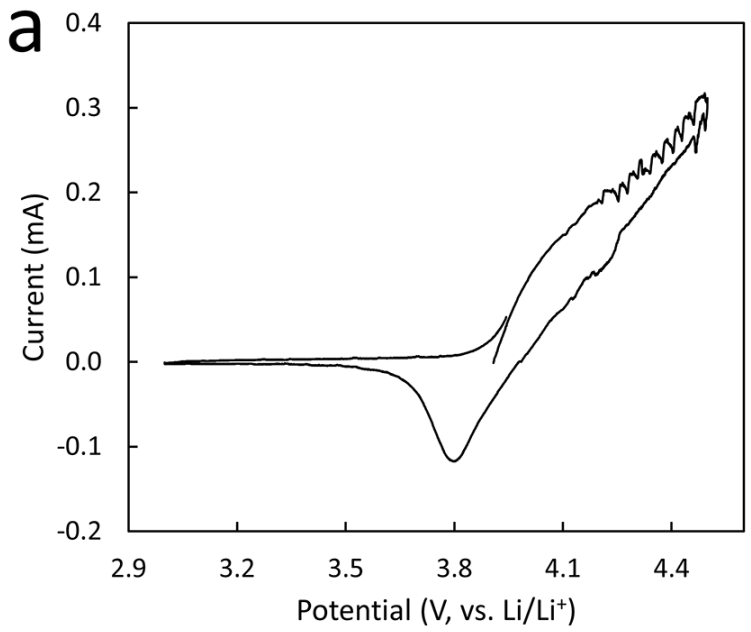

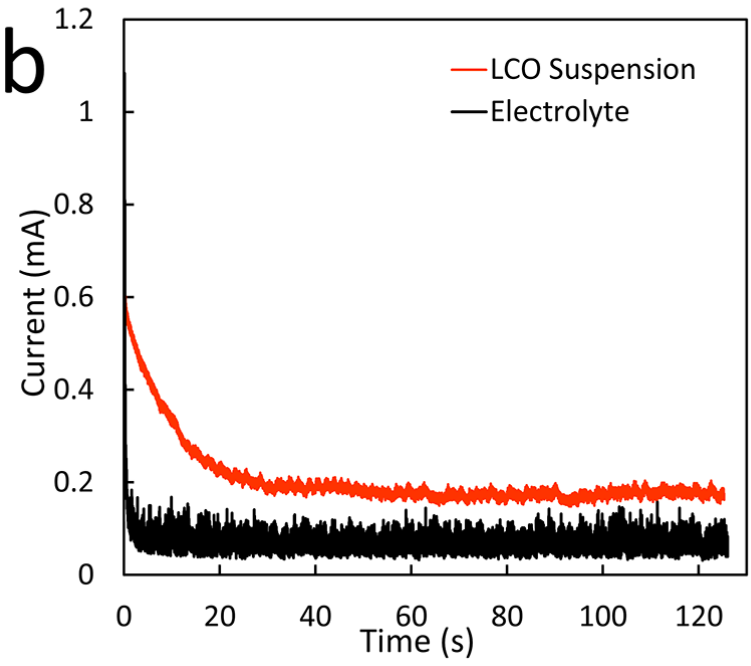

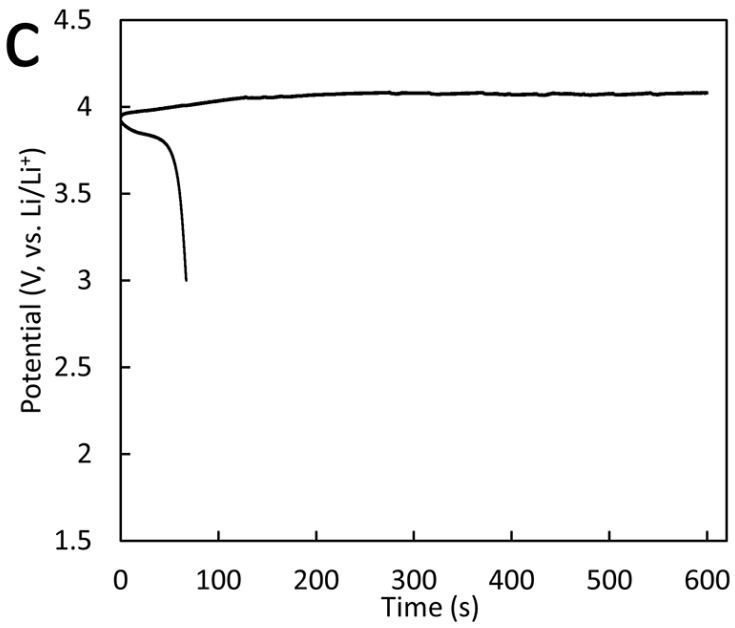

Figure 4. (a) CV scans at the rate of 5 mV/s between 3.0 and 4.5 V (vs. Li), (b) CA profiles for the control electrolyte (black) and electrolyte with 10 vol% dispersed LCO (red) with applied potential of 4.3 V, and (c) charge (10-minute cutoff time) and discharge curves for the vial cell with an LCO concentration of 10 vol% at a rate of 0.08 mA.

To demonstrate the ability of the LCO suspension to stably undergo charging of the LCO material, a Chronoamperometry (CA) test was conducted at a fixed charge potential of 4.3 V and the results are shown in Figure 4b. This voltage was chosen for the experiment because it was above the initial redox charging potential of LCO at ~3.9 V (Figure 2) and below a typical potential where corrosion has been reported to provide significant current for the aluminum current collector in the organic electrolyte.[55-58] A relatively short two-minute test was used because this amount of time was sufficient to provide a stable current signal. The control experiment with electrolyte free of LCO particles had a

measured current of 0.068 ± 0.017 mA over the last minute of the test. We attribute the measured current to be primarily the initial background current for electrolyte decomposition and aluminum corrosion in the organic electrolyte.[39, 41, 59, 60] The current measured with the LCO suspension for the last minute of the test was 0.175 ± 0.008 mA, which after adjusting for the current measured for the particle-free electrolyte suggests that ~0.107 mA current was due to the electrochemical oxidation and de-lithiation of the LCO particles in the suspension. The quickly dropping current in the first ~20 seconds of the CA test indicated that extra current was measured initially due to electrochemical double layer formation and possibly a very small amount of LCO particles attached on the aluminum current collector.[18, 61] We expect that the stable measured current of the last minute of the CA test was limited by LCO particle collision frequency, the mass of LCO particles participating in electrochemical oxidation at any given time, and the electronic/ionic conductivity of LCO particles in the suspension,[18, 20] rather than mass transfer diffusion limitations of lithium ions in the electrolyte.[62] The detailed mechanisms and limitations of the current density are currently under research, but the total mass of active material on average participating in the electrochemical reactions and in contact with the current collector likely plays a major role in the resistance to transferring current in the system.[63] We speculate that the amount of active material participation plays a role because a higher loading of electroactive material per current collector area has previously been reported to result in a lower resistance in coin cell studies with composite electrodes within a broad range of active material loading.[64-66] Previous reports on LTO suspensions also demonstrated that the measured current decreased for decreasing active material loadings.[18, 67]

A charge/discharge cycling test was performed to demonstrate the electrochemical reversibility of the LCO suspension in a flow battery-type environment. The test was performed with the 10 vol% LCO suspension after the CV and CA test, and the results are shown in Figure 4c. The suspension was first charged for 10 minutes at a current of 0.08 mA (0.008 mA cm^{-2}) before discharging at the same current. The charge potential quickly reached a plateau at ~4.0 V and remained steady at that potential during the test period. The discharge curve also showed a relatively stable voltage at ~3.8 V. This pair of charge and discharge potentials is consistent with the particle coin cell cycling potential profiles at low depth of charge range shown in Figure 2b. This not only further confirmed the reversible electrochemical reactions of LCO suspension, but also indicates that the suspension can provide stable power supply from the discharge of LCO particles at a low overpotential. We note that less discharge capacity was achieved relative to the charge capacity (0.013 mAh total charge capacity compared to 0.0015 mAh total discharge capacity resulting a coulombic efficiency of 11.5%). This was because only a small portion of the LCO had been charged during the 10-minute period (0.013 of the ~800 mAh total available capacity available, or ~0.002 % of the total capacity in the suspension). And due to this low concentration, most of the charged particles may not be able to collide with the current collector effectively to deliver capacity during the short discharge period, resulting a low coulombic efficiency. This cycling behavior is also similar to previous reports for LTO suspensions in terms of both voltage profile and coulombic efficiency.[18] We did not perform a full charge and discharge test because this 10-minute test was representative enough to show the cycling reversibility; and full

cycling of the suspensions for this dispersion flow battery are impractical with the existing current collector design. Due to the small surface area of the aluminum current collector, only a very small portion of active materials participate in the electrochemical reaction at any given time, while the majority of the particles are suspended in the electrolyte and do not contribute to the measured electrochemical activity, even though all particles will eventually exchange with those participating in electrochemical reactions and hence contribute to the total cell capacity. We estimate that with the current we are able to use for charge/discharge (that are kept low to avoid large voltage drops) and the total amount of active material in the suspensions, that a full charge and discharge of the LCO suspension would take ~7 months. We are actively investigating methods to increase the current density while avoiding a high viscosity interconnected carbon network, such as modified current collector designs that promote greater average amounts of active material being oxidized/reduced per area of current collector.

4.5.4. Full Dispersion Flow Cell Electrochemical Characterization

Before constructing an LTO/LCO dispersion full cell with the active materials dispersed in the electrolyte, first a conventional LTO/LCO coin cell was constructed to confirm the expected charge and discharge behavior for the paired materials in a full cell. Figure 5a shows the first cycle of a LTO/LCO conventional coin cell. The first charge capacity reached 177 mAh g^{-1} with a discharge capacity of 149 mAh g^{-1} (both based on the mass of LCO) for a cell cycled at a rate of 0.1C between the voltage window of 1.5 V to 2.8 V, resulting a coulombic efficiency of 84.4%. The initial capacity of the LTO electrode was approximately double the initial capacity of the LCO electrode to minimize the

possibility of lithium deposition during cycling. The charge curve first showed a plateau at ~2.4 V and then slowly increased to the cutoff voltage of 2.8 V. The discharge curve showed a corresponding behavior with voltage slowly decreasing to the ~2.4 V plateau. This was consistent with observations of LTO/LCO cells in the literature [68, 69]. Relative to Li/Li^+, LTO has a flat ~1.55 V charge/discharge plateau, while LCO begins charging at 3.95 V and the voltage slowly increases as the extent of delithiation increases.[22, 28, 29, 36, 37, 39, 69] We note that the discharge capacity was slightly lower but close to the LCO half-cell capacity. The discharge capacity being close to that observed for the LCO half-cells was consistent with the high first cycle coulombic efficiency of the LTO material (~0.7%).[18] However, the full cell charge capacity was slightly lower than the half-cell which we attributed to the relatively low charge cutoff for our LTO/LCO cell. The 2.8 V vs. LTO cutoff (~4.35 V vs. Li/Li^+) in the full cell was ~ 0.15 V lower than the 4.50 V charge cutoff voltage used in the half-cell. Overall, this test confirmed the electrochemical activity for the LTO/LCO full cell and provided expected potentials for electrochemical activity for the experiments with LTO and LCO suspensions.

A dispersed solid LTO/LCO full cell was constructed using the setup illustrated in Figure 1b and characterized electrochemically with 0.5 vol% LCO suspension as the catholyte and 1 vol% LTO suspension as the anolyte. Relatively low loadings of active materials were used in this cell in order to achieve relatively higher extents of charge in less time. The redox potentials for the LTO and LCO suspensions with lower active material loadings were confirmed to be comparable to the higher loading suspensions. Cyclic

voltammetry and galvanostatic charge/discharge testing indicated the same reversible redox reactions for both 0.5 vol% and 10 vol% LCO suspensions (see Appendix C, Figures C5a-b for 0.5 vol% LCO compared with Figures 4a,c for the 10 vol% LCO suspension), although the oxidation of LCO in the vial cell is more complex to interpret due to electrolyte decomposition and/or aluminum corrosion. The reversible redox behavior also has been observed to be at similar potentials for LTO suspensions within the range of 0.5 vol% and 20 vol%, as demonstrated in two previous reports.[18, 67] Chronopotentiometry results for a 1 vol% LTO suspension (the same loading as used in the LTO/LCO full cell experiment) in a vial cell paired with lithium metal can also be found in Figure C5c. The 1 vol% LTO suspension reached a plateau of ~1.55 V (vs. Li/Li^+) in less than 3 minutes, and the measured redox potential was consistent with measurements using the same material within a 10 vol% LTO suspension as well as conventional LTO electrodes in coin cells paired with lithium metal. A CV test on the LTO/LCO dispersion full cell was conducted to determine the redox potential of the electrochemical reactions in the full cell and the result is shown in Figure 5b. The measured current was relatively noisy during the experiment, likely because of the stochastic nature of the particle collisions necessary now at both current collectors to provide the charging current.[70] Due to the agitation and flow profile in the vial, the concentration of active materials was not perfectly homogeneous in the suspension and local collision frequencies of the active material particles on the current collector were likely not constant, i.e. the total mass of active materials that are contributing to the electrochemical reactions are not constant with time. Although the oxidation current increased continuously with the increasing potential in general, the current showed a

small peak at 2.52 V and became noisier above this potential. While the currents measured at higher potentials likely had contributions from the corrosion of aluminum wire and electrolyte decomposition,[39, 41, 59, 60] the increase in measured current at 2.26 V and the slight peak at 2.52 V (relative to LTO dispersion) were consistent with potentials expected for an LTO/LCO cell. The reduction peak at 2.26 V demonstrated that the redox reactions with the LTO/LCO cell suspensions were reversible. The approximate half-wave value, $E_{1/2}$ is 2.39 V.[71] This is consistent with the average potential at low state of charge in the LCO and LTO coin cell, indicating the source of the redox reaction was the LTO/LCO redox reaction pair. These results are the first demonstration of a reversible lithium-ion solid dispersion electrochemical flow cell, where all of the electrochemical activity is from collisions of lithium-ion active materials with current collectors placed in the anolyte and catholyte.

The oxidation peak was higher than the reduction peak in the CV measurement. This is due to a lower concentration of available active materials during the anodic compared to the cathodic reactions. The original suspension was pure pristine LCO and LTO. All of the LCO particles started in the reduced state and all of the LTO particles started in the oxidized state relative to the electrochemical processes of interest (effectively fully discharged LCO and LTO for full cell purposes). During the discharge sweep of the CV, only a tiny portion active material particles (<0.01%) had been reacted (delithiated LCO and lithiated LTO) and were available to have the electrochemical reactions reversed. Therefore, the concentration of active particles available for the discharge reactions was very low relative to the original active material concentration.

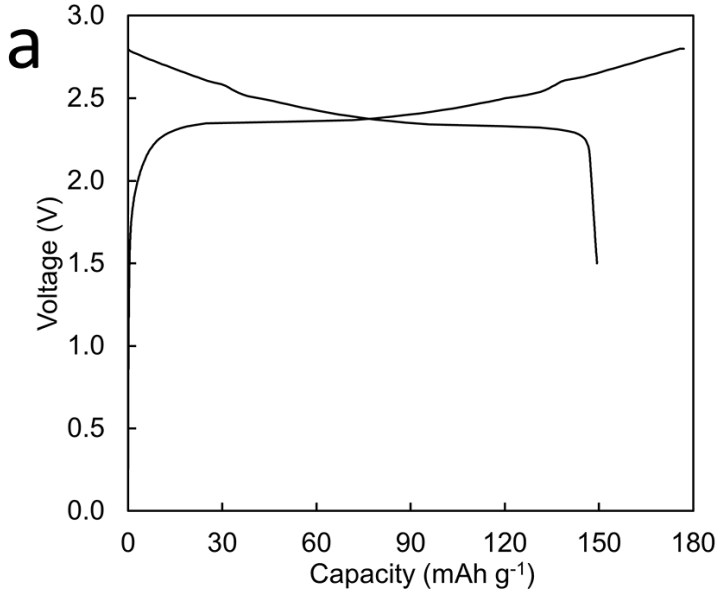
a
3.0
2.5
2.0
1.5
1.0
0.5
0.0
Voltage (V)
0
30
60
90
120
150
180
Capacity (mAh g-1)

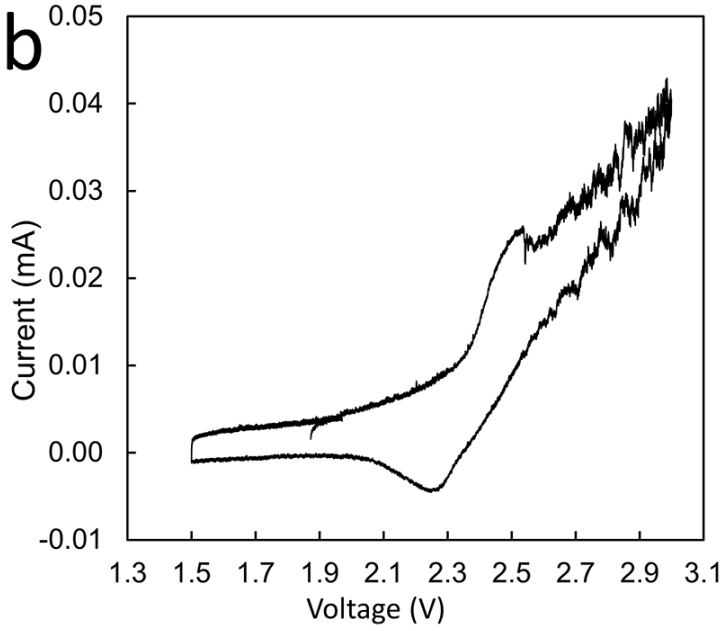
b
0.05
0.04
0.03
0.02
0.01
0.00
-0.01
Current (mA)
1.3
1.5
1.7
1.9
2.1
2.3
2.5
2.7
2.9
3.1
Voltage (V)

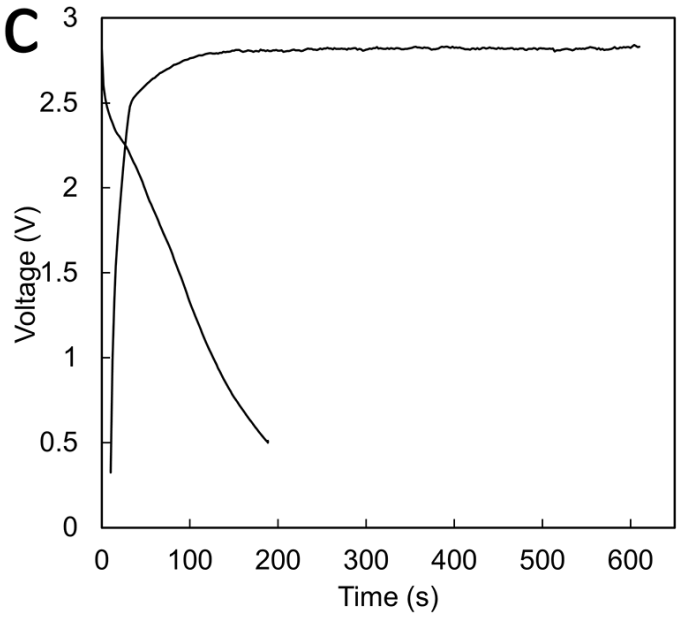

Figure 5. (a) First charge and discharge cycle of an LTO/LCO conventional coin cell; (b) CV scan at 20 mV s^{-1} between 1.5 - 3.0 volts (relative to the LTO anolyte) of the full cell containing a 1 vol% LTO anolyte and 0.5 vol% LCO catholyte while stirring at 400 rpm; (c) a constant current charge at 0.02 mA and discharge at 0.001 mA test (cutoff voltages of 0.5 and 3 V) on the same cell. The charge cycle was limited to 10 minutes.

The LTO/LCO dispersion electrochemical cell was also galvanostatically partially charged and discharged to demonstrate the potential to use the anolyte/catholyte in a flow battery system. Figure 5c shows a 10-minute charge of the cell at 0.02 mA and subsequent discharge of the cell down to a cutoff voltage of 0.5 V at 0.001 mA. The charge curve quickly reached a stable potential at 2.82 V, which was higher than the redox potential of ~2.4 V as indicated earlier in the CV test. The charging rate of 0.02 mA was relatively high for this cell configuration and resulted in additional overpotential due to the resistances in the system (charge transfer, diffusion and Ohmic resistance).[61]

On discharge the cell had a small capacity at ~2.2 V and quickly dropped to the lower cutoff voltage. We attribute the low coulombic efficiency (1.58%) to the low concentration of reacted active materials on both electrodes, similar to the explanation of the lower currents measured during the CV anodic sweep. Approaches to increase the participation rate of the active materials and hence faster cell charging are currently under investigation. This is the first report of an electrochemical cell comprised of only lithium-ion battery active material suspensions providing reversible redox couples in an electrochemical flow cell.

4.6. Conclusion

An LCO suspension dispersed in organic lithium-ion electrolyte was characterized electrochemically as a catholyte for a solid dispersion redox flow couple. A solid dispersion lithium-ion electrochemical flow cell was demonstrated for the first time by using the LCO suspension as a catholyte and pairing it with a LTO suspension anolyte. While the utilization of the active materials in this preliminary system are low, these results demonstrate the feasibility of reversible charge and discharge of a full cell comprised of lithium-ion active materials dispersed in electrolytes. Such a flow cell has a high operating potential relative to existing flow batteries as demonstrated in this manuscript, theoretically high capacity, and the ability to control the viscosity with active material loading. Future research efforts will need to be directed towards improving the current density and coulombic efficiency of the dispersed particle electrolytes.

4.7. References

1. Wang, W., et al., *Recent Progress in Redox Flow Battery Research and Development.* Advanced Functional Materials, 2013. **23**(8): p. 970-986.
2. Parasuraman, A., et al., *Review of material research and development for vanadium redox flow battery applications.* Electrochimica Acta, 2013. **101**: p. 27-40.
3. Skyllas-Kazacos, M., et al., *Progress in Flow Battery Research and Development.* Journal of the Electrochemical Society, 2011. **158**(8): p. R55-R79.
4. Alotto, P., M. Guarnieri, and F. Moro, *Redox flow batteries for the storage of renewable energy: A review.* Renewable and Sustainable Energy Reviews, 2014. **29**: p. 325-335.
5. de Leon, C.P., et al., *Redox flow cells for energy conversion.* Journal of Power Sources, 2006. **160**(1): p. 716-732.
6. Weber, A.Z., et al., *Redox flow batteries: a review.* Journal of Applied Electrochemistry, 2011. **41**(10): p. 1137-1164.
7. Janoschka, T., et al., *An aqueous, polymer-based redox-flow battery using non-corrosive, safe, and low-cost materials.* Nature, 2015. **527**(7576): p. 78-81.
8. Zhao, Y.F., et al., *Electrochemical Behavior of Polyaniline Microparticle Suspension as Flowing Anode for Rechargeable Lead Dioxide Flow Battery.* Journal of the Electrochemical Society, 2014. **161**(3): p. A330-A335.
9. Zhao, Y.F., et al., *Electrochemical study on polypyrrole microparticle suspension as flowing anode for manganese dioxide rechargeable flow battery.* Journal of Power Sources, 2014. **248**: p. 962-968.
10. Fan, F.Y., et al., *Polysulfide flow batteries enabled by percolating nanoscale conductor networks.* Nano Lett, 2014. **14**(4): p. 2210-8.
11. Pratt, H.D., et al., *A polyoxometalate flow battery.* Journal of Power Sources, 2013. **236**: p. 259-264.
12. Kaur, A.P., et al., *A Highly Soluble Organic Catholyte for Non-Aqueous Redox Flow Batteries.* Energy Technology, 2015. **3**(5): p. 476-480.
13. Takechi, K., Y. Kato, and Y. Hase, *A highly concentrated catholyte based on a solvate ionic liquid for rechargeable flow batteries.* Adv Mater, 2015. **27**(15): p. 2501-6.
14. Wang, W., et al., *A new hybrid redox flow battery with multiple redox couples.* Journal of Power Sources, 2012. **216**: p. 99-103.
15. Kang, S.-H., et al., *Study of Li1+x(Mn4/9Co1/9Ni4/9)1-xO2 Cathode Materials for Vehicle Battery Applications.* Journal of The Electrochemical Society, 2011. **158**(8): p. A936-A941.
16. Duduta, M., et al., *Semi-Solid Lithium Rechargeable Flow Battery.* Adv. Energy Mater., 2011. **1**(4): p. 511-516.
17. Viswanathan, V., et al., *Cost and performance model for redox flow batteries.* Journal of Power Sources, 2014. **247**: p. 1040-1051.
18. Qi, Z. and G.M. Koenig, *A carbon-free lithium-ion solid dispersion redox couple with low viscosity for redox flow batteries.* J. Power Sources, 2016. **323**: p. 97-106.

19. Park, M., et al., *A review of conduction phenomena in Li-ion batteries.* J. Power Sources, 2010. **195**(24): p. 7904-7929.
20. Li, H. and H. Zhou, *Enhancing the performances of Li-ion batteries by carbon-coating: present and future.* Chem. Commun. (Cambridge, U. K.), 2012. **48**(9): p. 1201-17.
21. Lai, W., et al., *Ultrahigh-energy-density microbatteries enabled by new electrode architecture and micropackaging design.* Adv Mater, 2010. **22**(20): p. E139-44.
22. Kim, J., et al., *Electrochemical Properties of Li1+xCoO2 Synthesized for All-Solid-State Lithium Ion Batteries with Li2S-P2S5 Glass-Ceramics Electrolyte.* J. Electrochem. Soc., 2015. **162**(6): p. A1041-A1045.
23. Otoyama, M., et al., *Raman imaging for LiCoO2 composite positive electrodes in all-solid-state lithium batteries using Li2S–P2S5 solid electrolytes.* Journal of Power Sources, 2016. **302**: p. 419-425.
24. Ensling, D., et al., *Nonrigid Band Behavior of the Electronic Structure of LiCoO2Thin Film during Electrochemical Li Deintercalation.* Chemistry of Materials, 2014. **26**(13): p. 3948-3956.
25. Ruffo, R., et al., *Electrochemical characterization of LiCoO2 as rechargeable electrode in aqueous LiNO3 electrolyte.* Solid State Ionics, 2011. **192**(1): p. 289-292.
26. Gummow, R.J. and M.M. Thackeray, *Structure and electrochemistry of lithium cobalt oxide synthesised at 400℃.* Material Research Bulletin, 1992. **27**: p. 327-337.
27. Whittingham, M.S., *Lithium Batteries and Cathode Materials.* Chemical Reviews, 2004. **104**(10): p. 4271-4301.
28. Tang, W., et al., *Nano-LiCoO2 as cathode material of large capacity and high rate capability for aqueous rechargeable lithium batteries.* Electrochem. Commun., 2010. **12**(11): p. 1524-1526.
29. Tan, K.S., et al., *High-performance LiCoO2 by molten salt (LiNO3 : LiCl) synthesis for Li-ion batteries.* J. Power Sources, 2005. **147**(1-2): p. 241-248.
30. Gaikwad, A.M., et al., *A High Areal Capacity Flexible Lithium-Ion Battery with a Strain-Compliant Design.* Advanced Energy Materials, 2015. **5**(3): p. 1401389.
31. Rahman, F. and M. Skyllas-Kazacos, *Vanadium redox battery: Positive half-cell electrolyte studies.* Journal of Power Sources, 2009. **189**(2): p. 1212-1219.
32. Qi, Z. and G.M.K. Jr., *High-Performance LiCoO2 Sub-Micrometer Materials from Scalable Microparticle Template Processing.* ChemistrySelect, 2016. **1**(13): p. 3992-3999.
33. Martha, S.K., et al., *Li4Ti5O12/LiMnPO4 Lithium-Ion Battery Systems for Load Leveling Application.* Journal of the Electrochemical Society, 2011. **158**(7): p. A790-A797.
34. Viswanathan, V.V., et al., *Effect of entropy change of lithium intercalation in cathodes and anodes on Li-ion battery thermal management.* Journal of Power Sources, 2010. **195**(11): p. 3720-3729.
35. Burukhin, A., et al., *Hydrothermal synthesis of LiCoO2 for lithium rechargeable batteries.* Solid State Ionics, 2002. **151**(1-4): p. 259-263.

36. Huang, B., et al., *Electrochemical evaluation of LiCoO2 synthesized by decomposition and intercalation of hydroxides for lithium-ion battery applications.* J. Appl. Electrochem., 1998. **28**(12): p. 1365-1369.
37. Liang, H.Y., et al., *Analysis of high rate performance of nanoparticled lithium cobalt oxides prepared in molten KNO3 for rechargeable lithium-ion batteries.* Electrochem. Commun., 2004. **6**(8): p. 789-794.
38. Liang, H., et al., *High performance lithium cobalt oxides prepared in molten KCl for rechargeable lithium-ion batteries.* Electrochem. Commun., 2004. **6**(5): p. 505-509.
39. Reddy, M.J.K., S.H. Ryu, and A.M. Shanmugharaj, *Synthesis of nanostructured lithium cobalt oxide using cherry blossom leaf templates and its electrochemical performances.* Electrochim. Acta, 2016. **189**: p. 237-244.
40. Pinson, M.B. and M.Z. Bazant, *Theory of SEI Formation in Rechargeable Batteries: Capacity Fade, Accelerated Aging and Lifetime Prediction.* Journal of the Electrochemical Society, 2012. **160**(2): p. A243-A250.
41. Xu, K., *Electrolytes and Interphases in Li-Ion Batteries and Beyond.* Chem. Rev. (Washington, DC, U. S.), 2014(114): p. 11503-11618.
42. Aurbach, D., et al., *Design of electrolyte solutions for Li and Li-ion batteries: a review.* Electrochimica Acta, 2004. **50**(2-3): p. 247-254.
43. Wang, H.F., et al., *TEM study of electrochemical cycling-induced damage and disorder in LiCoO2 cathodes for rechargeable lithium batteries.* Journal of the Electrochemical Society, 1999. **146**(2): p. 473-480.
44. Ohzuku, T., A. Ueda, and N. Yamamoto, *Zero-Strain Insertion Material of Li[Li1/3Ti5/3]O4 for Rechargeable Lithium Cells.* J. Electrochem. Soc, 1995. **142**(5): p. 1431-1435.
45. Ohzuku, T. and A. Ueda, *Why transition metal (di)oxides are the most attractive materials for batteries.* Solid State Ionics, 1994. **69**(3-4): p. 201-211.
46. Rieger, B., et al., *A New Method to Model the Thickness Change of a Commercial Pouch Cell during Discharge.* Journal of The Electrochemical Society, 2016. **163**(8): p. A1566-A1575.
47. Timofeeva, E.V., et al., *Base fluid and temperature effects on the heat transfer characteristics of SiC in ethylene glycol/H2O and H2O nanofluids.* Journal of Applied Physics, 2011. **109**(1): p. 014914.
48. Timofeeva, E.V., et al., *Particle size and interfacial effects on thermo-physical and heat transfer characteristics of water-based alpha-SiC nanofluids.* Nanotechnology, 2010. **21**(21): p. 215703.
49. Nguyen, C.T., et al., *Temperature and particle-size dependent viscosity data for water-based nanofluids-Hysteresis phenomenon.* International Journal of Heat and Fluid Flow, 2007. **28**(6): p. 1492-1506.
50. Tseng, W.J. and K.-C. Lin, *Rheology and colloidal structure of aqueous TiO2 nanoparticle suspensions.* Materials Science and Engineering: A, 2003. **355**(1-2): p. 186-192.
51. Mewis, J. and N.J. Wagner, *Colloidal suspension rheology*. Cambridge series in chemical engineering. 2012, Cambridge, UK New York: Cambridge University Press.

52. Madec, L., et al., *Surfactant for Enhanced Rheological, Electrical, and Electrochemical Performance of Suspensions for Semisolid Redox Flow Batteries and Supercapacitors.* ChemPlusChem, 2015. **80**(2): p. 396-401.
53. Sen, S., et al., *Surface Modification Approach to TiO2 Nanofluids with High Particle Concentration, Low Viscosity, and Electrochemical Activity.* ACS Appl Mater Interfaces, 2015. **7**(37): p. 20538-47.
54. Okubo, M., et al., *Nanosize Effect on High-Rate Li-Ion Intercalation in LiCoO2 Electrode.* J. Am. Chem. Soc., 2007. **129**: p. 7444-7452.
55. Zhang, S.S. and T.R. Jow, *Aluminum corrosion in electrolyte of Li-ion battery.* Journal of Power Sources, 2002. **109**(2): p. 458-464.
56. Markovsky, B., et al., *On the Electrochemical Behavior of Aluminum Electrodes in Nonaqueous Electrolyte Solutions of Lithium Salts.* Journal of The Electrochemical Society, 2010. **157**(4): p. A423-A429.
57. Zhang, X. and T.M. Devine, *Identity of Passive Film Formed on Aluminum in Li-Ion Battery Electrolytes with LiPF[sub 6].* Journal of The Electrochemical Society, 2006. **153**(9): p. B344-B351.
58. Morita, M., et al., *Anodic behavior of aluminum in organic solutions with different electrolytic salts for lithium ion batteries.* Electrochemica Acta, 2002. **47**(17): p. 2787-2793.
59. Arico, A.S., et al., *Nanostructured materials for advanced energy conversion and storage devices.* Nat. Mater., 2005. **4**(5): p. 366-377.
60. Handel, P., et al., *Thermal aging of electrolytes used in lithium-ion batteries – An investigation of the impact of protic impurities and different housing materials.* J. Power Sources, 2014. **267**: p. 255-259.
61. Hamann, C.H., A. Hamnett, and W. Vielstich, *Electrochemistry*. 2 ed. 2007: Wiley-VCH.
62. Ko, J.K., et al., *Transport, phase reactions, and hysteresis of iron fluoride and oxyfluoride conversion electrode materials for lithium batteries.* ACS Appl Mater Interfaces, 2014. **6**(14): p. 10858-69.
63. Gaberscek, M., R. Dominko, and J. Jamnik, *Is small particle size more important than carbon coating? An example study on LiFePO4 cathodes.* Electrochem. Commun., 2007. **9**(12): p. 2778-2783.
64. Gaberscek, M., *A Method for Fast Estimation of the Rate-Limiting Step in Lithium-Ion Batteries.* Acta Chim. Slov, 2014. **61**: p. 480-487.
65. Gallagher, K.G., P.A. Nelson, and D.W. Dees, *Simplified calculation of the area specific impedance for battery design.* Journal of Power Sources, 2011. **196**(4): p. 2289-2297.
66. Dees, D., et al., *Electrochemical Modeling of Lithium-Ion Positive Electrodes during Hybrid Pulse Power Characterization Tests.* Journal of The Electrochemical Society, 2008. **155**(8): p. A603-A613.
67. Qi, Z. and G.M.K. Jr., *Electrochemical Evaluation of Suspensions of Lithium-Ion Battery Active Materials as an Indicator of Rate Capability.* Journal of The Electrochemical Society, 2017. **164**(2): p. A151-A155.
68. Aliahmad, N., et al., *Paper-Based Lithium-Ion Batteries Using Carbon Nanotube-Coated Wood Microfibers.* IEEE Transactions on Nanotechnology, 2013. **12**(3): p. 408-412.

69. Takami, N., et al., *Electrochemical Kinetics and Safety of 2-Volt Class Li-Ion Battery System Using Lithium Titanium Oxide Anode.* Journal of The Electrochemical Society, 2009. **156**(2): p. A128-A132.
70. Fernando, A., S. Parajuli, and M.A. Alpuche-Aviles, *Observation of individual semiconducting nanoparticle collisions by stochastic photoelectrochemical currents.* J Am Chem Soc, 2013. **135**(30): p. 10894-7.
71. Bocarsly, A.B., *CV overview from Wiley Characterization of Materials*, in *Characterization of Materials*, E.N. Kaufmann, Editor. 2012, John Wiley & Sons.

Chapter V. Electrochemical Evaluation of Suspensions of Lithium-Ion Battery Active Materials by Dispersed Particle Resistance

5.1 Overview

This chapter describes the characterization of the resistance of the solid suspension based electrodes that can be used to identify materials in solid dispersion redox flow battery. $Li_4Ti_5O_{12}$ is adopted as the model material and three different $Li_4Ti_5O_{12}$ materials are characterized. The resistance of the active material suspensions is called "Dispersed Particle Resistance". It is also found to be correlated as an indicator of active material rate capability. This testing method has a fast throughput (each test within less than 30 min as opposed to a few weeks with the conventional method) and avoids the complication from other cell components such as additive composition, electrode microstructure, and cell assembly difference.

Elements of this chapter have been published in Journal of The Electrochemical Society: **Z. Qi**, G.M. Koenig, Electrochemical Evaluation of Suspensions of Lithium-Ion Battery Active Materials as an Indicator of Rate Capability, *Journal of The Electrochemical Society*, 164 (2017) A151-A155.

5.2. Abstract

A variety of physical and electrochemical properties are used to characterize lithium-ion battery active materials, both in the academic literature to understand the fundamental structure-property relationships of materials and in a manufacturing setting to provide quality control during battery material production. One important metric of battery performance is the ability to retain capacity at increasing rates of discharge, or rate capability; however, it can be influenced by a number of factors related to different electrode components and preparations and also requires time consuming cell fabrication and testing. Herein, we describe a relatively fast test that relies on electrochemical evaluation of battery active material particles in a suspension undergoing collisions with a current collector. While this technique does not provide a full rate capability characterization for a material, these results will demonstrate that the measured resistance provides the relative rate capability of the active materials without the potential interference of other composite electrode components.

5.3. Introduction

High performance battery active materials are a key enabler in the development and improvement of plug-in hybrid and battery electric vehicles, and lithium-ion (Li-ion) battery chemistry is the predominant battery technology within these applications.[1, 2] Among many physical and electrochemical evaluations conducted on Li-ion electrode active materials as part of material characterization and validation protocols, rate capability is an important metric in applications that require fast charge and/or high power output.[3, 4] Rate capability is the ability of active materials to retain electrochemical capacity at high cycling rates, i.e. high currents.[5, 6] It is highly dependent on the overpotential while discharging the cell, which is especially large at high rates of charge/discharge.[5, 7-9] This overpotential is dependent on many factors at the cell level that are not specific to the active material, including electrode contact to the current collector, pressure applied to the electrode and/or calendaring, connectivity of cell components, homogeneity of electrode slurry, conductive carbon loading, binder integrity, and other factors.[10] For the active material itself, rate capability can be dependent on additional attributes including material stoichiometry, crystal structure, particle size, and crystallinity;[3, 5, 6, 8, 9, 11] therefore, there is value in evaluating the electrochemical properties on active materials independent of the influences of other cell components or fabrication practices. Obtaining such material properties is important both from a research perspective to compare the electrochemical properties between candidate materials and from a quality control perspective of validating batch to batch variability between battery active materials in a manufacturing process.

Electrochemical evaluation of active materials is frequently reported in the literature by casting the material into thin film composite electrodes from slurries and then fabricating coin cells to undergo various electrochemical testing.[3, 8, 11] Including battery and electrode fabrication steps and charge/discharge cycling at multiple rates, electrochemical measurements such as rate capability on an active material can take weeks.[3, 8, 11] While these analyses are time consuming, they are important to quantify the rate capability of an active material and are thus frequently reported in the literature.[12-17] Another method to compare the rate capability of materials was reported recently by Gaberscek, et al.[18] The authors' extracted the potential of coin cells at the same state of charge at increasing cycling rates and demonstrated a linear relationship between current (per mass) and overpotential.[18] The slope of the regression line (defined as mass electrode resistance, or R_m in the report, units of Ω-g) is a single parameter that correlates with the rate capability of active materials because it shows the dependence of the overpotential on discharge current for a given material.[18] While this method is valuable for comparison between materials, especially of the same chemistry, it still requires electrode and cell fabrication. In this report we will demonstrate preliminary results for a simple resistance measurement that correlates to rate capability, much like R_m, but without electrode fabrication or coin cell assembly, resulting in faster material analysis.

An additional challenge in the coin cell electrochemical evaluation described above is that the resistance not only reflects the active material properties but also reflects the resistance from other cell components and the interaction between those components. For example, increasing and decreasing the pressure on a lithium-ion battery electrode results

in reversible decreases and increases in the resistance as measured using electrochemical impedance spectroscopy.[10] While such measurements provide insights into the improvements in electrode performance for common manufacturing steps such as electrode calendaring, they also highlight that electrochemical measurements on coin cells reflect more than the active material properties.[10] One way that such a challenge has been addressed in the literature is through electrochemical evaluation of individual lithium-ion battery particles.[19, 20] These measurements provide direct evaluation of the battery active material, however, they require relatively complex fabrication and are specific to the particle under evaluation, meaning that many individual particles would need to be assessed to provide information on the electrochemical properties of an ensemble average over a powder of many particles that will be processed into a composite electrode.

In this chapter, we will describe initial results for a method that 1) quickly provides a resistance measurement associated with the electrochemical charge/discharge of a lithium-ion battery material without electrode or coin cell fabrication and 2) provides this measurement that represents an average over an ensemble of many particles randomly distributed from a lithium-ion battery active material powder. This method to evaluate active material particles was adapted from a collision-based dispersion flow battery redox couple previously reported by our group.[21, 22] Within the flow battery redox couple system, battery active material was dispersed in electrolyte and either pumped or stirred to force the active material into collisions with a current collector. There are no conductive carbon additives in this system, and thus only active material in contact with

the current collector contributes to the observed electrochemical activity. The measurement process in this report follows similar methodology and requires three steps: 1) disperse the active material in the electrolyte; 2) flow the suspension into the customized cell and take measurements of voltage using sequential constant currents; 3) flow the suspension out. This method is fast and can accommodate multiple measurements performed in succession. Although the measurements do not give full rate capability in terms of the percentage of capacity at different rates, they result in a single resistance parameter which we demonstrate correlates to the relative rate capability for the three materials used to demonstrate the proof-of-concept in this report. This fast and simple technique specifically interrogates the active material without other composite electrode components and should enable fast screening and qualification of battery active materials, though validation across many more battery material samples will be needed to fully demonstrate the limits of this technique.

5.4. Experimental

5.4.1. Material Synthesis and Characterization

The lithium-ion battery active material used to demonstrate the method in this report was the anode material $Li_4Ti_5O_{12}$ (LTO). LTO was chosen because it is a well characterized lithium-ion battery anode material with high rate capability, and the rate capability has previously been demonstrated to vary significantly across LTO material produced using different methods.[9, 14] The flat discharge potential of LTO is beneficial for measuring a stable potential when using constant current testing.[9, 14, 21, 23] Three LTO materials from either different suppliers or synthesized in lab were first characterized in conventional coin cells using existing methods to measure the capacity retention at increased rates of discharge and the mass electrode resistance.[12-18] Three LTO materials were used in this study, which we refer to as LTO-1, LTO-2, and LTO-3. LTO-1 and LTO-3 were obtained from battery material vendors. LTO-2 material was synthesized following a solid state calcination method previously published in the literature.[9, 24, 25] A mixture of anatase titanium oxide (Acros Organics) and lithium hydroxide (Fisher Scientific, 4% excess than stoichiometric amount) was calcined in a Carbolite CWF 1300 box furnace in an air atmosphere by heating at an incremental rate of 3°C min^{-1} up to 800 °C and then holding at this temperature for 20 hours before turning off the furnace and allowing cooling down to ambient temperature without control over the cooling rate. To characterize the morphologies of the materials, scanning electron microscope (SEM) images were taken for all three LTO materials with a Quanta 650 SEM (see Appendix D, Figure D1). A Panalytical X'pert diffractometer with Cu Kα radiation was used to obtain the X-ray diffraction (XRD) patterns of the materials (see

Appendix D, Figure D2). Tap densities were measured with a tap density analyzer (Quantachrome Instruments). The focus of this manuscript is demonstrating the electrochemical evaluation of flowing particle dispersions and the correlation of the method to material rate capability, and thus the physical property characterization of the three LTO powders including SEM, XRD, and tap density can be found in Appendix D.

5.4.2. Coin Cell Fabrication and Electrochemical Characterization

Electrochemical characterizations were carried out using CR2032-type coin cells with LTO electrode as the working electrode and lithium foil as the counter and reference electrode, separated by a polypropylene / polyethylene / polypropylene trilayer membrane. LTO electrodes were prepared by first mixing 80 wt% LTO powder with 10 wt% carbon and 10 wt% polyvinylidene difluoride (PVDF) binder, which was dissolved in *N*-methylpyrrolidone (NMP, Sigma-Aldrich®). The mixtures were pasted on aluminum foil using a doctor blade. Electrodes were then dried in the oven at 70 °C overnight followed by further drying in a vacuum oven at 70 °C for three hours. Electrode disks of 1.6 cm^2 were prepared using a punch, and the loading of LTO active material in the electrodes for all samples was ~10 mg. The electrolyte used was 1.2 M lithium hexafluorophosphate ($LiPF_6$) in ethylene carbonate (EC) and ethyl methyl carbonate (EMC) with EC/EMC = 3:7 by volume ratio (BASF Corporation). The cells were assembled in an argon-filled glove box (with concentrations of both O_2 and H_2O < 1 ppm) at room temperature. The galvanostatic charge-discharge tests of coin cells were performed with a Maccor battery cycler. For experimental results where the C rate is given, 1C was assumed to be 175 mA g^{-1} LTO active material, with the rate scaled by the

amount of active material loaded into each individual electrode. The cycling window for LTO cells was 1.0 to 2.5 V (vs. Li/Li^+).

5.4.3. Active Material Suspensions Electrochemical Evaluation

LTO suspensions were prepared by dispersing the LTO powder in the electrolyte (using agitation provided by a magnetic stir bar at 400 rpm). Three different loadings of LTO suspensions (0.5 vol%, 1 vol% and 2 vol%) were prepared for each LTO material. Loadings were kept low to minimize the formation of larger particle flocculates. A customized cell was designed and assembled to characterize the suspensions. As shown in Figure 1, the cathode current collector was an aluminum wire (9.4 cm^2 total surface area immersed in the suspension, Fisher Scientific) surrounded by the LTO suspension, which was agitated by a stir bar. The active surface area of the aluminum wire was controlled by coating wax at the liquid-gas interface, creating an inert surface on the wire even if the interface underwent fluctuations due to the agitation of the suspension. The anode (and reference electrode) was a piece of lithium foil. The cathode and anode were separated by a glass tube and a polypropylene / polyethylene / polypropylene trilayer membrane. The cell was assembled and tested in the argon-filled glove box. All electrochemical tests on this customized device were performed with a Biologic SP-150.

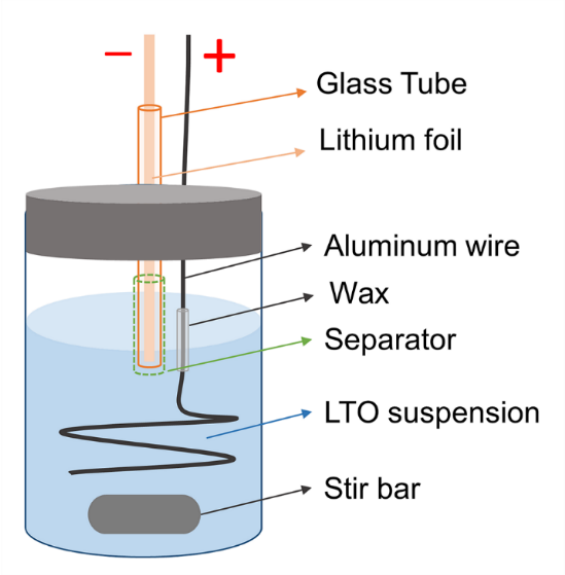

Figure 1. Cartoon illustration of the customized electrochemical cell with aluminum wire as the cathode current collector immersed in an LTO suspension and lithium foil as the anode.

5.5. Results and Discussion

5.5.1. Electrochemical Testing on Conventional Cells

The LTO materials were electrochemically tested in conventional coin cells to determine the rate capability for benchmarking. Both the discharge profiles and the discharge capacities at increasing rates of discharge (cells were cycled between 0.1C and 10C) are shown in Figure 2. All three LTO electrodes had flat discharge curves at ~1.5 V at low cycling rates, which is consistent with other reports on LTO materials in the literature.[9, 14-16, 26] Discharge capacities for all three LTO materials decreased with increasing rates, which is typical because of increasing overpotential at increasing discharge currents. At each C-rate, the capacity retention (in terms of the percentage of the discharge capacity relative to the capacity at 0.1C) follows the ranking order of LTO-1 > LTO-2 > LTO-3. This difference became more pronounced as the rate of discharge was increased. LTO-3 lost almost all discharge capacity when cycled at 10C. However, LTO-1 still maintained ~50% of the capacity at this rate. This test was highly reproducible and the standard deviation of capacity retention for three coin cells of each LTO material was below 1% for most rates tested (see Table D1 in Appendix D for standard deviation of capacity retentions at different C rates). We do note that while the low-rate capacities (0.1C) for LTO-1 and LTO-3 were very close (~165 mAh g^{-1}), LTO-2 had a significantly lower capacity (~148 mAh g^{-1}) which we attribute to significant rutile TiO_2 impurity phase in this material (see Appendix D). This electrochemical testing was primarily done to establish the baseline order of rate capability between the materials with LTO-1 having the highest rate capability and LTO-3 having the lowest rate capability.

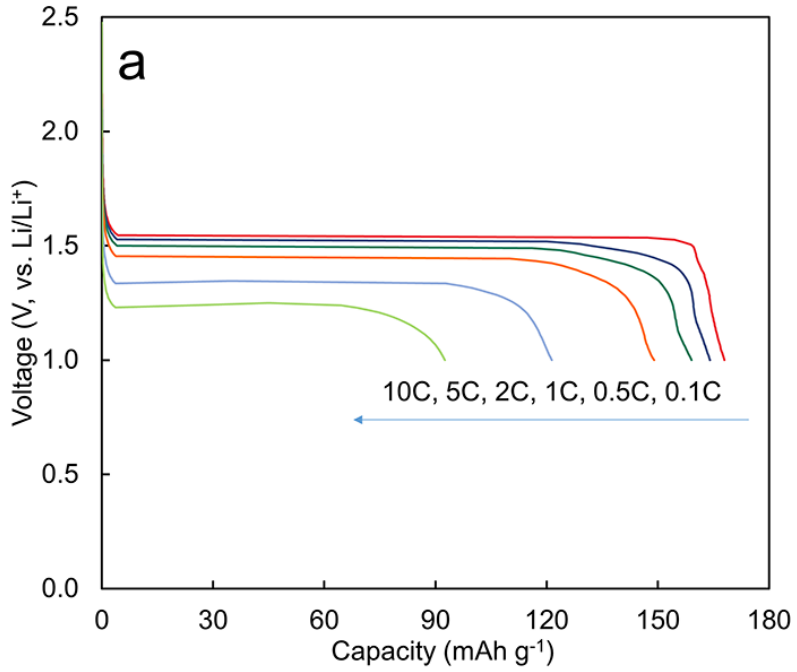
a
2.5
2.0
1.5
1.0
0.5
0.0
Voltage (V, vs. Li/Li+)
10C, 5C, 2C, 1C, 0.5C, 0.1C
0
30
60
90
120
150
180
Capacity (mAh g-1)

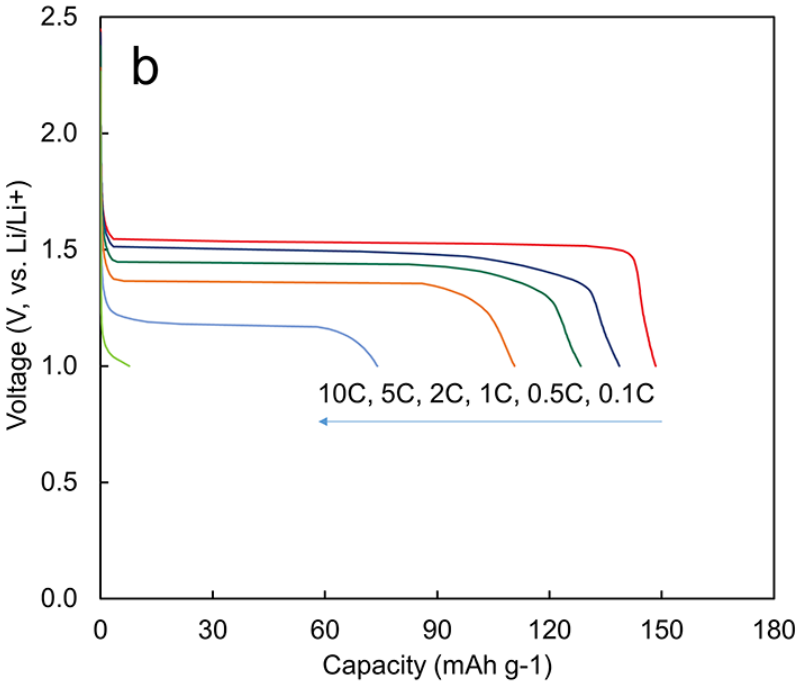
b
2.5
2.0
1.5
1.0
0.5
0.0
Voltage (V, vs. Li/Li+)
10C, 5C, 2C, 1C, 0.5C, 0.1C
0
30
60
90
120
150
180
Capacity (mAh g-1)

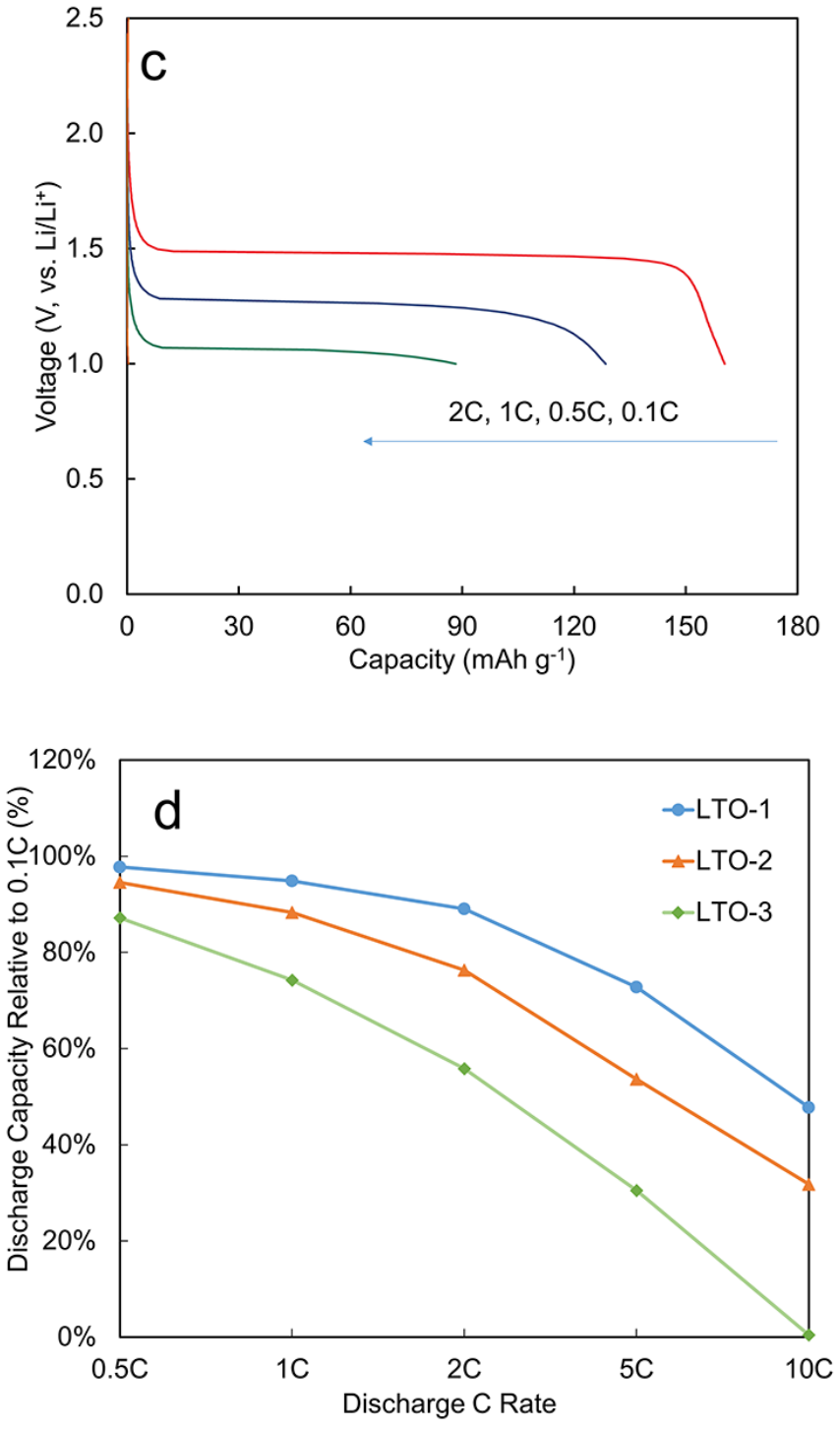

Figure 2. Constant current discharge profiles at increasing C-rates for (a) LTO-1, (b) LTO-2, and (c) LTO-3; (d) discharge capacity of all three materials (blue circles: LTO-1;

orange triangles: LTO-2; green diamonds: LTO-3) at different C-rates relative to the capacities at 0.1C (lines in (d) added to guide the eye).

Using the discharge profiles at various discharge currents in Figures 2a-c, the potential at 25 mAh g^{-1} (the same state of charge) was extracted to determine the mass electrode resistance (or R_m, units of Ω-g) using methods previously reported in the literature.[18] The potential as a function of the current (divided by the mass of active materials) displayed a linear relationship, with a representative example shown for LTO-3 in Figure 3. We note that for each current in Figure 3 there are four separate data points representing the potential measured for four successive discharge cycles under the same conditions, but that the high reproducibility of the measured potentials results in difficulty in distinguishing the four individual data points in the figure. A linear fit of data such as that displayed in Figure 3 provides a slope which is the parameter previously referred to as the R_m.[18] We measured the R_m values for LTO-1, 2, and 3 to be 0.693, 0.847, and 2.357 Ω-g, respectively. Increasing values of R_m correlated with decreasing rate capability of the LTO materials, consistent with previous reports on other lithium-ion battery electrode materials.[18] R_m is particularly useful in comparing between materials because it normalizes the effects of material loading on the resistance of the electrode and rate capability.[18] R_m provides a single straightforward parameter that can be used to compare the discharging resistance among different active electrode materials, and because lower resistance results in lower overpotential lower R_m materials have higher rate capabilities as long as everything else regarding the cells has been held equivalent.

Although R_m is a valuable parameter to use that correlates to the rate capability of active materials, it still requires electrode and cell fabrication and many charge/discharge cycles at different rates which take significant time. Also, while R_m in many cases is dominated by the resistance of the active material itself, it is also influenced by other factors in the electrode, such as the particle "wiring".[10, 27] Also, the influence of active material loading is compensated by the mass term in R_m only within a particular range of loading.[27] The electrode microstructure still influences the R_m value measured, and thus a method to interrogate the active material without electrode microstructure effects would be desirable. A technique that does not involve electrode fabrication to electrochemically probe the active materials could in principle remove the contributions from electrode microstructure and non-active material components.

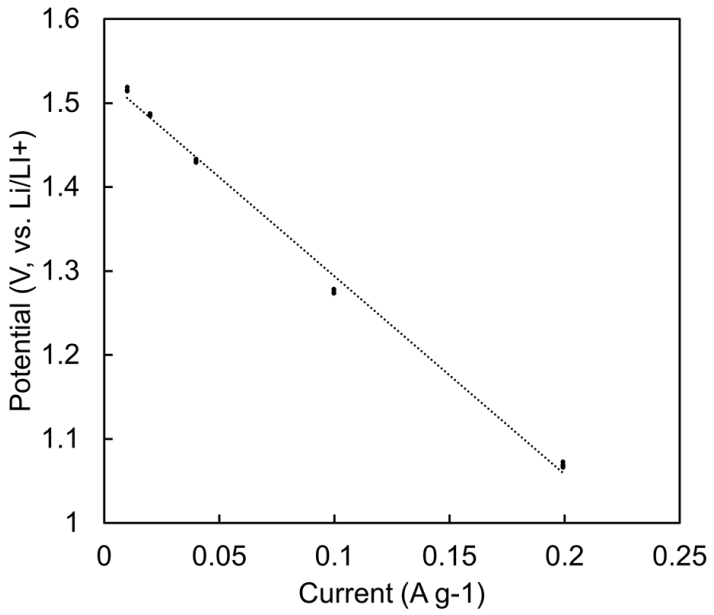

Figure 3. Potential at a capacity of 25 mAh g^{-1} at increasing current per mass of active material for LTO-3. Black dots are measured data points and the dashed line is the linear fit. The slope of the line is 2.357 Ω-g.

5.5.2. LTO Suspension Testing and Rate Capability Correlation

A customized electrochemical cell was designed (shown in Figure 1) to characterize LTO active material suspensions. After dispersing the powder in the electrolyte, a series of chronopotentiometry (CP) tests at systematically increasing discharge currents were performed. An example of a sequence of CP tests can be found in Figure D3, though this example has relatively few current steps compared to most of the measurements discussed below. The potential quickly stabilized after an initial drop in potential due to the capacitance of the electric double layer.[1, 28, 29] After reaching a stable plateau, the average potential of the final 20 seconds at a given current was determined. These average potentials have a linear decrease as the discharge current is increased (see Figure 4a as an example for LTO-2 with 2 vol% loading). Data such as that found in Figure 4a was used for a linear fit (dashed line, $R^2 = 0.999$) and the slope was extracted from this fit. We call this slope the dispersed particle resistance (DPR), which has units of Ω. DPR measures the increasing rate of overpotential over increasing current for the particles contacting the electrode in the dispersions. A higher DPR means a faster increase of overpotential while increasing the discharge current, which we hypothesized would indicate a material has a lower rate capability. Importantly, this technique provides a significant measured current from only the active material particles when the particles are actively colliding with the current collector (see Figure D4 in Appendix D for control experiment without LTO particles in electrolyte and reference [21] for demonstration that our experimental setup only provides electrochemical response when particles are actively agitated and colliding with the current collector). Thus, the DPR technique is probing a resistance that is the sum of many resistances in the system, including the

resistance of the active material particles, Ohmic resistance from the circuit, and resistance from the electrolyte. The combined value of these later two resistances was consistently found to be between 125 Ω and 140 Ω from the high frequency intercept of electrochemical impedance spectroscopy measurements, which was always less than 20% of DPR and can be subtracted from the measured resistance for normalizing between measurements. Thus, DPR was most sensitive to the active material particles and the variability due to electrolyte/cell resistance is low. The primary contribution to DPR is from the active material particles, which consists of resistance due to the particle electronic and ionic conductivity as well as activation resistance. Each of these factors are challenging to measure individually and vary across multiple orders of magnitude with different methods.[30] The DPR approach measures the sum of all of these factors and so only when one can be significantly assumed to dominate can an explicit electrochemical parameter be extracted; however, DPR does provide a collective measure that indicates the overall average resistance from an ensemble of the active material particles.

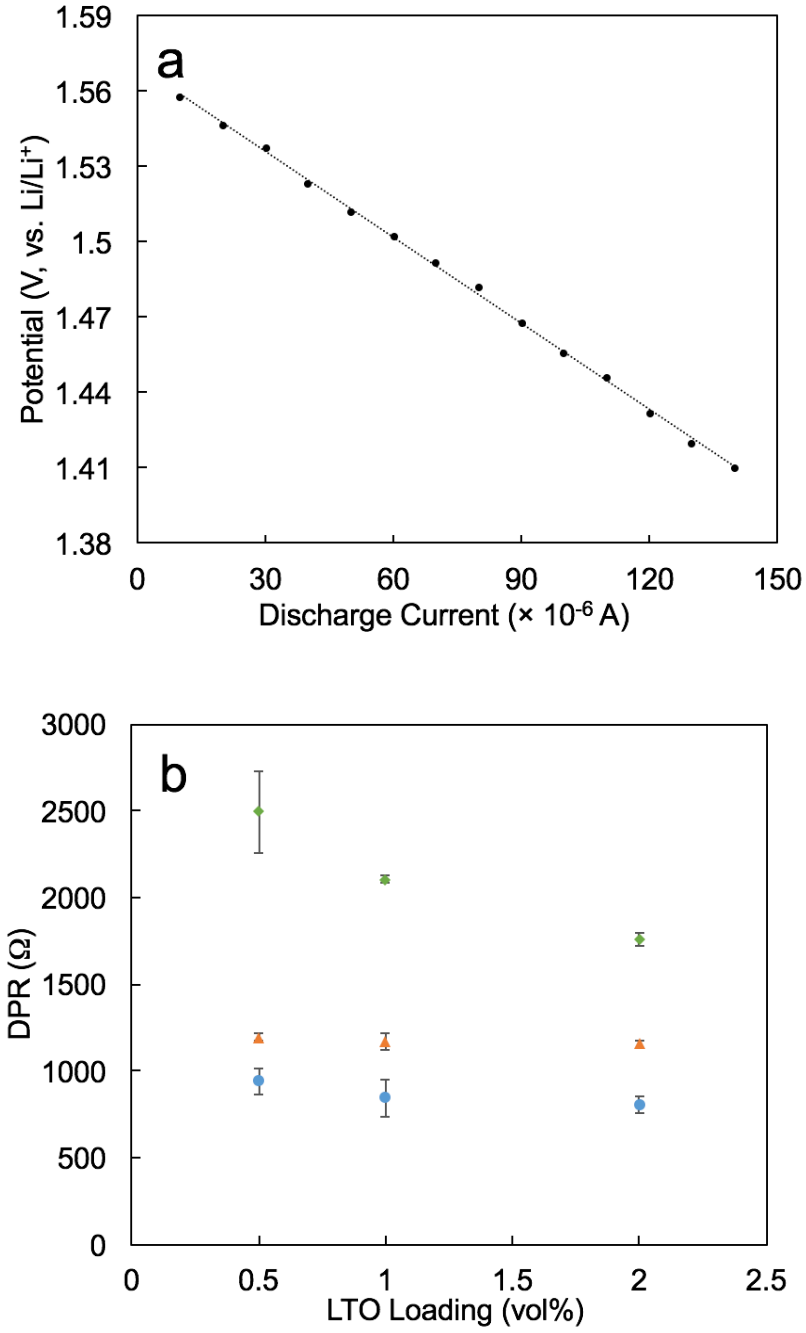

Figure 4. (a) Example of the average potentials after reaching a steady plateau in the measured potential at increasing CP discharge currents for a 2 vol% suspension of LTO-2 dispersed in electrolyte. Dashed line is a line plotted using parameters from a linear regression of the data. (b) The dispersed particle resistance (DPR) values determined

from the slopes of all fitted lines for three LTO materials at three different loadings (blue circles: LTO-1; orange triangles: LTO-2; green diamonds: LTO-3; error bars show the standard deviations of a series of three measurements).

To confirm the relative correlation between DPR and rate capability, we performed DPR measurements on all three LTO materials at 0.5, 1, and 2 vol% LTO loading in electrolyte and the results are shown in Figure 4b. The DPR across all suspension loadings went in the order of LTO-3 > LTO-2 > LTO-1. Notably, this is the same order as the R_m measurements and has the same general trend that a greater DPR value correlates with a lower rate capability of the active material. Figure 4b also shows that DPR decreased as the loading increased for each material. This increase of active material loading results in an increase in the particles in contact with the current collector on average, which increases the effective active material surface area and hence decreases the resistance. A similar effect has been shown previously for conventional coin cells in the literature. Atebamba *et al*. has shown that both contact resistance and lithium insertion resistance decrease as the mass loading of active materials increases.[10] Gallagher *et al*. and Dees *et al*. also have previously demonstrated that the area specific impedance (ASI) of the electrode is lower with thicker electrodes (corresponding to higher active material loading per unit area) below a critical thickness using both experimental analysis and computations.[31, 32] In the DPR system, a higher active material loading in the suspension increases the areal density of particles in the fluid contacting the current collector, which should result in more total active material particles in contact with the current collector and contributing to the electrochemical

reactions at any given time. Thus, the total electroactive material area in contact with the current collector is increased, similar to increasing the active material loading or thickness in a conventional coin cell as was the case in the studies mentioned above that measured and predicted decreased resistance under such conditions. These results demonstrated the sensitivity of the DPR technique both to the properties and the amount of electroactive material within the suspension. The DPR measurements and the previous literature discussed above lead us to expect that the measured DPR will decrease with increased active material loading in the electrolyte, decrease with an increase in the ionic and electronic conductivities of the active material, and increase with an increase in particle size. Detailed measurements with independent verification of each of these parameters being explicitly verified are the subject of ongoing and future experiments.

5.5.3. Discussion

A major benefit of the DPR method is that the measurement can be made in a convenient way without electrode fabrication, and thus is relatively fast and does not have contributions from other electrode components or the electrode microstructure and connectivity.[21] Additionally, because the suspension is agitated and there are many different particles that are coming into contact with the electrolyte, the measured resistance is an average of contributions from the ensemble of particles in the powder. Thus the technique is representative of the polydisperse particle population of interest, as opposed to single particles selected from within that population.[19-22] While more materials need to be tested to more generally affirm the DPR technique limits and reliability, these three materials show that a quick DPR measurement provides insights

into the relative rate capabilities of the active materials. Most of the DPR measurements took less than 30 minutes total in sample preparation and CP testing.

While the DPR technique is fast and has the advantages of probing the active material more explicitly than when it is within a composite electrode, the technique still has some limitations that will be the subject of future investigations. One limitation is that the technique is only probing the pristine dispersed particle resistance, and not the resistance at a set of state of charge as was used for R_m measurements. During the course of DPR measurements the total capacity discharged is <0.1% of the discharge capacity of the particles in the system. While this provides confidence that the particles are all in an effectively undischarged state when contacting the current collector, the technique would be challenging to implement after formation cycling on the material or at various states of charge because the current densities are very limited in dispersion redox couple experiments.[21, 22] Another limitation is that this technique would be challenging to interpret when using active materials outside of the electrolyte stability window. The resistance determined when using active materials outside of the electrolyte stability window would be complicated to interpret because the electrochemical current would be a combination of the active material intercalation reactions and electrolyte decomposition.[33] Thus, for some cathode and anode active materials the electrolyte would need to be changed such that stability window of the electrolyte contained the intercalation potential of the active material to be evaluated. Also, we do not have an independent verification of the average mass of active material in contact with the current collector. As can be seen in Figure 4b, as the volume fraction is increased the DPR

decreases for all samples. Other methods will need to be developed to independently estimate the mass of active material contacting the current collector and account for this effect. Finally, the measured resistance correlates to the active material rate capability but does not necessarily provide a means to diagnose the root cause of the rate capability differences. Other techniques will be needed in combination to diagnose the material qualities resulting in the measured resistances such as particle size, crystallinity, and other factors.[6, 7, 13, 15, 18, 34-37] The R_m method can be used to provide an estimate of the active material conductivity,[18] and the DPR method should provide similar insights if the average mass of particles contacting the current collector can be reliably and independently determined.

5.6. Conclusions

Three LTO lithium-ion battery active materials were electrochemically evaluated in particular with regards to rate capability and mass electrode resistance using conventional coin cells. Consistent with previous reports, materials with higher mass electrode resistance had lower rate capability. A new method to quantify the resistance of the active material, dispersed particle resistance, was demonstrated and also has a relationship of lower resistance correlating with increasing rate capability when the material is cycled in battery cells. The dispersed particle resistance measurements were conducted without fabricating electrodes and under conditions with flowing dispersions colliding with a current collector, providing a fast method to electrochemically evaluate ensembles of particles without the time commitments of electrode fabrication, cell fabrication, and rate capability testing. This simple technique demonstrates a platform to quickly provide one parameter to contribute to the electrochemical evaluation of battery active materials.

5.7. References

1. Omar, N., et al., *Rechargeable Energy Storage Systems for Plug-in Hybrid Electric Vehicles-Assessment of Electrical Characteristics.* Energies, 2012. **5**(8): p. 2952-2988.
2. Dunn, B., H. Kamath, and J.M. Tarascon, *Electrical Energy Storage for the Grid: A Battery of Choices.* Science, 2011. **334**(6058): p. 928-935.
3. Liang, B., Y. Liu, and Y. Xu, *Silicon-based materials as high capacity anodes for next generation lithium ion batteries.* J. Power Sources, 2014. **267**: p. 469-490.
4. Kang, S.-H., et al., *Study of Li1+x(Mn4/9Co1/9Ni4/9)1-xO2 Cathode Materials for Vehicle Battery Applications.* Journal of The Electrochemical Society, 2011. **158**(8): p. A936-A941.
5. Kang, K.S., et al., *Electrodes with high power and high capacity for rechargeable lithium batteries.* Science, 2006. **311**(5763): p. 977-980.
6. Kunduraci, M. and G.G. Amatucci, *The effect of particle size and morphology on the rate capability of 4.7 VLiMn1.5+delta Ni0.5-delta O4 spinel lithium-ion battery cathodes.* Electrochimica Acta, 2008. **53**(12): p. 4193-4199.
7. Bai, X., et al., *Enhancing the Long-Term Cyclability and Rate Capability of Li4Ti5O12 by Simple Copper-Modification.* Electrochimica Acta, 2015. **155**: p. 132-139.
8. Wang, W., et al., *A nanoparticle Mg-doped Li4Ti5O12 for high rate lithium-ion batteries.* Electrochimica Acta, 2013. **114**: p. 198-204.
9. Yi, T.-F., et al., *Synthesis and application of a novel Li4Ti5O12 composite as anode material with enhanced fast charge-discharge performance for lithium-ion battery.* Electrochimica Acta, 2014. **134**: p. 377-383.
10. Atebamba, J.-M., et al., *On the Interpretation of Measured Impedance Spectra of Insertion Cathodes for Lithium-Ion Batteries.* Journal of The Electrochemical Society, 2010. **157**(11): p. A1218.
11. Liu, J., et al., *Self-supported Li4Ti5O12-C nanotube arrays as high-rate and long-life anode materials for flexible Li-ion batteries.* Nano Lett, 2014. **14**(5): p. 2597-603.
12. Hsieh, C.T., et al., *Synthesis of lithium nickel cobalt manganese oxide cathode materials by infrared induction heating.* Journal of Power Sources, 2014. **269**: p. 31-36.
13. Tang, W., et al., *Nano-LiCoO2 as cathode material of large capacity and high rate capability for aqueous rechargeable lithium batteries.* Electrochem. Commun., 2010. **12**(11): p. 1524-1526.
14. Ge, H., et al., *Nanoparticles-Constructed Spinel Li4Ti5O12 with Extra Surface Lithium Storage Capability towards Advanced Lithium-ion Batteries.* Electrochimica Acta, 2016. **211**: p. 119-125.
15. Zhao, S., et al., *Effect of primary crystallite size on the high-rate performance of Li4Ti5O12 microspheres.* Electrochimica Acta, 2016. **206**: p. 17-25.
16. Lin, C.F., et al., *Monodispersed mesoporous Li4Ti5O12 submicrospheres as anode materials for lithium-ion batteries: morphology and electrochemical performances.* Nanoscale, 2014. **6**(12): p. 6651-6660.

17. Qi, Z. and G.M.K. Jr., *High-Performance LiCoO2 Sub-Micrometer Materials from Scalable Microparticle Template Processing.* ChemistrySelect, 2016. **1**(13): p. 3992-3999.
18. Gaberscek, M., R. Dominko, and J. Jamnik, *Is small particle size more important than carbon coating? An example study on LiFePO4 cathodes.* Electrochem. Commun., 2007. **9**(12): p. 2778-2783.
19. Dokko, K., et al., *Kinetic Characterization of Single Particles of LiCoO2 by AC Impedance and Potential Step Methods.* Journal of The Electrochemical Society, 2001. **148**(5): p. A422.
20. Takami, N., et al., *Electrochemical Kinetics and Safety of 2-Volt Class Li-Ion Battery System Using Lithium Titanium Oxide Anode.* Journal of The Electrochemical Society, 2009. **156**(2): p. A128.
21. Qi, Z. and G.M. Koenig, *A carbon-free lithium-ion solid dispersion redox couple with low viscosity for redox flow batteries.* J. Power Sources, 2016. **323**: p. 97-106.
22. Qi, Z. and G.M.K. Jr., *Carbon-free Solid Dispersion LiCoO2 Redox Couple Characterization and Electrochemical Evaluation for All Solid Dispersion Redox Flow Batteries.* Electrochim. Acta, submitted, 2016.
23. Song, M.S., et al., *Does Li4Ti5O12 need carbon in lithium ion batteries? Carbon-free electrode with exceptionally high electrode capacity.* Chemical Communications, 2012. **48**(4): p. 516-518.
24. Ohzuku, T., A. Ueda, and N. Yamamoto, *Zero-Strain Insertion Material of Li[Li1/3Ti5/3]O4 for Rechargeable Lithium Cells.* J. Electrochem. Soc, 1995. **142**(5): p. 1431-1435.
25. Belharouak, I., G.M. Koenig, and K. Amine, *Electrochemistry and safety of Li4Ti5O12 and graphite anodes paired with LiMn2O4 for hybrid electric vehicle Li-ion battery applications.* J. Power Sources, 2011. **196**(23): p. 10344-10350.
26. He, Z., et al., *Spherical Li4Ti5O12 synthesized by spray drying from a different kind of solution.* Journal of Alloys and Compounds, 2012. **540**: p. 39-45.
27. Gaberscek, M., *A Method for Fast Estimation of the Rate-Limiting Step in Lithium-Ion Batteries.* Acta Chim. Slov, 2014. **61**: p. 480-487.
28. Kotz, R. and M. Carlen, *Principles and applications of electrochemical capacitors.* Electrochimica Acta, 2000. **45**(15-16): p. 2483-2498.
29. Dennison, C.R., Y. Gogotsi, and E.C. Kumbur, *In situ distributed diagnostics of flowable electrode systems: resolving spatial and temporal limitations.* Phys Chem Chem Phys, 2014. **16**(34): p. 18241-52.
30. Park, M., et al., *A review of conduction phenomena in Li-ion batteries.* J. Power Sources, 2010. **195**(24): p. 7904-7929.
31. Dees, D., et al., *Electrochemical Modeling of Lithium-Ion Positive Electrodes during Hybrid Pulse Power Characterization Tests.* Journal of The Electrochemical Society, 2008. **155**(8): p. A603-A613.
32. Gallagher, K.G., P.A. Nelson, and D.W. Dees, *Simplified calculation of the area specific impedance for battery design.* Journal of Power Sources, 2011. **196**(4): p. 2289-2297.
33. Xu, K., *Electrolytes and Interphases in Li-Ion Batteries and Beyond.* Chem. Rev. (Washington, DC, U. S.), 2014(114): p. 11503-11618.

34. Madec, L., et al., *Electronic vs Ionic Limitations to Electrochemical Performance in Li4Ti5O12-Based Organic Suspensions for Lithium-Redox Flow Batteries.* Journal of the Electrochemical Society, 2014. **161**(5): p. A693-A699.
35. Chen, J., et al., *Performance of through-hole anodic aluminum oxide membrane as a separator for lithium-ion battery.* Journal of Membrane Science, 2014. **461**: p. 22-27.
36. Scott, I.D., et al., *Ultrathin Coatings on Nano-LiCoO2 for Li-Ion Vehicular Applications.* Nano Lett., 2011. **11**(2): p. 414-418.
37. Lin, M.C., et al., *An ultrafast rechargeable aluminium-ion battery.* Nature, 2015. **520**(7547): p. 325-8.

Chapter VI. Electrochemical Characterization of Lithium-Ion Battery Cathode Materials with Aqueous Flowing Dispersions

6.1 Overview

This chapter describes the demonstration of using Dispersed Particle Resistance technique to characterize $LiFePO_4$ cathode active material in aqueous suspensions as a continued study of Chapter V. A few improvements are made in this report: 1) a new custom cell design to increase the consistency and convenience; 2) the use of aqueous electrolyte to avoid the need of an isolated environment; 3) the demonstration of a new class of materials, lithium-ion cathode active materials; 4) more material samples (six materials as opposed to three in the previous chapter) to increase the trend reliability; 5) even higher throughput (10 minutes as opposed to 30 minutes).

Elements of this chapter have been written and prepared for publication titled "Electrochemical Characterization of Lithium-Ion Battery Cathode Materials with Aqueous Flowing Dispersions".

Respective author contribution

Hongxu Dong: optical emission spectroscopy (ICP) analysis.

6.2. Abstract

There are numerous ways to produce battery active materials and the electrochemical performance varies significantly across different synthesis methods and even different batches under the same method. Traditional ways to characterize these active materials need electrode fabrication, cell assembly and cycling. Although valuable, these procedures are time and effort consuming and the performance can be influenced by auxiliary parts of the cell instead of showing just the active material properties. In this report, an active material characterization method referred to as “Dispersed Particle Resistance” (DPR) is demonstrated to characterize lithium-ion cathode active materials by dispersing them into aqueous electrolyte and flowing the active materials through an electrochemical reaction cell. This DPR method takes much less effort, material and time to conduct the measurements. The total time needed is under 10 minutes as opposed to a few weeks with conventional methods. $LiFePO_4$ is chosen as a model material to demonstrate this technique.

6.3. Introduction

Lithium iron phosphate ($LiFePO_4$, LFP) is considered as a promising lithium-ion cathode active material due to its high capacity, cycling stability, and abundancy of raw materials used in its production.[1-4] However, the conductivity of LFP is low relative to other cathode material candidates; therefore, extensive research has been done to improve the high power performance of LFP by controlling the particle morphology, coating with conductive carbon, and doping with other elements.[1, 5-14] Although notable improvements have been achieved, the LFP performance varies significantly across different methods and between different batches from the same method.[1, 5-16] In addition, LFP material researchers synthesize significant numbers of variations of LFP materials during optimization through modification of synthesis parameters. These materials all need to be characterized to understand the electrochemical performance. In addition to characterization and testing of LFP materials during research and development, LFP producers need to test the LFP final products before shipping to electrode and cell manufacturers due to product variability. The conventional method to test electrode materials involves electrode fabrication, cell assembly, and battery cycling.[5, 17-19] Although valuable for materials comparison and/or validation, electrochemical cell testing requires extensive effort, materials, and time. In addition, battery cycling performance results can be ambiguous because the measured performance reflects not only the LFP material's properties but also the material properties of the other cell components, multiple material interfaces, the electrode microstructure, and heterogeneity of materials throughout the electrodes and cell. For example, the properties and distribution of carbon and binder additives impact the electrochemical performance

directly; and even the pressure applied to the electrode can influence the resulting cell resistance.[20] These variations are very challenging to control and to independently characterize and identify.

We previously reported a characterization method we refer to as "Dispersed Particle Resistance" (DPR) and applied the technique to characterize $Li_4Ti_5O_{12}$ (LTO) anode materials.[21] DPR was obtained through using a series of chronopotentiometry or chronoamperometry tests on active material suspensions. This series of tests resulted in a number of currents measured for successively varied potentials or potentials measured for successively varied currents, and in either case the slope from a linear fit of the potential-current relationship from these battery active material dispersions resulted in a resistance – the DPR of the suspension. This resistance was measured during the collision and electrochemical reactions of battery active material particles with an electrode, and the primary contribution to the resistance resulted from the particles themselves. The previous study demonstrated a correlation between DPR and the rate capability of the LTO active materials in identically prepared coin cells. The DPR method was demonstrated to be a relatively fast (<10 minutes), and could be operated in succession for different material batches or different particle loadings; however, the technique was still a batch-wise process which hindered continuous operation and high throughput.[21] Another challenge with the initial demonstration of the technique was the use of organic lithium-ion battery electrolyte as the dispersion fluid, resulting in the need to isolate the entire system from ambient conditions and requiring flammable and relatively expensive

electrolytes. The use of lithium metal as the counter electrode also contributed to additional safety concerns.[22, 23]

Herein, this chapter discribes a DPR characterization method applied to lithium-ion cathode materials in aqueous electrolyte with continuous operation. LFP was chosen as the first active material to demonstrate this analysis because 1) LFP has a flat charge/discharge plateau which improves accurate measurement of stable and consistent signals for DPR calculation, and 2) the electrochemical potential of LFP intercalation/deintercalation allows the use of aqueous carrier fluid for the suspension.[21, 24-26] A new custom electrochemical flow cell was designed for continuous characterization analysis. LFP was suspended in aqueous electrolyte, providing operation convenience and improved safety. Six different LFP materials were characterized using this DPR technique in a flow-through cell to provide confidence in the new method for the characterization of electrode materials and the correlation between rate capability and DPR with the new electrolyte and cell design. The ability of the DPR technique to detect aging effects of the LFP exposed to aqueous electrolyte will also be demonstrated.

6.4. Experimental

6.4.1. Material Synthesis and Characterization

Six different LFP materials were characterized, which we refer to as LFP-1, -2, -3, -4, -5, and -6. These materials were purchased from different suppliers and used as received. Scanning electron microscope (SEM) images were taken for all LFP materials with a Quanta 650 SEM to characterize the morphologies of the powders. A Panalytical X'pert diffractometer with Cu Kα radiation was used to obtain the X-ray diffraction (XRD) patterns of the materials. Tap densities were measured with a tap density analyzer (Quantachrome Instruments). Thermogravimetric analysis (TGA) of the LFP samples in air was conducted with a TA Instruments Q50. BET surface area of the LFP materials was determined with a surface area and pore size analyzer (NOVA 2200e). The Fe concentration of the electrolyte was measured using inductively coupled plasma optical emission spectroscopy (ICP) analysis (PerkinElmer Optima 8000). The typical concentration range for ICP analysis was 0.1 to 100 ppm for the element Fe. The original electrolyte was carefully filtered and diluted from the LFP suspensions. The Fe concentration reported was the average of three separate measurements. The standard deviation of all ICP measurements was less than 1% of the average value.

6.4.2. Coin Cell Fabrication and Electrochemical Characterization

All LFP materials were characterized electrochemically first using conventionally fabricated coin cells. Electrochemical characterizations were carried out using CR2032-type coin cells with LFP electrode as the working electrode and lithium foil as the counter and reference electrode, separated by a polypropylene / polyethylene /

polypropylene trilayer membrane. LFP electrodes were prepared by first mixing 60 wt% LFP powder with 20 wt% carbon black and 20 wt% polyvinylidene difluoride (PVDF) binder, which was dissolved in *N*-methylpyrrolidone (NMP, Sigma-Aldrich®). The mixtures were then pasted on aluminum foil using a doctor blade with a gap thickness of 125 μm. Electrodes were dried in an oven at 70 °C overnight and further dried in a vacuum oven at 70 °C for an additional three hours while applying vacuum. Electrode disks of 1.6 cm^2 were prepared using a punch, and the loading of LFP active material in the electrodes for all samples was ~4 mg. The electrolyte for the coin cell measurement was 1.2 M lithium hexafluorophosphate ($LiPF_6$) in ethylene carbonate (EC) and ethyl methyl carbonate (EMC) with EC/EMC = 3:7 by volume ratio (BASF Corporation). The cells were assembled in an argon-filled glove box (with concentrations of both O_2 and H_2O < 1 ppm) at room temperature. The galvanostatic charge-discharge tests of coin cells were performed with a Maccor battery cycler. Where C rates are reported, they were based on the actual measured capacities of the LFP materials at low rates (measured capacities varied between 145 and 160 mAh g^{-1}_{LFP}), and the current rates were scaled by the actual amount of active material loaded into each electrode. The cycling voltage window for LFP cells was 2.5 to 4.0 V (vs. Li/Li^+).

6.4.3. Active Material Suspensions Electrochemical Evaluation

LFP suspensions were prepared by dispersing LFP powders into the electrolyte agitated by a magnetic stir bar at 500 rpm for 5 minutes before measurement. Different loadings of LFP suspensions (0.2 vol%, 0.4 vol%, 0.7 vol%, 1 vol%, 1.5 vol%, 2 vol%, 3 vol%, and 4 vol%) were also prepared to characterize the effect of loading on the measured

resistance. A customized cell was designed and assembled to electrochemically characterize the suspensions (Figure 1). As shown in Figure 1, channels for both cathode and anode were carved using a scalpel (Fisher Scientific) and separated by a porous polypropylene membrane (25 μm thick, Celgard®). Both channel dimensions were 10 × 0.5 × 0.2 cm^3. The cathode current collector was a gold wire (0.25 mm diameter and 30 cm length, Fisher Scientific). The anode was a platinum wire (0.5 mm diameter and 8 cm long, Sigma Aldrich). the reference electrode was a Ag/AgCl electrode (Pine Instruments). Flow of the suspensions was provided by a MasterFlex peristatic pump (Cole-Parmer) at a rate of 82 mL min^{-1}. All electrochemical tests, including chronoamperometry test and electrochemical impedance spectroscopy (EIS), on this customized device were performed with a Biologic SP-150.

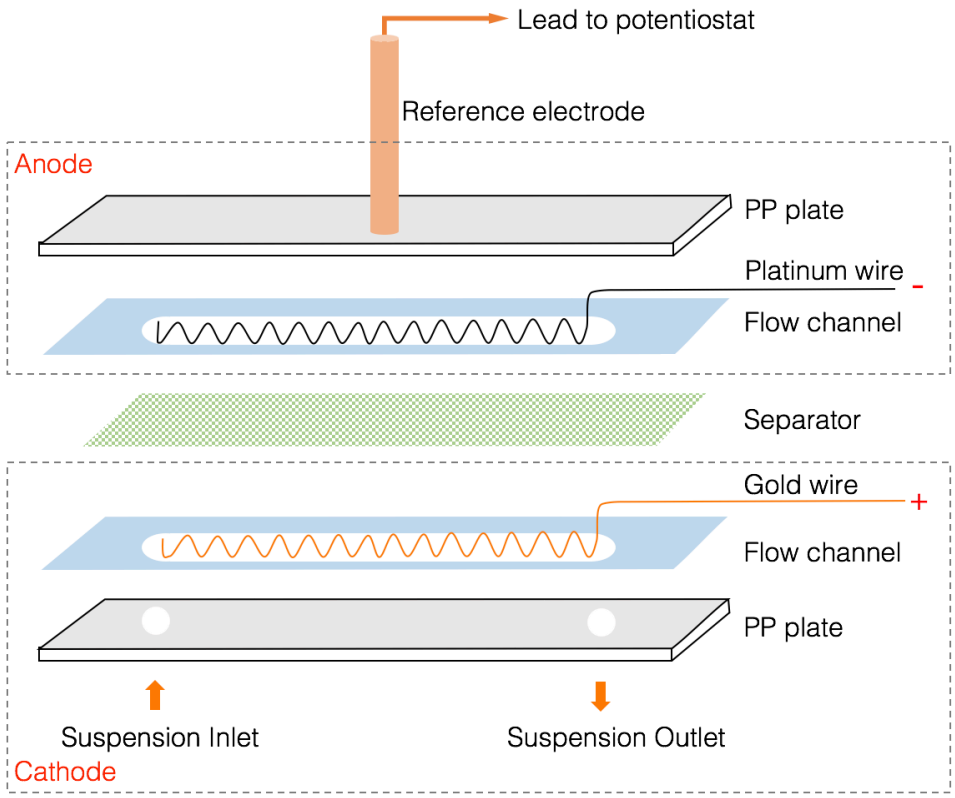

Figure 1. Cartoon illustration of the customized electrochemical cell with gold wire as the working electrode in the channel, platinum wire as the counter electrode, and Ag/AgCl reference electrode.

6.5. Results and Discussion

6.5.1. Electrochemical Testing on Conventional Coin Cells

The LFP materials were characterized using XRD, SEM, TGA, BET, and tap density first to confirm their material properties (material characterization for the LFP materials can be found in the Appendix E in Figures E1, E2, and E3 and in Table E1). Then conventional coin cells were fabricated and cycled to understand the electrochemical performance. The voltage profiles for the LFP materials at increasing rates of discharge (from 0.1C to 10C, all charge cycles were at 0.1C) are shown in Figure 2. All LFPs had a flat charge plateau at ~3.45 V, which was consistent with other reports on LFP materials.[1, 5-16, 26] LFP-1-LFP-5 had discharge similar capacities at low cycling rates that ranged from 145 – 160 mAh g^{-1}_{LFP}. These values are slightly lower than the theoretical capacity of LFP (170 mAh g^{-1}_{LFP}), but within a similar range of other reports on LFP materials.[1, 5-16, 26] LFP-6 showed a significantly lower capacity even at low rate of 0.1C. This was attributed to the high Li_3PO_4 and $LiFe_5O_8$ impurity content, which was identified the XRD pattern of this material (Figure E1 in Supplementary Materials). Discharge voltages and capacities for all six LFP materials decreased with increasing rate. This is typical and consistent with the literature due to increasing overpotential at increasing discharge current.[8-11, 14, 16, 19, 26-29] However, the percentage of the capacity retention (i.e., rate capability) varied for different materials. As shown in Figure 3, LFP-1 showed the highest rate capability performance and LFP-6 the lowest. The capacity retention (in terms of the percentage of the discharge capacity relative to the capacity at 0.1C) at increasing rates, or rate capability, generally followed the order of LFP-1 > LFP-2 > LFP-3 > LFP-4 > LFP-5 > LFP-6. These electrochemical

measurements established the benchmark order of rate capability among the six LFP materials which were within identically processed composite electrodes.

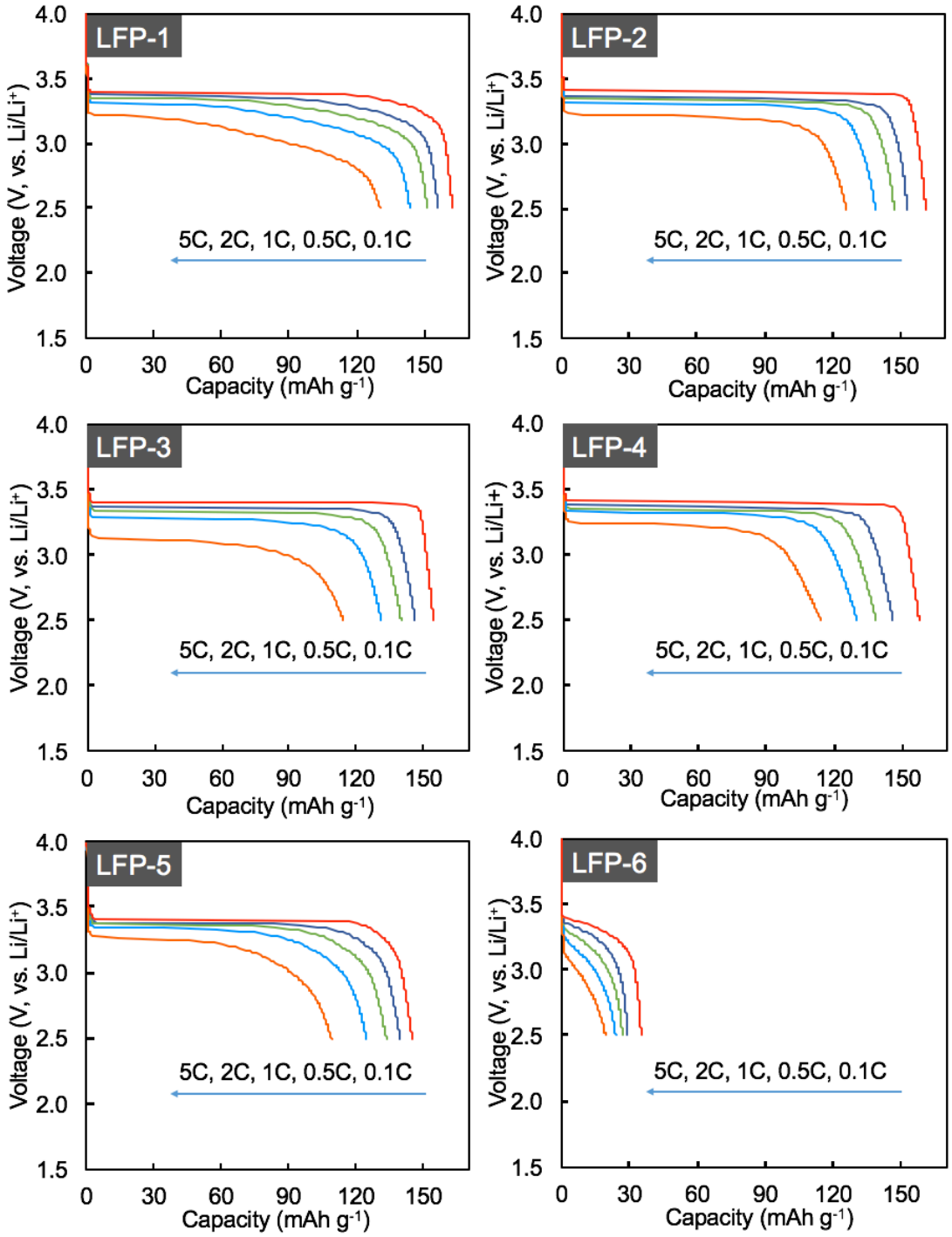

Figure 2. Voltage profiles during constant current discharges at increasing C-rates for all

six LFP materials. For all plots, the curves correspond to 0.1C (red), 0.5C (dark blue), 1C (dark green), 2C (light blue), 5C (orange), and 10C (light green). C rates were based on the gravimetric capacity of the material at 0.1C.

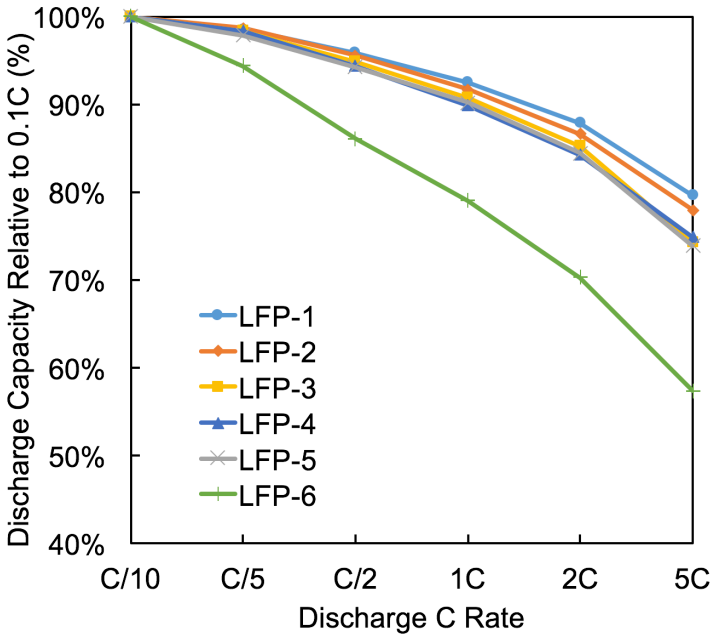

Figure 3. Discharge capacities of all six LFP materials (light blue circle: LFP-1; orange diamond: LFP-2; yellow square: LFP-3; dark blue triangle: LFP-4; gray "x": LFP-5; green "+": LFP-6) at different C-rates relative to the capacity at 0.1C (lines added to guide the eye).

6.5.2. LFP Suspension DPR Characterization

DPRs for LFP materials were measured using the following procedure. After dispersing a LFP powder in aqueous electrolyte, the suspension was electrochemically evaluated in a customized cell (shown in Figure 1). A series of chronoamperometry tests at sequentially increasing potentials were performed for each suspension. The potential and the average

stabilized current for each step were retained. A plot of the potential vs. current resulted in a straight line for all electrochemical tests, and the slope of a linear fit of each data set was the DPR corresponding to a given material at a given loading (vol% LFP in the electrolyte). An example of the linear potential vs. current data used to determine DPR, using 2 vol% LFP-3, is shown in Figure 4. A new increased current plateau resulted for each step increase of potential in Figure 4a. The average value of the current increased linearly with the increase in the applied potential. Figure 4b shows the resulting data extracted from the experiment in Figure 4a, with the applied potential vs. the average charging current after a plateau in the current was reached for that potential. For the example linear fit linear fit applied in Figure 4b, the slope was 400.7 Ω (the DPR value) and $R^2 = 0.998$, indicating a good linear fit. The measured DPR was the sum of all of the contributions to the electrode overpotential and was thus a combination of several resistances, including the resistance of the active material particles colliding on the current collector, ohmic resistance of the external electrical connections, and the ohmic resistance from the electrolyte. The combination of the latter two resistances were consistently measured to be ~3 Ω, as determined by the high frequency intercept of EIS measurements. The range of DPR values measured was between 38 and 1202 Ω, indicating that the resistance arising from the LFP particles undergoing electrochemical oxidation was the primary contributor to the measured DPR and not that the ohmic losses were small and were straightforward to independently measure. We note that our initial report of the DPR technique had much more significant ohmic contributions ranging from 125 - 140 Ω.[21] The reduction of this DPR resistance contribution in this report was attributed to: 1) the significantly higher ionic conductivity of the aqueous electrolyte

relative to the organic electrolyte (~100 compared to ~15 mS/cm);[30] 2) the change from an aluminum electrode in organic lithium-ion battery electrolyte to a gold electrode in aqueous electrolyte because the aluminum has both a lower conductivity and undergoes passivation reactions with the organic electrolyte that form a passivation layer that likely increases the measured resistance.[31-34] As discussed in a previous report, every contribution to DPR would be difficult to assess independently, but the dominant contribution is expected to be from the lesser of the ionic or electronic resistance from of the ensemble of active material particles colliding on the current collector and undergoing electrochemical reactions at any given time.[21]

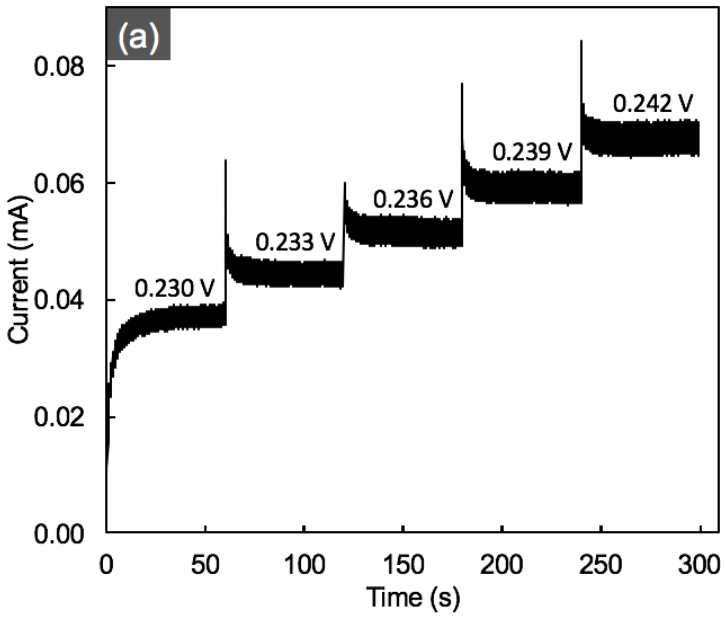

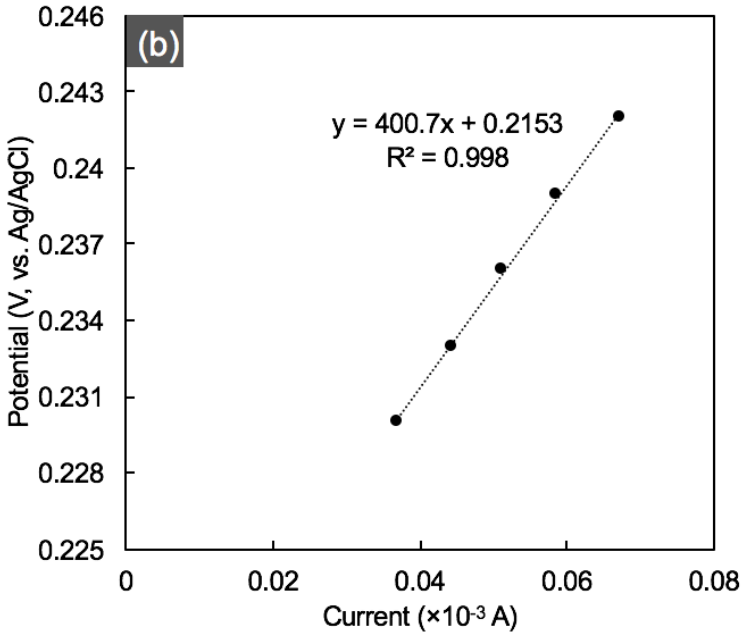

Figure 4. Example DPR measurement for 2 vol% LFP-3 dispersed in aqueous electrolyte. (a) Chronoamperometry tests from 0.230 V to 0.242 V (vs. Ag/AgCl reference electrode) and (b) the extracted potential vs. current pairs data set from (a). The dashed line is a linear fit, with the slope, intercept, and R^2 for the fit provided in the plot area.

DPR values of a material can be influenced by a few key factors besides the intrinsic electrochemical properties of the active material, including the electrochemical cell design (cell size, wire length and geometry), suspension flow rate, and active material loading. The same cell was used for each series of measurements to exclude any cell variability. Flow rate was also kept constant for all measurements. The effect of active material loading was probed in greater detail. LFP suspensions with different volumetric loadings were characterized in succession in a high throughput manner through the electrochemical flow cell (as an example LFP-1 is shown in Figure 5a). The DPR values decreased as LFP loadings increased for all LFP materials, and rate of decrease of DPR

with increasing loading decreased as the loading increased. Both observations were consistent with the proposed collision-dependent electrochemical reactions of dispersed particles.[4, 21, 24, 25] As active material loading increased, more particles were in contact with the current collector electrode on average at any given time and hence were participating in electrochemical reactions and measured oxidation currents. The particles in contact with the electrode can each be considered as resistors that are all connected in parallel. At higher volume fractions of LFP, there were more particles on the electrode surface, resulting in more resistors in parallel and hence decreased the total resistance due to the particles which decreased the measured DPR. Not only was the decrease in DPR with increased loading consistent with more resistors/particles in parallel, but the proportional relationship between LFP loading and resistance also supports this analysis. The resistance of from a single particle in contact with the current collector was R_i. Thus, the collective resistance of N particle resistors in parallel (R_N) can be calculated with Equation 1. If we assume the random sampling of the ensemble of R_i particles from a given sample powder to be relatively consistent, an average resistance for a particle from each LFP sample can be defined as R_0. This assumption should be reasonable because the number of particles was large even at low loadings and for a large batch of LFP sample there was not any particle sorting or separation to bias any particular dispersion. Using the assumption of a representative average single resistance for each LFP sample, R_N would be R_0/N. Thus, the resistance due to the active materials, which dominates DPR measurements, would be expected to be inversely related with the number of active material particles in contact with the current collector and hence inversely related with the volumetric active material loading – at least at relatively low loadings of active

material where the current collector surface was readily accessible. The inverse relationship between volumetric active material loading and DPR was supported by a least squares fit of the DPR measurements as collected at increasing loadings shown in Figure 5a. DPR was inversely related with the LFP loading and the R^2 value of 0.992 indicates that the inverse relationship gives a good fit of the collected data. The inverse relationship between DPR and volumetric particle loading provided further evidence that DPR measured the collective resistance of the active material particles. Volumetric loading of 2 vol% LFP was chosen for further comparison between LFP materials because 1) the change in resistance above 2 vol% was relatively small, 2) higher loadings required more material in contrary to the desire of devoting less material to the DPR analytical technique, and 3) at very low loadings of LFP in some cases the variation in the measured resistance was relatively high, likely because at lower loadings the DPR measurement became a more stochastic technique which resulted in more significant swings in the distribution of particles on the current collector relative to the mean distribution.

$$R_N = \frac{1}{\sum_{i=1}^{N} \frac{1}{R_i}} \qquad (1)$$

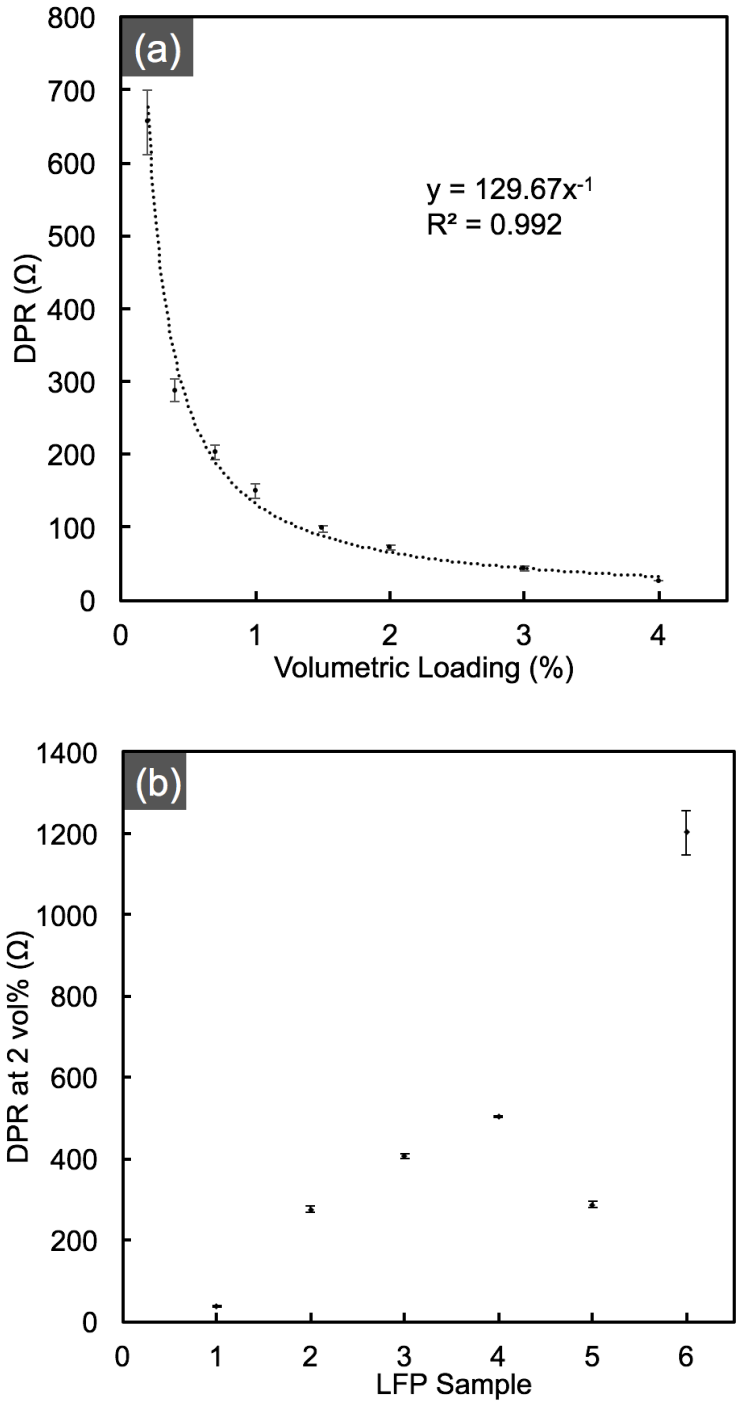

Figure 5. (a) DPR of LFP-1 at different volumetric loadings from 0.2 vol% to 4 vol%. Dashed line represents a power fit, with the resulting equation and R^2 value displayed in the plot area. shown as a dashed line; (b) DPR of all six LFP materials measured at 2

vol% LFP loading. The red bars represent the standard deviations of three measurements for each sample.

Lower DPR for a given material indicates a slower increase of overpotential at increasing current, and thus for appropriate materials processed into equivalent electrodes and battery cells, a material with a lower DPR would in general be expected to correlate to a higher voltage and better capacity retention at increasing currents.[7, 21] Thus, for a given set of materials those with lower DPR values would be expected to have higher rates. DPRs for all six LFP materials at 2 vol% were measured and the results are shown in Figure 5b. Recall that the materials were numbered in order of decreasing rate capability where LFP-1 had the highest rate capability and LFP-6 had the lowest rate capability in identically processed and assembled coin cells. With the exception of LFP-5, the DPR showed an increasing trend from LFP-1 to LFP-6, with LFP-1 having the lowest DPR and LFP-6 having the highest DPR. This DPR trend was generally consistent with expectations based on the relative rate capability order of these LFP materials, where the material with the lowest DPR had the highest rate capability and the material with the highest DPR had the lowest rate capability. The standard deviations were also very small relative to the measured DPR values, indicating good data consistency. LFP-5 was the outlier in the DPR analysis with regards to the correlation to relative rate capability. We speculate that this deviation was due to the significantly higher carbon loading of 3.3 wt% (from TGA measurements, TGA results for all LFP materials can be found in Figure E3 in Appendix E), compared to 0-2 wt% for the other LFP materials. This large amount of carbon additive likely decreased the DPR due to the formation of a

conductive network within the suspension that effectively increased the number of particles in contact with the current collector via the carbon network and reduced the overall resistance.[35, 36] Future research in our lab will aim to validate this carbon network influence hypothesis. The additional carbon, however, was not as effective in improving the rate capability in coin cell measurements because an additional 20 wt% carbon was added to each LFP electrode. The relatively high 20 wt% carbon was originally chosen to minimize the contact and matrix resistance in the electrode such that the electrochemical performance of the electrode was primarily limited by the resistance from the LFP active materials. To further demonstrate the impact of the high carbon in the LFP-5 material, coin cells were fabricated without any added carbon (composite electrode contained only active material and binder) and these electrodes were cycled in coin cells (for cycling profiles see Figure E4 in Appendix E). LFP-5 had better electrochemical performance than both LFP-3 and LFP-4 with regards to capacity at 0.1C. The results above demonstrate that DPR can provide relative rate capabilities for materials with similar physical properties. Materials with different properties such as composition can be easily differentiated while combining other techniques such as TGA.

6.5.3. DPR Sensitivity to LFP Aged in Electrolyte

As an example to demonstrate the sensitivity of the DPR technique, DPR measurements were made on the same LFP material both pristine and after aging in the electrolyte. LFP has previously been reported to have reduced electrochemical performance after being aged in water or aqueous electrolyte.[13, 37-40] After aging, measured impacts to LFP

include increased electrode polarization, decreased capacity, dissolution of chemical species, and in some cases a change in the crystalline phases observed in the material. [13, 37-40] These performance decays can even occur during storage in humid environments, thus the storage history of LFP materials can be very important.[41] The changes for LFP in contact with water; however, in many cases proceed slowly and detecting these changes in some cases can be challenging without fabricating electrodes with the LFP material and performing electrochemical evaluation. As mentioned in Section 1, this procedure is very time consuming although accurate. DPR could be a potential candidate for fast characterization of this electrochemical performance decay.

As an initial demonstration of the concept of detecting LFP aging using DPR, LFP-3 was mixed with 1 M Li_2SO_4 electrolyte and aged for 15 days. After aging, the LFP was rinsed, dried, and then fabricated into electrodes used in conventional coin cells via identical procedures to those used for all other LFP materials used in this study. A representative example of LFP-3 coin cell discharge capacity at different cycling rates for LFP-3 before and after aging in electrolyte for 15 days is shown in Figure 6. ICP measurements on the electrolyte confirmed that ~0.2% of the Fe present in the LFP had dissolved after 15 days. While the discharge capacity at low discharge rates only dropped ~1% after aging in electrolyte, the high rate capacity retention dropped significantly. The aged LFP-3 was only able to achieve ~80% of the capacity of unaged LFP-3 at 10C. This performance change was consistent with other reports on aged LFP materials in aqueous electrolyte or water. [13, 37-40] DPR tests were conducted for both unaged and aged LFPs. The aged LFP had a 30% increase of DPR from the unaged material (from 467.8 Ω

to 626.1Ω). This 10-minute DPR measurement detected a significant change in the aged material, indicating that DPR has sensitivity to aging effects in LFP that can dramatically impact rate capability. We note that the aged LFP did not have any significant changes in the XRD pattern relative to the pristine material (see Appendix E, Figure E1) and that the DPR analysis required a timescale three orders of magnitude less than the coin cell validation of the aging impact on rate capability.

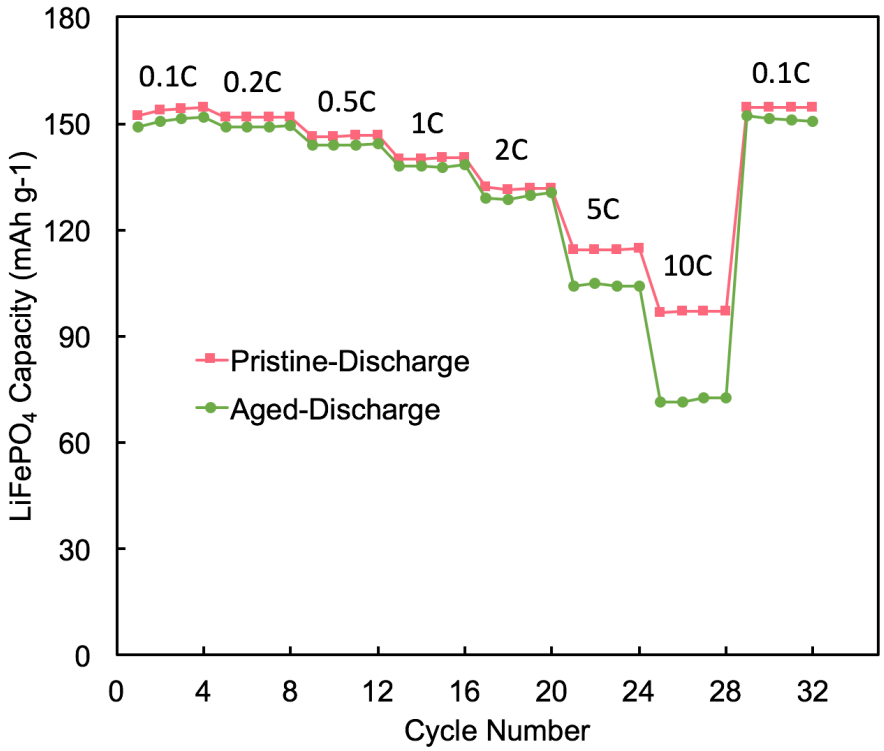

Figure 6. Representative coin cell discharge capacity at different rates (0.1C to 10C) for pristine LFP-3 (red squares) and LFP-3 aged in 1 M Li_2SO_4 electrolyte for 15 days (green circles). Lines are added between data points to guide the eye.

6.6. Conclusions

LFP cathode materials were characterized electrochemically via a measured resistance during oxidation of the particles in flowing aqueous dispersions. This resistance, referred to as DPR, generally was an indicator of rate capability for coin cells fabricated using the active materials. The only outlier in the analysis was a LFP sample with much higher carbon loading, further demonstrating the sensitivity of DPR conductivity and the need for other techniques to complement the analysis of the particles. DPR measurements on suspensions of systematically increasing volume fractions of LFP particles demonstrated an inverse relationship between DPR and particle concentrations. This inverse relationship was consistent with previous measurements done on coin cells with increasing active material loading within composite electrodes, indicating that the particle loading relationship to resistance in the dispersions was analogous to each additional particle in contact with the electrode represented an additional resistor connected in parallel. The sensitivity of DPR technique was additionally used to identify changes in LFP electrochemical performance during aging in aqueous electrolyte. DPR provides a fast and sensitive approach to detect relative differences in electrochemical performance for LFP active materials, and this analysis technique should be extendable to other battery electrode materials.

6.7. References

1. Vu, A. and A. Stein, *Lithium iron phosphate spheres as cathode materials for high power lithium ion batteries.* J. Power Sources, 2014. **245**: p. 48-58.
2. Axsen, J., K.S. Kurani, and A. Burke, *Are batteries ready for plug-in hybrid buyers?* Transport Policy, 2010. **17**(3): p. 173-182.
3. Zhang, W.J., *Structure and performance of LiFePO4 cathode materials: A review.* Journal of Power Sources, 2011. **196**(6): p. 2962-2970.
4. Qi, Z. and G.M. Koenig, *Review Article: Flow battery systems with solid electroactive materials.* Journal of Vacuum Science & Technology B, Nanotechnology and Microelectronics: Materials, Processing, Measurement, and Phenomena, 2017. **35**(4): p. 040801.
5. Liang, B., Y. Liu, and Y. Xu, *Silicon-based materials as high capacity anodes for next generation lithium ion batteries.* J. Power Sources, 2014. **267**: p. 469-490.
6. Li, Y., et al., *Effects of Particle Size, Electronic Connectivity, and Incoherent Nanoscale Domains on the Sequence of Lithiation in LiFePO4 Porous Electrodes.* Adv. Mater. (Weinheim, Ger.), 2015. **27**(42): p. 6591-7.
7. Gaberscek, M., R. Dominko, and J. Jamnik, *Is small particle size more important than carbon coating? An example study on LiFePO4 cathodes.* Electrochem. Commun., 2007. **9**(12): p. 2778-2783.
8. Miao, C., et al., *A novel synthesis and characterization of LiFePO4 and LiFePO4/C as a cathode material for lithium-ion battery.* J. Power Sources, 2014. **246**: p. 232-238.
9. Yu, F., et al., *Optimized electrochemical performance of three-dimensional porous LiFePO4/C microspheres via microwave irradiation assisted synthesis.* Journal of Power Sources, 2014. **271**: p. 223-230.
10. Chen, Z., et al., *Polyacene coated carbon/LiFePO4 cathode for Li ion batteries: Understanding the stabilized double coating structure and enhanced lithium ion diffusion kinetics.* Electrochimica Acta, 2013. **109**: p. 262-268.
11. Wang, S., et al., *A simple and inexpensive synthesis route for LiFePO4/C nanoparticles by co-precipitation.* J. Power Sources, 2013. **233**: p. 43-46.
12. Wang, J., et al., *Size-dependent surface phase change of lithium iron phosphate during carbon coating.* Nat Commun, 2014. **5**: p. 3415.
13. Zhong, K., et al., *Study on the stability of the LiFePO4 Li-ion battery via an electrochemical method.* Journal of Power Sources, 2014. **250**: p. 296-305.
14. Lva, Y.-J., et al., *Synthesis of bowl-like mesoporous LiFePO4/C composites as cathode materials for lithium ion batteries.* Electrochim. Acta, 2014. **119**: p. 155-163.
15. Yamada, A., S.C. Chung, and K. Hinokuma, *Optimized LiFePO4 for lithium battery cathodes.* J. Electrochem. Soc., 2001. **148**(3): p. A224-A229.
16. Lou, X.M. and Y.X. Zhang, *Synthesis of LiFePO4/C cathode materials with both high-rate capability and high tap density for lithium-ion batteries.* Journal of Materials Chemistry, 2011. **21**(12): p. 4156-4160.
17. Wang, W., et al., *A nanoparticle Mg-doped Li4Ti5O12 for high rate lithium-ion batteries.* Electrochimica Acta, 2013. **114**: p. 198-204.

18. Liu, J., et al., *Self-supported Li4Ti5O12-C nanotube arrays as high-rate and long-life anode materials for flexible Li-ion batteries.* Nano Lett, 2014. **14**(5): p. 2597-603.
19. Qi, Z. and G.M.K. Jr., *High-Performance LiCoO2 Sub-Micrometer Materials from Scalable Microparticle Template Processing.* ChemistrySelect, 2016. **1**(13): p. 3992-3999.
20. Atebamba, J.-M., et al., *On the Interpretation of Measured Impedance Spectra of Insertion Cathodes for Lithium-Ion Batteries.* Journal of The Electrochemical Society, 2010. **157**(11): p. A1218.
21. Qi, Z. and G.M.K. Jr., *Electrochemical Evaluation of Suspensions of Lithium-Ion Battery Active Materials as an Indicator of Rate Capability.* Journal of The Electrochemical Society, 2017. **164**(2): p. A151-A155.
22. Ji, X.L., et al., *Spatially heterogeneous carbon-fiber papers as surface dendrite-free current collectors for lithium deposition.* Nano Today, 2012. **7**(1): p. 10-20.
23. Zhamu, A., et al., *Reviving rechargeable lithium metal batteries: enabling next-generation high-energy and high-power cells.* Energy & Environmental Science, 2012. **5**(2): p. 5701-5707.
24. Qi, Z. and G.M. Koenig, *A carbon-free lithium-ion solid dispersion redox couple with low viscosity for redox flow batteries.* J. Power Sources, 2016. **323**: p. 97-106.
25. Qi, Z., A.L. Liu, and G.M.K. Jr., *Carbon-free Solid Dispersion LiCoO2 Redox Couple Characterization and Electrochemical Evaluation for All Solid Dispersion Redox Flow Batteries.* Electrochimica Acta, 2017. **228**: p. 91-99.
26. Liu, T., et al., *Carbon-coated single-crystalline LiFePO4 nanocomposites for high-power Li-ion batteries: the impact of minimization of the precursor particle size.* RSC Adv., 2014. **4**: p. 9.
27. Eftekhari, A., *LiFePO4/C nanocomposites for lithium-ion batteries.* Journal of Power Sources, 2017. **343**: p. 395-411.
28. Kim, J.-K., et al., *Effect of carbon coating methods on structural characteristics and electrochemical properties of carbon-coated lithiumiron phosphate.* Solid State Ionics, 2014. **262**: p. 25-29.
29. Srinivasan, V. and J. Newman, *Design and optimization of a natural graphite/iron phosphate lithium-ion cell.* Journal of the Electrochemical Society, 2004. **151**(10): p. A1530-A1538.
30. Ruffo, R., et al., *Electrochemical characterization of LiCoO2 as rechargeable electrode in aqueous LiNO3 electrolyte.* Solid State Ionics, 2011. **192**(1): p. 289-292.
31. Zhang, S.S. and T.R. Jow, *Aluminum corrosion in electrolyte of Li-ion battery.* 2002.
32. Honda, C., et al., *Evaluation of Contact Resistance of Aluminum Current Collector Surfaces for Energy Storage Systems.* Electrochemistry, 2014. **82**(5): p. 328-330.
33. Zhang, X. and T.M. Devine, *Identity of Passive Film Formed on Aluminum in Li-Ion Battery Electrolytes with LiPF[sub 6].* Journal of The Electrochemical Society, 2006. **153**(9): p. B344-B351.

34. Markovsky, B., et al., *On the Electrochemical Behavior of Aluminum Electrodes in Nonaqueous Electrolyte Solutions of Lithium Salts*. Journal of The Electrochemical Society, 2010. **157**(4): p. A423-A429.
35. Li, Z., et al., *Aqueous semi-solid flow cell: demonstration and analysis.* Physical Chemistry Chemical Physics, 2013. **15**(38): p. 15833-15839.
36. Duduta, M., et al., *Semi-Solid Lithium Rechargeable Flow Battery.* Adv. Energy Mater., 2011. **1**(4): p. 511-516.
37. Liu, P., et al., *Aging Mechanisms of LiFePO[sub 4] Batteries Deduced by Electrochemical and Structural Analyses.* Journal of The Electrochemical Society, 2010. **157**(4): p. A499.
38. Yin, Y., et al., *Electrochemical Performance and Capacity Fading Mechanism of LiFePO4 at Different pH Aqueous Electrolyte Solutions.* Chinese Journal of Chemical Physics, 2015. **28**(3): p. 315-322.
39. Koltypin, M., et al., *On the Stability of LiFePO4 Olivine Cathodes under Various Conditions (Electrolyte Solutions, Temperatures).* Electrochemical and Solid-State Letters, 2007. **10**(2): p. A40.
40. Porcher, W., et al., *Stability of LiFePO4 in water and consequence on the Li battery behaviour.* Ionics, 2008. **14**(6): p. 583-587.
41. Iltchev, N., et al., *LiFePO4 storage at room and elevated temperatures.* Journal of Power Sources, 2003. **119-121**: p. 749-754.

Chapter VII. Conclusions and Recommendations

7.1. Overview

This chapter briefly summarizes the key findings of this dissertation as concluding remarks. Prospects on future work is also suggested.

7.2. Summary and Conclusions

Lithium-ion active material suspensions were demonstrated as the energy carrier for redox flow batteries for the first time and their operating principles were explored. Efforts to understand the performance limitations of dispersed particle flow batteries led to a new technique to determine the relative resistance of lithium-ion active material particles to electrochemical charge and discharge without the fabrication of electrodes and battery cells. A few key findings are summarized below:

(a) This work contains the first report of reversible electrochemical charge and discharge of carbon-free lithium-ion active material suspensions. The redox reaction in these suspensions was dependent on the collisions of active material with current collectors within the carrier fluid, which is a new operating principle for flow batteries. This reversible collision dependent and rheologically coupled system was demonstrated for both anode and cathode lithium-ion materials including $Li_4Ti_5O_{12}$, $LiCoO_2$, and $LiFePO_4$. Due to the use of solid intercalation active materials, the theoretical energy density of flow batteries based on lithium-ion solid dispersions is very high, although the power density is still too low for practical applications.

(b) A new technique was developed, referred to as “Dispersed Particle Resistance”, to characterize the resistance of electroactive particles in suspensions to charge and discharge. This technique was demonstrated for both anode and cathode materials and in both organic and aqueous electrolyte suspensions. Under a specific particle loading, this resistance was also found to be inversely correlated with the active material rate capability in conventional coin cells. This technique provides a fast experimental method to probe relative differences in the tolerance of materials to high rates of charge and discharge without electrode and cell fabrication steps and without concern over the influence of other battery components and electrode microstructure impacts to electrochemical performance.

7.3. Recommendations for Future Work

Recommendations to further understand and improve the systems that were the subject of this thesis are briefly discussed below.

(a) The operation of flow batteries based on lithium-ion active material suspensions at significant deviations of state of charge has not been investigated due to the charge/discharge current limitation. There are significant differences of electrochemical properties at different states of charge in conventional composite electrode lithium-ion batteries as reported in the literature. For example, the conductivity of $Li_4Ti_5O_{12}$ changes by orders of magnitude depending on the extent of lithiation. Therefore, it is valuable to investigate the electrochemical performance in this active material suspension based electrodes at different states of charge. The different states of charge can possibly

obtained by chemically lithiating or delithiating the active materials before adding to the flow cell or very long time charge/discharge experiments, which can be shortened by increasing the active material participation of the reaction with optimized 3D current collector designs.

(b) The Dispersed Particle Resistance technique showed promising performance to characterize lithium-ion active materials. But only two kinds of materials were demonstrated and the sample sizes were limited (three for $Li_4Ti_5O_{12}$ and six for $LiFePO_4$). Therefore, more kinds of materials (even beyond lithium-ion active materials) with larger sample sizes can be characterized through this technique in the future to study the adaptability and accuracy of this technique. For example, $LiMn_2O_4$ can be a material to characterize for the next step because 1) it has flat potential profiles (though there are two) like $Li_4Ti_5O_{12}$ and six for $LiFePO_4$; 2) it is a commercially emerging non-toxic lithium-ion cathode materials; 3) it would be a good test case for understanding the performance of dispersions that are less stable with regards to sedimentation because $LiMn_2O_4$ is typically desirable and available as larger particles; 4) it is valuable to investigate the influence of side reactions with the technique because the potential is near water splitting window. In addition, applying the technique to chemistries other than lithium-ion can also help understand the role of ion conductivity in the solid particles. For example, sodium-ion battery active materials can be characterized in this system and further investigate the influence of the significantly different ion conductivity between sodium ions and lithium ions.

Acknowledgements

I would like to thank my thesis advisor Professor Gary Koenig for his advice and guidance throughout the research. I want to thank my committee members Professor Geoffrey Geise, Professor Joshua Choi, Professor Robert Kelly, and Professor David Green for the valuable advice and suggestions. I also want to thank the current and past graduate students and undergraduate researchers who have worked with me in Koenig Group, Ethan Paharik, Pierce Robinson, Charles Michaelis, Spring Dong, Aaron Liu, Peter Marr, and Devanshi Gupta for their help of both valuable discussion and help on operating instruments. I give my thanks to Professor David Green for use of his lab's rheometer, Professor Geoffrey Geise for use of his lab's TGA instrument, and Ricky Buchanan for making different designs of flow cells. I also thank all faculties, staffs, and graduate students in Chemical Engineering Department and in Engineering School who have given me help, advice and support.

I want to thank all my family and friends for their continuous support, especially my parents Chunmou Qi and Mei Zhang, my wife Cuiting Yang, my little sister Jinghan Qi, and my grandparents Quanrong Zhang and Xinzhen Hu. I cannot have the work done without their encouragement and support.

This research was financially supported by the National Science Foundation through award ECCS-1405134 and by start-up funding at the University of Virginia. The LTO powder was initially provided by the U.S. Department of Energy's (DOE) CAMP (Cell Analysis, Modeling and Prototyping) Facility, Argonne National Laboratory. The CAMP

Facility is fully supported by the DOE Vehicle Technologies Program (VTP) within the core funding of the Applied Battery Research (ABR) for Transportation Program.

Appendix

Appendix A

This section of appendix provides additional information for Chapter II.

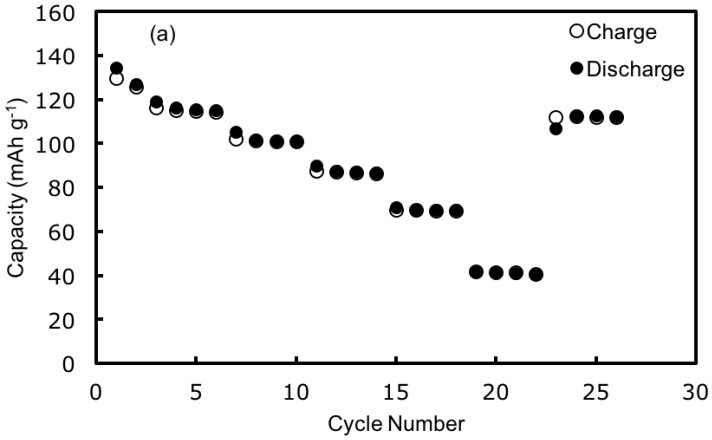

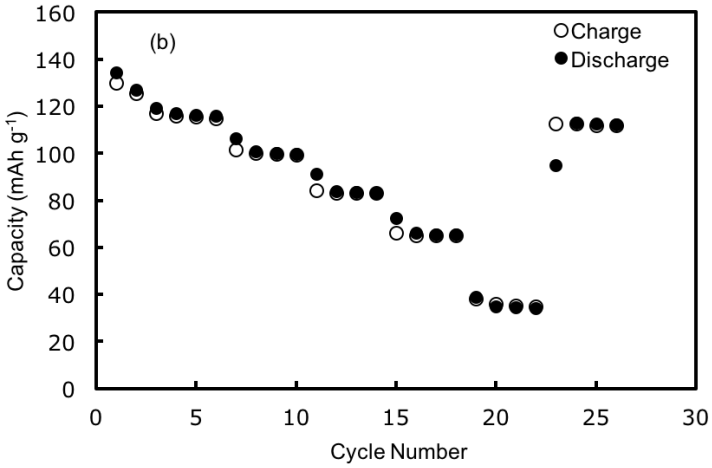

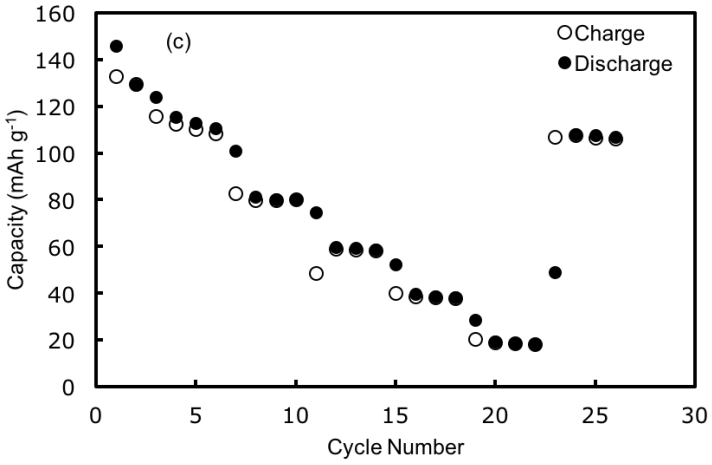

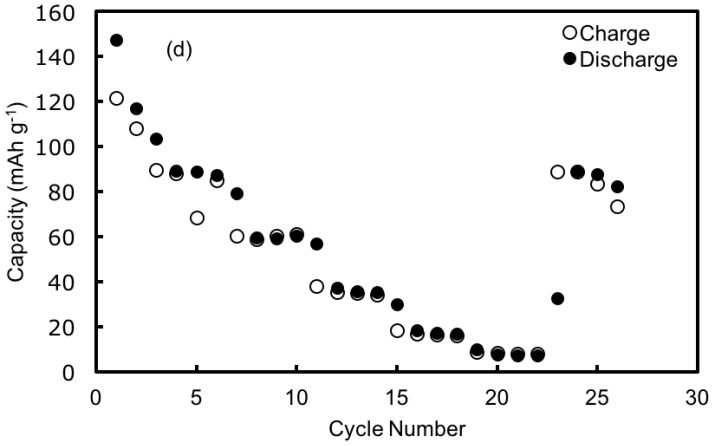

Figure A1. Cycling performance of LTO particle coin cells loaded with (a) 5.35, (b) 8.74, (c) 26.75, and (d) 40.14 mg LTO. Cycling currents relative were the same (adjusted for active material mass) for the different LTO loadings. The charge/discharge rates used were 0.1C (first 2 cycles), 0.2C (cycles 3-6), 0.5C (cycles 7-10), 1C (cycles 11-14), 2C (cycles 15-18), and 5C (cycles 19-22), and 0.2 C (cycles 23-26). 1C assumed to correspond to 174.55mA g^{-1} for calculation of C rate. For comparison, the cell with 5.35 mg at the rate of 5C showed 27.4% capacity of the initial capacity, while the 40.14 mg cell at 5C showed only 6.1% capacity of the initial capacity.

Appendix B

This section of appendix provides additional information for Chapter III.

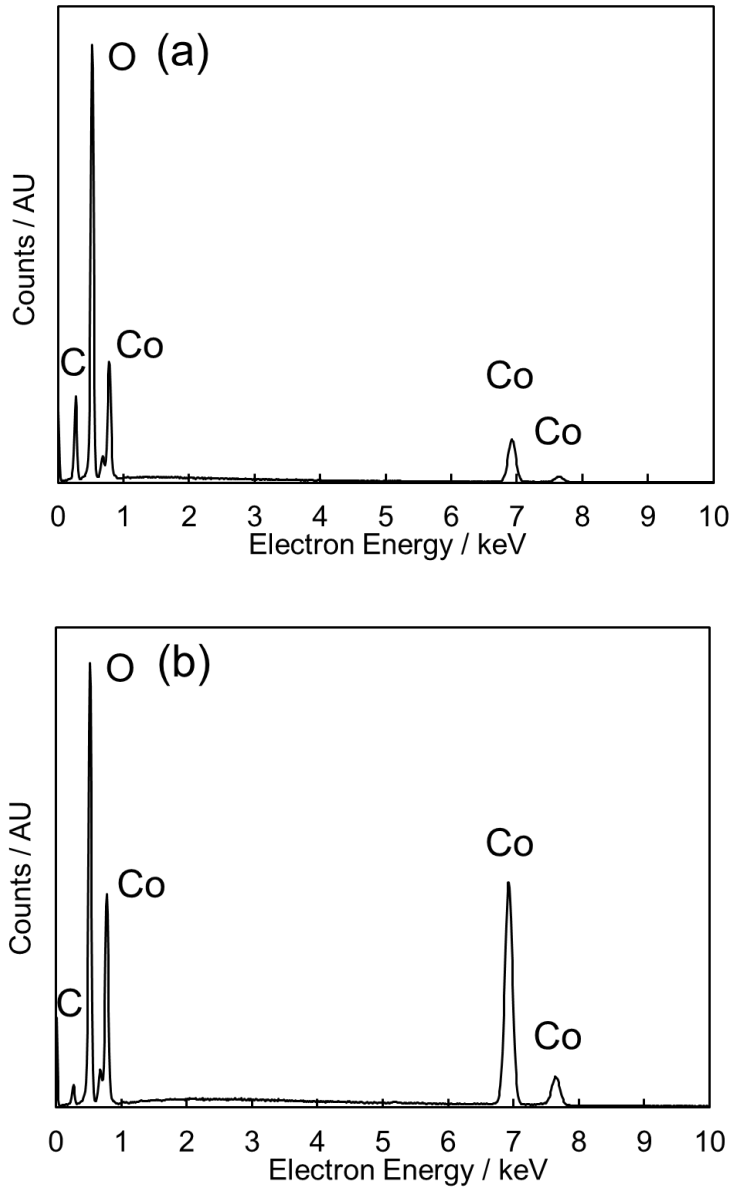

Figure B1. Energy dispersive x-ray spectroscopy (EDS) profiles for (a) $CoC_2O_4 \cdot 2H_2O$ and (b) $LiCoO_2$ powders.

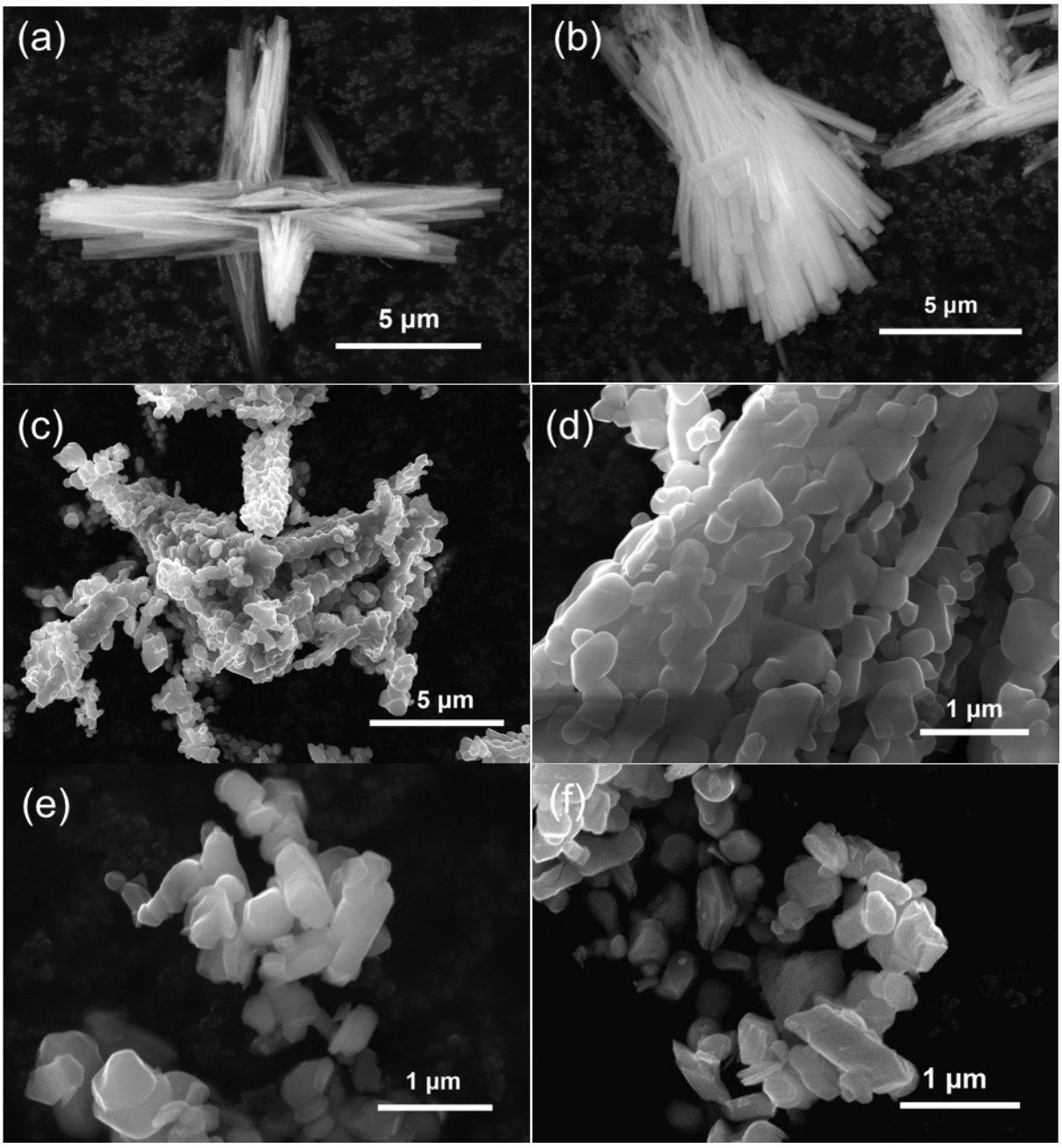

Figure B2. Scanning electron micrograph (SEM) images of (a, b) $CoC_2O_4 \cdot 2H_2O$ rods and (c, d) calcined $LiCoO_2$ materials templated from the rods in (a, b) after firing at 800 °C. (e, f) $LiCoO_2$ morphology after soft milling the material shown in (c, d).

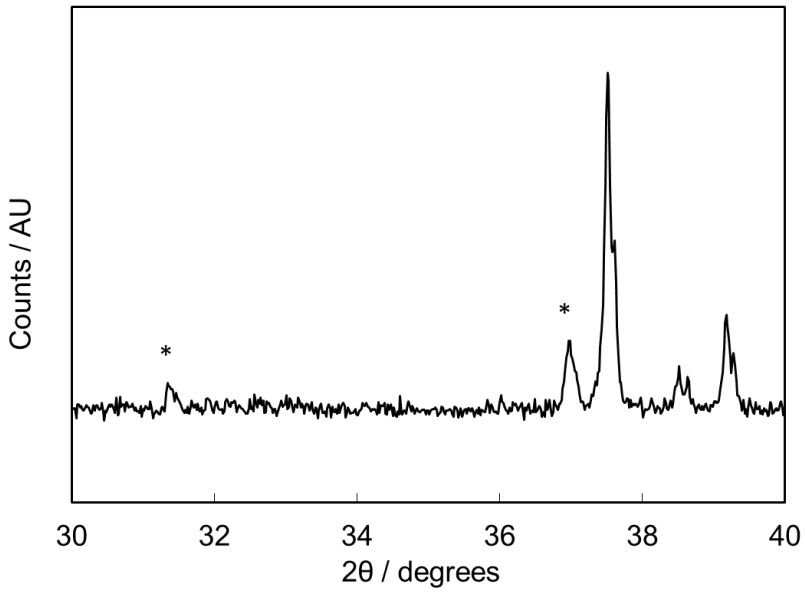

Figure B3. X-ray diffraction (XRD) pattern for $LiCoO_2$ calcined at 750 °C. Peaks attributed to the Co_3O_4 impurity phase are indicated with stars.

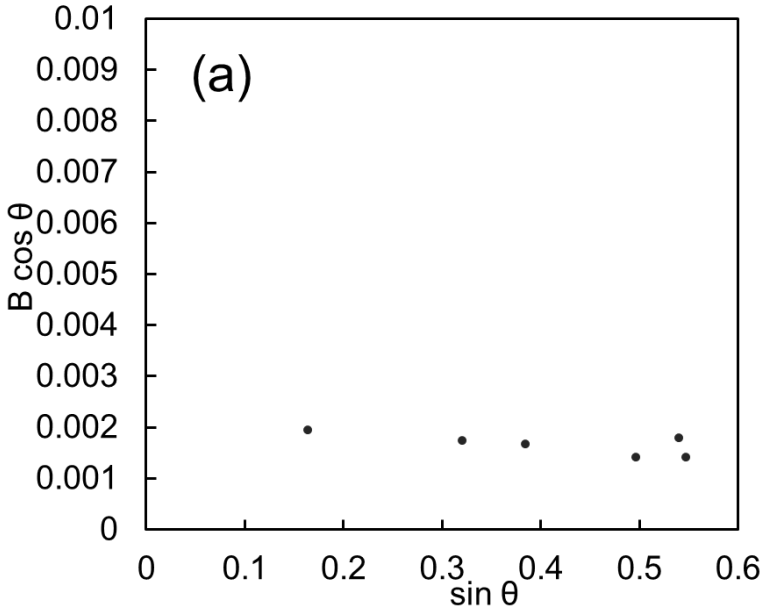

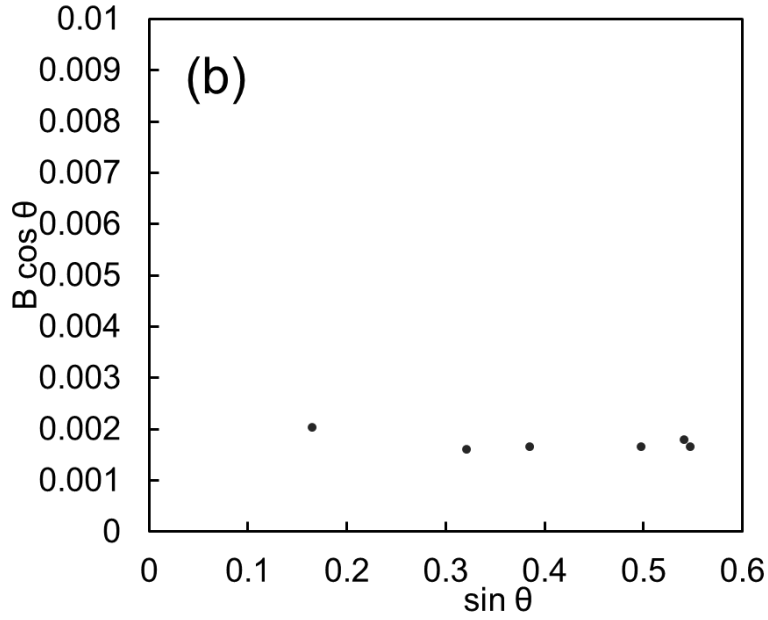

Figure B4. Williamson−Hall plot from the X-ray diffraction (XRD) patterns of (a) unmilled $LiCoO_2$ and (b) milled $LiCoO_2$ calcined at 800 °C.

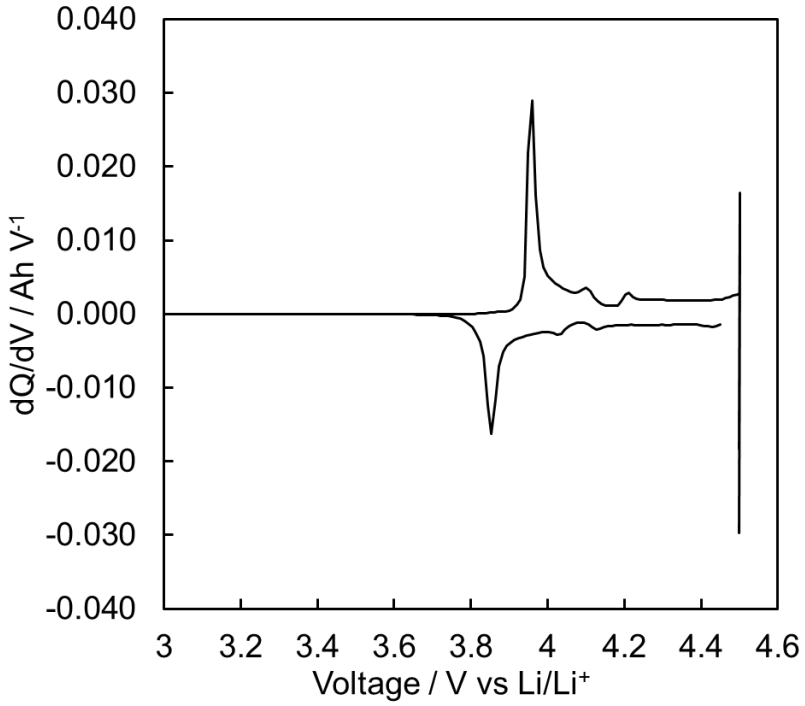

Figure B5. dQ/dV profile of a Li/ $LiCoO_2$ half-cell at a cycling rate of 0.1C.

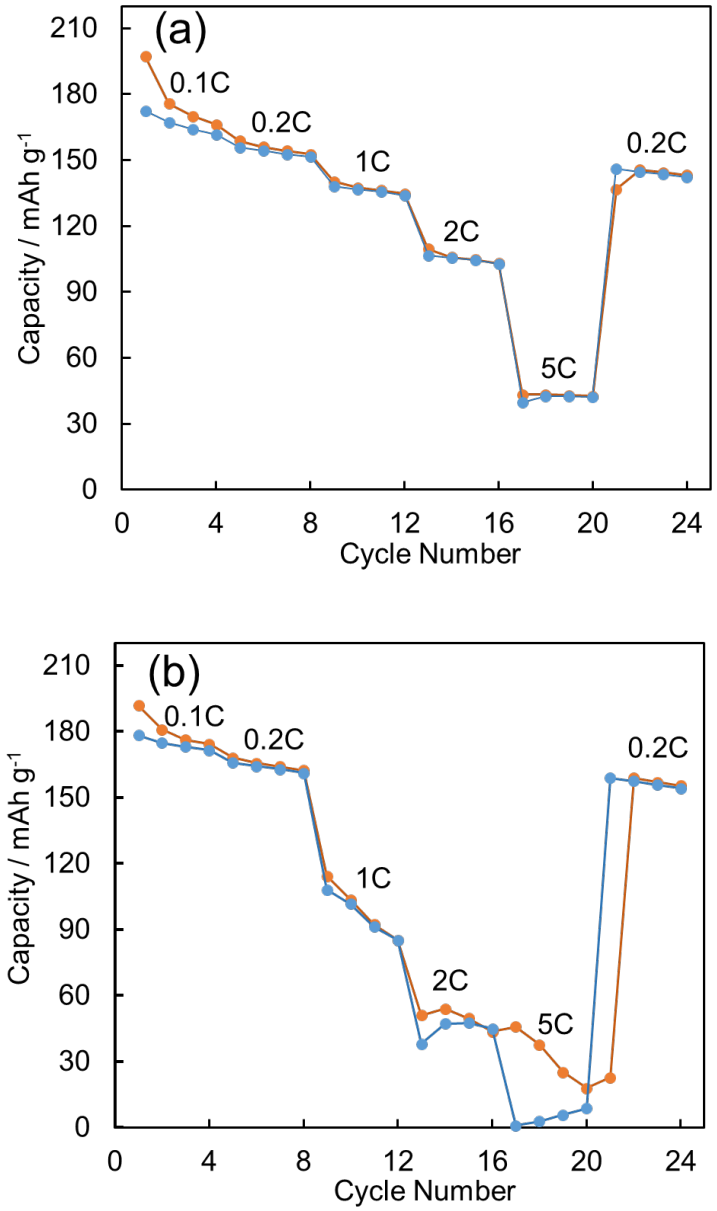

Figure B6. Charge (orange) and discharge (blue) capacity of a Li/ $LiCoO_2$ cell with $LiCoO_2$ material calcined at (a) 800°C (the sub-micrometer sized material) and (b) 900°C (the bulk $LiCoO_2$ material with similar synthesis route and particles many micrometers in size, morphology of material can be seen in Figure 3d in the text) at increasing charge/discharge rates of 0.1C, 0.2C, 1C, 2C, and 5C. Four charge/discharge cycles were conducted at each rate.

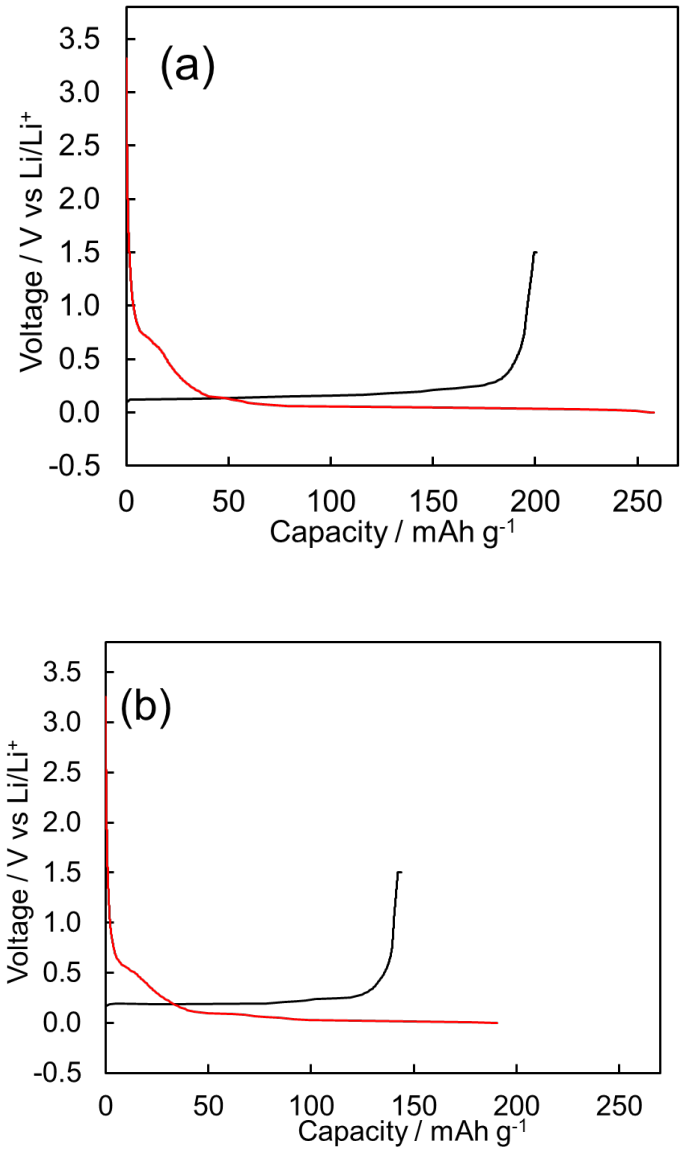

Figure B7. First discharge (red) and charge (black) curves for Li/graphite cells cycled at a rate of (a) 0.2C and (b) 1C.

Appendix C

This section of appendix provides additional information for Chapter IV.

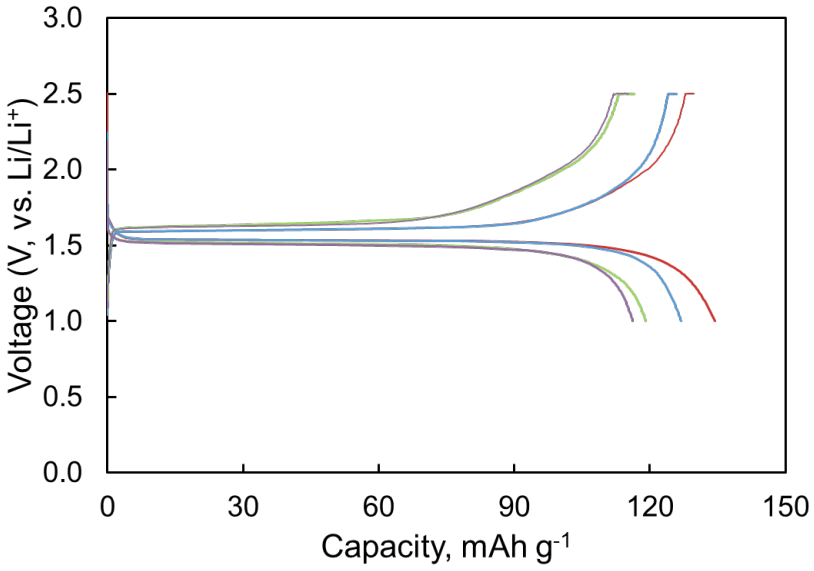

Figure C1. Charge and discharge cycles 1 (red), 2 (blue), 3 (green), and 4 (purple) of a Li/LTO particle coin cell at the rate of 0.1C (17.5 mA g^{-1}) cycled between 1.0 and 2.5 V.

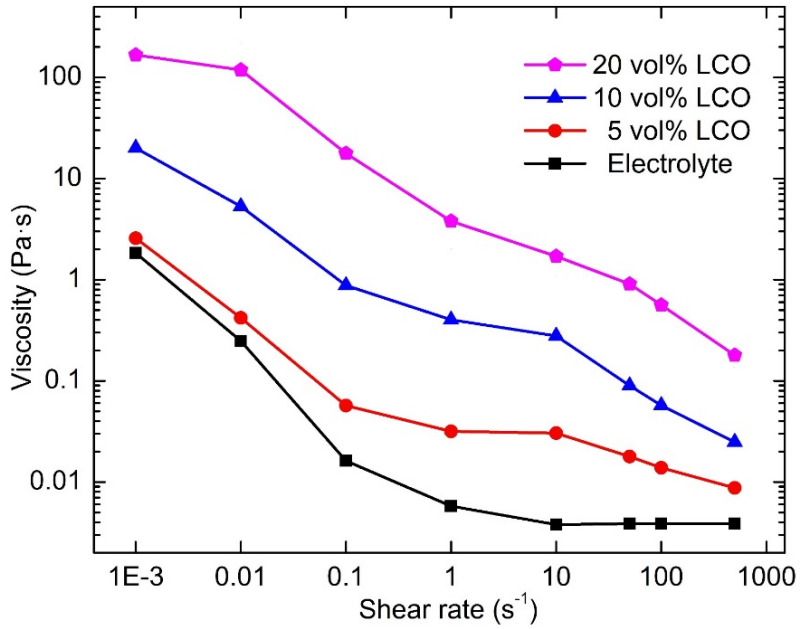

Figure C2. The viscosity for the particle-free electrolyte (1.2 M $LiPF_6$ in EC/EMC solvents) and the electrolyte laden with 5 (red circles), 10 (blue triangles), and 20 (purple pentagons) vol% LCO measured at different shear rates.

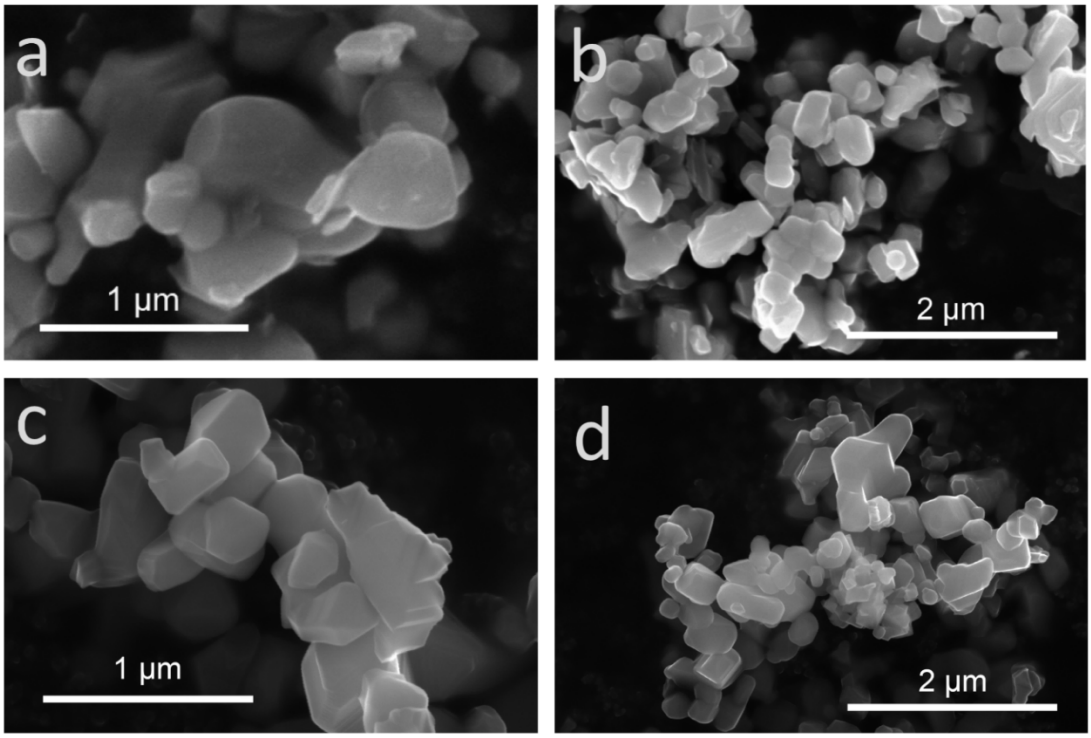

Figure C3. Representative SEM images of the LCO (a and b) and LTO (c and d) particles.

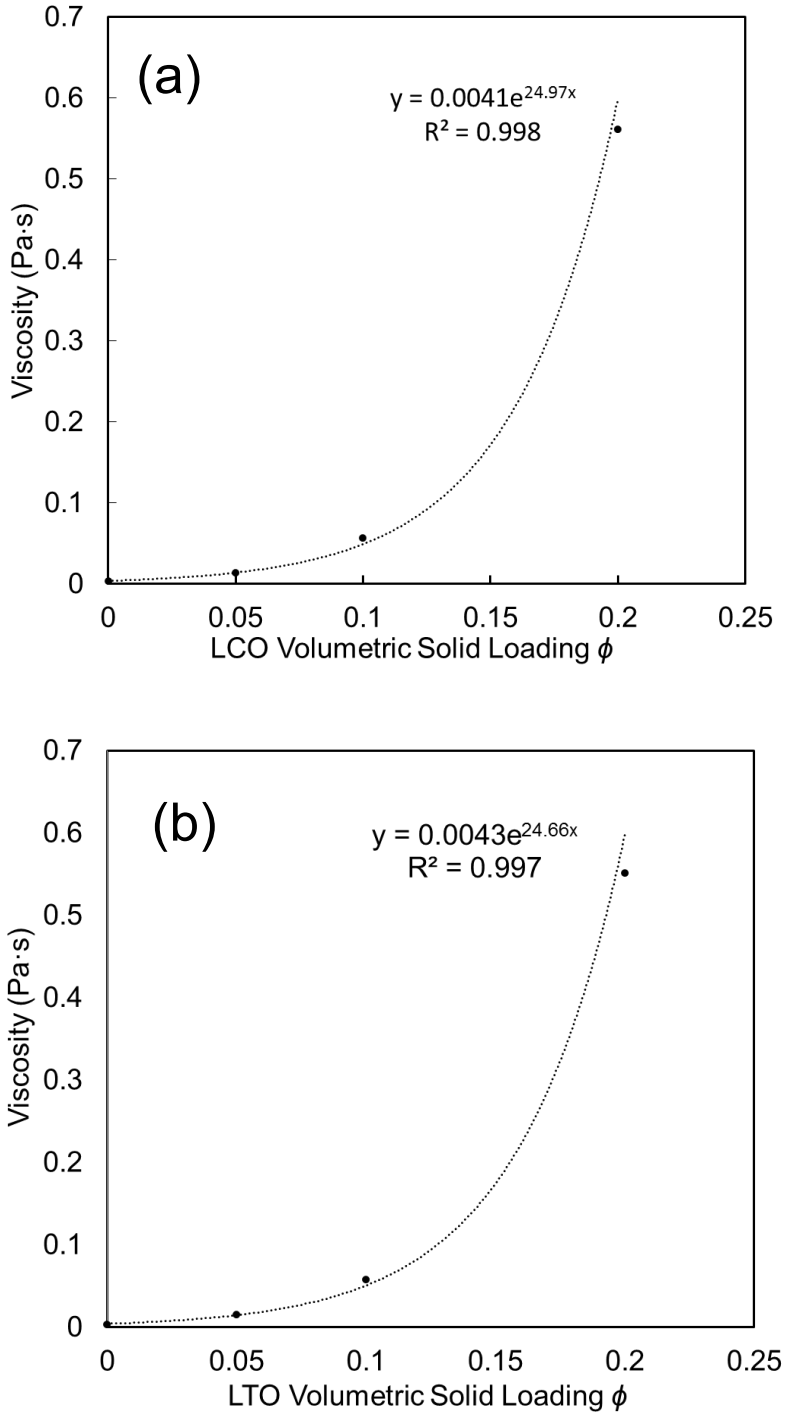

Figure C4. Viscosities of (a) LCO and (b) LTO suspensions at a shear rate of 100 s^{-1} at increasing volume fractions of solids loaded into the electrolytes. Dashed lines represent the best fit of the data to an exponential function.

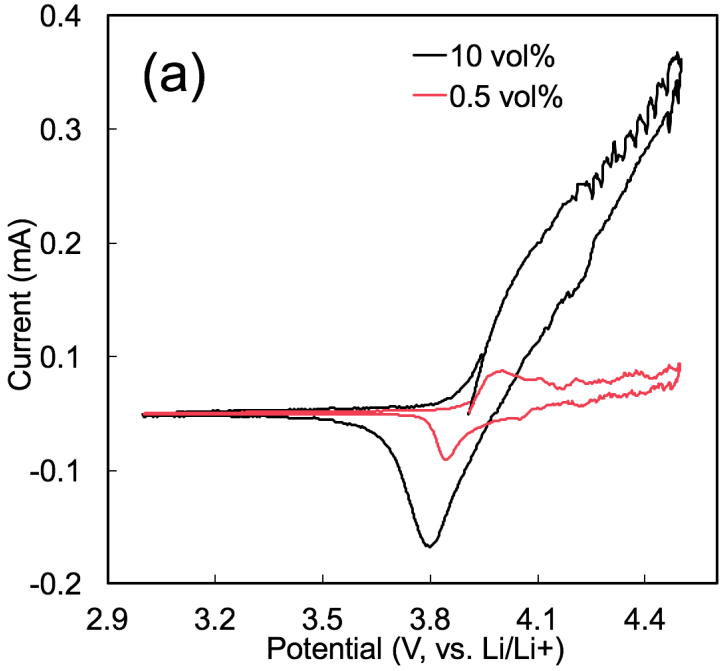
(a)
10 vol%
0.5 vol%
Current (mA)
0.4
0.3
0.2
0.1
-0.1
-0.2
2.9
3.2
3.5
3.8
4.1
4.4
Potential (V, vs. Li/Li+)

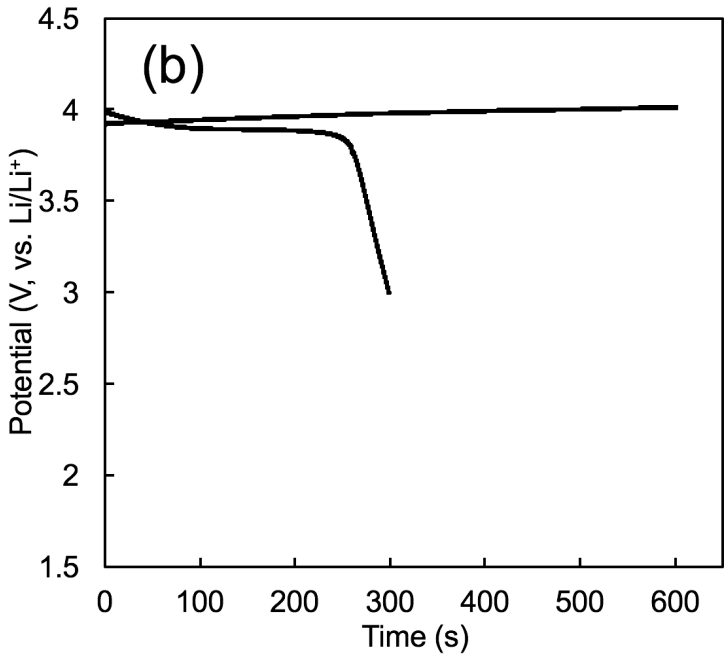
(b)
Potential (V, vs. Li/Li+)
4.5
4
3.5
3
2.5
2
1.5
0
100
200
300
400
500
600
Time (s)

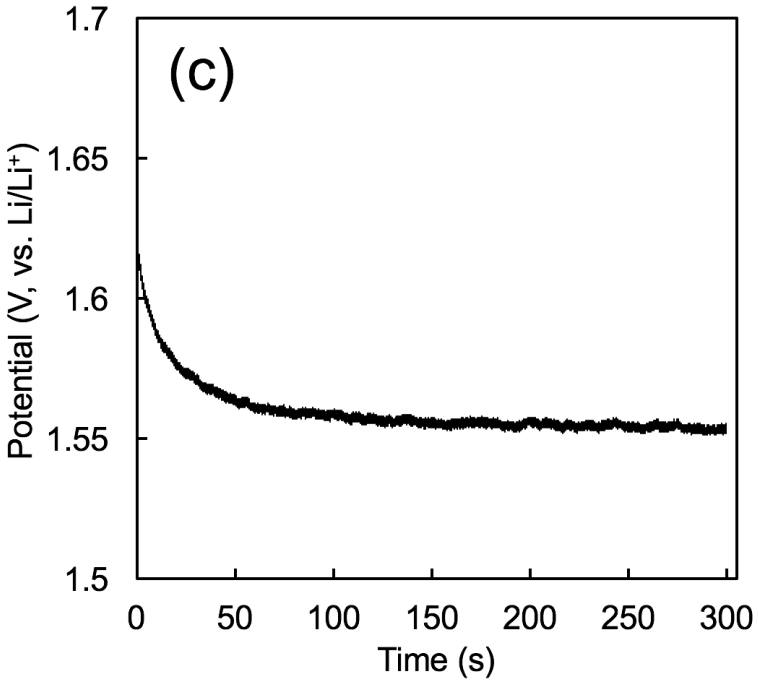

Figure C5. (a) CV scans at a rate of 5 mV/s between 3.0 and 4.5 V (vs. Li) for 0.5 vol% LCO suspension (red) and 10 vol% (black), showing similar locations for onset potential and peak reduction potential and indicating lower current response with lower LCO loading. (b) charge (10-minute cutoff time) and discharge curves at a rate of 0.01 mA for 0.5 vol% LCO suspension, showing reversible electrochemical activity at ~ 3.9 V. A lower cycling current (0.01 mA instead of 0.08 mA on the 10 vol% LCO suspension) was used because the potential reached the cutoff voltage immediately at 0.08 mA, without effectively charging the LCO material. (c) Chronopotentiometry profile for 1 vol% LTO suspension at a current of 0.02 mA, showing stable electrode potential at ~1.55 V (the same as 10 vol% LTO suspension and conventional LTO electrode).

Appendix D

This section of appendix provides additional information for Chapter V.

Material Characterization

SEM images were taken for all three LTO materials to determine the size and morphology of the particles (Figure D1). All samples are polydisperse sub-micrometer sized particles. Particle sizes were determined by measurements of the average of the longest and shortest dimension for each particle of 100 randomly selected particles using SEM images. LTO-1 had a particle size of 0.35 μm ± 0.15 μm, LTO-2 had a size of 0.64 μm ± 0.28 μm and LTO-3 has a size of 0.62 μm ± 0.24 μm.

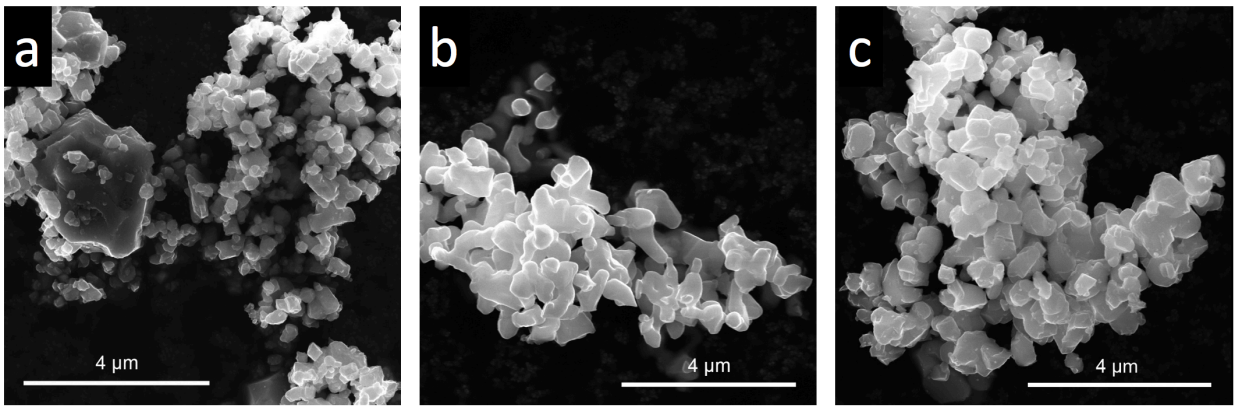

Figure D1. Representative scanning electron microscopy (SEM) images of (a) LTO-1, (b) LTO-2, and (c) LTO-3 particles.

XRD patterns for all three LTO materials were also analyzed. The patterns of the LTO samples and the reference pattern for LTO can be found in Figure D2. The patterns for all three materials contained peaks consistent with the reference pattern for *Fd-3m* LTO [1],

although LTO-1 and LTO-2 contained rutile TiO_2 impurity phases (marked with stars in Figure S2) [2]. The lattice parameters for LTO-1, 2, and 3 determined from a refinement of just the cubic *Fd-3m* phase were a = 8.3498 Å, 8.3435 Å, and 8.3241 Å, respectively. These values for the lattice parameters were consistent with other reports in the literature for LTO materials [3-5].

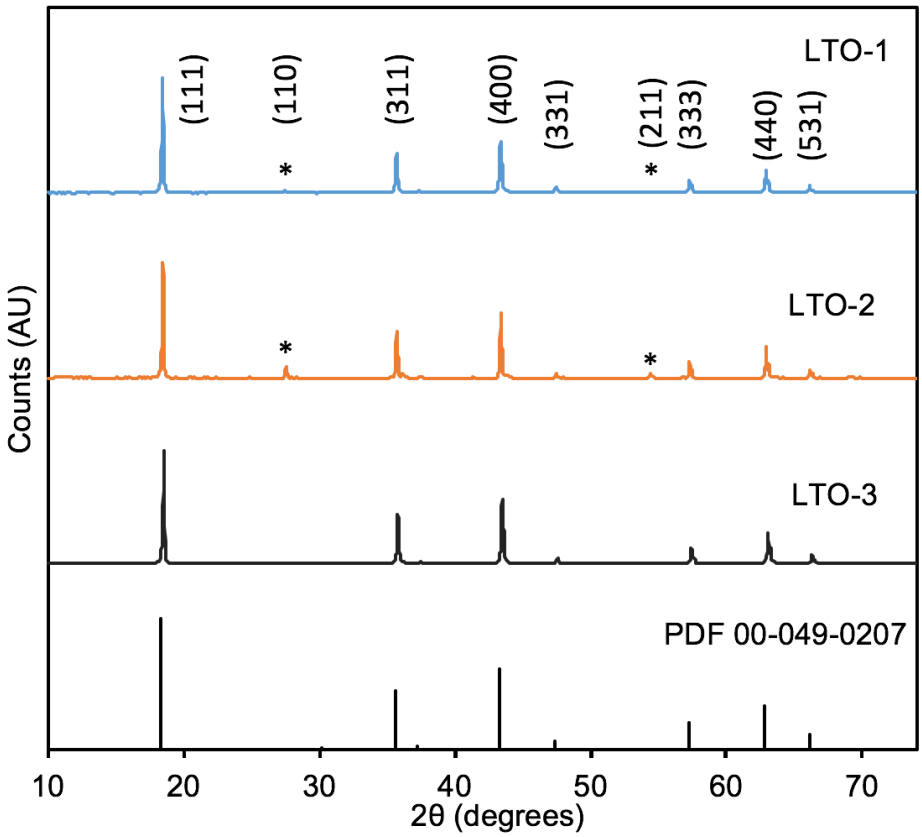

Figure D2. X-ray diffraction (XRD) patterns for LTO-1, LTO-2, LTO-3, and the LTO reference pattern.

Tap densities for all three materials were also determined to be 0.92 ± 0.01 g mL^{-1}, 1.05 ± 0.01 g mL^{-1}, 0.85 ± 0.01 g mL^{-1} for LTO-1, 2, and 3 respectively (all based on 5 separate

measurements of the powders). These tap densities are within ranges commonly reported for sub-micrometer lithium-ion battery active material powders [6-10].

Electrochemical Tests

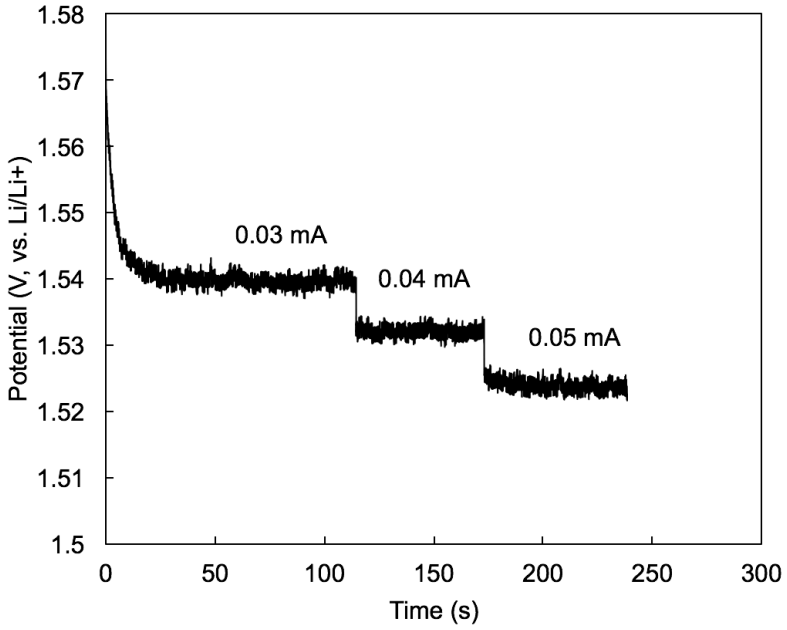

Figure D3. Chronopotentiometry (CP) profile on a 0.5 vol% LTO-1 suspension at sequential steps in the discharge currents of 0.03, 0.04, 0.05 mA.

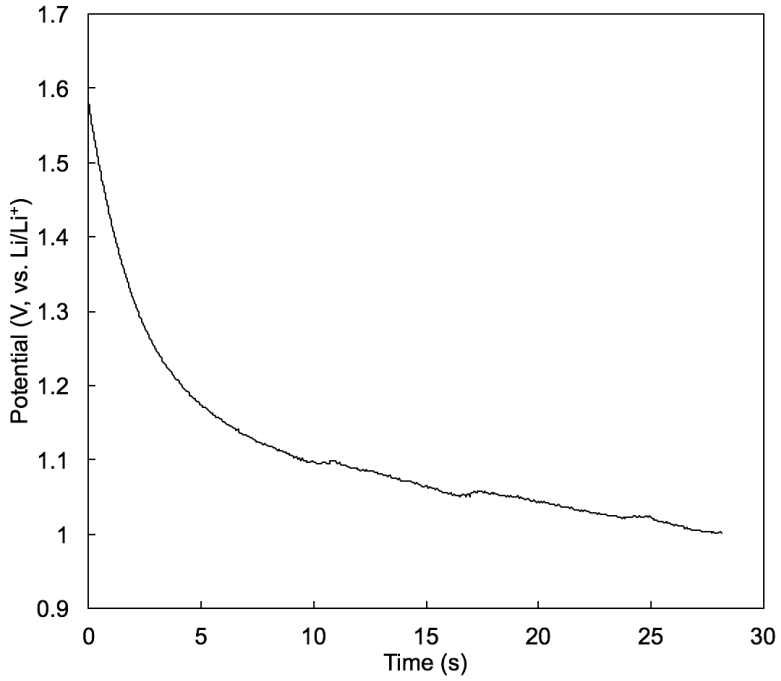

Figure D4. Chronopotentiometry (CP) profile on LTO-free electrolyte at a discharge current of 0.02 mA. The experiment was stopped upon hitting a cutoff voltage of 1.0 V.

Table D1. Standard deviations of three coin cells of each LTO material of the discharge capacity relative to 0.1C at increasing C rates for the data shown in Figure 2d.

Material \ C Rate	0.5C	1C	2C	5C	10C
LTO-1	0.09%	0.08%	0.07%	0.70%	4.23%
LTO-2	0.06%	0.10%	0.15%	0.28%	1.40%
LTO-3	0.60%	0.28%	0.15%	1.04%	0.24%

Appendix E

This section of appendix provides additional information for Chapter VI.

Material Property Characterizations

Six $LiFePO_4$ (LFP) materials from different suppliers were first characterized with XRD, SEM, and coin cell electrochemical measurements. Figure E1 shows the XRD patterns for these LFP materials. All samples matched well with the reference pattern for LFP,[1] although LFP-6 also contained significant impurity peaks attributed to Li_3PO_4 and $LiFe_5O_8$ (marked with asterisks above the peaks).[2, 3] The patterns indicated all materials predominantly had the same Orthorhombic crystal structure.

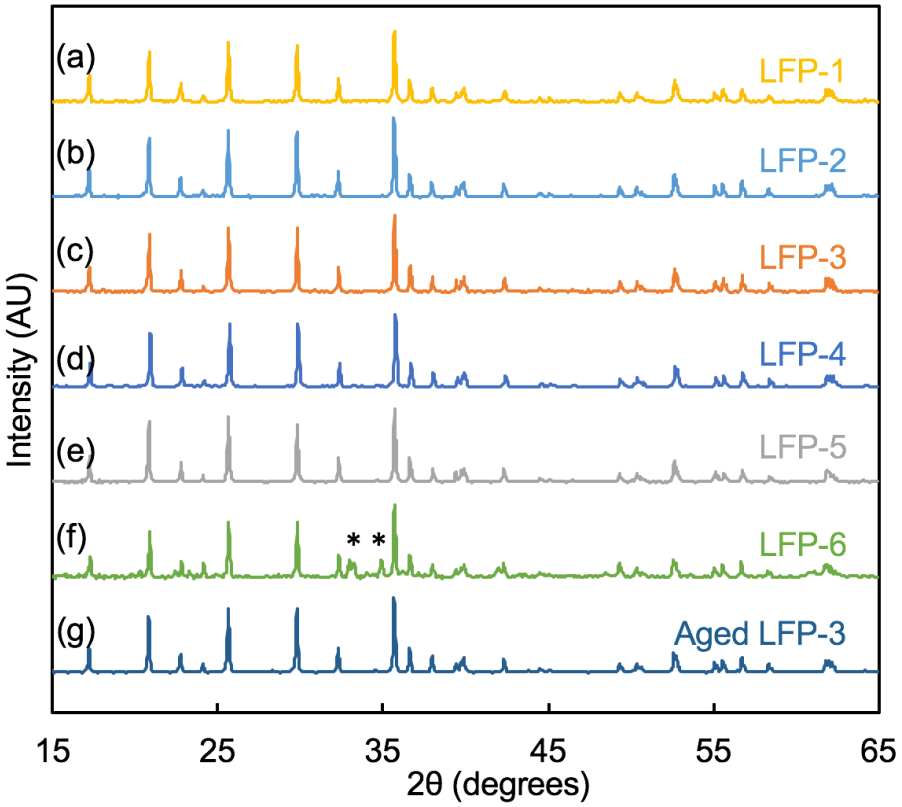

Figure E1. X-ray Diffraction (XRD) patterns for LFP-1, -2, -3, -4, -5, and -6; and LFP-3 after aging for 15 days in the aqueous carrier fluid electrolyte. Asterisks represent impurity peaks of Li_3PO_4 and $LiFe_5O_8$.

SEM images were taken for all six LFP materials for observation of material size and morphology (Figure E2). Although all LFP samples were polydisperse particles, LFP-1 through LFP-5 showed similar particle sizes whereas LFP-6 had significantly larger particles. Note that all LFP samples except LFP-1 were carbon coated as indicated in TGA results shown in Figure E3.[4-6] In one sample, LFP-3, long carbon wires were observed in the sample. Tap densities for all six LFP materials were measured and can be found in Table E1. With the exception of LFP-3 (relatively low tap density of 0.64), the

tap densities of all LFP samples were within a similar range of 1.04-1.17 g mL^{-1}. The significantly lower tap density for LFP-3 may have been due to the carbon wire particles in the sample, which reduced the ability of the LFP particles to pack efficiently. The BET surface areas for all materials were determined and can be found in Table E1. The BET surface areas vary significantly even for the materials with similar particle sizes. We suspect this variation was largely due to the variation in the porosity of the carbon coatings and residual carbon particles in the different LFP materials.

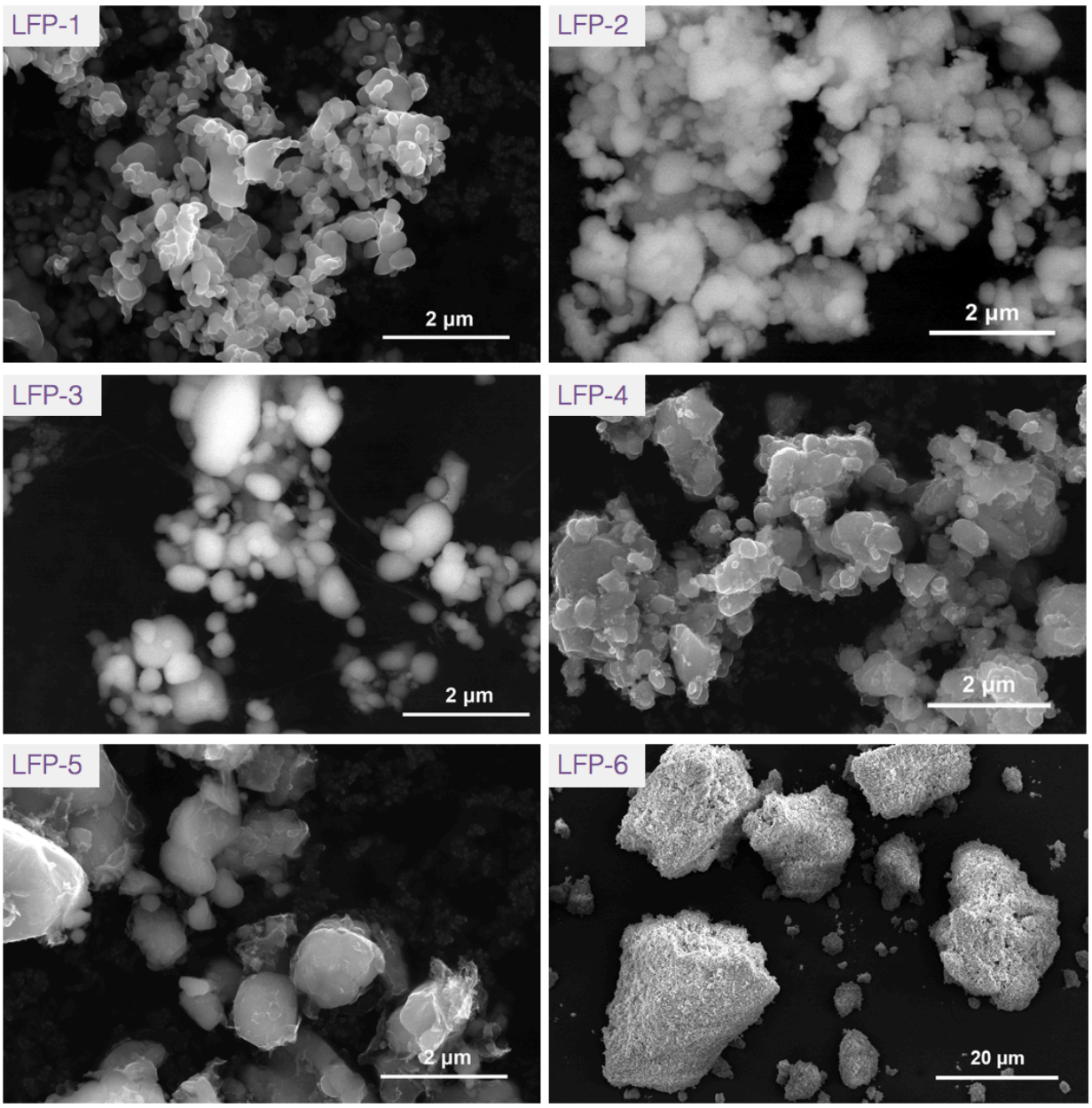

Figure E2. Scanning electron micrograph (SEM) images of LFP-1-6.

Table E1. Tap density and BET surface area of the LFP materials (values reported are the averages and standard deviations for three independent measurements for each material).

Material	Tap Density (g mL^{-1})	BET Surface Area (m^2 g^{-1})
LFP-1	1.08 ± 0.01	7.5 ± 0.2
LFP-2	1.07± 0.01	11.3 ± 0.1
LFP-3	0.64 ± 0.01	14.9 ± 0.1
LFP-4	1.15 ± 0.01	9.7 ± 0.2
LFP-5	1.17 ± 0.01	17.5 ± 0.4
LFP-6	1.04 ± 0.01	1.5± 0.3

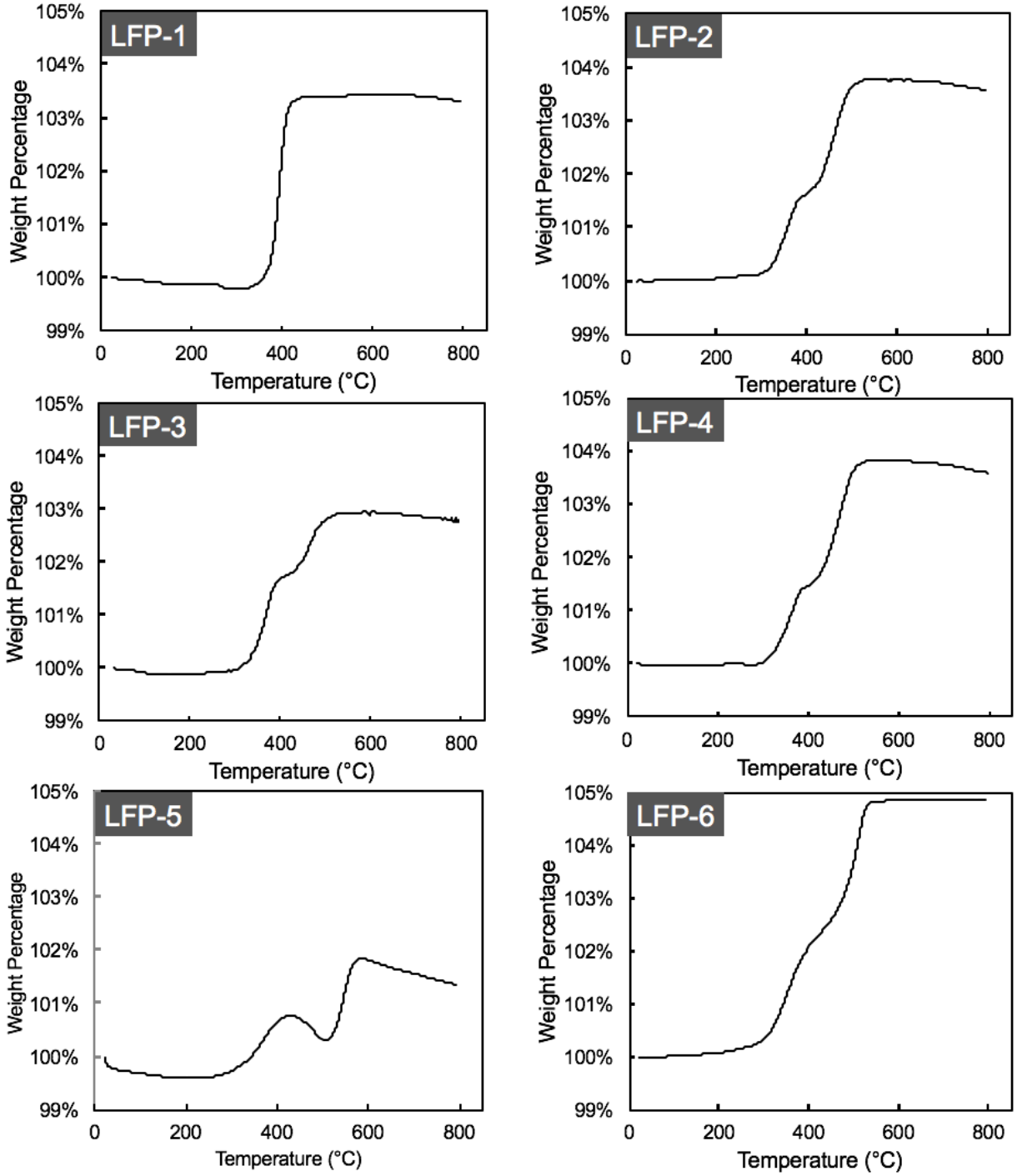

Figure E3. Thermogravimetric analysis (TGA) profiles for the six LFP materials.

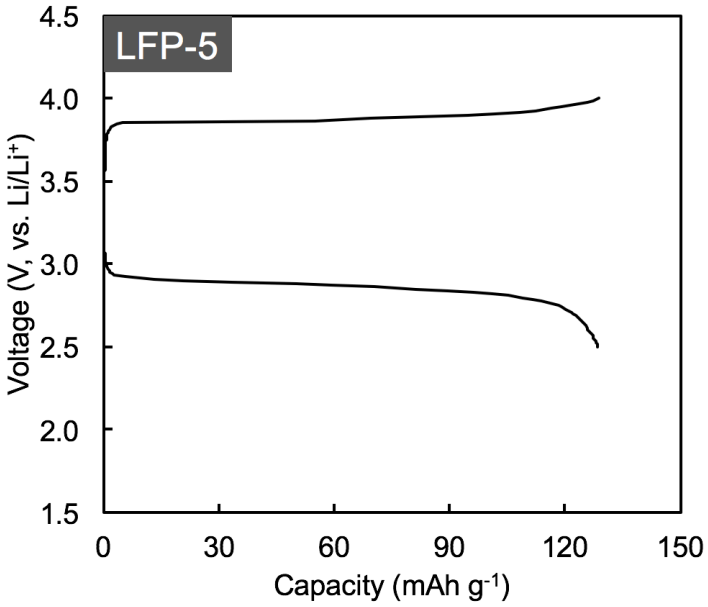
LFP-5
Voltage (V, vs. Li/Li+)
4.5
4.0
3.5
3.0
2.5
2.0
1.5
0
30
60
90
120
150
Capacity (mAh g-1)

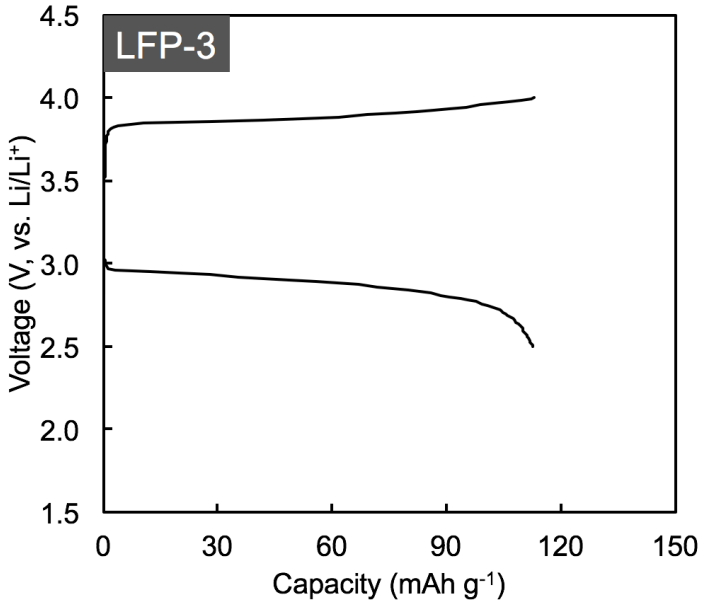
LFP-3
Voltage (V, vs. Li/Li+)
4.5
4.0
3.5
3.0
2.5
2.0
1.5
0
30
60
90
120
150
Capacity (mAh g-1)

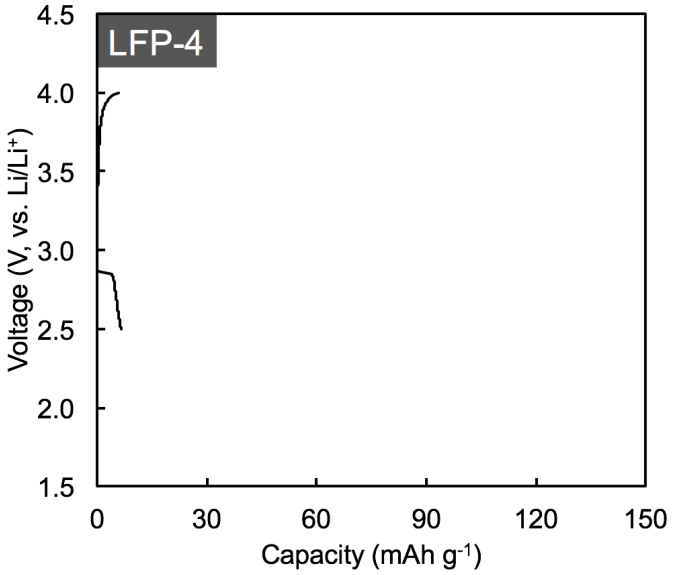

Figure E4. Charge/discharge profile of the 4th cycle of LFP-5, LFP-3, and LFP-4 electrodes fabricated without any additional conductive additive at 0.1C (128.6 mA g^{-1}_{LFP-5}, 112.7 mA g^{-1}_{LFP-3}, 6.5 mA g^{-1}_{LFP-4}). Relative to electrodes with the same materials fabricated with conductive additives, LFP-5 obtained 87.5% of the discharge capacity, LFP-3 73.2%, and LFP-4 4.0%.

Reference:

1. M. Bini, M. C. Mozzati, P. Galinetto, D. Capsoni, S. Ferrari, M. S. Grandi, and V. Massarotti, *J. Solid State Chem.,* **182** 1972 (2009).
2. M. Shieber, *J. Inorg. Nucl. Chem.,* **26** 1363 (1964).
3. Fisher, *Am. Mineral.,* **43** 761 (1958).
4. Z. Zheng, W. K. Pang, X. Tang, D. Jia, Y. Huang, and Z. Guo, *J Alloy Compd,* **640** 95-100 (2015).
5. I. Belharouak, C. Johnson, and K. Amine, *Electrochem Commun,* **7** (10), 983-988 (2005).
6. X. M. Lou and Y. X. Zhang, *J Mater Chem,* **21** (12), 4156-4160 (2011).